Cytochrome *c*: Folding Triggered by Electron Transfer. Rates of Heme Oxidation and Reduction at High Driving Forces

Thesis by

Gary Alan Mines

In Partial Fulfillment of the Requirements

for the Degree of

Doctor of Philosophy

California Institute of Technology

Pasadena, California

1997

(Submitted May 7, 1997)

Acknowledgments

Many people have impacted me both scientifically and otherwise during my time at Caltech. Firstly I would like to thank Harry Gray for always being there for me when I needed him most, for his unyielding spirit and energy, for his unmatched generosity, and for sincerely caring about my well being and happiness. I would like to thank Sunney Chan for supporting me over the years, even as my path took me farther and farther away from the one originally anticipated. I thank Jay Winkler for tolerating my many questions, for providing details and insight on so many topics, and for being essentially another advisor to me during my time here. I thank my committee for being kind, supportive and generally enthusiastic about my efforts.

I thank Jack Richards and Tom Meade for allowing me to use equipment in their labs for certain phases of my research. I thank Skip Williams and Torbjörn Pascher for their help and advice during our jam-packed week in Los Alamos. I thank Ruth Ann Bertsch for introducing me to the interesting topic of protein folding, and for being so understanding when things became a bit complicated.

I have enjoyed working with and interacting with so many wonderful people in the Gray group over the years. Debbie Wuttke, Danny Casimiro, Jorge Colón, I-Jy Chang, Morten Bjerrum, Yi Lu, Mark McCleskey, Jim Baily, Vinny Miskowski, Kara Bren, Jack Mizoguchi, Toshi Takeuchi, Don Low, Eva Birnbaum, Bill Connick, Mike Hill, Claire Slutter, Torbjörn Pascher, Sonny Lee, John Chesick, Tim Karpishin, Angelo Di Bilio, Jens Duus, Hans Nikol, David Wiedenfeld, Kevin Hoke, Ben Ramirez, Phil Dawson, Jeff Regan, Jeff Rack, Jason Telford, Ofer Blum, Jonathan Wilker, Akif Tezcan, Elizabeth Krider, and Randy Villahermosa. Thanks go to all of you, as well as those whom I may have unwittingly omitted. Thanks to I-Jy Chang in particular for mentoring me when I began doing research at Caltech, and for becoming and remaining a wonderful

friend. Debbie Wuttke, Morten Bjerrum, and Randy Larsen were extremely supportive and helpful to me in the early years as well, and I sincerely thank them for that.

Special thanks go to Phil Dawson and Don Low for their help during my thesis-writing days. Phil proofread my thesis at crucial phases, which helped me more than he may know. Don helped both in tangible and intangible ways which are hard to describe; there is simply nothing quite like writing a thesis, and I am so thankful that it happened to work out that Don and I wrote up at the same time so that we could help each other through the various phases and ups and downs. Don also listened to my practice defense talk, which proved to be extremely helpful to me. I cannot thank him enough.

Tom Dunn has always been extremely nice whenever I needed his (amazing) technical assistance on just about anything; I thank him for the interaction as much as for the assistance! I thank Pat Anderson, Catherine May, Dian Buchness, Beth Kerns, and Mo Renta for general assistance in many miscellaneous tasks and inquiries. In general, all the staff I have interacted with at Caltech have been kind and helpful, and I thank them all for that.

I have been fortunate to meet many interesting and fun people during activities outside of the lab. These experiences kept me sane at times, and have left me with many fond memories. I thank Bill and Delores Bing for the opportunities to play clarinet while at Caltech. I can't believe I had never played chamber music before I arrived here! Thanks to all those with whom I have shared the joy of music, and Connie Josias in particular for clarinet information, advice and for introducing me to the Claremont Winds. Thanks to Martha Ter Maat, Jim Smith, and the others involved in Amnesty International. Thanks to Pam Croomes, Branislav Kecman, Jon Melvin, Derrick Key, Lisa Wang and the others involved in Open Line. It was a great idea which I am happy to have been a part of. I thank Zack Berger for his patience in attempting to teach me Yiddish, and for leading the most informative and enjoyable Seder I've ever attended. I

also thank Caty Konigsberg and the others involved in Hillel as well. Thanks to Kathleen Bartle-Schulweis for all the talks, and for being a friend. I thank Yonchu Jenkins for getting me involved in ballroom dancing, and for being my Lindy Hop partner. That was always so much fun! I thank all those members of the Gray group softball team over the years; I'm glad I hung around long enough for us to beat the Hogs! I can't thank Coach Bob Lynn enough for reviving my interest and confidence in doing gymnastics; oh, how I wish the program had not been canceled when Braun Gym opened up! I thank Dana and Arnold Brod for getting me back into racquetball, a truly fantastic sport!

Thanks to Yonchu Jenkins, Ai Ching Lim, Hoa Nguyen, Jérôme Claverie, Jack Mizoguchi, Toshi Takeuchi, Silvia Cavagnero, Howie Choset, and Mike Hill for their friendship and support, and for all the talks, concerts, lunches, and other fun diversions we shared together.

I thank my high school chemistry teacher, Frank Cardulla, for exposing me to chemistry in such a fun and lucid manner; I doubt this thesis would have been written had it not been for him. I also thank my undergraduate research advisor and friend, Marty Ackermann for helping me in the past as a student, and in the present as a colleague.

I would like to thank my parents and grandparents for always supporting me in my scholastic as well as non-scholastic endeavors. Their support has always meant a great deal to me, and it has been particularly important during my grad-school years. I also thank my aunt, uncle and the rest of the "Kaplan clan" for providing me a "home away from home" while I've been on the West Coast. I have truly enjoyed the time we have had to spend together while I have been geographically close. I lastly thank Dana Brod for her love, support, friendship, and patience; it has been a long trek, Dane, but it is finally over! Let's celebrate!

Abstract

Rates of various intramolecular heme oxidations and reductions in a series of closely related $RuL_2(X)$(His33)cytochromes *c* [L = bipyridine or phenanthroline derivatives; X = imidazole (im) or cyanide (CN^-)] have been measured over a free-energy range of 0.54 to 1.89 eV. The driving-force dependence of $Fe^{2+} \rightarrow Ru^{3+}$ electron transfer (ET) is well described by semiclassical ET theory with a coupling-limited rate (k_{max}) of 2.8 x 10^6 s^{-1} and a reorganization energy of 0.74 eV. As predicted by theory, the rate of an exergonic ($-\Delta G^\circ$ = 1.3 eV) heme reduction reaction, $*Ru^{2+}(bpy)_2(im)(His) \rightarrow Fe^{3+}$, falls in the inverted region (k = 2.0 x 10^5 s^{-1}). In contrast, the rates of three highly exergonic heme reductions, $*Ru^{2+}(phen)_2(CN)(His) \rightarrow Fe^{3+}$ (3.1 x 10^5 s^{-1}; 1.4 eV), $Ru^{+}(4,4'\text{-}(CONH(C_2H_5))_2\text{-}bpy)_2(im)(His) \rightarrow Fe^{3+}$ (2.3 x 10^5 s^{-1}; 1.44 eV), and $Ru^{+}(phen)_2(CN)(His) \rightarrow Fe^{3+}$ (4.5 x 10^5 s^{-1}; 1.89 eV), are much higher than expected for reactions directly to ground-state products. Agreement with theory is greatly improved by assuming that an electronically excited ferroheme ($Fe^{2+} \rightarrow *Fe^{2+}$ ~ 1.05 eV) is the initial product in each of these reactions.

In a separate investigation, rates of folding of ferrocytochromes *c* from horse (h-cyt *c*) and yeast (y-cyt *c*) were measured over a range of denaturant concentrations (guanidine hydrochloride, GuHCl) and folding free energies (ΔG_f) using a new ET triggering technique. The backbone structures of the two homologs are similar, but y-cyt *c* is ~15 kJ mol^{-1} less stable than h-cyt *c* and is unfolded at concentrations of GuHCl ~1.5 M lower than for h-cyt *c*. Activation free energies exhibit a linear dependence on GuHCl and ΔG_f for both proteins, with folding rates decreasing with increasing concentration of GuHCl (less negative ΔG_f). At a given denaturant concentration, the folding rates for y-cyt *c* are about an order of magnitude slower than those for h-cyt *c*, but when the folding free energies are matched, folding rates of the two homologs are comparable.

Table of Contents

List of Tables and Figures

Appendix A

Chapter 1

Thesis Overview

Cytochrome *c* is one of the most extensively investigated electron-transfer proteins.[1-3] Numerous detailed accounts of the properties of this protein in various intramolecular[4-6] and bimolecular[7-9] electron-transfer reactions are available. This thesis explores the development of new methodologies for the study of photoinduced electron transfer in cytochrome *c*. Chapter 2 details several photochemical reaction schemes that can be used to study intramolecular electron transfer in Ru-polypyridyl-modified proteins, using $Ru(phen)_2(CN)$(His33)cytochrome *c* as an example. This new label is found to possess photophysical properties which make it more amenable to very high driving force heme reductions than its predecessor, $Ru(bpy)_2$(im)(His).[10] This chapter also describes the preparation and characterization of the modified protein, as well as $Ru(phen)_2(CN)(im)^+$, the compound used to model the photophysical properties of the protein-bound moiety. Chapter 3 presents a study of the driving-force dependence of electron-transfer rates in a series of closely related Ru(His33)cytochromes *c*, using the methods illustrated in Chapter 2. By varying the ligands on the ruthenium complex and by measuring heme reduction reactions as well as heme oxidations, a very wide range of driving forces, including several deep in the Marcus inverted region, is explored.

In Chapter 4, a novel application of photoinduced electron transfer to a very important biological problem, protein folding,[11] is discussed. Techniques which can initiate folding of proteins on submillisecond timescales are actively being sought in this field.[12] It is shown that for redox proteins in which the stability of the oxidized and reduced forms are substantially different, rapid electron transfer under suitable conditions will trigger the process of protein folding. The relationship between the folding rate and the free energy of folding in horse and yeast ferrocytochromes *c* is explored using this method.

REFERENCES

(1) *Cytochrome c: a multidisciplinary approach*; Scott, R. A.; Mauk, A. G., Eds.; University Science Books: Sausalito, 1996, pp 738.

(2) Moore, G. R.; Pettigrew, G. W. *Cytochromes c: Biological Aspects*; Springer-Verlag: New York, 1987, pp 282.

(3) Moore, G. R.; Pettigrew, G. W. *Cytochromes c: Evolutionary, Structural, and Physicochemical Aspects*; Springer-Verlag: New York, 1990, pp 478.

(4) Winkler, J. R.; Gray, H. B. *Chem. Rev.* **1992**, *92*, 369-379.

(5) Millett, F.; Durham, B. In *Metal Ions in Biological Systems*; H. Sigel and A. Sigel, Eds.; Marcel Dekker, Inc.: New York, 1991; Vol. 27; pp 223-264.

(6) Casimiro, D. R.; Beratan, D. N.; Onuchic, J. N.; Winkler, J. R.; Gray, H. B. In *Mechanistic bioinorganic chemistry*; H. H. Thorp and V. L. Pecoraro, Eds.; American Chemical Society: Washington, D. C., 1995; Vol. 246; pp 471-485.

(7) Turró, C.; Zaleski, J. M.; Karabatsos, Y. M.; Nocera, D. G. *J. Am. Chem. Soc.* **1996**, *118*, 6060-6067.

(8) Millett, F.; Miller, M. A.; Geren, L.; Durham, B. *J. Bioenerg. and Biomembr.* **1995**, *27*, 341-351.

(9) Hoffman, B. M.; Natan, M., J.; Nocek, J. M.; Wallin, S., A. *Struct. Bond.* **1991**, *75*, 85-108.

(10) Chang, I.-J.; Gray, H. B.; Winkler, J. R. *J. Am. Chem. Soc.* **1991**, *113*, 7056-7057.

(11) *Protein Folding*; Creighton, T., E., Ed.; W. H. Freeman and Company: New York, 1992, pp 547.

(12) Eaton, W. A.; Muñoz, V.; Thompson, P. A.; Chan, C.-K.; Hofrichter, J. *Curr. Op. Struct. Biol.* **1997**, *7*, 10-14.

Chapter 2

Preparation, Characterization, and Electron-Transfer Reactions of $Ru(phen)_2(CN)(His33)$cytochrome *c*

INTRODUCTION

An oxidative flash-quench scheme utilizing a $Ru(bpy)_2(im)$- label bound to a surface histidine of a protein has recently been developed to study long-range electron transfer (ET) in biomolecules.[1] In this scheme, bimolecular oxidative quenching of the excited state of the label allows facile measurement of intramolecular oxidations of native redox centers in proteins. This methodology has been particularly useful in determining the medium dependence of the electronic couplings of ET reactions in proteins such as cytochrome *c*,[2,3] myoglobin,[4] and azurin.[5]

However, the $Ru(bpy)_2(im)(His)$- label, due in large part to its relatively short excited-state lifetime (~70 ns),[6] is much less useful in photoreduction schemes. Direct photoinduced reduction of ferricytochrome *c* from the ruthenium excited state occurs in such a small yield that investigators initially failed to observe it.[6] In addition, attempts to quench the excited state *reductively* have met with little success.

It is well known that the photophysical properties of ruthenium-polypyridyl complexes can be modulated by manipulation of the ligands.[7,8] Perusal of a vast compilation of photophysical data[9] indicates that ruthenium polypyridyls containing phenanthroline (phen) tend to exhibit lifetimes that are ~50% longer than analogous compounds containing bipyridine (bpy) (e.g., $\tau_o[Ru(phen)_3^{2+}] \sim 1.0$ μs; $\tau_o[Ru(bpy)_3^{2+}] \sim 0.6$ μs),[10] and complexes having a cyanide ligand in place of an imidazole (im) often display lifetime enhancements of up to three to fourfold (e.g., $\tau_o[Ru(bpy)_2(CN)_2] \sim 250$ ns;[11] $\tau_o[Ru(bpy)_2(im)_2^{2+}] \sim 70$ ns). These observations suggest that incorporation of phenanthroline and cyanide ligands into a histidine-bound ruthenium label might lead to an enhanced excited-state lifetime and potentially improved behavior in photophysical ET schemes. This chapter describes the synthesis and characterization of $Ru(phen)_2(CN)$(His33)cyt *c*. The photophysical properties of the modified label are indeed improved over $Ru(bpy)_2(im)$-: yields in both photoreduction and reductive

quenching experiments are significantly higher. Detailed descriptions of the measurement of ET rates using these reductive kinetic schemes, as well as the oxidative flash-quench scheme, are provided.

MATERIALS AND METHODS

General

Protein solutions were concentrated using ultrafiltration units (stirred cells or centricon devices) from Amicon containing YM3 or YM10 membranes. G-25 Sephadex (Pharmacia) was used for gel filtration chromatography, and unless otherwise specified, columns were preequilibrated and eluted with $\mu = 0.1$ sodium phosphate buffer, pH 7.0. Unless stated otherwise, cation-exchange chromatography was performed using an HR 16/10 Mono S prepacked column attached to an FPLC system (Pharmacia). Linear NaCl gradients were used for elution (loading buffer (pump A) $\mu = 0.1$ sodium phosphate, pH 7; limit buffer (pump B) 0.25 M NaCl, buffered to pH 7.0 using sodium phosphate (~25 mM)).

Horse heart cytochrome c (type VI) was obtained from Sigma and was typically purified by cation-exchange chromatography (FPLC) before use. Bovine cytochrome *c* oxidase (CcO) was prepared by members of Sunney Chan's research group using the method of Hartzell and Beinart.[12] Buffers were prepared using reagent grade chemicals and distilled house water purified by passage through a Barnstead NANOpure system. 1,10-phenanthroline (phen), 2,2'-bipyridine (bpy), 4,4'-dimethyl-2,2'-bipyridine (4,4'-$(CH_3)_2$-bpy), and imidazole (im) were purchased from either Merck or Aldrich and used as received. *p*-methoxy-*N,N*- dimethylaniline (MeODMA) was obtained from *p*-methoxyaniline (TCI) by reaction with dimethylsulfate according to a published procedure,[13] followed by room temperature sublimation under static vacuum; it was stored in the dark under argon until just prior to use. Ruthenium(III) chloride hydrate

(Johnson Matthey or Aldrich) and Tris(2,2'-bipyridine)-ruthenium(II) chloride (Strem or Aldrich) were used as received. Hexaammineruthenium(III) chloride (Aldrich) was recrystallized from warm 1 M HCl (<40 °C) before use. $Ru(phen)_2Cl_2$, $Ru(phen)_2(im)_2Cl_2$, and $Ru(phen)_2CO_3$ were prepared by literature procedures for the analogous $Ru(bpy)_2Cl_2$,[14] $Ru(bpy)_2(im)_2Cl_2$,[15] and $Ru(bpy)_2CO_3$[16] compounds, with minor modifications.

[Ru(phen)$_2$(CN)(im)]Cl

$Ru(phen)_2Cl_2$ (297 mg, 0.53 mmol), KCN (48 mg, 0.79 mmol), and im (47 mg, 0.69 mmol) were refluxed in water/ethanol (1:1) for 3 hours, and the red solution was roto-evaporated to dryness. The residue was redissolved in a minimum of water/ethanol (~5:1), and the solution was applied to a cation-exchange column preequilibrated with water (SP-Sephadex, 12 cm x 4 cm i.d.). A small amount of $Ru(phen)_2(CN)_2$ eluted in the void volume (with water). $Ru(phen)_2(CN)(im)^+$ was eluted with 0.5 M NaCl (~500 mL). The volume was reduced to ~60 mL by rotary evaporation, yielding an orange precipitate. After incubation at 0 °C for 2 hours, the solid was isolated by filtration, washed with ether, and air dried. See Results and Discussion section for ^1H NMR spectrum.

Ru(phen)$_2$(CN)(His33)cytochrome *c*

A solution of ferricytochrome *c* (0.5 mM, 15 mL; $\mu = 0.1$ phosphate buffer, pH 7.0) was stirred under Ar with $Ru(phen)_2CO_3 \cdot 2H_2O$ (43 mg, ~5 mM) at room temperature in the dark for ~40-50 hours. During this time the reaction was monitored (approximately every 10 hours) by passing a 10-50 μL aliquot of the reaction mixture down a small G-25 Sephadex column (PD 10, Pharmacia) and measuring the absorption spectrum of the protein fraction. The reaction was stopped when the average modification ratio was ~1:1 (Ru:heme), as indicated by an absorbance ratio of

Abs_{266}/Abs_{410} ~ 0.86 (see Figure 2.16). After removal of excess $Ru(phen)_2(H_2O)_2$ by gel filtration (G-25 Sephadex, 30 cm x 2.5 cm i.d.), the protein solution was loaded onto a cation-exchange "screening" column (SP Sepharose, 3 cm x 2.5 cm i.d.) and eluted with 0.25 NaCl (buffered to pH 7.0). This step was performed to remove multiply modified and/or other highly binding side products which were seen to semipermanently contaminate Mono S FPLC columns. The solution which passed through the screening column was desalted by repetitive concentration/dilution cycles in an Amicon ultrafiltration cell, and loaded onto a Mono S column for purification by FPLC. The band eluting at ~60% Buffer B ($Ru(phen)_2(H_2O)$(His33)cyt *c*) was concentrated to ~0.7 mM, reduced with excess sodium dithionite, and passed through a gel filtration column preequilibrated and eluted with 0.2 M diethanolamine, pH 9.1. Solid KCN was added (to make 0.22 N KCN) and the solution (~0.2 mM Ru-cyt *c*) was stirred under argon in the dark for 3 days. The reaction was stopped by passage down a gel filtration column, and the protein solution was oxidized overnight at 4 °C by addition of >100-fold excess of solid KCoEDTA. The solution was then loaded onto a Mono S column, and $Ru(phen)_2(CN)$(His33)cyt *c* eluted at 45% Buffer B. Numerous side products were observed (see Results and Discussion), including unreacted $Ru(phen)_2(H_2O)$(His33)cyt *c*, and one or two additional FPLC runs were necessary to achieve baseline separation.

Spectroscopic Characterization

Absorption spectra were measured using a Hewlett-Packard 8452A Diode-Array Spectrophotometer. ^1H NMR spectra of metal complexes were recorded at 500 MHz using a Bruker AM500 Spectrometer. The solvent was D_2O and sample concentrations were >1 mM. Emission spectra were obtained using an in-house apparatus described elsewhere;[17] the excitation source was a 150 W Xe/Hg lamp (436 nm line).

UV CD spectra (200-350 nm) of (Ru-modified) cyt *c* solutions in quartz cells of 0.1 cm pathlength (12 μM cyt *c*, 200 μL; μ = 0.1 phosphate buffer, pH 7.0) were obtained

at room temperature using a Jasco J-600 spectropolarimeter. A blank spectrum was recorded and saved before each spectral acquisition, and was subtracted from the protein spectrum after the measurement using Jasco software or Kaleidagraph (Abelbeck/Synergy Software). Each spectrum is the average of 4-8 scans. The output from the instrument (ψ, in degrees) is converted to molar ellipticity, $[\theta]_M$ (in the odd but conventional units of deg cm^2 $dmol^{-1}$), using the formula:[18]

$$[\theta]_M = 100\psi / ml \qquad (2.1)$$

where l is path length (in cm), m is the concentration (in M), and 100 is a conversion factor (100 cm^2 $dmol^{-1}$ = M^{-1} cm^{-1}). Mean residue ellipticity, $[\theta]$ (without the subscript "M"), which applies only to peptides/proteins, is the *average* molar ellipticity per amino-acid residue in the sequence, and is simply equal to $[\theta]_M$ divided by the number of residues in the peptide/protein (104 for horse cytochrome *c*).

Tryptic Digestion of Cytochromes *c*

A solution of (Ru-modified) cytochrome *c* (0.5-2 mg) was equilibrated with 0.1 M NH_4HCO_3 (pH 8.5) concentrated to 2 mg/mL (~160 μM) using centricon devices, and transferred to a 15 mL disposable conical tube. 16 μL of a trypsin stock solution (2 mg/mL in 0.001 M HCl) was then added for every mL of protein solution, and the solution was incubated at 37 °C. After 6 hours, a second addition of trypsin was made (16 μL trypsin stock/mL solution). The reaction was stopped after 20 hours (total) by adjusting the pH to ≤ 2 with a few drops of 1 M HCl. The solutions were flash frozen in an ethanol/dry ice bath and lyophilized. The lyophilized protein fragments were dissolved in ~100 μL of aqueous trifluoroacetic acid (TFA) (0.1% by weight) per mg of protein digested, and loaded onto a PepRPC 5/5 HR reversed-phase column connected to an FPLC system (Pharmacia). Purification was achieved using a linear gradient from 0 to

40% (by volume) acetonitrile [loading solvent (pump A) was 0.1% TFA in water; limit solvent (pump B) was 0.1% TFA in acetonitrile]; 280 nm absorption was used to monitor the separation. The ruthenium-containing peptide (as determined by absorption spectroscopy) was collected and subjected to N-terminal sequencing by the University of Southern California Cancer Center's Microchemical Facility.

Kinetics Measurements

Instrumentation

Kinetics were measured by laser-flash photolysis/transient-absorption and transient emission spectroscopy using the facilities in the Beckman Institute Laser Resource Center. The excitation source was a dye laser (Lambda Physik FL3002; Coumarin 480, 25 ns/pulse, 480 nm, 1-3 mJ/pulse) pumped by a XeCl excimer laser (Lambda Physik LPX210i). Single-wavelength transient-absorption traces were collected by directing light from a 75 W xenon arc lamp through the sample, colinearly with the excitation beam, into a 160B Instruments SA double monochromator. The signal was detected by a Hamamatsu R928 photomultiplier tube, amplified using a DSP 1402E programmable amplifier, and digitized with a Tektronix R710 200-MHz 10-bit transient digitizer connected to a 386-based microcomputer. Kinetic traces are averages of 500-2000 laser shots, acquired in cycles of 50-100 shots/cycle at a repetition rate of 10 Hz. Samples were stirred throughout data collection. All kinetics traces were fit to single or biexponential functions using the KINFIT program written by Dr. Jay Winkler, and adapted for use on a Macintosh by Torbjörn Pascher. Uncertainties in measured rate constants are estimated to be 10%.

Determination of Transient Difference Spectra

The difference spectra of various transient ruthenium and MeODMA redox species were determined by monitoring the single-wavelength kinetics of laser-excited

solutions of appropriate reagents (see below) by transient absorption at a variety of wavelengths between 300 and 700 nm. All kinetic traces for a given spectral determination were acquired on the same sample on the same day. All experiments were performed in $\mu = 0.1$ sodium phosphate buffer, pH 7.0; solution volumes ranged from 2-4 mL. Solutions were Ar-degassed by repetitive pump/fill cycles in vacuum cells fitted with 1 cm quartz cuvette side arms.

The difference spectrum of the Ru^{3+} state ($Ru^{3+} - Ru^{2+}$) of $Ru(phen)_2(CN)(im)^+$ was determined using solutions of $[Ru(phen)_2(CN)(im)]Cl$ (20 μM) and $Ru(NH_3)_6Cl_3$ (12 mM). A solution containing $Ru(bpy)_3Cl_2$ (18 μM), $Ru(NH_3)_6Cl_3$ (5 mM), and MeODMA (~200 μM) was used to determine the spectrum of $MeODMA^{\bullet+}$. The sum of the Ru^+ difference spectrum of $Ru(phen)_2(CN)(im)^+$ ($Ru^+ - Ru^{2+}$) and the spectrum of $MeODMA^{\bullet+}$ was determined using solutions of $[Ru(phen)_2(CN)(im)]Cl$ (~35 μM) and MeODMA (~5 mM); the excited-state difference spectrum ($*Ru^{2+} - Ru^{2+}$) was measured during these experiments as well. Concentrations of ground-state species were determined using the following extinction coefficients: $Ru(bpy)_3^{2+}$ ($\varepsilon_{452} = 14600$ M^{-1} cm^{-1}),[19] MeODMA ($\varepsilon_{239} = 10320$ M^{-1} cm^{-1}).[20]

Ru-cytochrome c Electron-Transfer Experiments

Protein solutions for oxidative flash-quench measurements were reduced by excess sodium dithionite and passed through a gel filtration column just prior to each experiment. Solutions (1.5-4 mL) of 12-20 μM Ru-cyt *c* and either 1-12 mM $Ru(NH_3)_6Cl_3$ (for oxidative flash-quench experiments) or 5-9 mM MeODMA (for reductive flash-quench experiments) in $\mu = 0.1$ sodium phosphate buffer, pH 7.0, were Ar-degassed as noted above. Mild warming was necessary to solubilize MeODMA.

Power-Dependence Experiments

Transient absorption kinetics of a solution of 18 μM $Ru(phen)_2(CN)(His33)$cyt $c(Fe^{3+})$ were measured at 339 nm over a pulse power (incident intensity) range of 0 to 4.9

mJ/pulse to determine the $\Delta\varepsilon$ values for *Ru(phen)$_2$(CN)(His).[21] The pulse power was adjusted between 0 and 3.2 mJ/pulse using a pair of polarizers in the path of the laser beam; rotation of one polarizer relative to the other results in a diminished intensity passing through the set. A power of 4.9 mJ/pulse was attained by removing the polarizers from the path entirely. Pulse power was measured using a Scientech 372 Power and Energy Meter.

It can be shown that the concentration of an excited-state species, C^*, produced by laser excitation with incident intensity I, depends upon I according to the following relation:[21]

$$C^* = C_0(1 - e^{-bI}) \tag{2.2}$$

in which C_0 is the concentration of the photoexcitable species in solution (b is a product of constants relating to the probability of absorption of light; the details are not important to this analysis). Substituting this expression into Beer's Law, $\Delta Abs_\lambda = \Delta\varepsilon_\lambda C^* d$ (d is the path length) yields:

$$\Delta Abs_\lambda = \Delta\varepsilon_\lambda C_0 d(1 - e^{-bI}) \tag{2.3}$$

ΔAbs/pulse-power data were fit to Equation 2.3 using Kaleidagraph to obtain $\Delta\varepsilon_\lambda$. It is important to note that Equation 2.3 is not valid at very high powers since excited states of the excited state can be generated (i.e., two-photon excitation can occur).

RESULTS AND DISCUSSION

Synthesis and Characterization of [Ru(phen)$_2$(CN)(im)]Cl

The idea of making small inorganic complexes as models for more complicated protein-bound inorganic species is a pervasive concept in bioinorganic chemistry.[22] We

have prepared $Ru(phen)_2(CN)(im)^+$ to model the properties of a putative $Ru(phen)_2(CN)(His)^+$- moiety, in which the histidine (His) is a surface-exposed residue of a protein. Our purposes for making this model are threefold: 1) to use the model compound, which is easy to make in large quantities, to determine whether or not to pursue the more complicated and costly procedure of actually modifying a protein with this reagent; 2) if the protein is in fact made, to use the model compound to characterize spectral and photophysical properties of the protein-bound complex which are difficult to determine directly due to the presence of the protein; and 3) to help verify the identity and integrity of the labeled protein once it has been prepared.

Cation-exchange chromatography of the products of the reaction of $Ru(phen)_2Cl_2$ with KCN and imidazole yields three major bands. The first band elutes with the void volume, has an MLCT absorption band with a maximum at about 400-410 nm, and emits bright orange upon irradiation with 366 nm light (handheld UV lamp). These properties are characteristic of $Ru(phen)_2(CN)_2$.[11] The third band has an absorption maximum at 484 nm and emits red light upon irradiation, characteristic of $Ru(phen)_2(im)_2^{2+}$ (Appendix A). The middle fraction exhibits an MLCT band roughly midway between that for $Ru(phen)_2(CN)_2$ and $Ru(phen)_2(im)_2^{2+}$ (Figure 2.1; λ_{max} = 442 nm), as expected for the desired product: $Ru(phen)_2(CN)(im)^+$.

The ^1H NMR spectrum is consistent with this assignment. Unlike $Ru(phen)_2(CN)_2$ or $Ru(phen)_2(im)_2^{2+}$, $Ru(phen)_2(CN)(im)^+$ has no C_2 axis of symmetry, and thus all 16 phenanthroline protons are distinct in the ^1H NMR spectrum (Figure 2.2; compare with Figure 3.1). The splitting patterns and integrations are as expected; phenanthroline protons: d at 9.89 (1), d at 8.68 (1), d at 8.54 (1), d at 8.45 (1), d at 8.31 (1), d at 8.17 (1), d at 8.02 (1), d at 7.99 (1), m at 7.91 (3), dd at 7.81 (1), d at 7.74 (1), d at 7.70 (1), dd at 7.32 (1), dd at 7.16 (1); imidazole protons: s at 7.61 (1), s at 6.86 (1), s at 6.64 (1).

The ^{3}MLCT state emits with a λ_{max} of ~680 nm and an estimated E_{00} of 2.2 eV (560 nm); a time-resolved emission measurement yields an excited-state lifetime of 500 ns (Figure 2.3). This is seven times longer than the corresponding ^{3}MLCT state of $Ru(bpy)_2(im)_2^{2+}$ (70 ns),[1] consistent with the trends noted above in comparing other ruthenium polypyridyl compounds with similar ligand swaps.

Difference Spectra

All ET measurements described in this thesis were made using transient absorption spectroscopy. In our setup, absorption is recorded in difference mode. That is, measured absorption values represent the post-laser-flash absorbance minus the pre-laser-flash absorbance (ΔAbs). In order to meaningfully plan kinetics experiments and interpret kinetics data, it is essential to know the difference spectra of the species present during ET reactions. The cyt *c* heme iron exists in only two possible states (Fe^{3+} and Fe^{2+}) during the ET reactions discussed in this thesis, and both of these states can be easily prepared as steady-state species under normal conditions. The spectra of each redox form and the corresponding (Fe^{2+} – Fe^{3+})cyt *c* difference spectrum are shown in Figure 2.4. The ruthenium center in $Ru(phen)_2(CN)(His)$, on the other hand, accesses several states ($*Ru^{2+}$, Ru^{3+}, and Ru^{+}) in the photoinduced ET reaction schemes described in this thesis. These species are not stable under normal conditions. In order to determine the difference spectra of these short-lived states, oxidative and reductive quenching schemes involving the model compound $Ru(phen)_2(CN)(im)^+$ were employed. Working with the model compound is more convenient than studying the Ru-modified protein directly, since in the latter case absorption contributions from the protein complicate the spectrum, and ET processes involving the heme can occur as well, complicating the analysis even further. An oxidative quenching scheme is also used to determine the spectrum of the oxidized state of one of the quenchers, $MeODMA^{\bullet+}$,

which is only transiently stable as well. Results from these experiments are described below.

($Ru^{3+} - Ru^{2+}$) Difference Spectrum

The ($Ru^{3+} - Ru^{2+}$) difference spectrum of $Ru(phen)_2(CN)(im)$ was determined using a simple oxidative photochemical quenching scheme (Figure 2.5, *top*; Q_1 = $Ru(NH_3)_6^{3+}$). The excited state of $Ru(phen)_2(CN)(im)$ is efficiently quenched via electron transfer to $Ru(NH_3)_6^{3+}$ to form $Ru^{3+}(phen)(CN)(im)$ and $Ru(NH_3)_6^{2+}$ in less than a microsecond ($k_q = 1.8 \times 10^9\ M^{-1}\ s^{-1}$). Data collected at 450 nm, at which both $*Ru^{2+}$ and Ru^{3+} difference spectra exhibit a bleach, are shown in Figure 2.5 (*bottom*). Owing to the optical transparency of $Ru(NH_3)_6$ in both oxidation states over the wavelength range of interest, the difference spectrum just after the fast kinetic phase (at 2.5 μs), obtained from multiple single-wavelength kinetics traces, describes the $Ru(phen)_2(CN)(im)$ ($Ru^{3+} - Ru^{2+}$) difference spectrum (Figure 2.6). Bimolecular recombination of the photoproducts occurs on a much longer timescale (~ms) due to the low concentration of species generated (~μM).

Spectrum of MeODMA$^{\bullet+}$

A variant of the simple oxidative quenching scheme was used to determine the spectrum of the radical cation of *p*-methoxy-*N,N*-dimethylaniline ($MeODMA^{\bullet+}$) (Figure 2.7, *top*; $Q_1 = Ru(NH_3)_6^{3+}$; "Ru" in this scheme refers to $Ru(bpy)_3$ rather than $Ru(phen)_2(CN)(im)$). Laser excitation of solutions of $Ru(bpy)_3^{2+}$, $Ru(NH_3)_3^{2+}$, and MeODMA yields biphasic kinetics on a fast timescale (<25 μs) (Figure 2.7, *bottom*). The first phase ($k_{obs} = 7 \times 10^6\ s^{-1}$) represents oxidation of $*Ru(bpy)_3^{2+}$ by $Ru(NH_3)_6^{3+}$ to form $Ru(bpy)_3^{3+}$ and $Ru(NH_3)_6^{2+}$. The second phase ($k_{obs} = 4 \times 10^5\ s^{-1}$) represents thermal bimolecular oxidation of MeODMA by $Ru(bpy)_3^{3+}$; this phase is pseudo first order due to the greater than tenfold excess of MeODMA over photogenerated

$Ru(bpy)_3^{3+}$. Again, due to the optical transparency of $Ru(NH_3)_6$, the ΔAbs values after the second kinetic phase (at 25 μs) are ascribed entirely to $MeODMA^{\bullet+}$ (Figure 2.8). The spectrum was scaled assuming a value of 7200 M^{-1} cm^{-1} at 484 nm.[23] Equal-concentration bimolecular recombination between $Ru(NH_3)_6^{2+}$ and $MeODMA^{\bullet+}$ occurs on a long timescale (~ms).

The key to this experiment is in choosing the appropriate concentrations of reagents. Q_1 is in 25-fold excess over MeODMA to ensure that the vast majority of $*Ru^{2+}$ molecules are quenched by Q_1 rather than MeODMA. But the concentration of MeODMA is still 10-20 times greater than the amount of Q_1^- generated by the quenching (~10 μM), so that MeODMA gets oxidized by $Ru(bpy)_3^{3+}$ before the recombination of $Ru(bpy)_3^{3+}$ with Q_1^-.

($Ru^+ - Ru^{2+}$) Difference Spectrum (plus $MeODMA^{\bullet+}$)

"Ru^+" denotes the species in which ruthenium is in the +2 oxidation state and one of the ligands is a radical anion [Ru^{2+}-(diimine$^{\bullet-}$)] (regardless of the overall charge on the complex). A simple *reductive* quenching scheme (Figure 2.9, *top*; Q_2 = MeODMA), analogous to the scheme in Figure 2.5, was used to determine the ($Ru^+ - Ru^{2+}$) difference spectrum. A kinetic trace, monitored at 339 nm, is shown in Figure 2.9 (*bottom*). Unlike in the oxidative quenching scheme, the quencher is not optically transparent in both oxidation states, and thus the observed spectrum at 2.5 μs is the sum of the oxidized quencher, $MeODMA^{\bullet+}$, and the ($Ru^+ - Ru^{2+}$) difference spectrum (Figure 2.10).

It should be noted that further ΔAbs changes were observed on a ~100 μs timescale, which is too fast for bimolecular recombination at such low concentrations. We suspect that the Ru^+ species undergoes some type of degradation chemistry, perhaps involving reduction of unreacted MeODMA molecules.

The successful demonstration of reductive quenching of the model compound in aqueous solution with measurable yields of ET photoproducts is a significant

accomplishment. *$Ru(bpy)_3^{2+}$ has been utilized much more extensively as a photoreductant than as a photooxidant,[24] perhaps indicating the greater difficulties in achieving reductive quenching in unsubstituted bpy complexes of ruthenium. Furthermore, of those studies involving reductive quenching of *$Ru(bpy)_3^{2+}$, the majority have been carried out in organic solvent. We attempted experiments with many quenchers that have been reported to yield reductive photoproducts in experiments with $Ru(bpy)_3$. Excitation of $Ru(phen)_2(CN)(im)^+$ in the presence of $Co(phen)_3^{2+}$[25] or $Ru(NH_3)_6^{2+}$[26] yielded quenching but no photoproducts. Excitation in the presence of *p*-methoxyphenol[27] was also attempted, but no quenching was observed using up to 90 mM of the quencher. Photoproducts were observed using $Fe(CN)_6^{4-}$,[26,28] but the yields were very small (at least five times smaller than seen with MeODMA) and Stern-Volmer plots displayed curvature. Tetramethlyphenylenediamine (TMPD)[29] quenched *$Ru^{2+}(phen)_2(CN)(im)$ to yield a significant amount of photoproducts, but its reduction potential is too low for use in an ET experiment with cyt *c*; it reduces the ferriheme thermally before the laser flash.

**Ru^{2+} Spectrum; Δε determination*

The spectrum of the $Ru(phen)_2(CN)(im)$ excited-state species was determined by extrapolation to "time 0" of each kinetic trace acquired during the reductive quenching experiment described above; the spectrum is shown in Figure 2.11A. This spectrum was scaled to give Δε values by measuring the transient absorption kinetics at 339 nm as a function of power in $Ru(phen)_2(CN)$(His33)cyt *c*(Fe^{3+}) (Figure 2.11B); 339 nm is an isosbestic point for cyt *c*, and so no interference from the absorption of the protein occurs. The observed ΔAbs values, extrapolated to "time 0" for each trace, vary with the pulse power as dictated by Equation 2.3, yielding a value of $\Delta\varepsilon_{339}$ =7300 M^{-1} s^{-1} (C_0 = 18 μM; d = 1 cm).

Preparation of $Ru(phen)_2(CN)$(His33)cytochrome *c*

The advantageous photophysical properties of the model compound clearly indicated that preparation of $Ru(phen)_2(CN)$(His33)cyt *c* was worth pursuing. The procedure involved two basic steps: modification of native cyt *c* with $Ru(phen)_2(H_2O)$- to form $Ru(phen)_2(H_2O)$(His33)cyt *c*, and subsequent incubation with cyanide to produce $Ru(phen)_2(CN)$(His33)cyt *c* (Figure 2.12). The first reaction is analogous to modification with $Ru(bpy)_2(H_2O)$-.[6] $Ru(phen)_2CO_3$ dissolved in aqueous solution readily aquates to form $Ru(phen)_2(H_2O)_2^{2+}$ which will react with nitrogenous ligands such as the imidazole moiety of histidine residues with a modest rate at room temperature. A cation-exchange chromatogram of the protein reaction products displays three major peaks: the first band to elute is unmodified cyt *c*, the second band is composed of cyt *c* modified with one ruthenium compound, and the third peak is largely composed of doubly-modified cyt *c* proteins (Figure 2.13). The elution sequence is consistent with the fact that each ruthenium complex adds a net charge of +2 to the already positive cyt *c* molecule. The majority of the singly-modified protein in band II is composed of $Ru(phen)_2(H_2O)$(His33)cyt *c*; however, it is clear from the chromatogram that several other products having spectra consistent with a singly-modified cyt *c* elute both before and after the presumed His33 band. A prior investigation of $Ru(bpy)_2$(im)-cyt *c* identified four components (one major and three minor) within the singly-modified band "envelope," representing the four combinations resulting from placement of either the Λ or Δ enantiomer of the Ru complex at position His33 or His26.[30] It is presumed that the other products seen here are the analogous $Ru(phen)_2(H_2O)$- variants; however, only the major peak, verified to be a His33-modified protein (see next section), has been extensively characterized and used in the experiments described in this thesis.

Although the modification reaction has not been carefully optimized, several conditions have been tried, and a few observations warrant mention. The yield of crude

$Ru(phen)_2(H_2O)$(His33)cyt *c* ranges from 10-19%. The highest yields occurred when the reaction was carried out on a relatively large scale (>150 mg cyt *c*), and when using *reduced* cyt *c* rather than oxidized, but we have not specifically tested the reproducibility of this observation. Changing the ratio of reactants from ~10:1 (Ru:Fe) to ~1.25:1 (using approximately the same absolute cyt *c* concentration) resulted in a much longer reaction time (about 11 days), did not increase selectivity for His33 (as assessed by the distribution of peaks in the FPLC chromatograms), and resulted in a relatively small yield of crude $Ru(phen)_2(H_2O)$(His33)cyt *c* (~8%). Similarly, running the reaction in 300 mM carbonate buffer (pH 8.0) and at tenfold diluted concentration of both reactants led to reaction times of about 25 days and gave a yield of only 3%.

A cation-exchange chromatogram of the products of the cyanide incubation exhibits more products than anticipated (Figure 2.14A). The major peak, eluting at 45% Buffer B (~100 mL; marked with an asterisk), accounts for only about 30% of the starting material after purification to homogeneity by further FPLC runs. As described in the next section, this protein is the expected product, $Ru(phen)_2(CN)$(His33)cyt *c*. Of the other peaks in the chromatogram, one (marked by a "#") can be ascribed to unreacted $Ru(phen)_2(H_2O)$(His33) (note that this elutes later than the main peak, consistent with the charge difference between H_2O and CN^-), but the others remain undetermined. In a control experiment in which native cyt *c* was incubated with cyanide under the same conditions as in the $Ru(phen)_2(H_2O)$(His33)cyt *c* reaction, a similar pattern of degradation was observed (Figure 13B). Evidently, this is a consequence of the relatively long reaction time of the ligand-exchange reaction. The extent to which the presence of the ruthenium complex may affect these degradation pathways or elicit other ones was not pursued.

Attempts to use $Ru(phen)_2(CN)(H_2O)$ (crude preparation) as a modification reagent in order to eliminate the CN^- step were unsuccessful. It is possible that cyanide-bridged ruthenium dimers or oligomers [31] form faster than modification of the protein.

Tryptic Digests

To identify the residue to which $Ru(phen)_2(CN)$- was bound, the protein was enzymatically cleaved by trypsin, and the resulting protein fragments were separated by reversed-phase chromatography. The sequence of horse heart cyt *c*, divided into the expected fragments resulting from tryptic digestion, is shown in Figure 2.15A. The FPLC chromatogram of the digestion products of native horse heart cyt *c* (Figure 2.15B) exhibits a profile similar to that expected for a complete digestion reaction (monitored at 280 nm): the largest peak corresponds to the heme-containing peptide (T4), the medium-sized peak is due to the fragment bearing a Trp residue (T10), and multiple smaller peaks arise from those fragments containing Tyr residues (T8, T11, T12, T16). The profile of the digestion products of the Ru-modified cyt *c* accords well with that for native cyt *c*, except for the presence of a large peak eluting at 30% acetonitrile (Figure 2.15C). The absorption spectrum of this peptide is characteristic of $Ru(phen)_2(CN)(im)^+$; the sizable absorbance value at 280 nm (relative to the other fragments in the chromatogram) originates from the tail of the phen (π to π^*) transition occurring at 266 nm ($\varepsilon_{280} \sim 24{,}000$ $M^{-1}\ s^{-1}$; see Figure 2.1). The purity of this material was verified by capillary-zone-electrophoresis (Caltech core facility), and the peptide was subjected to N-terminal sequencing. The resulting sequence, Thr_{28}-Gly-Pro-Asn-Leu-___-Gly-Leu_{35}- [Gly34 and Leu35 appear in extremely small amounts], matches that of the N-terminal portion of T7, the fragment containing His33. This strongly suggests that the ruthenium complex is bound to His33 since no other good ligands for ruthenium are present in this fragment, and the spectral properties of the label on the protein match those for an imidazole-bound ruthenium complex. As has been observed previously, no signal shows up in the

sequencing cycle in which His33 is expected; either the presence of ruthenium complex inhibits the cleavage reaction that occurs during the sequencing protocol, or the fragment elutes "off-scale". The fact that severely diminished signals are seen for Gly34 and Leu35, the residues just after His33 in the sequence, indicates the former explanation. This observation is thus taken as further evidence that the ruthenium complex is bound at His33.

Spectroscopic Characterization of Ru(phen)$_2$(CN)(His33)cytochrome *c*

The absorption spectrum of Ru(phen)$_2$(CN)(His33)cyt *c* can be duplicated almost exactly by a sum of the spectra of Ru(phen)$_2$(CN)(im)$^+$ and unmodified cyt *c* (Figure 2.16). The excellent match indicates that the addition of the metal complex to the protein does not significantly perturb the protein structure. Since only approximate extinction coefficients were determined for the model complex, whereas accurate extinction coefficients for cyt *c* are known from the literature,[32] the spectrum of Ru(phen)$_2$(CN)(im)$^+$ in Figure 2.16 was multiplied by a scaling factor to achieve the best superposition with Ru(phen)$_2$(CN)(His33)cyt *c*. These "scaled" extinction coefficients for the Ru(phen)$_2$(CN)(im)$^+$ are the values used for determining the concentration of model compound, and are those plotted in Figure 2.1.

The far-UV circular dichroism (CD) spectrum of Ru(phen)$_2$(CN)(His33)cyt *c* matches closely that for unmodified cyt *c* (Figure 2.17), providing further evidence that the addition of the metal does not perturb the structure of the protein. Interestingly, the Ru-cyt *c* spectrum exhibits an additional pair of features, a negative peak at 260 nm and a positive band at 269 nm, corresponding to the phenanthroline π to π^* transition in the ruthenium complex. This demonstrates that the modification site prefers a particular enantiomer of the label (Λ or Δ). The same enantiomer also is favored in the reaction of cyt *c* with Ru(bpy)$_2$CO$_3$, in which the major product at His33 was tentatively assigned to be the Λ isomer.[30]

Direct Photoinduced Reduction

Intramolecular $*Ru^{2+} \rightarrow Fe^{3+}$ ET ($*k_{ET}$) and $Fe^{2+} \rightarrow Ru^{3+}$ ET ($^{O}k_{ET}$) were determined using a scheme involving excitation of oxidized Ru(phen)$_2$(CN)(His33)cyt *c* (Ru^{2+}-Fe^{3+}) (Figure 2.18, *top*). The ruthenium excited state can decay via three competing first order processes: ET ($*k_{ET}$), energy transfer ($k_{en.t.}$), and intrinsic decay back to ground state (k_d). The observed rate constant for decay, which dictates the observed rate constant for formation of ET products (Ru^{3+}-Fe^{2+}), is the sum of the rate constants for these processes:

$$k_{obs} = *k_{ET} + k_{en.t.} + k_d \tag{2.4}$$

Comparison of the observed luminescence decay rate constant of $*Ru^{2+}$-Fe^{3+} (k_{obs} = 3.7 x 10^6 s^{-1}) to that of $*Ru^{2+}$-Fe^{2+} (k_{obs} = 2.5 x 10^6 s^{-1}) cyt *c* indicates significant quenching of $*Ru^{2+}$ by Fe^{3+} ($k_q = *k_{ET} + k_{en.t.}$ = 1.2 x 10^6 s^{-1}). Transient absorption measurements demonstrate that at least part of the quenching is due to ET; kinetics are biphasic at 377 nm (an isosbestic point for the ruthenium complex) corresponding to formation (k_{obs} = 3.7 x 10^6 s^{-1}) and disappearance ($^{O}k_{ET}$ = 1.0 x 10^7 s^{-1}) of ET products (Fe^{2+}) (Figure 2.18, *bottom*). Determination of the yield of ET (Φ_{ET}), which is needed to evaluate the value of $*k_{ET}$ (see Equation 2.6), requires calculation of the concentration of ET products and excited states generated per laser flash:

$$\Phi_{ET} = \frac{[\text{products}]}{[\text{reactants}]} = \frac{[Fe^{2+}]}{[*Ru^{2+}]} \tag{2.5}$$

Using the ΔAbs amplitudes from fits of kinetic traces at 377 nm (Ru^{3+}-Fe^{2+}) and 339 nm ($*Ru^{2+}$) (Figure 2.19), and the corresponding Δε values (–16800 M^{-1} cm^{-1} and 7300 M^{-1} cm^{-1} respectively), the yield for ET is found to be ~0.084 [0.89 μM Ru^{3+}-Fe^{2+}, 11 μM $*Ru^{2+}$]. This yield represents about a sixfold improvement over the yield of photoreduction achieved using a $Ru(bpy)_2(im)$- label at His33,[1] which makes this system more suitable for applications such as protein-protein ET (see below).

From the following relation:

$$\Phi_{ET} = \frac{{}^*k_{ET}}{{}^*k_{ET} + k_{en.t.} + k_d} = \frac{{}^*k_{ET}}{k_{obs}} \quad \Rightarrow \quad {}^*k_{ET} = \Phi_{ET} k_{obs} \tag{2.6}$$

${}^*k_{ET}$ = (0.084)(3.7 x 10^6 s^{-1}) = 3.1 x 10^5 s^{-1}, and hence $k_{en.t.}$ = 8.7 x 10^5 s^{-1}. Thus, ~75% of the quenching of $*Ru^{2+}$ is attributed to energy transfer and ~25% is due to electron transfer.

Oxidative Flash-Quench Experiments

$Fe^{2+} \rightarrow Ru^{3+}$ ET (${}^Ok_{ET}$) was also measured using an oxidative flash-quench method described previously (Figure 2.20; Q_1 = $Ru(NH_3)_6^{3+}$).[1] Excitation of reduced $Ru(phen)_2(CN)$(His33)cyt *c* (Ru^{2+}-Fe^{2+}) leads to biphasic kinetics. The first phase corresponds to bimolecular oxidative quenching of $*Ru^{2+}$ by $Ru(NH_3)_6^{3+}$ to form the transiently stable Ru^{3+}-Fe^{2+} form; Ru^{3+}-Fe^{2+} then undergoes intramolecular electron transfer ($Fe^{2+} \rightarrow Ru^{3+}$) to form Ru^{2+}-Fe^{3+} in a second phase. On longer timescales (>1 ms) photoproduced $Ru(NH_3)_6^{2+}$ rereduces the heme to return the system to its original state (Ru^{2+}-Fe^{2+}; $Ru(NH_3)_6^{3+}$). Kinetics monitored at 378 nm are shown in Figure 2.21; the initial phase exhibits a small decrease in ΔAbs due to the formation of Ru^{3+}, and the second phase displays a sizable increase due to the formation of Fe^{3+} (the loss of Ru^{3+} contributes to the increase as well). As demonstrated in the direct-photoinduced-reduction scheme noted above, ${}^Ok_{ET}$ in $Ru(phen)_2(CN)$(His33)cyt *c* is considerably

greater than the (unquenched) excited-state decay rate (1.0×10^7 s^{-1} vs. 2.5×10^6 s^{-1}). This leads to an interesting dependence of the kinetics on quencher concentration: at low quencher concentrations ($[Q_1]$ d 7 mM), the observed rate of formation of Fe^{2+} is limited by the rate of excited-state decay since $(k_q[Q]_1 + k_d) < {}^{O}k_{ET}$; at high concentrations of quencher ([Q] t 7 mM), the rate of formation is simply ${}^{O}k_{ET}$ (Figure 2.21; for $[Q_1] = 1$ mM, $k_{obs} = 3.2 \times 10^6$ s^{-1}, ${}^{O}k_{ET} = 9 \times 10^6$ s^{-1}; for $[Q_1] = 12$ mM, $k_{obs} = 1.4 \times 10^7$ s^{-1}; ${}^{O}k_{ET} = 9.9 \times 10^6$ s^{-1}). The value obtained from the trace with 1 mM Q_1 is much more approximate than the one determined from the $[Q_1] = 12$ mM experiment due to the small size of the signal for that phase. Note that the value for ${}^{O}k_{ET}$ obtained using the flash-quench method agrees with the value obtained in the direct-photoinduced-reduction experiment.

Reductive Flash-Quench Experiments

$Ru^+ \rightarrow Fe^{3+}$ ET (${}^{R}k_{ET}$) was measured using a reductive flash-quench procedure (Figure 2.22), in which MeODMA was the quencher, Q_2.[8] Excitation of Ru^{2+}-Fe^{3+} results in biphasic kinetics. The first phase represents loss of $*Ru^{2+}$-Fe^{3+}, accelerated by bimolecular reductive quenching by MeODMA ($k_q \sim 6 \times 10^8$ M^{-1} s^{-1}). The transient absorption spectrum immediately after the fast kinetic phase accords with the difference spectrum (Fe^{2+} – Fe^{3+})cyt *c*, indicating some direct intramolecular ET quenching of $*Ru^{2+}$ by Fe^{3+} followed by reductive *scavenging* by MeODMA (Figure 2.25; S = MeODMA). A second kinetic phase corresponds to intramolecular reduction of the ferriheme by Ru^+. Identical kinetics were observed at wavelengths corresponding (primarily) to the oxidation state of the heme (385, 420, 550 nm; see Figure 2.4B) and the Ru complex (339, 504 nm; see Figure 2.10) (Figure 2.23; ${}^{R}k_{ET} = 4.5 \times 10^5$ s^{-1}). The transient absorption spectrum just after the second phase accords closely with the sum of the spectra of (Fe^{2+} – Fe^{3+})cyt *c*[32] and $MeODMA^{\bullet+}$ (Figure 2.24).[23] On a millisecond timescale, $MeODMA^{\bullet+}$ reoxidizes the heme. After many shots, reduced protein is

observed in the steady-state absorption spectrum indicating some irreversibility. This is most likely due to dimerization of some of the $MeODMA^{\bullet+}$ radicals.[23]

Flash-Scavenge Scheme; Application to Protein-Protein ET

As noted above, the yield of photoreduction using $Ru(phen)_2(CN)(His)$- at position 33 in cyt *c* is about six times greater than the corresponding yield using a $Ru(bpy)_2(im)(His)$- label. This yield enhancement extends the applicability of the Ru(His33)cyt *c* system; certain experiments which were not practical previously can now be performed. One such example involves using Ru(His33)cyt *c* to inject electrons into physiological redox partners such as cytochrome *c* oxidase (CcO). The $Ru(phen)_2(CN)(His33)$- system has several properties that make it well suited for this purpose, especially compared with a similar system that has been reported in which lysines are modified with ruthenium labels.[33,34] His33 lies on the backside of cytochrome *c* (i.e., on the side facing away from docked physiological partners)[35] and the label is therefore not likely to interfere with the protein-protein binding interface, in contrast to many of the Ru-Lys modified cytochromes *c*.[36] In addition, the $Ru(phen)_2(CN)(His)$ label is held more closely to the cyt *c* surface than the Lys-modified labels,[37] further decreasing the likelihood that the native protein-protein binding interaction will be disrupted. Lastly, the net charge on the $Ru(phen)_2(CN)(His)$ label is +1, compared to +2 for $Ru(bpy)_2(im)(His)$ and for one type of Lys-modified label (the other has a charge of +1). This is important since the physiological redox partners of cyt *c* are typically negatively charged, and many of the ET experiments are performed at very low ionic strength. Under these conditions, direct interaction of the Ru moiety with the redox partner is a distinct possibility;[38] a decreased charge on the ruthenium complex as in $Ru(phen)_2(CN)(His)$ decreases the likelihood of this type of interaction. We note that the recent development of a new class of ruthenium labels in which modified cysteines

are labeled rather than lysine alleviates many of the problems associated with the Ru-Lys technology.[39]

Excitation of $Ru(phen)_2(CN)$(His33)cyt *c* in the presence of NADH as a reductive scavenger leads to rapid irreversible reduction of cytochrome *c* (Figure 2.25, *top*). NADH bimolecularly reduces the transiently produced Ru^{3+}-Fe^{2+}, thereby inhibiting the back reaction ($^{O}k_{ET}$). Kinetics monitored at 550 nm show a rapid increase due to cyt *c* reduction, but then no further change out to >50 ms (Figure 2.25, *bottom*); the oxidized NADH radical apparently undergoes decomposition before reoxidation of the ferroheme occurs. When the same experiment is carried out in the presence of bovine CcO (0.1 M HEPES, 0.1% Brij detergent), transient absorption kinetic signals consistent with intermolecular ET between cyt *c* and CcO are observed: specifically, after initial rapid reduction of cyt *c*, a decrease is seen at 550 nm, corresponding to cyt *c* oxidation, and an increase in signal is seen at 605 nm, corresponding to reduction of the cytochrome *a* center in CcO (Figure 2.26).[40] The signal sizes and rate constant of the major phase (k_{obs} ~ 2 x 10^3 s^{-1}) are comparable to those observed under similar conditions (~physiological ionic strength) using other photoreductants,[41,42] indicating that the system is well behaved.

REFERENCES AND NOTES

(1) Chang, I.-J.; Gray, H. B.; Winkler, J. R. *J. Am. Chem. Soc.* **1991**, *113*, 7056-7057.

(2) Wuttke, D. S.; Bjerrum, M. J.; Winkler, J. R.; Gray, H. B. *Science* **1992**, *256*, 1007-1009.

(3) Casimiro, D. R.; Richards, J. H.; Winkler, J. R.; Gray, H. B. *J. Phys. Chem.* **1993**, *97*, 13073-13077.

(4) Bjerrum, M. J.; Casimiro, D. R.; Chang, I.-J.; Di Bilio, A. J.; Gray, H. B.; Hill, M. G.; Langen, R.; Mines, G. A.; Skov, L. K.; Winkler, J. R.; Wuttke, D. S. *J. Bioenerg. and Biomembr.* **1995**, *27*, 295-302.

(5) Langen, R.; Chang, I.-J.; Germanas, J. P.; Richards, J. H.; Winkler, J. R.; Gray, H. B. *Science* **1995**, *268*, 1733-1735.

(6) Durham, B. D.; Pan, L. P.; Hahm, S.; Long, J.; Millett, F. In *ACS Advances in Chemistry Series*; M. K. Johnson, R. B. King, D. M. Kurtz, C. Kutal, M. L. Norton and R. A. Scott, Eds.; American Chemical Society: Washington, DC, 1990; Vol. 226; pp 180-193.

(7) Lin, C.-T.; Böttcher, W.; Chou, M.; Creutz, C.; Sutin, N. *J. Am. Chem. Soc.* **1976**, *98*, 6536-6544.

(8) Kalyanasundaram, K. In *Photosensitization and Photocatalysis Using Inorganic and Organometallic Compounds*; K. Kalyanasundaram and M. Grätzel, Eds.; Kluwer Academic Publishers: Dordrecht, 1993; pp 113-160.

(9) Juris, A.; Balzani, V.; Barigelletti, F.; Campagna, S.; Belser, P.; Von Zelewsky, A. *Coord. Chem. Rev.* **1988**, *84*, 85-277.

(10) Demas, J. N.; Addington, J. W. *J. Am. Chem. Soc.* **1976**, *98*, 5800-5806.

(11) Demas, J. N.; Addington, J. W.; Peterson, S. H.; Harris, E. W. *J. Phys. Chem.* **1977**, *81*, 1039-1043.

(12) Hartzell, C. R.; Beinert, H. *Biochim. Biophys. Acta* **1974**, *368*, 318-338.

(13) Sekiya, M.; Tomie, M.; Leonard, N. J. *J. Org. Chem.* **1968**, *33*, 318-322.

(14) Sullivan, B. P.; Salmon, D. J.; Meyer, T. J. *Inorg. Chem.* **1978**, *17*, 3334-3341.

(15) Long, C.; Vos, J. G. *Inorg. Chim. Acta* **1984**, *89*, 125-131.

(16) Johnson, E. C.; Sullivan, B. P.; Adeyemi, S. A.; Meyer, T. J. *Inorg. Chem.* **1978**, *17*, 2211-2215.

(17) McCleskey, T. M. Thesis, California Institute of Technology, 1994.

(18) Woody, R. W. In *The Peptides*; E. R. Blout, F. A. Bovey, M. Goodman and N. Lotan, Eds.; Academic Press, Inc.: New York, 1985; Vol. 7; pp 15-114.

(19) Kalyanasundaram, K. *Coord. Chem. Rev.* **1982**, *46*, 159-244.

(20) Fickling, M. M.; Fischer, A.; Mann, B. R.; Packer, J.; Vaughan, J. *J. Am. Chem. Soc.* **1959**, *81*, 4225.

(21) Lachish, U.; Infelta, P. P.; Grätzel, M. *Chem. Phys. Lett.* **1979**, *62*, 317-319.

(22) Lippard, S. J.; Berg, J. M. *Principles of Bioinorganic Chemistry*; University Science Books: Mill Valley, 1994, pp 411.

(23) Sassoon, R. E.; Gershuni, S.; Rabani, J. *J. Phys. Chem.* **1992**, *96*, 4692-4698.

(24) Hoffman, M. Z.; Bolletta, F.; Moggi, L.; Hug, G. L. *J. Phys. Chem. Ref.* **1989**, *18*, 219-544.

(25) Creutz, C.; Sutin, N. *Inorg. Chem.* **1976**, *15*, 496-499.

(26) Creutz, C.; Sutin, N. *J. Am. Chem. Soc.* **1976**, *98*, 6384-6385.

(27) Miedlar, K.; Das, P. K. *J. Am. Chem. Soc.* **1982**, *104*, 7462-7469.

(28) Mallouk, T. E.; Krueger, J. S.; Mayer, J. E.; Dymond, C. M. G. *Inorg. Chem.* **1988**, *28*, 3507-3510.

(29) Bock, C. R.; Connor, J. A.; Gutierrez, A. R.; Meyer, T. J.; Whitten, D. G.; Sullivan, B. P.; Nagle, J. K. *J. Am. Chem. Soc.* **1979**, *101*, 4815-4824.

(30) Wuttke, D. S. Ph.D. Thesis, California Institute of Technology, 1994.

(31) Bignozzi, C. A.; Roffia, S.; Chiorboli, C.; Davila, J.; Indelli, M. T.; Scandola, F. *Inorg. Chem.* **1989**, *28*, 4350-4358.

(32) Margoliash, E.; Frohwirt, N. *Biochem. J.* **1959**, *71*, 570-572.

(33) Pan, L. P.; Durham, B.; Wolinska, J.; Millett, F. *Biochemistry* **1988**, *27*, 7180-7184.

(34) Millett, F.; Durham, B. In *Metal Ions in Biological Systems*; H. Sigel and A. Sigel, Eds.; Marcel Dekker, Inc.: New York, 1991; Vol. 27; pp 223-264.

(35) Moore, G. R.; Pettigrew, G. W. *Cytochromes c: Biological Aspects*; Springer-Verlag: New York, 1987, pp 282.

(36) Pan, L. P.; Hibdon, S.; Liu, R. Q.; Durham, B.; Millett, F. *Biochemistry* **1993**, *32*, 8492-8498.

(37) Durham, B.; Pan, L. P.; Long, J.; Millett, F. *Biochemistry* **1989**, *28*, 8659-8665.

(38) Liu, R. Q.; Hahm, S.; Miller, M.; Durham, B.; Millett, F. *Biochemistry* **1995**, *34*, 973-983.

(39) Geren, L. M.; Beasley, J. R.; Fine, B. R.; Saunders, A. J.; Hibdon, S.; Pielak, G. J.; Durham, B.; Millett, F. *J. Biol. Chem.* **1995**, *270*, 2466-2472.

(40) Blair, D. F.; Ellis, W. R., Jr.; Wang, H.; Gray, H. B.; Chan, S. I. *J. Biol. Chem.* **1986**, *261*, 11524-11537.

(41) Larsen, R. W.; Winkler, J. R.; Chan, S. I. *J. Phys. Chem.* **1992**, *96*, 8023-8027.

(42) Pan, L.-P.; Hazzard, J. T.; Lin, J.; Tollin, G.; Chan, S. I. *J. Am. Chem. Soc.* **1991**, *113*, 5908-5910.

Figure 2.1. Absorption spectrum of $Ru(phen)_2(CN)(im)^+$ (μ = 0.1 sodium phosphate, pH 7.0).

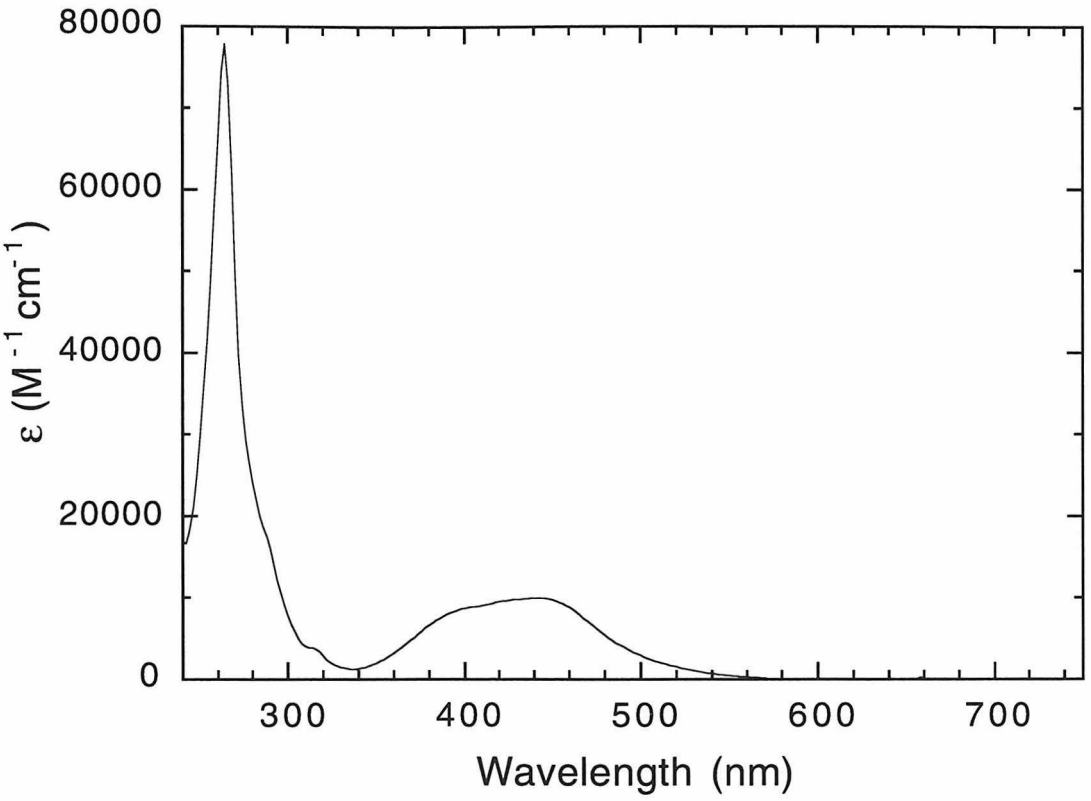
80000
60000
40000
20000
0
ε (M -1 cm-1)
300
400
500
600
700
Wavelength (nm)

Figure 2.2. ^{1}H NMR spectrum of $Ru(phen)_2(CN)(im)^+$ in D_2O.

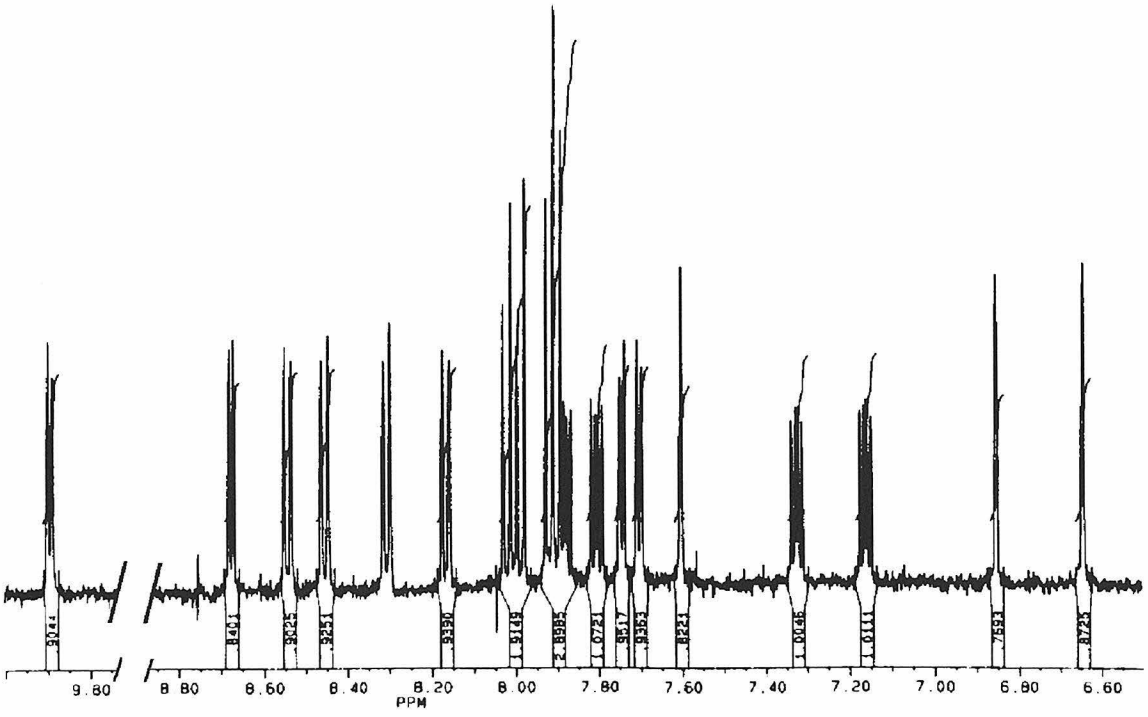
9.80
8.80
8.60
8.40
8.20
8.00
7.80
7.60
7.40
7.20
7.00
6.80
6.60
PPM

Figure 2.3. Time-resolved luminescence decay profile of *[$Ru(phen)_2(CN)(im)^+$]. λ_{ex} = 480 nm, 20 ns, 1-2 mJ/pulse; λ_{obs} = 645 nm; [Ru] = 15 μM; μ = 0.1 sodium phosphate, pH 7.0. The smooth line is a best fit to a single exponential function; the function, fitted parameters, and residual (ΔY is the difference between the data and the best fit line) are shown above the trace.

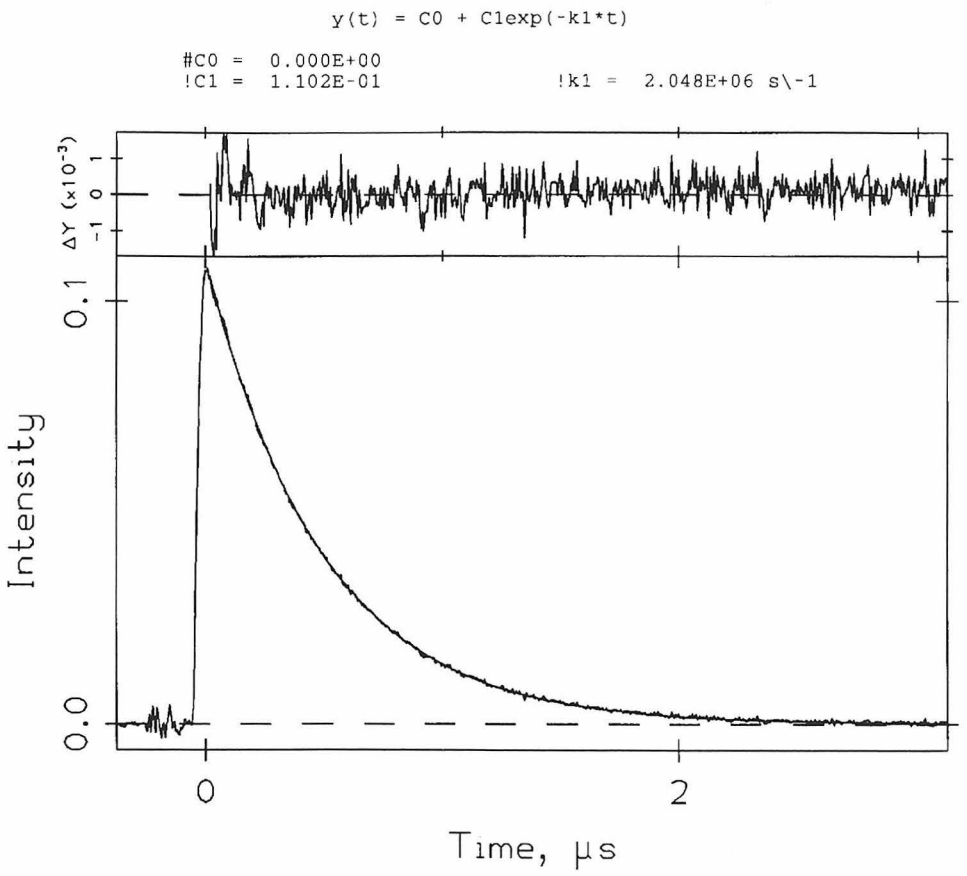
y(t) = C0 + C1exp(-k1*t)
#C0 = 0.000E+00
!C1 = 1.102E-01
!k1 = 2.048E+06 s\-1
ΔY (x10⁻³)
-1 0 1
0.1
0.0
Intensity
0
2
Time, μs

Figure 2.4. (A) Absorption spectra of oxidized (dashed line) and reduced (solid line) cyt *c* (μ = 0.1 sodium phosphate, pH 7.0). Spectra were scaled using ε_{410} = 106100 M^{-1} cm^{-1} (oxidized) and ε_{550} = 27700 M^{-1} cm^{-1} (Margoliash, E.; Frohwirt, N. *Biochem. J.* **1959**, *71*, 570-572). (B) The (Fe^{2+} – Fe^{3+})cyt *c* difference spectrum calculated from the spectra in (A).

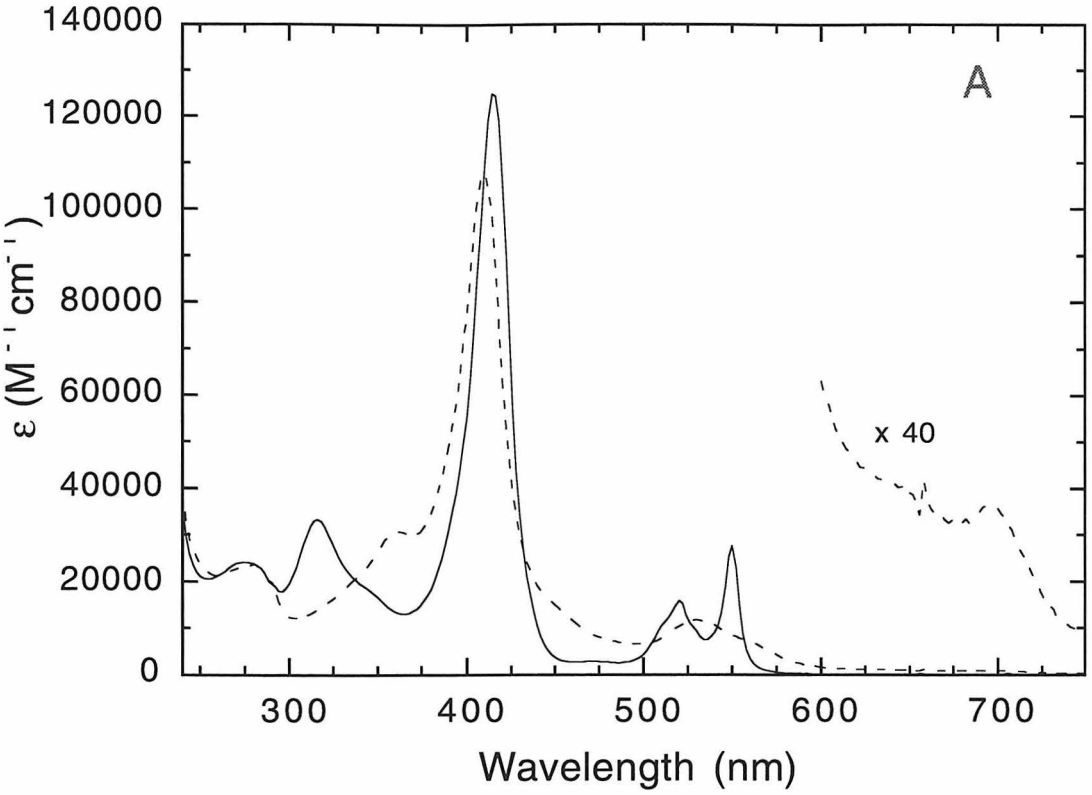
A
x 40
ε (M⁻¹cm⁻¹)
Wavelength (nm)
140000
120000
100000
80000
60000
40000
20000
0
300
400
500
600
700

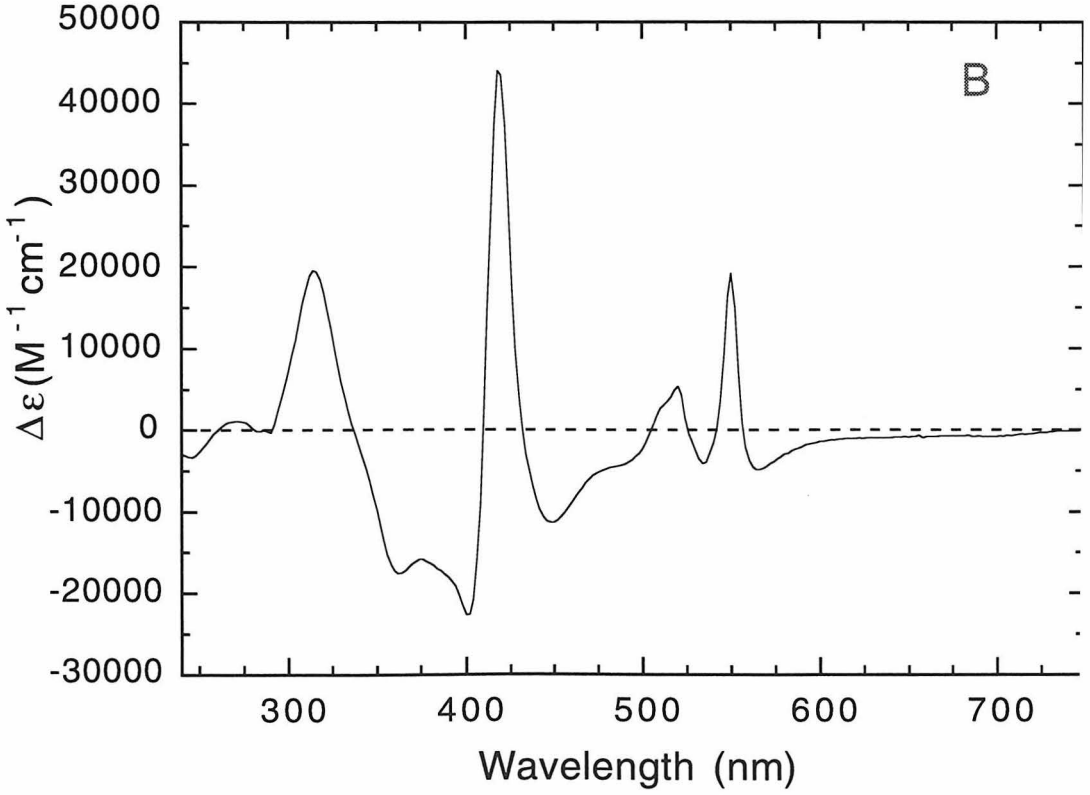
B
Δε(M⁻¹cm⁻¹)
Wavelength (nm)
50000
40000
30000
20000
10000
0
-10000
-20000
-30000
300
400
500
600
700

Figure 2.5. Kinetic determination of the ($Ru^{3+} - Ru^{2+}$) difference absorption spectrum of $Ru(phen)_2(CN)(im)$. Top: Oxidative quenching scheme. Q_1 is $Ru(NH_3)_6^{3+}$ and L represents a coordinated phenanthroline ligand. The metal-to-ligand charge-transfer character of the excited state is explicitly depicted. Bottom: Transient absorption kinetics monitored at 450 nm ([Ru] = 20 mM, [Q_1] = 12 mM; μ = 0.1 sodium phosphate, pH 7.0). The smooth line is the best fit to a single exponential function as in Figure 2.3.

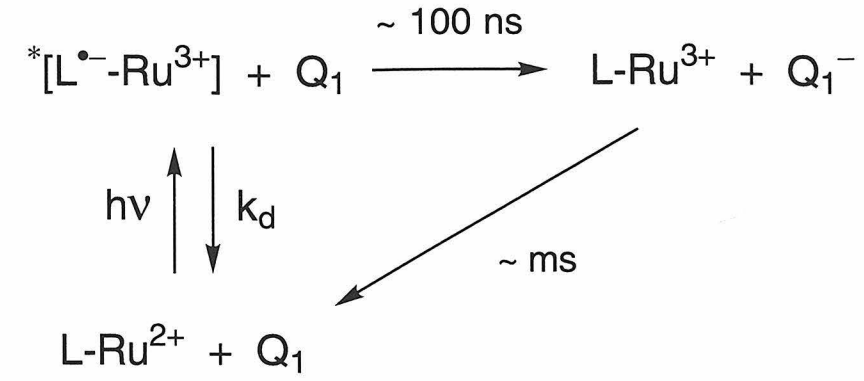
~ 100 ns
*[L•−-Ru3+] + Q1
L-Ru3+ + Q1−
hν
kd
~ ms
L-Ru2+ + Q1

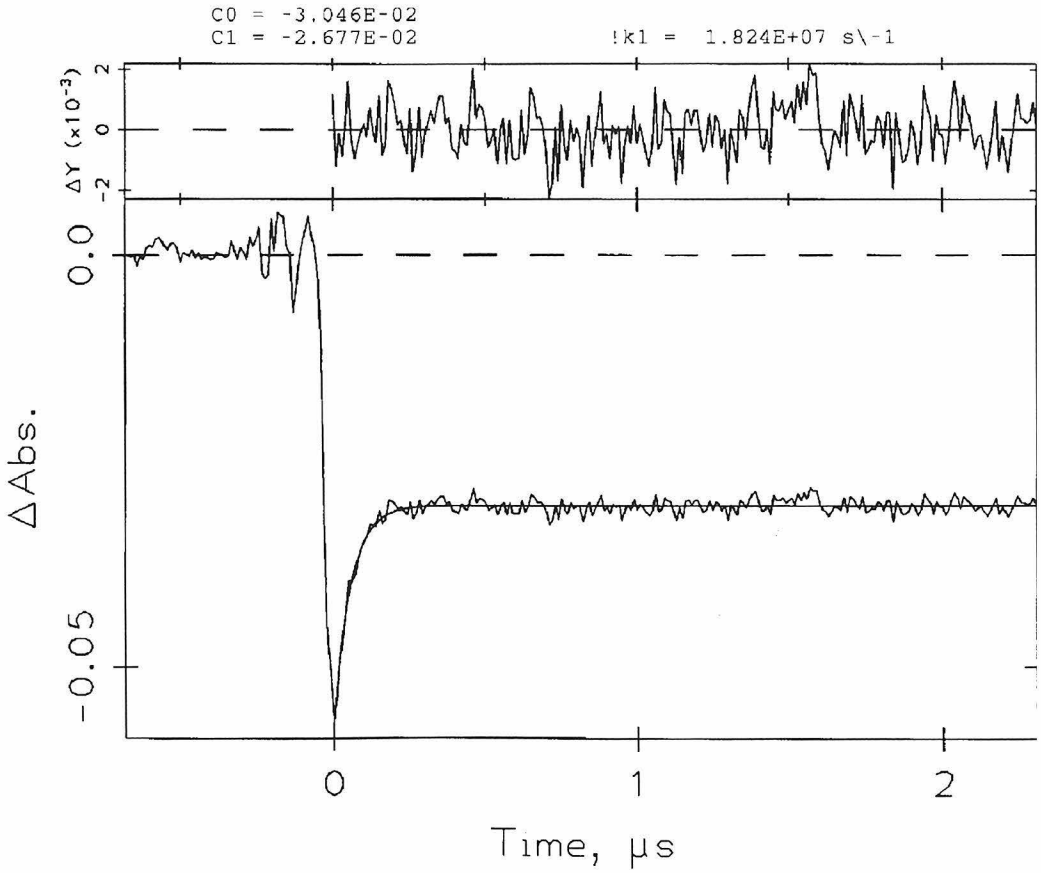
C0 = -3.046E-02
C1 = -2.677E-02
!k1 = 1.824E+07 s\-1
ΔY (x10-3)
2
0
-2
0.0
-0.05
ΔAbs.
0
1
2
Time, μs

Figure 2.6. ($Ru^{3+} - Ru^{2+}$) difference absorption spectrum of $Ru(phen)_2(CN)(im)$ determined from fits of transient absorption traces obtained as described in Figure 2.5.

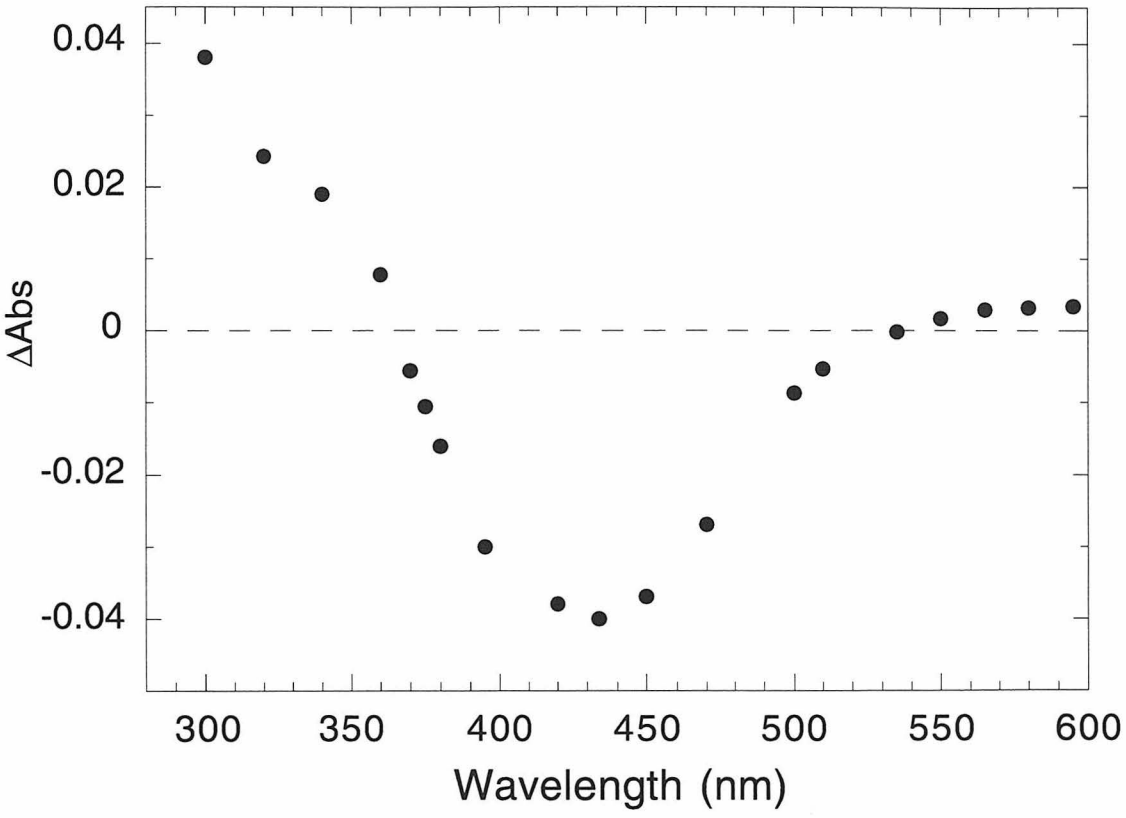
0.04
0.02
0
-0.02
-0.04
ΔAbs
300
350
400
450
500
550
600
Wavelength (nm)

Figure 2.7. Kinetic determination of the absorption spectrum of MeODMA$^{\bullet+}$. Top: Photochemical scheme. L-Ru represents $Ru(bpy)_3$ and Q_1 is $Ru(NH_3)_6^{3+}$. MeODMA$^{\bullet+}$ is bolded for emphasis. Bottom: Transient absorption kinetics monitored at 450 nm ($[Ru(bpy)_3^{2+}]$ = 18 μM; $[Q_1]$ = 5 mM; [MeODMA] ~ 200 μM; μ = 0.1 sodium phosphate, pH 7.0). The smooth line is a best fit to a biexponential function; the function, fitted parameters, and residual are shown.

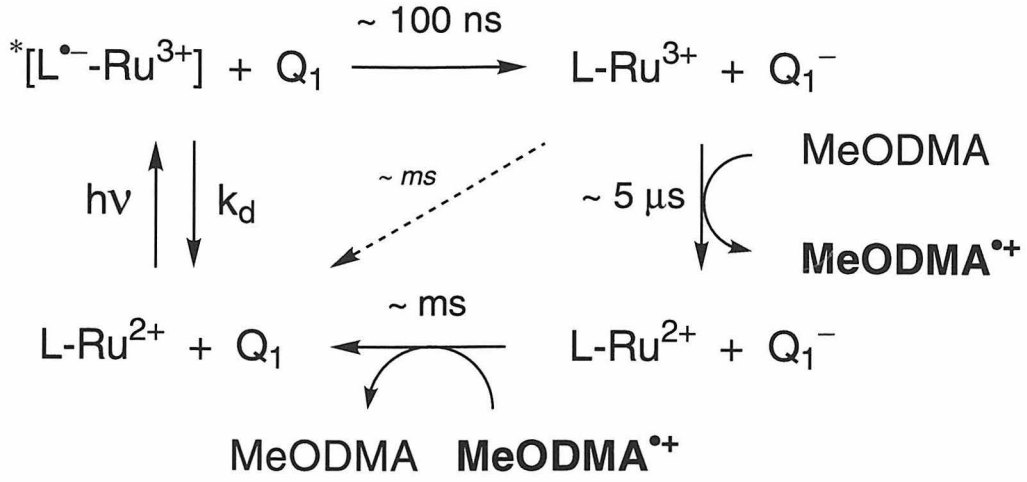
~ 100 ns
*[L•−-Ru3+] + Q1
L-Ru3+ + Q1−
hν
kd
~ ms
~ 5 µs
MeODMA
MeODMA•+
~ ms
L-Ru2+ + Q1
L-Ru2+ + Q1−
MeODMA
MeODMA•+

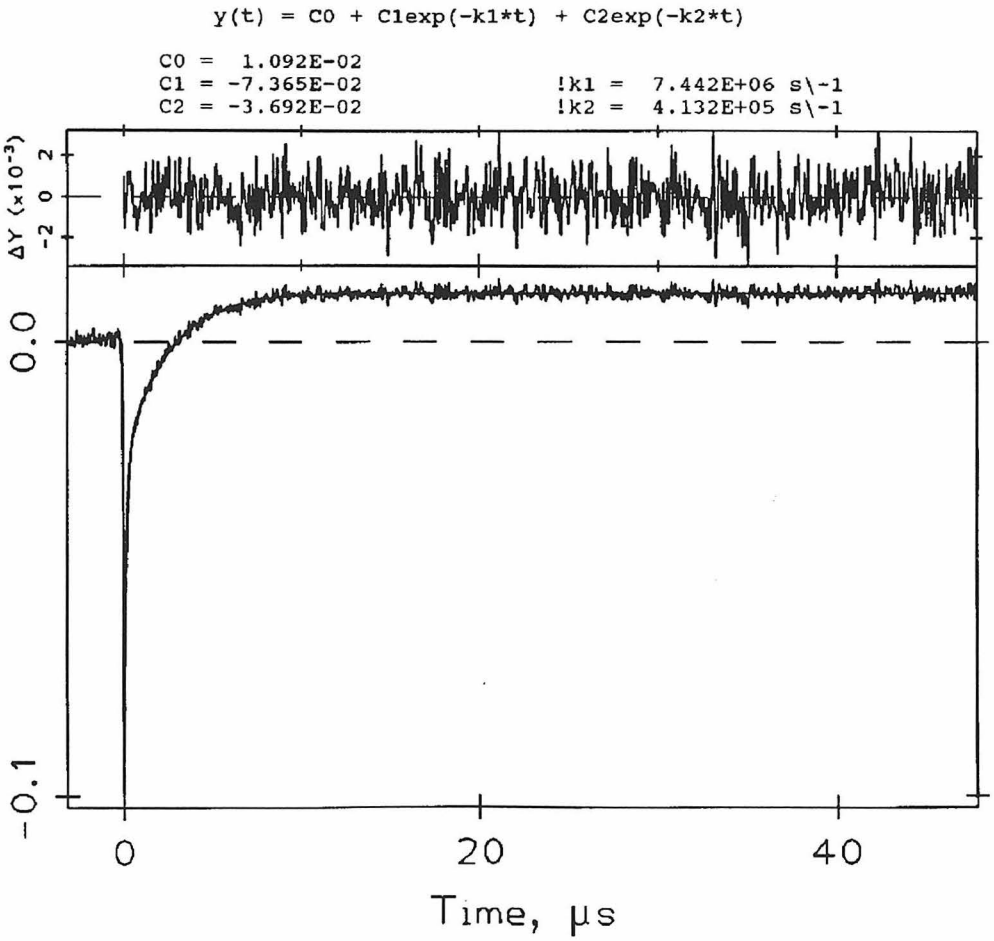
y(t) = C0 + C1exp(-k1*t) + C2exp(-k2*t)
C0 = 1.092E-02
C1 = -7.365E-02
C2 = -3.692E-02
!k1 = 7.442E+06 s\-1
!k2 = 4.132E+05 s\-1
ΔY (x10-3)
2
0
-2
0.0
-0.1
0
20
40
Time, µs

Figure 2.8. Absorption spectrum of MeODMA$^{\bullet+}$ determined from fits of transient absorption traces obtained as described in Figure 2.7. The spectrum was scaled using $\varepsilon_{484} = 7200\ M^{-1}\ cm^{-1}$ (Sassoon, R. E.; Gershuni, S.; Rabani, J. *J. Phys. Chem.* **1992**, *96*, 4692-4698).

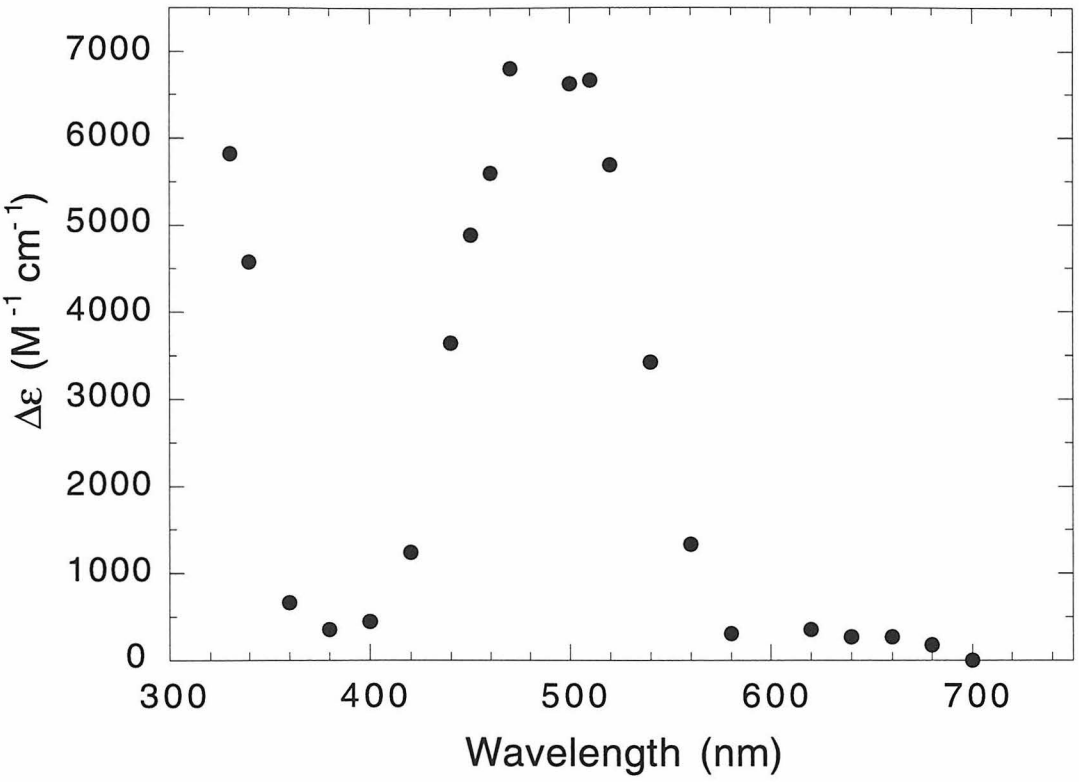
7000
6000
5000
4000
3000
2000
1000
0
Δε (M-1 cm-1)
300
400
500
600
700
Wavelength (nm)

Figure 2.9. Kinetic determination of the sum of the ($Ru^{+} - Ru^{2+}$) difference absorption spectrum of $Ru(phen)_2(CN)(im)^{+}$ and the absorption spectrum of $MeODMA^{\bullet+}$. Top: Reductive quenching scheme. Q_2 is MeODMA. L represents a phenanthroline ligand. Bottom: Transient absorption kinetics monitored at 339 nm ([Ru] = 35 μM; $[Q_2]$ = 5 mM; μ = 0.1 sodium phosphate, pH 7.0). Fitting is as described in Figure 2.3.

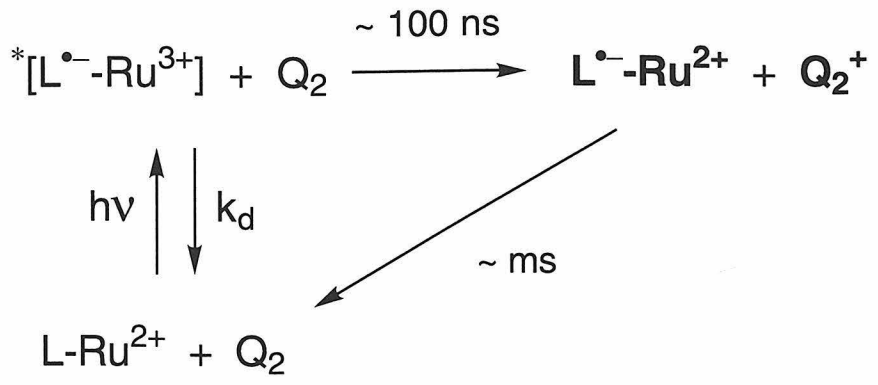
~ 100 ns
*[L•−-Ru3+] + Q2
L•−-Ru2+ + Q2+
hν
kd
~ ms
L-Ru2+ + Q2

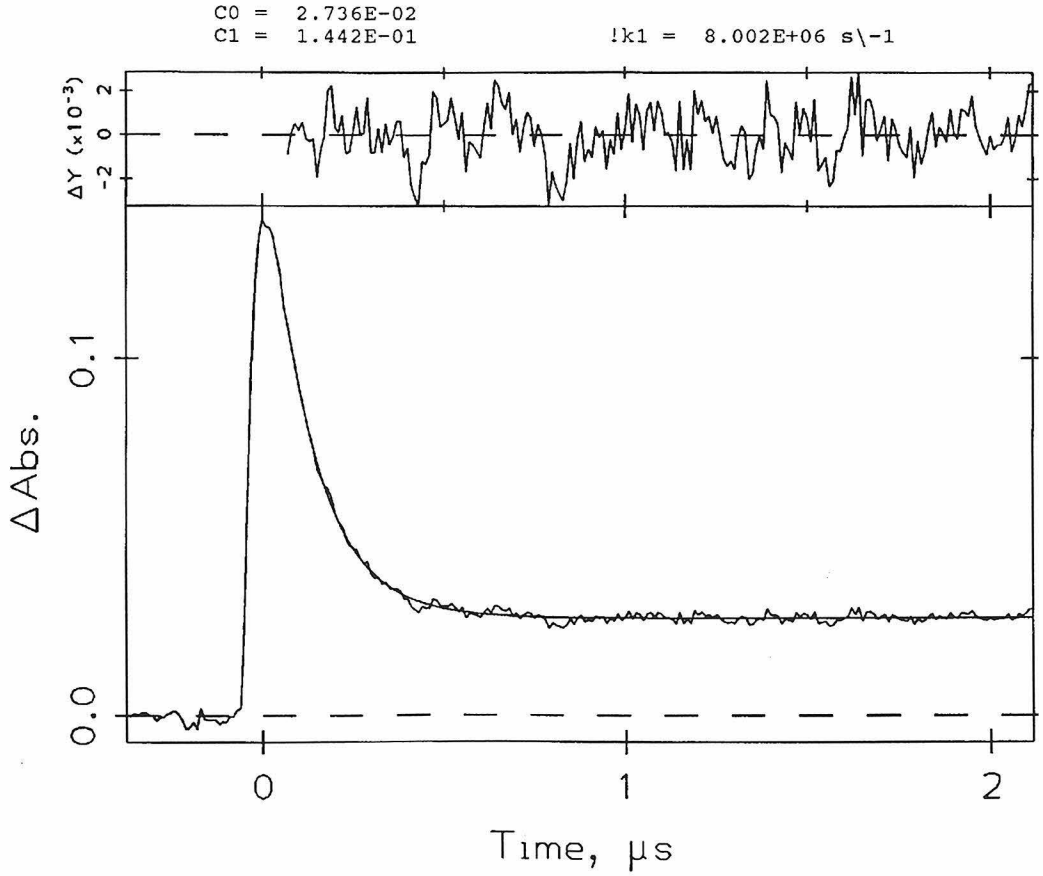
C0 = 2.736E-02
C1 = 1.442E-01
!k1 = 8.002E+06 s\-1
ΔY (x10-3)
2
0
-2
ΔAbs.
0.1
0.0
0
1
2
Time, μs

Figure 2.10. Sum of the absorption spectra of (Ru^{+} – Ru^{2+}) $Ru(phen)_2(CN)(im)$ and $MeODMA^{\bullet+}$, determined from fits of transient absorption traces obtained as described in Figure 2.9.

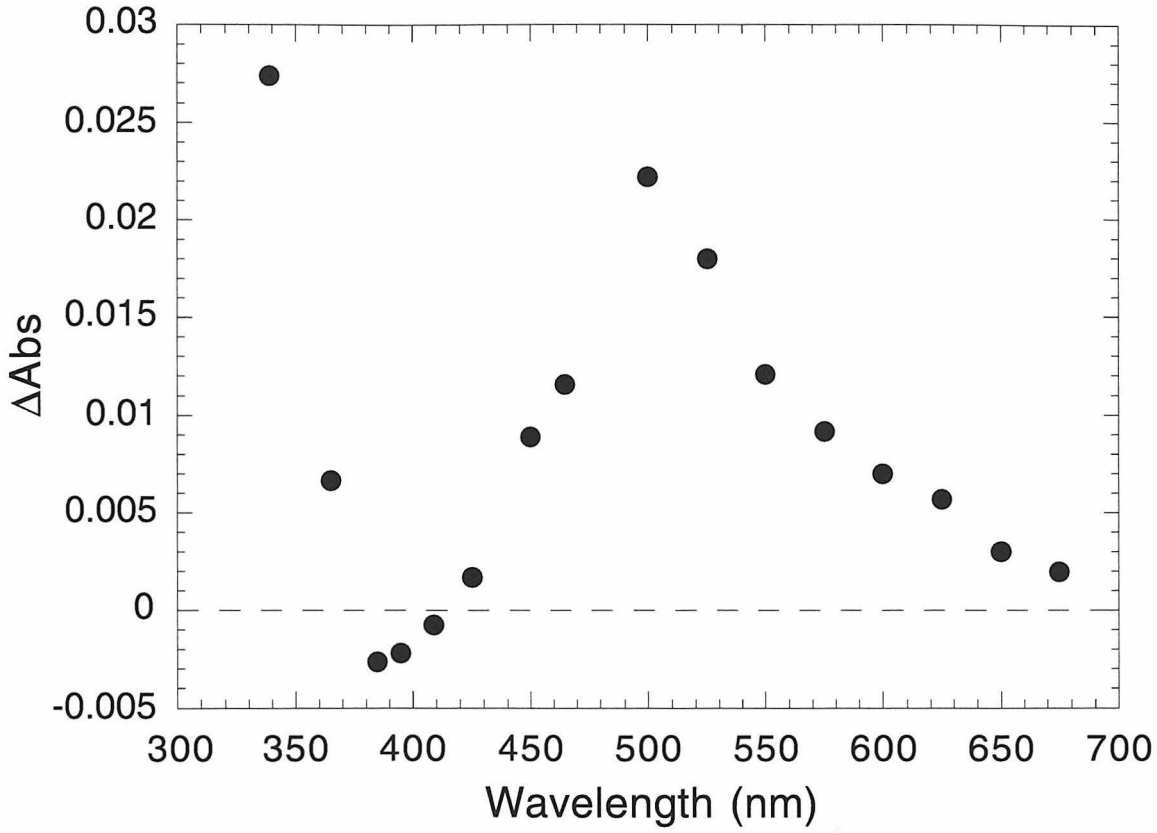
0.03
0.025
0.02
0.015
0.01
0.005
0
-0.005
ΔAbs
300
350
400
450
500
550
600
650
700
Wavelength (nm)

Figure 2.11. (A) ($*Ru^{2+} - Ru^{2+}$) difference absorption spectrum of $Ru(phen)_2(CN)(im)$, determined from fits of transient absorption traces obtained as described in Figure 2.9. (B) Power dependence of the ($*Ru^{2+} - Ru^{2+}$) ΔAbs signal at 339 nm following excitation of a solution of $Ru(phen)_2(CN)$(His33)cyt *c* ([Ru-cyt *c*] = C_o = 18 μM; μ = 0.1 sodium phosphate, pH 7.0). The curve is the best fit to Equation 2.3, and corresponds to $\Delta\varepsilon_{339}$ = 7300 M^{-1} cm^{-1} and b = 0.653. This Δε value was used to scale the spectrum in (A).

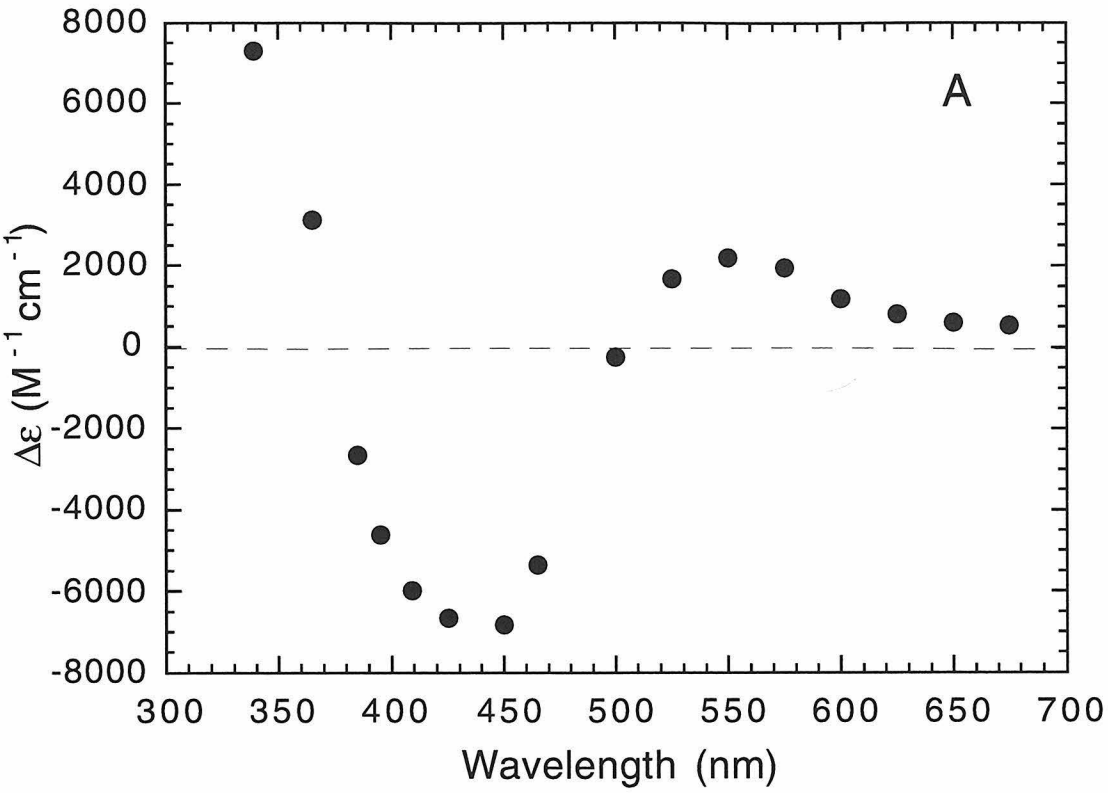
8000
6000
4000
2000
0
-2000
-4000
-6000
-8000
Δε (M -1 cm -1)
300
350
400
450
500
550
600
650
700
Wavelength (nm)
A

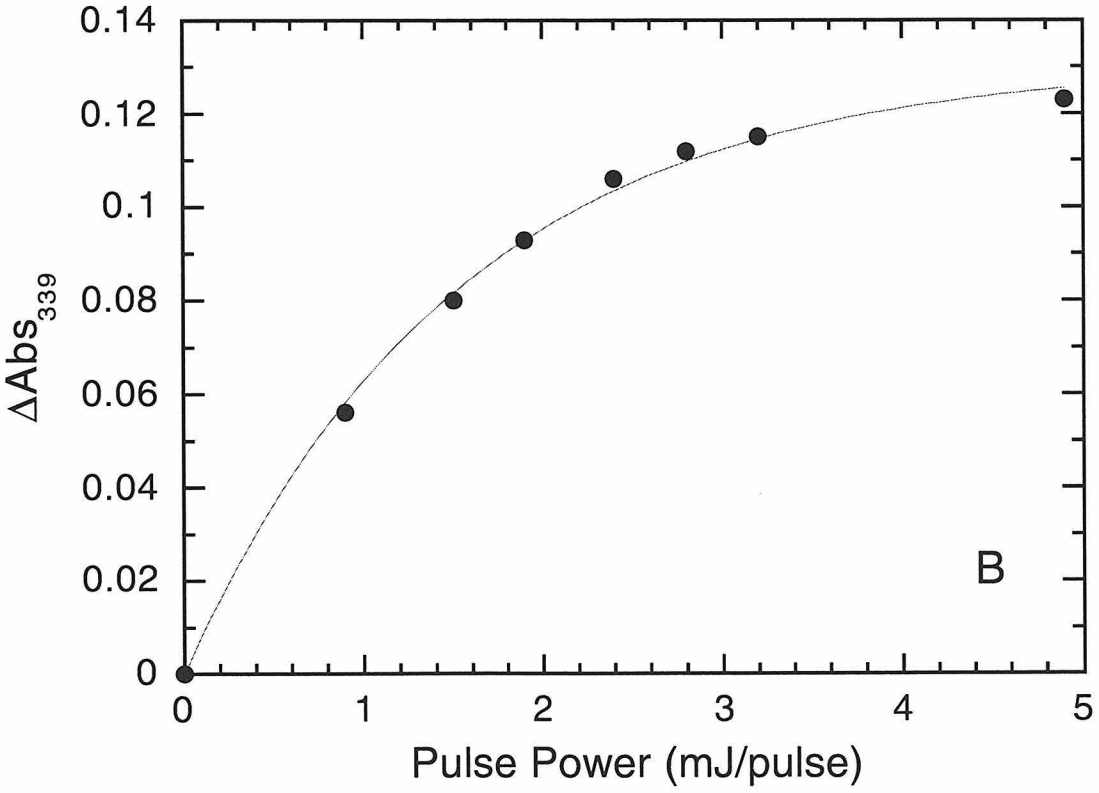
0.14
0.12
0.1
0.08
0.06
0.04
0.02
0
ΔAbs339
0
1
2
3
4
5
Pulse Power (mJ/pulse)
B

Figure 2.12. Procedure for preparing $Ru(phen)_2(CN)(His33)$cyt *c*.

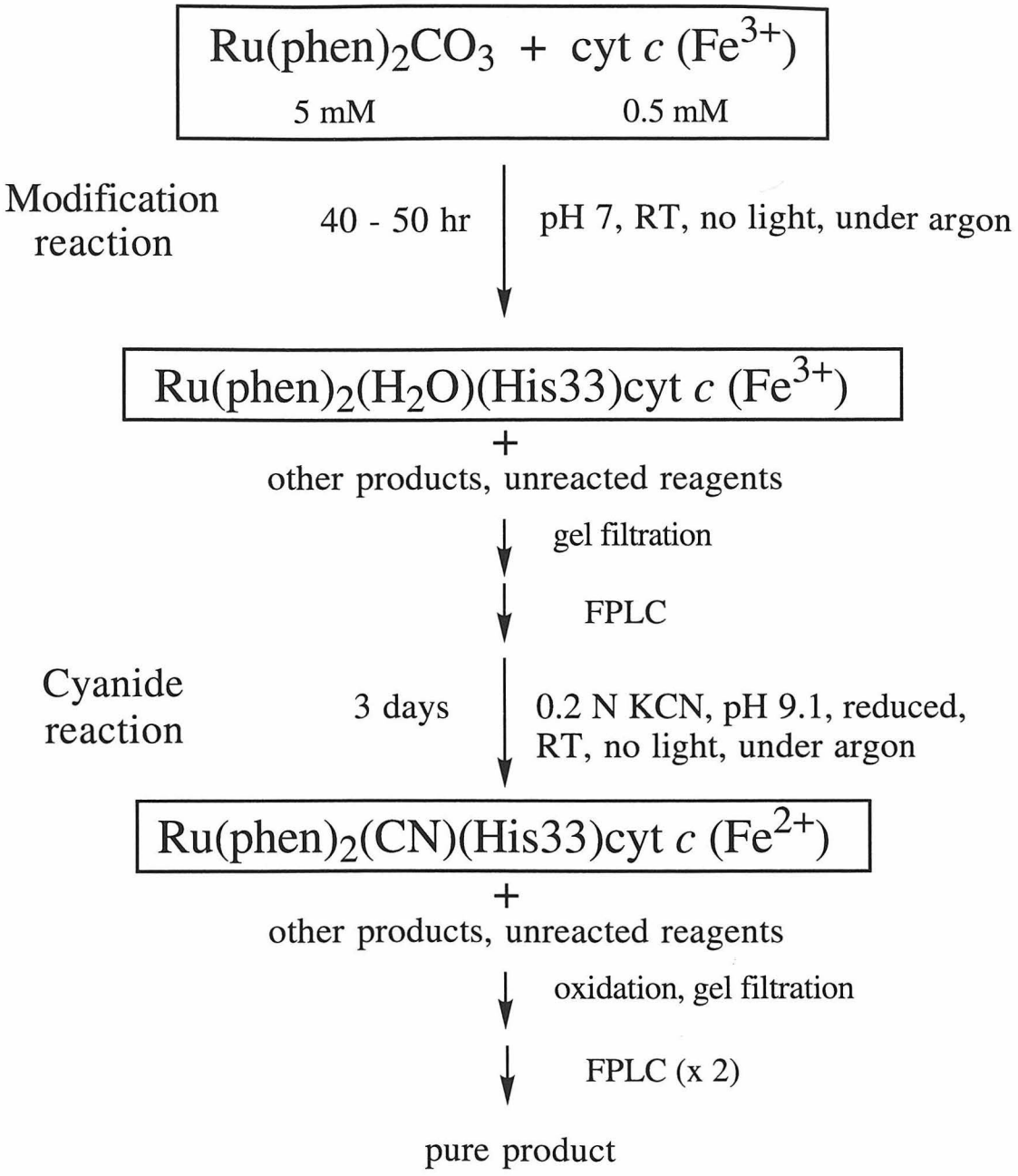
Ru(phen)2CO3 + cyt c (Fe3+)
5 mM
0.5 mM
Modification reaction
40 - 50 hr
pH 7, RT, no light, under argon
Ru(phen)2(H2O)(His33)cyt c (Fe3+)
+
other products, unreacted reagents
gel filtration
FPLC
Cyanide reaction
3 days
0.2 N KCN, pH 9.1, reduced, RT, no light, under argon
Ru(phen)2(CN)(His33)cyt c (Fe2+)
+
other products, unreacted reagents
oxidation, gel filtration
FPLC (x 2)
pure product

Figure 2.13. Cation-exchange FPLC chromatogram of the products of the $Ru(phen)_2CO_3$/cyt *c* reaction. 16/10 Mono S column; buffer A (loading) $\mu = 0.1$ sodium phosphate, pH 7.0; buffer B (limit) 0.25 M NaCl, ~25 mM sodium phosphate, pH 7.0. The final value for the gradient line is 100% buffer B. The first band off the column is unmodified cyt *c*, the second is comprised of cyt *c* modified by one ruthenium complex, and the third peak is made up of doubly modified cyt *c*. All cytochromes *c* are in the oxidized form.

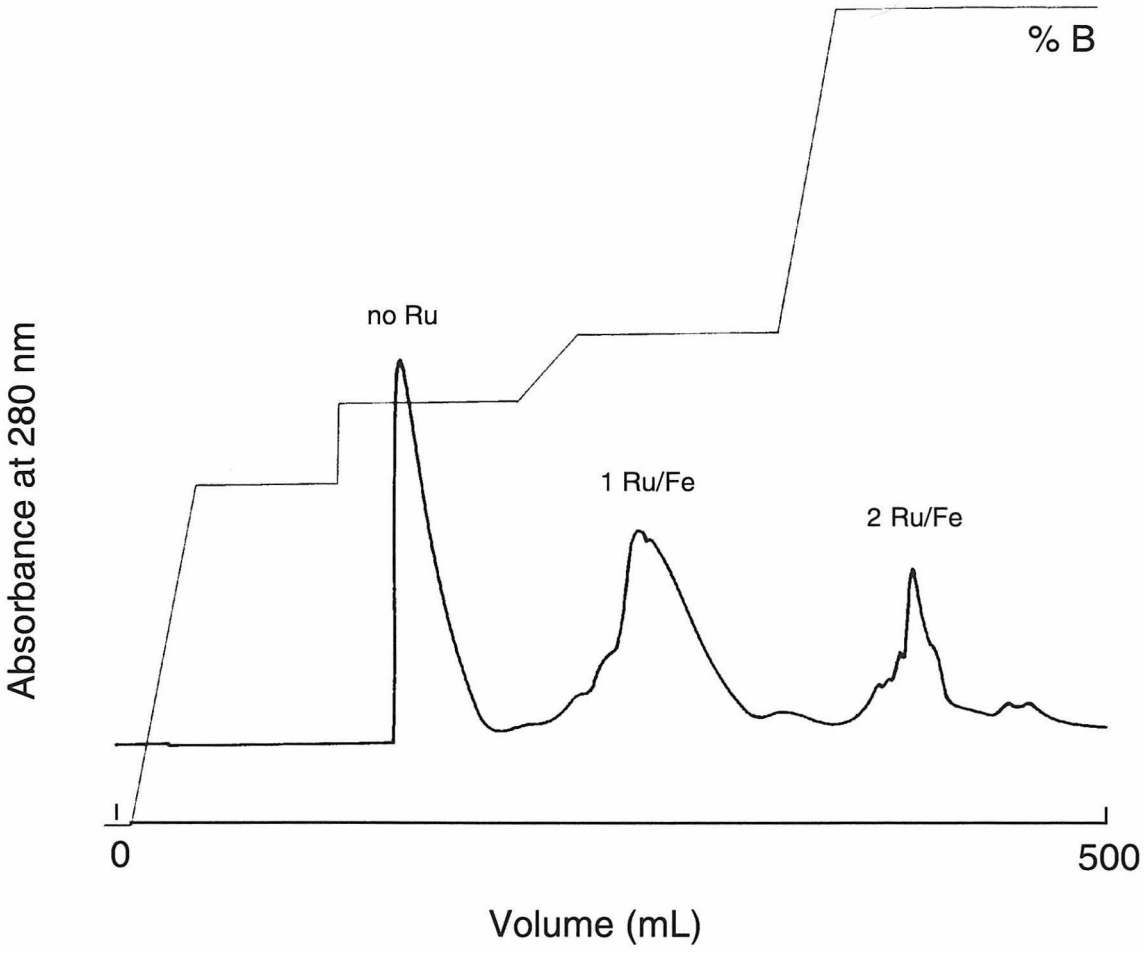
% B
no Ru
1 Ru/Fe
2 Ru/Fe
Absorbance at 280 nm
0
500
Volume (mL)

Figure 2.14. Cation-exchange FPLC chromatograms of Ru(phen)$_2$(H_2O)(His33)cyt *c* (A) and unmodified cyt *c* (B) after incubation with cyanide as described in Figure 2.12. FPLC conditions are the same as in Figure 2.13. Samples were oxidized before purification. The peak marked by an asterisk is Ru(phen)$_2$(CN)(His33)cyt *c*. The one marked with "#" is Ru(phen)$_2$(H_2O)(His33)cyt *c*. The band in (B) bearing the symbol "@" is pure unmodified cyt *c*.

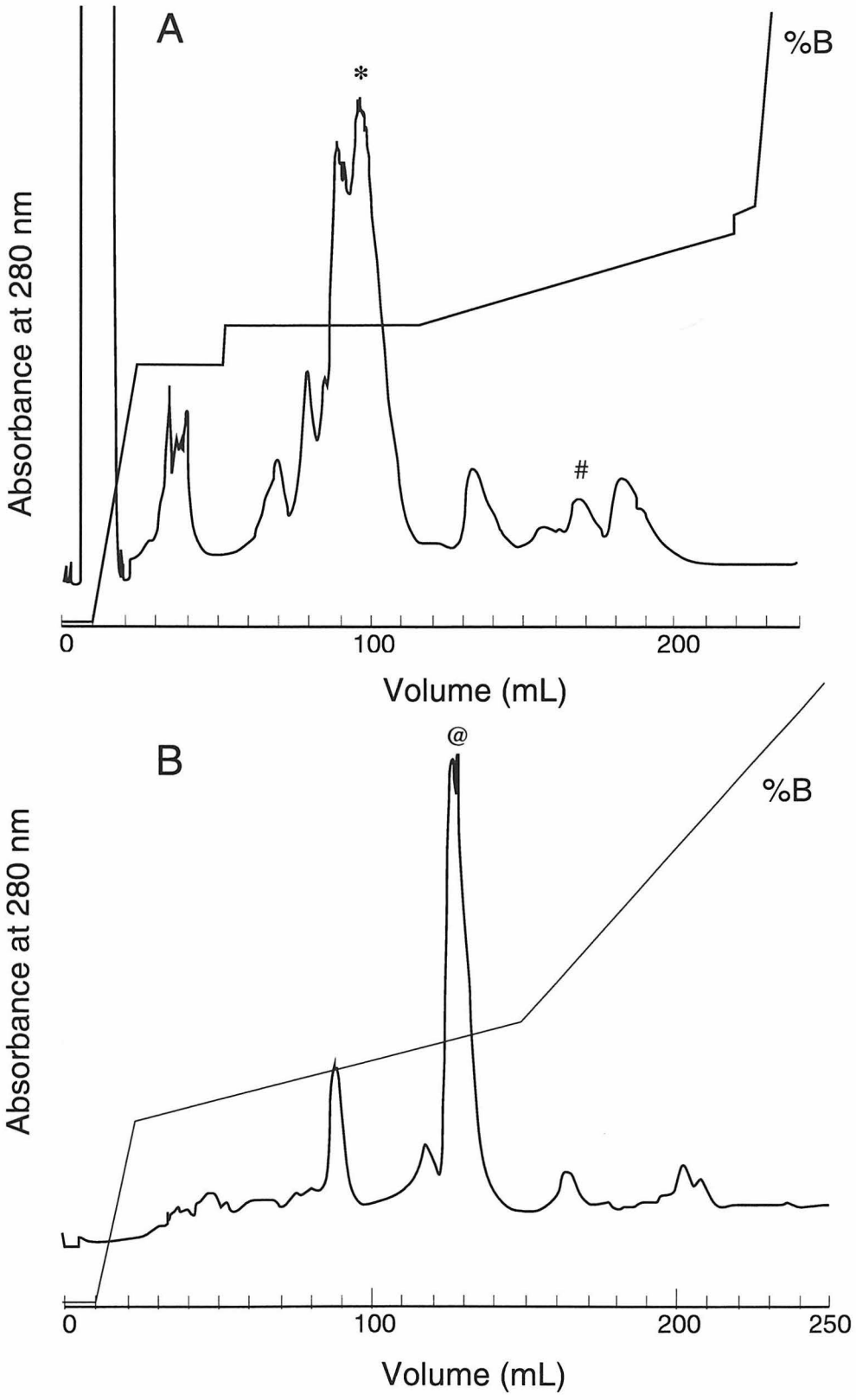
A
%B
*
#
Absorbance at 280 nm
0
100
200
Volume (mL)
B
@
%B
Absorbance at 280 nm
0
100
200
250
Volume (mL)

Figure 2.15. Map of cytochrome *c* fragments expected from digestion with trypsin (A), and reversed phase FPLC chromatograms of tryptic digests of unmodified (B) and $Ru(phen)_2(CN)$(His33)-modified (C) cyt *c*. PepRPC 5/5 HR column. Eluent A was 0.1% TFA in water, and eluent B was 0.1% TFA in acetonitrile.

A

```
                T1                  T2                  T3
1   Acetyl-Gly-Asp-Val-Glu-Lys  Gly-Lys   Lys   Ile-Phe-Val-Gln-Lys

                T4                                T5          T6
14  Cys-Ala-Gln-Cys-His-Thr-Val-Glu-Lys  Gly-Gly-Lys   His-Lys
    └─ heme ─┘

                T7
28  Thr-Gly-Pro-Asn-Leu-His-Gly-Leu-Phe-Gly-Arg  Lys

                T8                                          T9
40  Thr-Gly-Gln-Ala-Pro-Gly-Phe-Thr-Tyr-Thr-Asp-Ala-Asn-Lys  Asn-Lys

          T10                 T11
56  Gly-Ile-Thr-Trp-Lys   Glu-Glu-Thr-Leu-Met-Glu-Tyr-Leu-Glu-Asn-Pro-Lys

                T12                 T13                 T14
73  Lys   Tyr-Ile-Pro-Gly-Thr-Lys   Met-Ile-Phe-Ala-Gly-Ile-Lys   Lys-Lys

          T15                 T16                 T17                 T18
89  Thr-Glu-Arg   Glu-Asp-Leu-Ile-Ala-Tyr   Leu-Lys   Lys   Ala-Thr-Asn-Glu-COOH
```

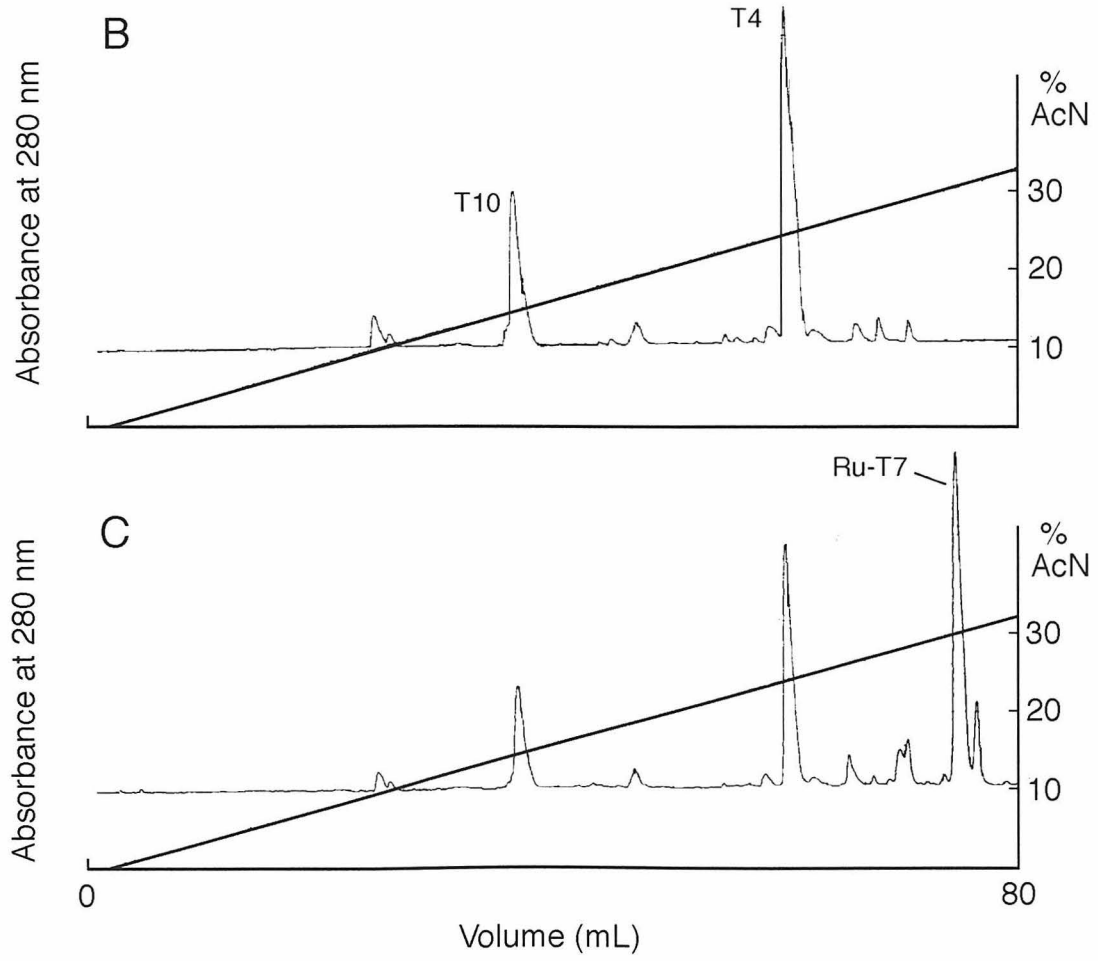

Figure 2.16. Absorption spectra of $Ru(phen)_2(CN)(im)^+$ (dashed), oxidized cytochrome *c* (dotted), the sum of $Ru(phen)_2(CN)(im)^+$ and oxidized cytochrome *c* (long dashes), and oxidized $Ru(phen)_2(CN)$(His33)cyt *c* (solid line) ($\mu = 0.1$ sodium phosphate, pH 7.0). The Ru-cyt *c* spectrum is plotted using a smaller thickness in order to allow observation of the spectrum of the sum.

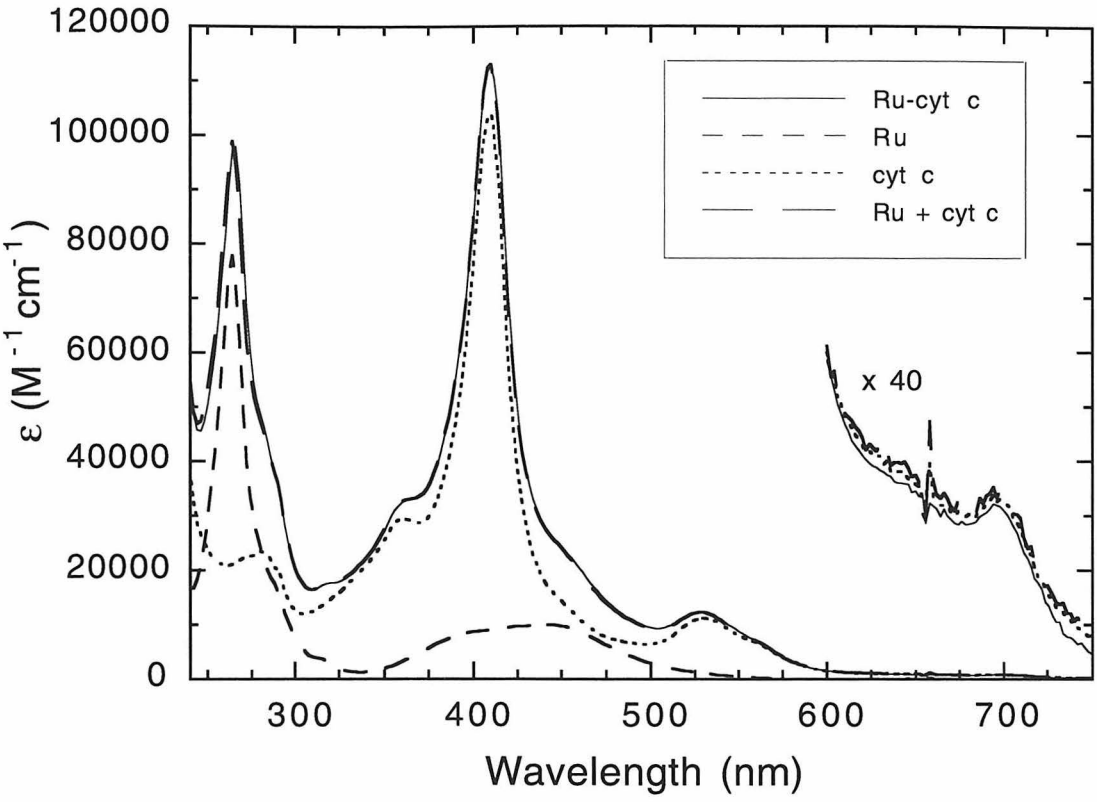
120000
100000
80000
60000
40000
20000
0
ε (M⁻¹ cm⁻¹)
300
400
500
600
700
Wavelength (nm)
Ru-cyt c
Ru
cyt c
Ru + cyt c
x 40

Figure 2.17. UV CD spectra of cyt *c* (A) and $Ru(phen)_2(CN)$(His33)cyt *c* (B). Both proteins are oxidized. Samples are 12 mM in protein, in 0.1 cm path length cuvettes (μ = 0.1 sodium phosphate, pH 7.0). Mean residue ellipticity is plotted; multiplication by 104 yields molar ellipticity.

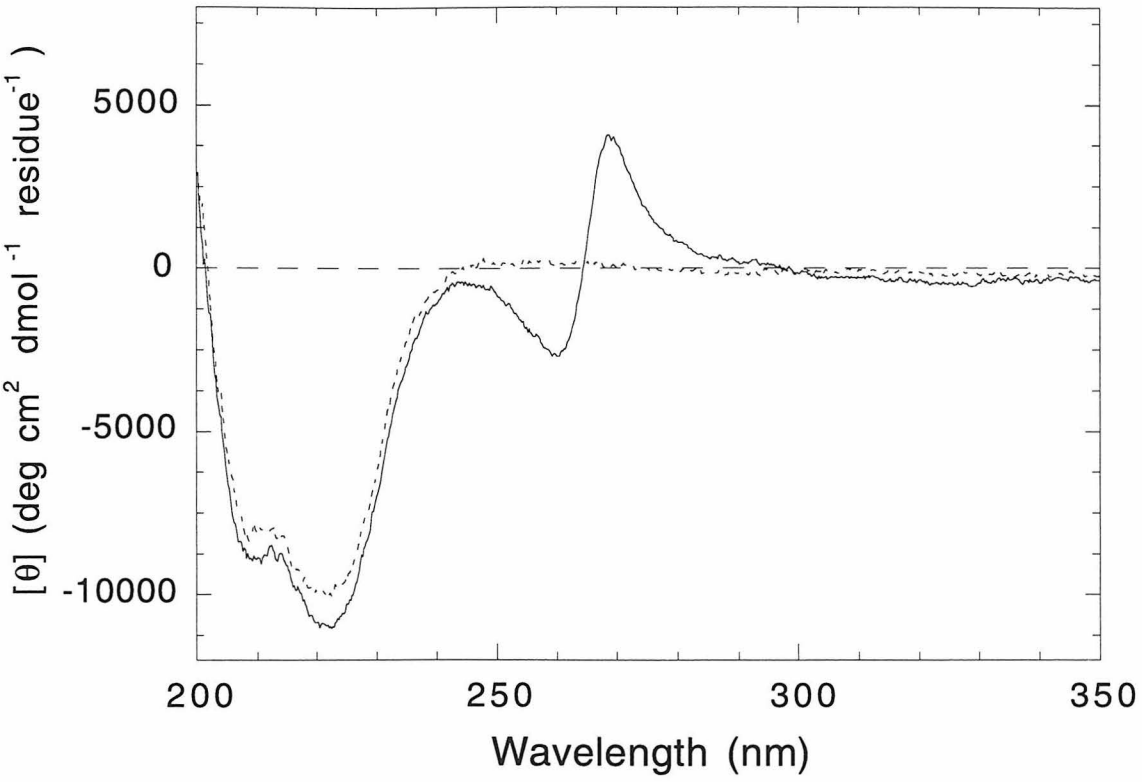
5000
0
-5000
-10000
[θ] (deg cm^2 dmol^{-1} residue^{-1})
200
250
300
350
Wavelength (nm)

Figure 2.18. Photoinduced reduction and reoxidation of the cyt *c* heme. Top: Scheme depicting processes which could occur upon excitation of $Ru(phen)_2(CN)(His33)$cyt *c* (L-Ru---Fe; L represents a phenanthroline ligand). Bottom: Transient absorption kinetics monitored at 377 nm after excitation of a 20 μM solution of $Ru(phen)_2(CN)(His33)$cyt *c* (μ = 0.1 sodium phosphate, pH 7.0). The smooth line is the best fit to a biexponential function; one phase corresponds to $*Ru^{2+} \rightarrow Fe^{3+}$ ET (k_{obs} = 3.7 x 10^6) and the other corresponds to $Fe^{2+} \rightarrow Ru^{3+}$ ET ($^{O}k_{ET}$ = 1.0 x 10^7 s^{-1}). The observed reoxidation of ferroheme is limited by the rate of excited-state decay (k_{obs}); see text for further explanation. Residuals and fitting parameters are shown above the trace.

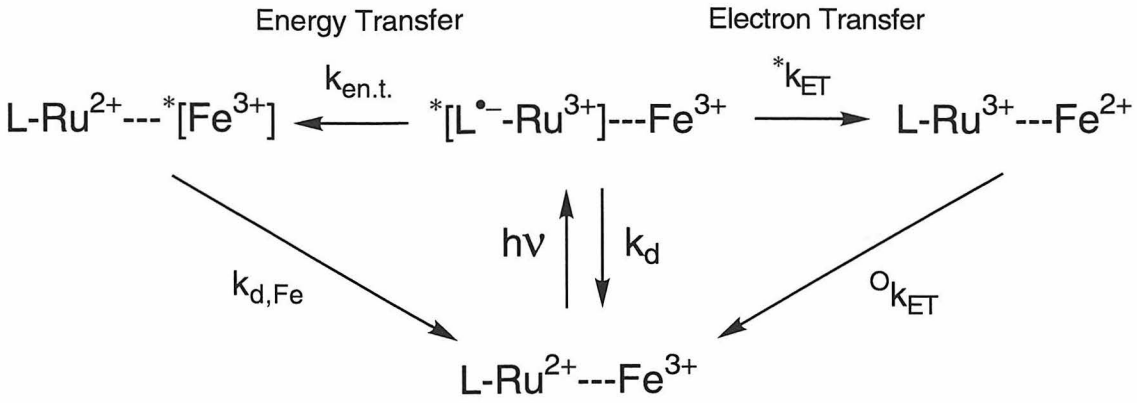
Energy Transfer
Electron Transfer
$k_{en.t.}$
$^*k_{ET}$
L-Ru^{2+}---*[Fe^{3+}]
*[L$^{\bullet-}$-Ru^{3+}]---Fe^{3+}
L-Ru^{3+}---Fe^{2+}
hν
k_d
$k_{d,Fe}$
$^o k_{ET}$
L-Ru^{2+}---Fe^{3+}

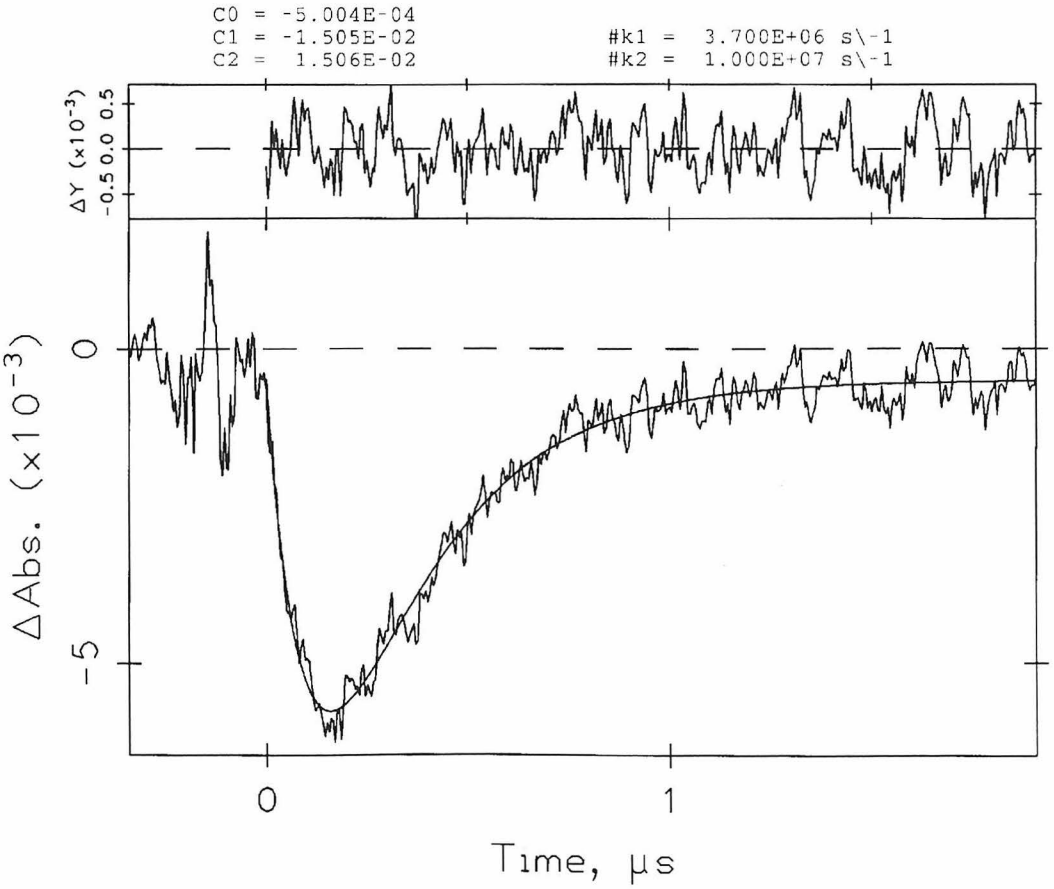
C0 = -5.004E-04
C1 = -1.505E-02
C2 = 1.506E-02
#k1 = 3.700E+06 s\-1
#k2 = 1.000E+07 s\-1
ΔY (x10^{-3})
-0.5 0.0 0.5
ΔAbs. (x10^{-3})
0
-5
0
1
Time, μs

Figure 2.19. Transient absorption kinetics of excited-state decay in the same solution as described in Figure 2.18. λ_{obs} = 339 nm. The smooth line is the best fit to a single exponential function. Fit parameters and residuals are shown above the trace.

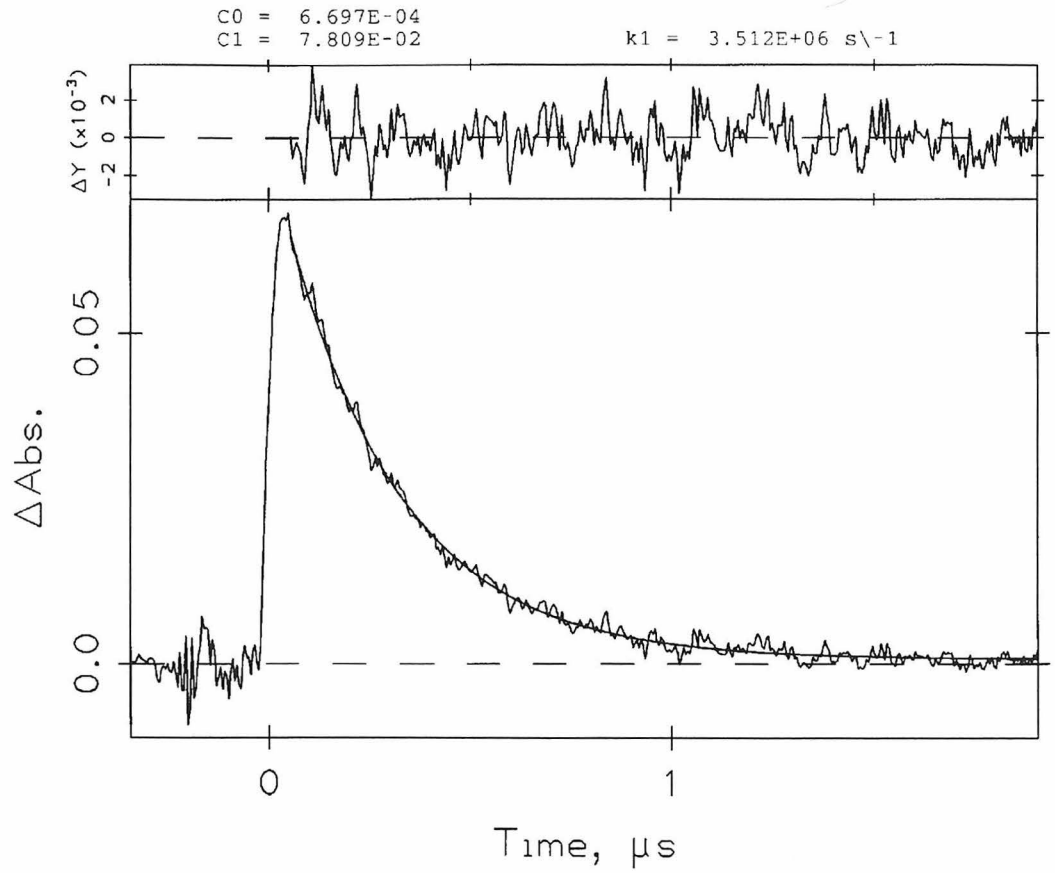
C0 = 6.697E-04
C1 = 7.809E-02
k1 = 3.512E+06 s\-1
ΔY (x10-3)
2
0
-2
0.05
0.0
ΔAbs.
0
1
Time, μs

Figure 2.20. Oxidative flash-quench scheme for measuring $Fe^{2+} \rightarrow Ru^{3+}$ ET in Ru-cyt *c* (L-Ru---Fe; L represents a diimine ligand). Q_1 is $Ru(NH_3)_6^{3+}$.

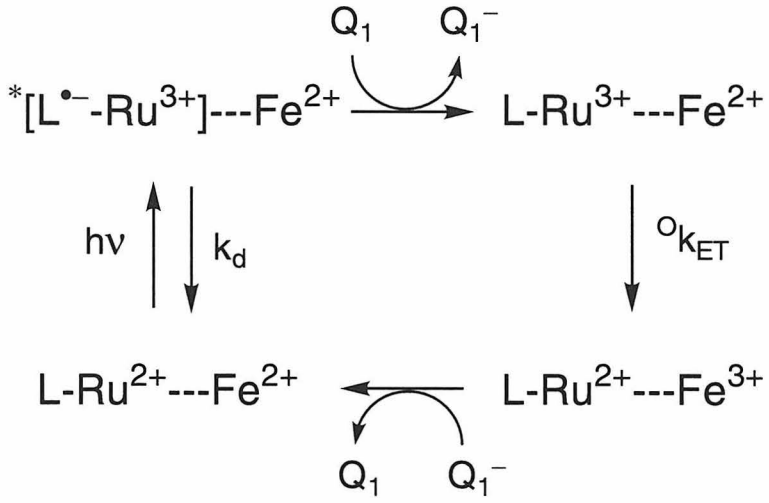
Q1
Q1−
*[L•−-Ru3+]---Fe2+
L-Ru3+---Fe2+
hν
kd
oket
L-Ru2+---Fe2+
L-Ru2+---Fe3+
Q1
Q1−

Figure 2.21. Transient absorption kinetics monitored at 378 nm following excitation of a solution of reduced $Ru(phen)_2(CN)(His33)$cyt *c* (20 μM) in the presence of either 1 or 12 mM $Ru(NH_3)_6^{3+}$. Best fits to a biexponential function are shown (smooth lines), along with the residuals. See the text for a detailed description of the measured rates and the meaning ascribed to them.

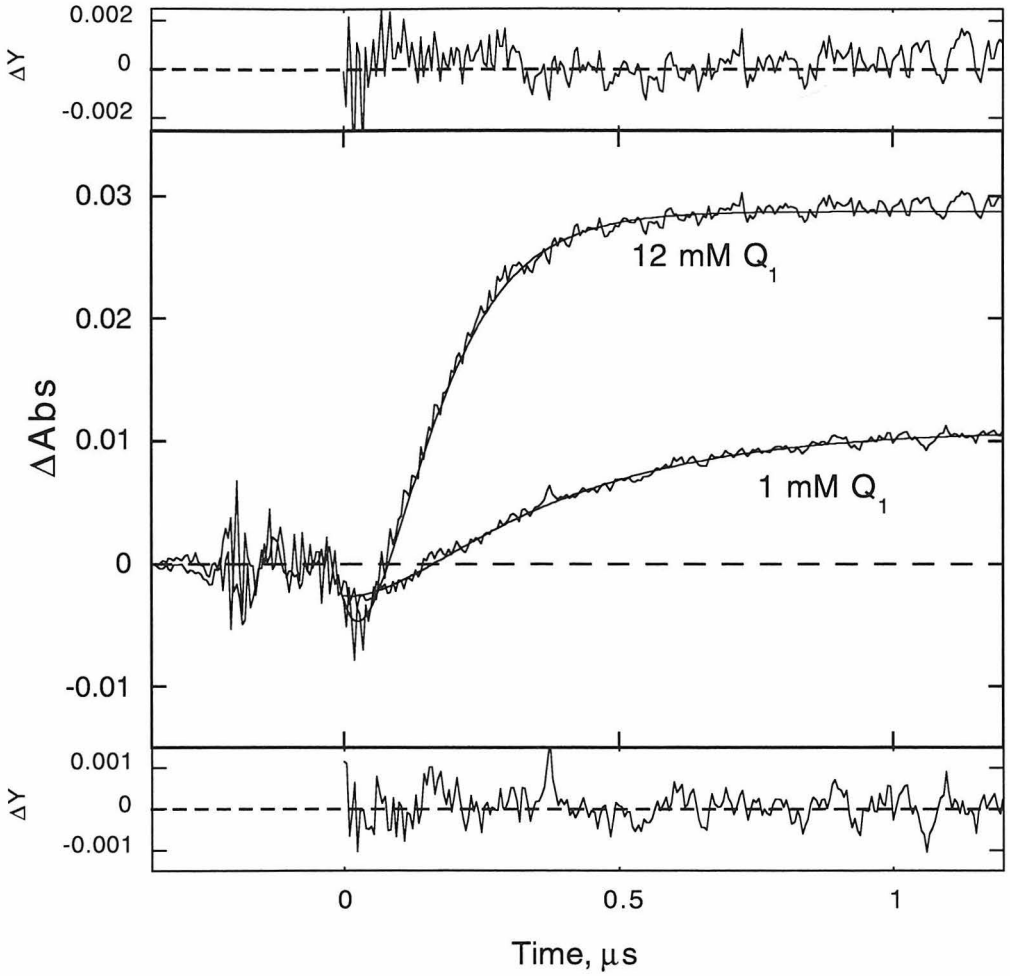
0.002
0
-0.002
ΔY
0.03
0.02
0.01
0
-0.01
ΔAbs
12 mM Q1
1 mM Q1
0.001
0
-0.001
ΔY
0
0.5
1
Time, μs

Figure 2.22. Reductive flash-quench scheme for measuring $Ru^{+} \rightarrow Fe^{3+}$ ET in Ru-cyt *c* (L-Ru---Fe; L represents a diimine ligand). Q_2 is MeODMA.

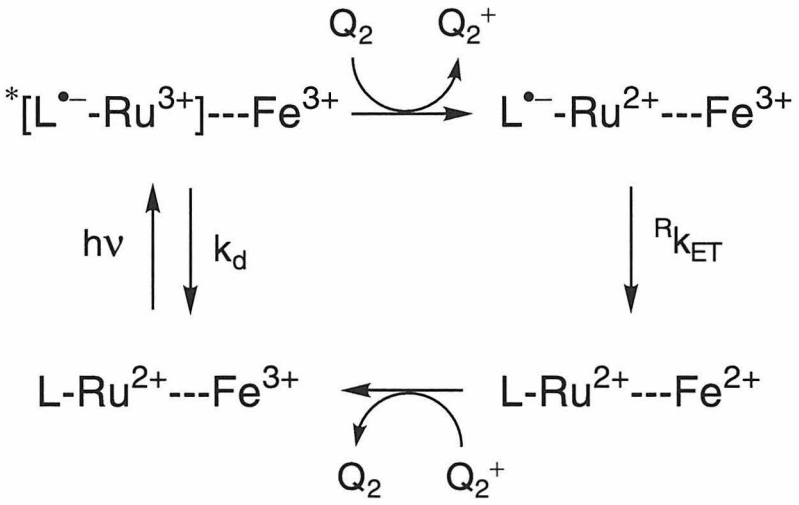
Q2
Q2+
*[L•−-Ru3+]---Fe3+
L•−-Ru2+---Fe3+
hν
kd
RkET
L-Ru2+---Fe3+
L-Ru2+---Fe2+
Q2
Q2+

Figure 2.23. Transient absorption kinetics monitored at (A) 420 nm and (B) 339 nm following excitation of a solution of oxidized $Ru(phen)_2(CN)(His33)$cyt *c* (18 μM) in the presence of 9 mM MeODMA. Best fits to a biexponential function are shown (smooth lines), along with the residuals. The fast phase corresponds to loss of $*Ru^{2+}$ (k_{obs} = 9.4 x 10^6 s^{-1}. The slower component corresponds to $Ru^{+} \rightarrow Fe^{3+}$ ET ($^{R}k_{ET}$ = 4.5 x 10^5 s^{-1}).

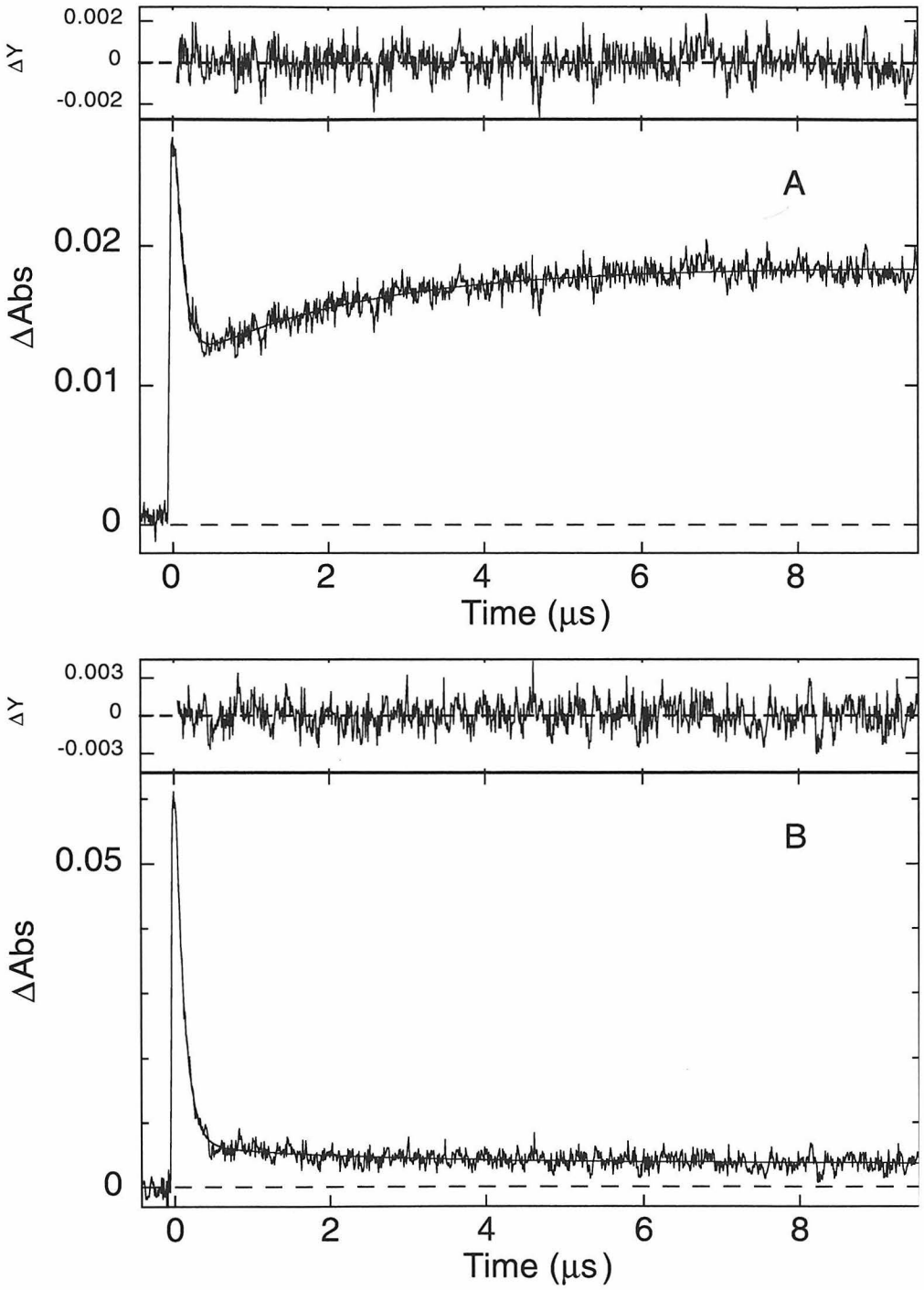
0.002
0
-0.002
ΔY
A
0.02
0.01
0
ΔAbs
0
2
4
6
8
Time (μs)
0.003
0
-0.003
ΔY
B
0.05
0
ΔAbs
0
2
4
6
8
Time (μs)

Figure 2.24. Transient absorption spectrum after the slow phase in the reaction described in Figure 2.23 (dots), and the sum of the absorption spectra of (Fe^{2+} – Fe^{3+})cyt *c* and MeODMA$^{\bullet+}$ (line).

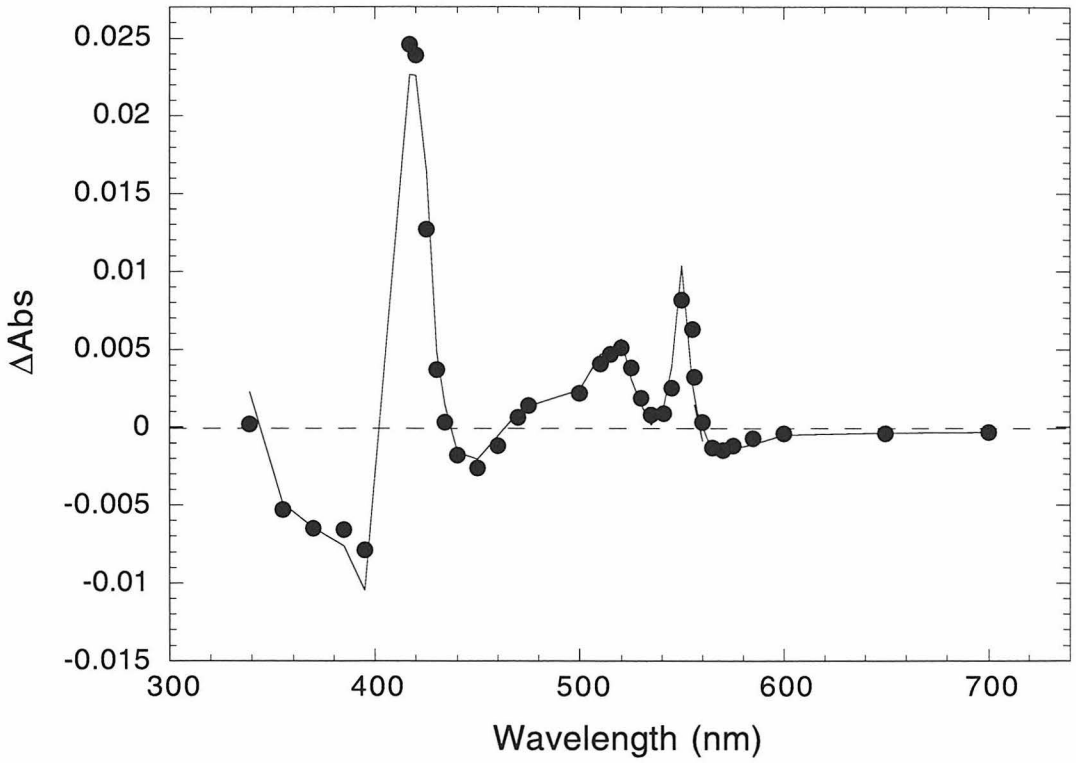
0.025
0.02
0.015
0.01
0.005
0
-0.005
-0.01
-0.015
ΔAbs
300
400
500
600
700
Wavelength (nm)

Figure 2.25. Direct photoreduction of ferricytochrome *c* by *$Ru(phen)_2(CN)(His33)$. Top: Reductive flash-scavenge scheme. S is NADH. Bottom: Transient absorption kinetics monitored at 550 nm after excitation of a solution of oxidized $Ru(phen)_2(CN)(His33)$cyt *c* (18 μM) in the presence of 1 mM NADH (μ = 0.1 sodium phosphate, pH 7.0).

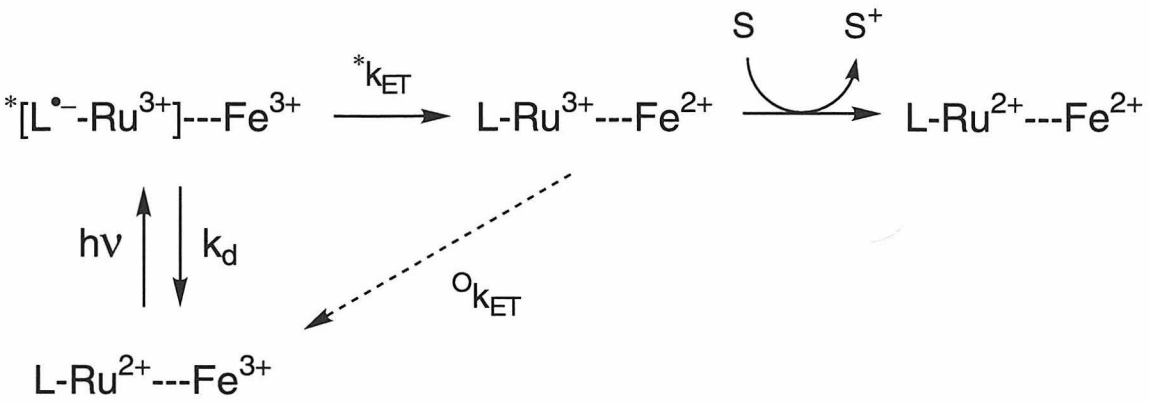
S
S+
*k_ET
*[L•−-Ru3+]---Fe3+
L-Ru3+---Fe2+
L-Ru2+---Fe2+
hν
k_d
oK_ET
L-Ru2+---Fe3+

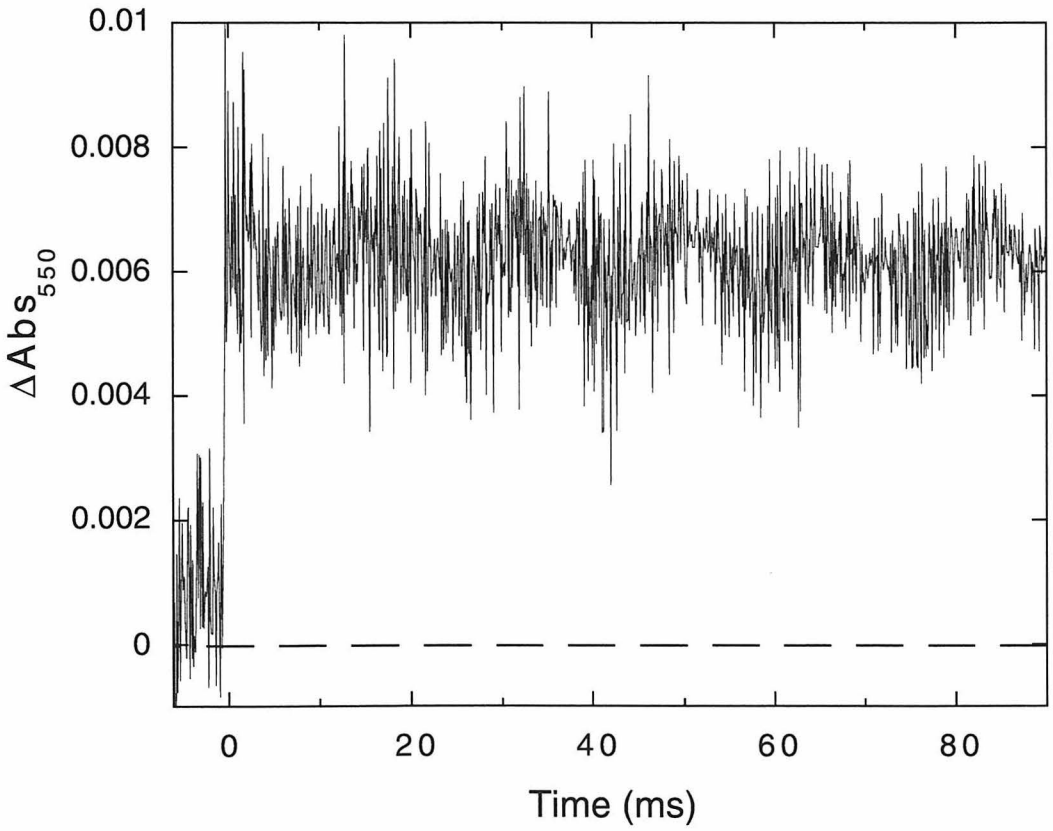
0.01
0.008
0.006
0.004
0.002
0
ΔAbs550
0
20
40
60
80
Time (ms)

Figure 2.26. Transient absorption kinetics monitored at 550 nm (A) and 605 nm (B) after excitation of a solution of $Ru(phen)_2(CN)$(His33)cyt *c* (20 μM), NADH (2 mM), and bovine CcO (20 μM) in 0.1 M HEPES, pH 7.4, 0.1% Brij (detergent). The smooth lines are best fits to a biexponential function. Fit parameters and residuals are shown above each trace.

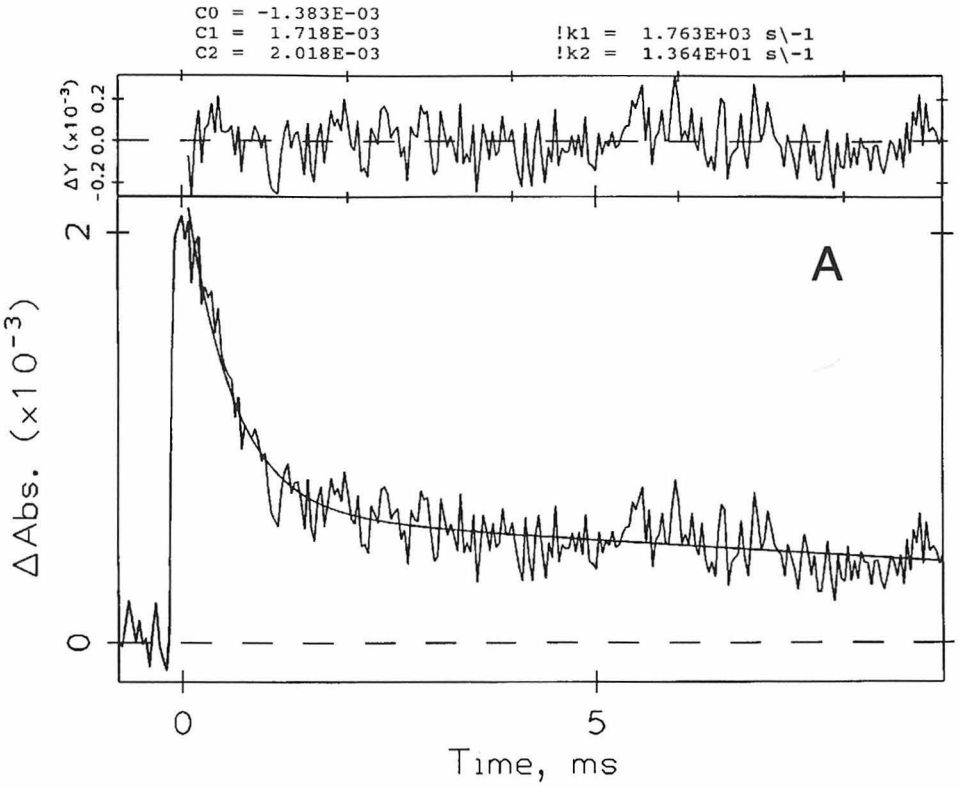
C0 = -1.383E-03
C1 = 1.718E-03
C2 = 2.018E-03
!k1 = 1.763E+03 s\-1
!k2 = 1.364E+01 s\-1
ΔY (x10⁻³)
-0.2 0.0 0.2
A
ΔAbs. (x10⁻³)
2
0
0
5
Time, ms

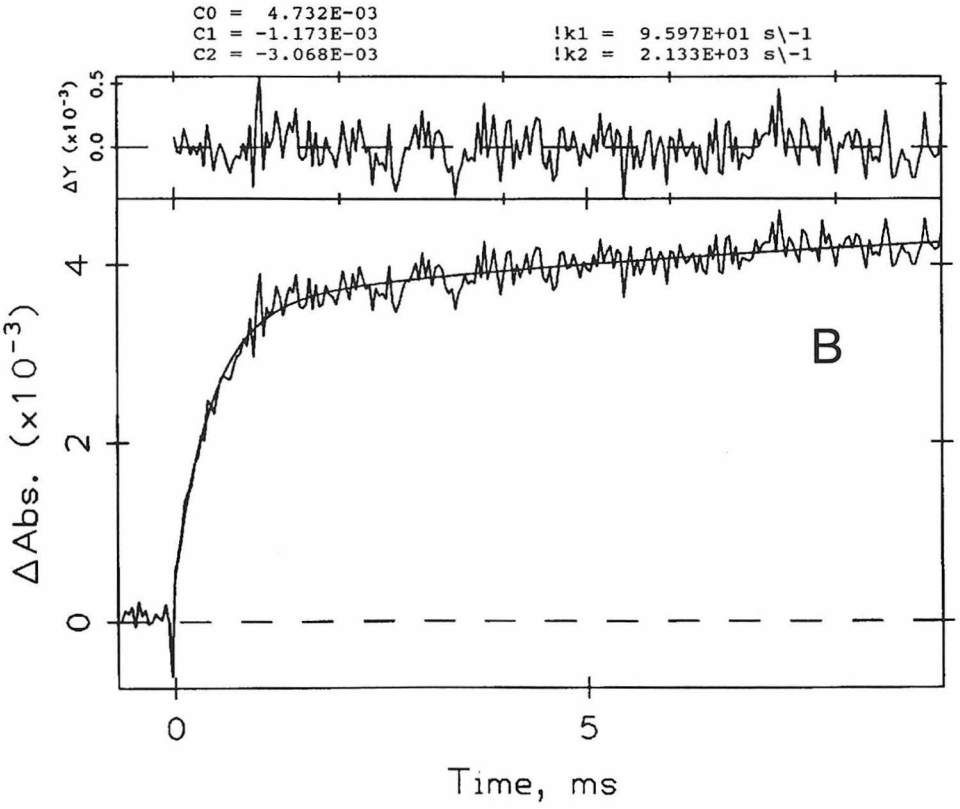
C0 = 4.732E-03
C1 = -1.173E-03
C2 = -3.068E-03
!k1 = 9.597E+01 s\-1
!k2 = 2.133E+03 s\-1
ΔY (x10⁻³)
0.0 0.5
B
ΔAbs. (x10⁻³)
4
2
0
0
5
Time, ms

Chapter 3

Rates of Heme Oxidation and Reduction in Ru(His33)cytochrome c
at Very High Driving Forces

Acknowledgment. The bulk of the work involving bipyridine complexes discussed in this chapter was performed by Morten Bjerrum and I-Jy Chang. Many of the electrochemical measurements were performed by Michael Hill, with contributions from Morten Bjerrum and Danilo Casimiro as well.

INTRODUCTION

According to semiclassical theory, electron-transfer (ET) rates should exhibit a Gaussian dependence on the reaction driving force ($-\Delta G°$); at the optimum driving force, $-\Delta G° = \lambda$ (λ is the nuclear reorganization energy), the rate is fixed by the donor-acceptor electronic coupling (H_{AB}):[1]

$$k_{ET} = \sqrt{\frac{4\pi^3}{h^2 \lambda k_b T}} (H_{AB})^2 \exp\left[\frac{-(\Delta G° + \lambda)^2}{4\lambda k_b T}\right] \tag{3.1}$$

In the region of driving forces greater than λ (the inverted region), ET rates are predicted to decrease with increasing driving force (the inverted effect). Experimental verification of the inverted effect has come from extensive investigations of ET reactions involving both organic[2-9] and inorganic[10-16] molecules.

Owing to our interest in biological ET processes,[17,18] we would like to establish experimentally the magnitudes of inverted effects in proteins and other biomolecules. Some work in this area has been done,[17-26] but no single study has involved a driving-force range sufficiently wide to probe behavior far in the inverted region. In the previous chapter photochemical schemes were described which allow the measurement of various oxidation and reduction reactions in cytochrome *c* modified at His33 with a $Ru(phen)_2(CN)$- moiety. In this chapter analogous ET processes are measured in additional, closely related Ru(His33)cytochromes *c* using these techniques. Reaction driving forces, determined using electrochemical methods, range from 0.54 to 1.89 eV. Inverted behavior is observed, but it is limited; at the highest driving forces, the ET reactions are much faster than predicted. Agreement with theory is vastly improved by assuming that these reactions involve the formation of an electronically excited ferroheme.

MATERIALS AND METHODS

Many materials and methods relevant to this chapter are described in the corresponding section of Chapter 2. Those introduced in this chapter are detailed below.

General

All RuL_2Cl_2, $RuL_2(im)_2Cl_2$, and RuL_2CO_3 complexes were prepared by literature procedures for the analogous $Ru(bpy)_2Cl_2$,[27] $Ru(bpy)_2(im)_2Cl_2$,[28] and $Ru(bpy)_2CO_3$[29] compounds, with minor modifications. Transient absorption experiments were performed as described in Chapter 2, except that excitation of Ru(4,4'-$(CONH(C_2H_5))_2$-bpy)$_2$(im)$(His)^{2+}$ was sometimes accomplished using a YAG laser (532 nm, 20 ns, 2 mJ/pulse).

4,4',5,5'-tetramethyl-2,2'-bipyridine (4,4',5,5'-$(CH_3)_4$-bpy)[30]

2,3-dimethylpyridine (30 mL) was refluxed with a Pd/C catalyst (10% Pd, Aldrich) for 8 days. A solid material was obtained upon cooling. Toluene/chloroform (~1:1) was added to dissolve the solid, and the solution was filtered hot. Rotary evaporation of the filtrate yielded a white precipitate that was isolated by filtration and washed with a small amount of toluene/chloroform. Yield: 6 g. ^{1}H NMR spectrum (in DCl, pH 1, uncorrected): singlets at 8.25 (1), 7.75 (1), 2.34 (3), and 2.25 (3). The product was recrystallized from ethyl acetate.

4,4'-di(*N*-ethyl-carbamoyl)-2,2'-bipyridine (4,4'-$(CONH(C_2H_5))_2$-bpy)

4,4'-dicarboxy-2,2'-bipyridine[31] (3 g, 12 mmol) was refluxed in 30 mL of thionyl chloride for 3-4 hours, producing a yellow solution. Excess thionyl chloride was removed under vacuum, and the resulting residue was dried at 50 °C under vacuum. Dry benzene (80 mL) was added, and treatment of the suspension with excess freshly distilled ethylamine (3 mL, 45 mmol) yielded instant precipitation of the white product. The

mixture was refluxed for another hour. Chloroform (100 mL) was added to dissolve impurities, and the reaction mixture was filtered. The white solid was washed with ether and dried in air. Yield: 2.1 g. ^{1}H NMR spectrum (in 0.25 M DCl): d at 8.98 (2), s at 8.77 (2), d at 8.15 (2) q at 3.47 (4), and t at 1.24 ppm (6).

RuL_2(im)(His33)cytochrome *c*

$Ru(bpy)_2$(im)(His33)cyt *c* was prepared according to a published procedure[32] with minor modifications. A solution of ferricytochrome *c* (0.5 mM, 15 mL; $\mu = 0.1$ phosphate buffer, pH 7.0) was stirred under Ar with $Ru(bpy)_2CO_3$ (36 mg, ~5 mM) for 18-24 hours at room temperature in the dark. Excess $Ru(bpy)_2(H_2O)_2$ was separated by gel filtration (G-25 Sephadex, 30 cm x 2.5 cm i.d.). Solid imidazole was added to the protein fraction (to make ~1 M), and the solution sat in the dark for 1-3 days (pH unadjusted). After gel filtration to remove excess imidazole, the protein band was concentrated by ultrafiltration (Amicon), and loaded onto a Mono S column for purification by FPLC (Pharmacia). The band eluting at ~60% Buffer B was concentrated, desalted by gel filtration, and purified one to two more times by FPLC; the absorption spectrum indicated the presence of a single $Ru(bpy)_2$(im)(His) moiety per cyt *c* (e.g., $Abs_{292}/Abs_{410} = 0.67$; 292 nm corresponds primarily to a bpy(π to π^*) transition, and 410 nm is the Soret peak maximum of oxidized cyt *c*). The site of modification was determined by tryptic digestion of the modified protein, followed by purification and amino-acid sequencing of the Ru-containing peptide, as described in Chapter 2.

The other RuL_2(im)(His33)cyt *c* molecules were prepared as above, with the following modifications: In the preparation of Ru(4,4'5,5'-$(CH_3)_4$-bpy)$_2$(im)(His33)cyt *c*, Ru(4,4'5,5'-$(CH_3)_4$-bpy)$_2Cl_2$, dissolved in 100-200 µL methanol, was used instead of the carbonato complex. The modification reaction involving Ru(4,4'-CONH(C_2H_5))$_2$-bpy)$_2CO_3$ used 2-3 times greater concentrations of both reagents and required 2-4 days at 30-35 °C; the subsequent imidazole reaction was

conducted at 30-35 °C and pH 8.5. In the preparation of $Ru(phen)_2(im)(His33)$cyt *c*, the modification reaction took ~2 days, and as noted in Chapter 2 for $Ru(phen)_2(H_2O)(His)$cyt *c*, protein solutions were passed through a screening column (SP Sepharose, 3 cm x 2.5 cm i.d.; eluent: 0.25 M NaCl, pH 7.0) to remove highly binding side products prior to loading on the FPLC column (the solution off the screening column was desalted by repetitive concentration/dilution cycles in an Amicon ultrafiltration cell).

vis/NIR Absorption Spectroscopy

The absorption spectrum of a solution of ferrocytochrome *c* (2.0 mL,1.9 mM) in deuterated sodium phosphate buffer ($\mu = 0.1$, pD = 7.0 [observed pH = 6.56]) was measured from 570 to 1070 nm using a Cary 14 spectrophotometer modernized by On-Line Instruments Systems, Inc. (OLIS). Measurements were made under an atmosphere of Ar using a vacuum cell fitted with a 1 cm quartz cuvette sidearm; a slight excess of sodium dithionite was used to ensure that the protein was completely reduced during the course of the measurement.

Electrochemistry

All electrochemical measurements were made using a BAS (Model 100 or Model CV-50W) electrochemical analyzer. Cyclic Voltammetry (CV) was performed at ambient temperature with a normal three-electrode configuration consisting of a highly polished glassy carbon or platinum working electrode, a platinum auxiliary electrode, and either an SCE or AgCl/Ag reference. The working electrode was separated from the reference compartment by a modified Luggin capillary. Aqueous solutions contained sodium phosphate buffer ($\mu = 0.1$, pH = 7.0); acetonitrile solutions contained 0.1 M tetrabutylammonium hexafluorophosphate as the supporting electrolyte. All potentials

are reported vs. NHE, using the relationships E°(NHE) = E°(SCE) + 0.241 V and E°(NHE) = E°(AgCl/Ag) + 0.197 V.

$Ru^{3+/2+}$ potentials of model complexes were measured in water. The $Ru^{3+/2+}$ potentials of Ru(4,4',5,5'-$(CH_3)_4$-bpy)$_2$(im)(His33)cyt *c* (**II**) and Ru(4,4'-$(CONH(C_2H_5))_2$-bpy)$_2$(im)(His33)cyt *c* (**V**) were measured as previously described.[33] $Ru^{2+/+}$ potentials[34] were recorded vs. AgCl/Ag at an edge-plane graphite electrode in acetonitrile and corrected for the junction potential using ferrocenium/ferrocene as an internal standard. In our cell, cyclic voltammetry of a 0.05 mM ferrocenium nitrate solution in 1.00 M KCl gave $E^o(Fc^+/Fc)$ = 0.139 V vs. SCE. Junction potentials in acetonitrile were found to be ~150-300 mV.

RESULTS AND DISCUSSION

Model Compounds

As discussed in Chapter 2, model compounds are useful in determining the approximate properties of protein-bound metal species, since some measurements may be more difficult, if not impossible, to perform on complexes bound to protein. For example, $Ru^{2+/+}$ redox potentials of labels cannot be measured directly since they can only be determined in non-aqueous solvent (see below). Model compounds for all of the Ru(His)cyt *c* labels in this study have been synthesized, and characterization data (absorption spectra, emission spectra, NMR spectra) for some of the compounds are presented in Appendix A.

Photodissociation of Imidazole in $Ru(phen)_2(im)_2^{2+}$

Due to observation of light-induced changes in the transient absorption kinetics of ET reactions involving Ru(phen)$_2$(im)(His33)cyt *c* (see below), photodecomposition of $Ru(phen)_2(im)_2^{2+}$ was monitored by ^{1}H NMR. The ^{1}H NMR spectrum of

$Ru(phen)_2(im)_2Cl_2$ in D_2O exhibits eight signals corresponding to phenanthroline protons and three singlets corresponding to coordinated imidazole, consistent with the presence of a C_2 axis of symmetry which makes the two coordinated phenanthroline ligands and imidazole ligands chemically equivalent (Figure 3.1A). A second ^1H NMR of the same sample, taken after ~36 hours of exposure to room light, exhibits new peaks corresponding to a ruthenium complex with 16 distinct phenanthroline protons, as well as peaks corresponding to free imidazole (Figure 3.1B). These observations are consistent with the photoinitiated loss of one imidazole ligand from the complex, as has been observed in other $Ru(bpy)_2(X)(Y)$ compounds such as $Ru(bpy)_2(py)_2^{2+}$.[35]

Electrochemistry

$Ru^{3+/2+}$ couples for most of the model compounds displayed reversible oxidations in aqueous solution (Figure 3.2A; $E°[Ru^{3+/2+}(4,4'\text{-}(CH_3)_2\text{-bpy})_2(im)_2] = 0.86$ V vs. NHE). The exception was $Ru(4,4'\text{-}CONH(C_2H_5))_2\text{-bpy})_2(im)_2^{2+}$, which exhibited a chemically irreversible oxidation under normal scanning conditions, likely due to its substantially up-shifted potential (Figure 3.2B). Using a microelectrode (d = 30 μm) and a very fast scan rate (50,000 V/s), a reversible oxidation of this compound was obtained ($E°[Ru^{3+/2+}(4,4'\text{-}CONH(C_2H_5))_2\text{-bpy})_2(im)_2] = 1.26$ V vs. NHE). The small electrode was required to keep the cell resistance sufficiently low, and the fast scan rates were necessary to outcompete the degradation reaction.

Several attempts were made to obtain $Ru^{2+/+}$ potentials in water. Mercury drop and gold working electrodes have very large overpotentials for reduction of hydronium ion to hydrogen in water, allowing very negative potentials to be accessed. However, in experiments involving either electrode, large catalytic currents were observed at potential values significantly higher than the solvent threshold, suggesting that the reduced ruthenium complex acts as a catalyst for hydronium ion reduction. The pH dependence of the process supports this conclusion, as the catalytic potential was inversely related to

the concentration of hydronium ion. Direct measurement of the $Ru^{2+/+}$ potentials in aqueous solution was therefore impossible. Reversible reductions, however, were observed in acetonitrile solution (Figure 3.3; $E°[Ru^{2+/+}(phen)_2(CN)(im)] = -1.63$ V vs. NHE), and in solutions of acetonitrile doped with small amounts of water (up to ~35 mol%). However, a complex dependence of the potential was seen as a function of the mole fraction of water present even after correction for the junction potential, and it was not possible to extrapolate to 100% water with a sufficient degree of confidence. Thus the values obtained in non-doped acetonitrile were used for the determination of the driving forces for $Ru^{+} \rightarrow Fe^{3+}$ ET reactions (Tables 3.1 and 3.2).

Comments About Redox Potentials and Driving Forces

Several assumptions and approximations have gone into the determination of the driving forces for the reactions described in this chapter. The actual driving force for an intramolecular ET reaction between a covalently bound label and the heme in cyt *c* is determined by the redox potentials of the label *bound to the protein* and the heme group of cyt *c with the label bound to the protein.* When these are not the actual measurements made, some error is introduced. We have used the standard value for the redox potential of cyt *c* (+0.260 V)[36] for all of the modified proteins described here. Prior work in this group[33,37] has demonstrated that heme potentials typically vary by no more than 20 mV upon addition of a $Ru(bpy)_2(im)$- label to various surface histidine residues, so relatively little error is introduced by this assumption. Measurements of the $Ru^{3+/2+}$ potentials for the complexes bound to the protein have been made for only two of the six cases (**II** and **V**); the model compound $[RuL_2(X)(im)^{n+}]$ values have been determined for the other four (Table 3.1). $Ru^{3+/2+}$ potentials for **II** and **V** are 100 and 70 mV more positive than the values obtained for the respective model complexes, indicating that significant error could be introduced by using the model compound values. It is likely that the observed 70-100 mV shift to more positive potential is systematic, arising from a positive

electrostatic potential at the surface of the protein near His33 (oxidized cyt *c* has a net charge of +11 at pH 7). Thus we have included for comparison an "adjusted" set of driving forces for the $Fe^{2+} \rightarrow Ru^{3+}$ ET reactions, in which +85 mV (the average of +70 and +100 mV) has been added to the $Ru^{3+/2+}$ redox potentials measured for model complexes (Table 3.2).

$Ru^{2+/+}$ potentials could only be obtained for model complexes in acetonitrile solution (see above). Thus, two sources of error are associated with these values: the use of the potential of a model compound as opposed to the actual ruthenium complex bound to the protein, and the use of a potential obtained in a solvent other than water. The former error should be similar to that seen for the corresponding $Ru^{3+/2+}$ potentials ($E°$(complex at His33) – $E°$(model) ≈ 100 mV). Concerning the latter error, others have used correction terms of 30-70 mV to estimate aqueous values for $M(bpy)_3^{2+/+}$ (M = Ru, Os) from potentials obtained in other solvents (*N,N*-dimethlyformamide and acetonitrile),[38] and a similar error is expected for the ruthenium complexes used in this study (we have chosen not to attempt such a correction). Though the actual total systematic errors (degree of inaccuracy) associated with $Ru^{2+/+}$ potentials may not be insignificant (≈ 200 mV), these values are far too small to provide an explanation for the anomalous rate/energy behavior observed in this study (see Figure 3.12).

Electron-Transfer Kinetics

We have examined three different ET processes in closely related $RuL_2(X)$(His33)cyt *c* molecules (Table 2). Methods for measuring these ET reactions have been described in detail in Chapter 2, and thus only brief descriptions will be presented here. $Fe^{2+} \rightarrow Ru^{3+}$ ET ($^{O}k_{ET}$) was measured using an oxidative flash-quench method (Figure 3.4: **6**→**4**→**3**→**1**; $Q_1 = Ru(NH_3)_6^{3+}$).[39] In a first phase, a fraction of the ruthenium excited states produced by laser excitation of reduced Ru-cyt *c* (Ru^{2+}-Fe^{2+}) are quenched oxidatively by $Ru(NH_3)_6^{3+}$ to form Ru^{3+}-Fe^{2+}, which then undergoes

intramolecular electron transfer ($^{O}k_{ET}$) in a second kinetic phase to form Ru^{2+}-Fe^{3+}. Representative data, monitored at either 550 or 420 nm, are shown in Figure 3.5 (A: $^{O}k_{ET}$ (**I**) = 1.6 x 10^6 s^{-1}; B: $^{O}k_{ET}$ (**VI**) = 1.2 x 10^6 s^{-1}). In the case of Ru(phen)$_2$(im)(His33)cyt *c*, an additional kinetic phase was typically observed after excited-state decay (Figure 3.6: k_{fast} = 3.5 x 10^6 s^{-1}; k_{slow} = 4.5 x 10^5 s^{-1}; λ_{obs} = 395 nm). The amplitude of the fast phase steadily decreased relative to that for the slow phase during the course of the experiment (as the sample was subjected to more laser shots); after a sufficient number of laser shots, only a single phase, having a rate constant equal to that of the slow phase, was observed (Figure 3.7A; k_{obs} = 4.5 x 10^5 s^{-1}). These kinetics are identical to those observed for a sample of independently prepared Ru(phen)$_2$(H_2O)(His33)cyt *c* (**VII**) (Figure 3.7B: $^{O}k_{ET}$ (**VII**) = 4.3 x 10^5 s^{-1}; λ_{obs} = 399 nm), indicating that the slow phase observed in the Ru(phen)$_2$(im)(His33)cyt *c* experiment is due to Ru(phen)$_2$(H_2O)(His33)cyt *c* generated via photodissociation of imidazole during the experiment (see Figure 3.1). The faster phase in the Ru(phen)$_2$(im)(His33)cyt *c* experiment corresponds to Fe^{2+}→Ru^{3+} ET in the unphotolyzed Ru(phen)$_2$(im)(His) protein ($^{O}k_{ET}$(**III**) = 3.5 x 10^6 s^{-1}).

*Ru^{2+}→Fe^{3+} rate constants ($^{*}k_{ET}$) were extracted by determining the yield of Ru^{3+}-Fe^{2+} formed after excitation of Ru^{2+}-Fe^{3+} without quencher (Figure 3.4: **1**→**2**→**3**→**1**). Kinetics for Ru(bpy)$_2$(im)(His33)cyt *c* are biphasic at 420 nm. The first phase represents the decay of the excited state and simultaneous formation of Ru^{3+}-Fe^{2+} (the excited state absorbs a bit at 420 nm); the second phase corresponds to reoxidation of the heme by Ru^{3+}, the same process measured in the oxidative flash-quench experiment (Figure 3.4: **3**→**1**). The amplitude of the second phase corresponds to production of 0.16 μM of Ru^{3+}-Fe^{2+} (Figure 3.8A). The ruthenium excited-state absorption dominates at 370 nm, and the amplitude of this excited-state decay phase corresponds to production

of 14 μM of $*Ru^{2+}$ (Figure 8B, k_{obs} = 1.6 x 10^7 s^{-1}). The quantum yield (Φ) of reduction is thus ~0.011, and $*k_{ET}$ (= Φk_{obs}) is 1.8 x 10^5 s^{-1}.

$Ru^+ \rightarrow Fe^{3+}$ ET ($^Rk_{ET}$) was measured using a reductive flash-quench procedure [Figure 3.4: **1**→**2**→**5**→**6**;[40] Q_2 = *p*-methoxy-*N,N*- dimethylaniline (MeODMA)]. In this scheme, excitation leads to bimolecular *reductive* quenching of the ruthenium excited state to produce the highly reducing Ru^+ species; intramolecular ET to the ferriheme follows in a second kinetic phase. Kinetics for Ru(4,4'-$CONH(C_2H_5)$)$_2$-bpy)$_2$(im)(His33)cyt *c*, monitored at 395 and 550 nm, are shown in Figure 3.9 ($^Rk_{ET}$(**VI**) = 2.3 x 10^5).

A fourth ET process, $Fe^{2+} \rightarrow *Ru^{2+}$ ($*k_{ET}$'), was observed in one of the complexes, Ru(4,4'-$CONH(C_2H_5)$)$_2$-bpy)$_2$(im)(His33)cyt *c*, after excitation of the reduced protein with no quencher present (Figure 3.4: **6**→**4**→**5**→**6**). The rate constant for this process was not determined. Nonetheless, achievement of direct photooxidation of the heme by tuning the $Ru^{3+/2+}$ redox potential to sufficiently high values is notable, and the recombination ET in this scheme provides an independent means of measuring $^Rk_{ET}$(**VI**). Kinetics monitored at 395 and 550 nm are shown in Figure 3.10. The rates are identical to those observed in the reductive flash-quench scheme (compare Figures 3.9 and 3.10).

Analysis of the driving-force dependence of the $Fe^{2+} \rightarrow Ru^{3+}$ reaction using the "as-measured" redox potentials for the model complexes corresponding to **I**, **III**, and **VI** gives λ = 0.74(4) eV and H_{AB} = 0.096(5) cm^{-1} (Figure 3.11A). Using adjusted redox potentials assuming E°[RuL_2X(His33)] = E°[RuL_2X(im)] + 85 mV (see above) yields λ = 0.83(4) eV and H_{AB} = 0.100(5) cm^{-1} (Figure 3.11B). The differences provide a rough measure of the errors introduced by the use of model compound values: the coupling is not significantly affected, but the difference between the reorganization energy obtained using model compounds and the actual value could be statistically significant (but

reasonably small). The Ru(phen)$_2$(CN)(His33)cyt *c* $Fe^{2+}\rightarrow Ru^{3+}$ rate constant, while consistent with the analysis, is statistically an outlier, and was not included in the fits of the RuL$_2$(im)(His)cyt *c* data. Cyanide binding to ruthenium evidently perturbs the Ru-heme electronic coupling relative to Ru-im ligation. Indeed, calculations indicate that the $Fe^{2+}\rightarrow Ru^{3+}$ rate constant is sensitive to the Ru orbital that provides the coupling to the bridge,[41] and experimental work shows that varying X in RuL$_2$(X)(His) could slightly alter the Ru-His coupling.[42]

One of the $*Ru^{2+}\rightarrow Fe^{3+}$ rates [$*k_{ET}$(**V**)] is well described by the $Fe^{2+}\rightarrow Ru^{3+}$ analysis; however, the other $*Ru^{2+}\rightarrow Fe^{3+}$ rate [$*k_{ET}$(**IV**)], as well as the $Ru^{+}\rightarrow Fe^{3+}$ rates [$^{R}k_{ET}$(**IV**) and $^{R}k_{ET}$(**VI**)], are higher than expected for the driving forces involved (Figure 3.12). In particular, $^{R}k_{ET}$(**IV**) is more than five orders of magnitude larger than predicted. We can rule out variations in outer-sphere reorganization energies (λ_O) as an explanation for this anomalous rate/energy behavior: according to dielectric continuum models,[43,44] λ_O depends on donor-acceptor properties, such as size and separation distance, that do not vary significantly for the different types of ET reactions in Ru(His33)cyt *c* molecules.

Electronic-coupling variations cannot explain the rate/energy behavior either. The donor electron in the $*Ru^{2+}\rightarrow Fe^{3+}$ and $Ru^{+}\rightarrow Fe^{3+}$ reactions is localized in a diimine π^* orbital. The first step in the ET pathway involves coupling to the Ru or directly to the protein. In either case, the coupling should be slightly *weaker* than that for $Fe^{2+}\rightarrow Ru^{3+}$ ET: the former case involves an additional covalent bond relative to the $Fe^{2+}\rightarrow Ru^{3+}$ pathway, and the latter involves a through-space jump (van der Waals interaction) having no counterpart in the $Fe^{2+}\rightarrow Ru^{3+}$ pathway.

Deviations from inverted behavior involving anomalously fast inverted rates often are attributable to quantum effects: specifically, the inverted effect can be attenuated at high driving forces by nuclear tunneling along one or more coordinates of high-frequency vibrational modes.[45] Tunneling efficiency depends on the magnitude of the distortion

along the high-frequency vibrational coordinates (λ_i). The λ_i associated with $Ru^{+/2+}$(diimine) reactions should be similar to that for $Ru(bpy)_3^{2+}$ MLCT [$Ru(d\pi)\rightarrow bpy(\pi^*)$] excitation (0.17 eV).[46] However, in order to accommodate ${}^{R}k_{ET}$(**IV**) in the fit, we must postulate a value of $\lambda_i \sim 1$ eV; this is unreasonably large, and thus we do not favor this as an explanation for our observations.

It has been suggested that $Ru^{+}\rightarrow Fe^{3+}$ reactions are so exergonic that formation of an electronically excited species (at lower driving force) is faster than the (highly inverted) reaction directly to ground-state Ru^{2+}-Fe^{2+}.[47] Although the lowest Ru^{2+} excited states are out of reach ($\geq$ 2.0 eV),[33] those for ferrocytochrome *c* are not: based on the NIR absorption spectrum, the origin of the ^{1}MLCT [$Fe(d\pi)\rightarrow P(\pi^*)$, P = porphyrin] excited state is at roughly 1.3 eV (Figure 3.13).[48,49] The ^{3}MLCT state is estimated at ~1.05 eV assuming a singlet-triplet gap of ~0.25 eV, the value observed in $Fe(bpy)_3^{2+}$.[50] Indeed, the rates predicted for the Ru^{+}-$Fe^{3+} \rightarrow Ru^{2+}$-*$Fe^{2+}$(^{3}MLCT) reactions of complexes **VI** and **IV** (Figure 3.4: **5**$\rightarrow$**7**) are close to those observed for $Ru^{+}\rightarrow Fe^{3+}$ ET (Figure 4.14). The fact that the energy-adjusted ${}^{R}k_{ET}$(**IV**) point falls slightly below the value predicted from the $Fe^{2+}\rightarrow Ru^{3+}$ analysis may reflect the slightly weaker electronic coupling expected for $Ru^{+}\rightarrow Fe^{3+}$ reactions as noted above. Similar analysis indicates that the *Ru^{2+}-$Fe^{3+} \rightarrow Ru^{3+}$-*$Fe^{2+}$(^{3}MLCT) reaction of complex **IV** (Figure 3.4: **2**$\rightarrow$**8**) is faster than inverted ET directly to a ground-state ferroheme.[51] Subsequent ferriheme excited-state deactivation (Figure 3.4: **8**$\rightarrow$**3** and **7**$\rightarrow$**6**) should be very fast (>10^{11} s^{-1})[52,53] and thus will not be observed in our experiments.

The phenomenon of rate/energy leveling is common for photoinduced charge separation;[54] most examples of inverted behavior involve recombination reactions.[55] Invoking the formation of excited-state products is one explanation of rate leveling:[9,15,16,54,56,57] photoinduced charge separation generally produces open-shell species (radicals) possessing low-lying excited states, whereas recombination reactions

yield closed-shell products.[15,16] A key role played by electronic structure in ET kinetics is underscored by our finding that a relatively low-lying excited state of a closed-shell product can open a noninverted decay channel deep in the inverted region–the region in which thermal (energy wasting) recombinations of photogenerated charge-separated states are usually inhibited.

REFERENCES AND NOTES

(1) Marcus, R. A.; Sutin, N. *Biochim. Biophys. Acta* **1985**, *811*, 265-322.

(2) Miller, J. R.; Calcaterra, L. T.; Closs, G. L. *J. Am. Chem. Soc.* **1984**, *106*, 3047-3049.

(3) Closs, G. L.; Miller, J. R. *Science* **1988**, *240*, 440-447.

(4) Wasielewski, M. R.; Niemczyk, M. P.; Svec, W. A.; Pewitt, E. B. *J. Am. Chem. Soc.* **1985**, *107*, 1080-1082.

(5) Gould, I. R.; Moser, J. E.; Armitage, B.; Farid, S. J. *J. Am. Chem. Soc.* **1989**, *111*, 1917-1919.

(6) Levin, P. P.; Pluzhnikov, P. F.; Kuzmin, V. A. *Chem. Phys.* **1989**, *137*, 331-344.

(7) Irvine, M. P.; Harrison, R. J.; Beddard, G. S.; Leighton, P.; Sanders, J. K. M. *Chem. Phys.* **1986**, *104*, 315-324.

(8) Grampp, G.; Hetz, G. *Ber. Bunsenges. Phys. Chem.* **1992**, *96*, 198-200.

(9) Beitz, J. V.; Miller, J. R. *J. Chem. Phys.* **1979**, *71*, 4579-4595.

(10) Fox, L. S.; Kozik, M.; Winkler, J. R.; Gray, H. B. *Science* **1990**, *247*, 1069-1071.

(11) Chen, P.; Duesing, R.; Tapolsky, G.; Meyer, T. J. *J. Am. Chem. Soc.* **1989**, *111*, 8305-8306.

(12) Yonemoto, E. H.; Riley, R. L.; Kim, Y. I.; Atherton, S. J.; Schmehl, R. H.; Mallouk, T. E. *J. Am. Chem. Soc.* **1992**, *114*, 8081-8087.

(13) Ohno, T.; Yoshimura, A.; Mataga, N. *J. Phys. Chem.* **1986**, *90*, 3295-3297.

(14) MacQueen, D. B.; Schanze, K. S. *J. Am. Chem. Soc.* **1991**, *113*, 7470-7479.

(15) McCleskey, T. M.; Winkler, J. R.; Gray, H. B. *J. Am. Chem. Soc.* **1992**, *114*, 6935-6937.

(16) McCleskey, T. M.; Winkler, J. R.; Gray, H. B. *Inorg. Chim. Acta* **1994**, *225*, 319-322.

(17) Winkler, J. R.; Gray, H. B. *Chem. Rev.* **1992**, *92*, 369-379.

(18) Bjerrum, M. J.; Casimiro, D. R.; Chang, I.-J.; Di Bilio, A. J.; Gray, H. B.; Hill, M. G.; Langen, R.; Mines, G. A.; Skov, L. K.; Winkler, J. R.; Wuttke, D. S. *J. Bioenerg. and Biomembr.* **1995**, *27*, 295-302.

(19) McLendon, G.; Hake, R. *Chem. Rev.* **1992**, *92*, 481-490.

(20) Simmons, J.; McLendon, G.; Qiao, T. *J. Am. Chem. Soc.* **1993**, *115*, 4889-4890.

(21) Zhou, J. S.; Rodgers, M. A. J. *J. Am. Chem. Soc.* **1991**, *113*, 7728-7734.

(22) Scott, J. R.; Willie, A.; McLean, M.; Stayton, P. S.; Sligar, S. G.; Durham, B.; Millett, F. *J. Am. Chem. Soc.* **1993**, *115*, 6820-6824.

(23) Gunner, M. R.; Robertson, D. E.; Dutton, P. L. *J. Phys. Chem.* **1986**, *90*, 3783-3795.

(24) Brooks, H. B.; Davidson, V. L. *J. Am. Chem. Soc.* **1994**, *116*, 11201-11202.

(25) Lin, X.; Williams, J. C.; Allen, J. P.; Mathis, P. *Biochemistry* **1994**, *33*, 13517-13523.

(26) Jia, Y.; DiMagno, T. J.; Chan, C.-K.; Wang, Z.; Du, M.; Hanson, D. K.; Schiffer, M.; Norris, J. R.; Fleming, G. R.; Popov, M. S. *J. Phys. Chem.* **1993**, *97*, 13180-13191.

(27) Sullivan, B. P.; Salmon, D. J.; Meyer, T. J. *Inorg. Chem.* **1978**, *17*, 3334-3341.

(28) Long, C.; Vos, J. G. *Inorg. Chim. Acta* **1984**, *89*, 125-131.

(29) Johnson, E. C.; Sullivan, B. P.; Adeyemi, S. A.; Meyer, T. J. *Inorg. Chem.* **1978**, *17*, 2211-2215.

(30) This procedure is based on a literature method for making symmetrically substituted bipyridines (Sasse, W. H. F.; Whittle, C. P. *J. Chem. Soc.* **1961**, 1347-1350).

(31) Sprintschnik, G.; Sprintschnik, H. W.; Kirsch, P. P.; Whitten, D. G. *J. Am. Chem. Soc.* **1977**, *99*, 4947-4954.

(32) Durham, B. D.; Pan, L. P.; Hahm, S.; Long, J.; Millett, F. In *ACS Advances in Chemistry Series*; M. K. Johnson, R. B. King, D. M. Kurtz, C. Kutal, M. L. Norton and R.

A. Scott, Eds.; American Chemical Society: Washington, DC, 1990; Vol. 226; pp 180-193.

(33) Casimiro, D. R. Ph.D. Thesis, California Institute of Technology, 1994.

(34) "Ru^{+}" denotes the species in which ruthenium is in the +2 oxidation state and one of the ligands is a radical anion [Ru^{2+}-(diimine$^{\bullet-}$)] regardless of the overall charge on the complex.

(35) Durham, B.; Walsh, J. L.; Carter, C. L.; Meyer, T. J. *Inorg. Chem.* **1980**, *19*, 860-865.

(36) Taniguchi, V. T.; Sailasuta-Scott, N.; Anson, F. C.; Gray, H. B. *Pure Appl. Chem.* **1980**, *52*, 2275-2281.

(37) Wuttke, D. S. Ph.D. Thesis, California Institute of Technology, 1994.

(38) Sutin, N.; Creutz, C. In *Inorganic and Organometallic Photochemistry*; M. S. Wrighton, Ed.; American Chemical Society: Washington, DC, 1978; Vol. 168; pp 1-27.

(39) Chang, I.-J.; Gray, H. B.; Winkler, J. R. *J. Am. Chem. Soc.* **1991**, *113*, 7056-7057.

(40) Mines, G. A.; Winkler, J. R.; Gray, H. B.; Chan, S. I. *J. Inorg. Biochem.* **1993**, *51*, 236.

(41) Stuchebrukhov, A. A.; Marcus, R. A. *J. Phys. Chem.* **1995**, *99*, 7581-7590.

(42) LaChance-Galang, K. J.; Doan, P. E.; Clarke, M. J.; Rao, U.; Yamano, A.; Hoffman, B. M. *J. Am. Chem. Soc.* **1995**, *117*, 3529-3538.

(43) Marcus, R. A. *Ann. Rev. Phys. Chem.* **1964**, *15*, 155-196.

(44) Brunschwig, B. S.; Ehrenson, S.; Sutin, N. *J. Phys. Chem.* **1986**, *90*, 3657-3668.

(45) Brunschwig, B. S.; Sutin, N. *Comments Inorg. Chem.* **1987**, *6*, 209-235.

(46) Sutin, N.; Brunschwig, B. S.; Creutz, C.; Winkler, J. R. *Pure Appl. Chem.* **1988**, *60*, 1817-1830.

(47) Heacock II, D. H.; Harris, M. R.; Durham, B.; Millett, F. *Inorg. Chim. Acta* **1994**, *226*, 129-135.

(48) Eaton, W. A.; Charney, E. *J. Chem. Phys.* **1969**, *51*, 4502-4505.

(49) Makinen, M. W.; Churg, A. K. In *Iron Porphyrins, Part One*; A. B. P. Lever and H. B. Gray, Eds.; Addison-Wesley Publishing Company: Reading, 1983; pp 141-235.

(50) Kober, E. M.; Meyer, T. J. *Inorg. Chem.* **1982**, *21*, 3967-3977.

(51) LF(Ru^{3+}) excited states also could be formed in $*Ru^{2+} \rightarrow Fe^{3+}$ ET reactions. These states, however, are at relatively low energies (~1000 cm^{-1}; LaChance-Galang *et al.* in ref. 42) and their population is not likely to significantly affect $*Ru^{2+} \rightarrow Fe^{3+}$ ET rates.

(52) Huppert, D.; Straub, K. D.; Rentzepis, P. M. *Proc. Natl. Acad. Sci. U.S.A.* **1977**, *74*, 4139-4143.

(53) Li, P.; Sage, J. T.; Champion, P. M. *J. Chem. Phys.* **1992**, *97*, 3214-3227.

(54) Rehm, H.; Weller, A. *Isr. J. Chem* **1970**, *8*, 256-271.

(55) Suppan, P. *Top. Curr. Chem.* **1992**, *163*, 95-130.

(56) Kikuchi, K.; Niwa, T.; Takahashi, Y.; Ikeda, H.; Miyashi, T. *J. Phys. Chem.* **1993**, *97*, 5070-5073.

(57) Siders, P.; Marcus, R. A. *J. Am. Chem. Soc.* **1981**, *103*, 748-752.

Table 3.1. Measured $Ru^{3+/2+}$ and $Ru^{2+/+}$ potentials of $RuL_2(X)(im)$ and $RuL_2(X)(His33)$cytochrome *c* complexes.

complex	$E°(Ru^{3+/2+})^a$ (V)	$E°(Ru^{2+/+})^b$ (V)
$Ru(4,4',5,5'\text{-}(CH_3)_4\text{-}bpy)_2(im)_2^{2+}$	0.80	----
$Ru(4,4'\text{-}(CH_3)_2\text{-}bpy)_2(im)_2^{2+}$	0.86	----
$Ru(4,4'\text{-}(CH_3)_2\text{-}bpy)_2(im)(His33)^{2+}$ **(II)**	0.96[c]	N/A
$Ru(phen)_2(im)_2^{2+}$	0.98	-1.48
$Ru(phen)_2(CN)(im)^{+}$	1.02	-1.63
$Ru(bpy)_2(im)_2^{2+}$	1.00	-1.48
$Ru(bpy)_2(im)(His33)^{2+}$ **(V)**	1.07[c]	N/A
$Ru(4,4'\text{-}(CONH(C_2H_5))_2\text{-}bpy)_2(im)_2^{2+}$	1.26	-1.18

a In aqueous buffer (pH 7, phosphate).

b In acetonitrile, as described in text.

c Casimiro, D. R. Ph.D. Thesis, California Institute of Technology, 1994.

Table 3.2. Rate constants and driving forces for intramolecular ET in RuL2(X)(His33)cytochromes *c*.

complex	reaction	k_{ET} (s^{-1})	$-\Delta G°$ (eV)[a]
$Ru(4,4',5,5'\text{-}(CH_3)_4\text{-}bpy)_2(im)(His)^{2+}$ **(I)**	$Fe^{2+}\rightarrow Ru^{3+}$	1.6(2) x 10^6	0.54 [0.625][b]
$Ru(4,4'\text{-}(CH_3)_2\text{-}bpy)_2(im)(His)^{2+}$ **(II)**	$Fe^{2+}\rightarrow Ru^{3+}$	2.0(2) x 10^6	0.70
$Ru(phen)_2(im)(His)^{2+}$ **(III)**	$Fe^{2+}\rightarrow Ru^{3+}$	3.5(4) x 10^6	0.72 [0.805][b]
$Ru(phen)_2(CN)(His)^{+}$ **(IV)**	$Fe^{2+}\rightarrow Ru^{3+}$	1.0(1) x 10^7	0.76 [0.845][b]
$Ru(bpy)_2(im)(His)^{2+}$ **(V)**	$Fe^{2+}\rightarrow Ru^{3+}$	2.6(3) x 10^6	0.81
$Ru(4,4'\text{-}(CONH(C_2H_5))_2\text{-}bpy)_2(im)(His)^{2+}$ **(VI)**	$Fe^{2+}\rightarrow Ru^{3+}$	1.1(1) x 10^6	1.00 [1.085][b]
$Ru(bpy)_2(im)(His)^{2+}$ **(V)**	$*Ru^{2+}\rightarrow Fe^{3+}$	1.8(10) x 10^5	1.3
$Ru(phen)_2(CN)(His)^{+}$ **(IV)**	$*Ru^{2+}\rightarrow Fe^{3+}$	3.1(10) x 10^5	1.4 [0.35][c]
$Ru(4,4'\text{-}(CONH(C_2H_5))_2\text{-}bpy)_2(im)(His)^{2+}$ **(VI)**	$Ru^{+}\rightarrow Fe^{3+}$	2.3(2) x 10^5	1.44 [0.39][c]
$Ru(phen)_2(CN)(His)^{+}$ **(IV)**	$Ru^{+}\rightarrow Fe^{3+}$	4.5(5) x 10^5	1.89 [0.84][c]

[a] Redox potentials of model compounds were used in all cases except for $Ru^{3+/2+}$[**II,V**] (values are listed in Table I); E°[cyt *c*($Fe^{3+/2+}$)] = 0.26 V *vs.* NHE; $E_{00}(*Ru^{2+})$[**V**] = 2.1 eV; $E_{00}[*Ru^{2+}(phen)_2(CN)(im)]$ = 2.2 eV; $E_{00}[*Ru^{2+}(4,4'\text{-}(CONH(C_2H_5))_2\text{-}bpy)_2(im)_2]$ = 2.0 V.

[b] Assuming $Ru^{3+/2+}$ potentials for His33-bound labels are 85 mV more positive than the corresponding model complex values (see text).

[c] Assuming formation of the ferroheme ^{3}MLCT excited state.

Figure 3.1. ^{1}H NMR spectra of $Ru(phen)_2(im)_2^{2+}$ in water, acquired immediately after preparation of the sample (A) and after 36 hours of exposure to room light (B). Inset: (left) chemical structure of phenanthroline with its eight protons numbered; (right) a depiction of $Ru(phen)_2(im)_2^{2+}$ showing the C_2 axis of symmetry (dotted arrow) which makes apparent the equivalence of the two phenanthroline ligands. Peaks due to coordinated imidazole are highlighted in (A). Appearance of peaks corresponding to uncoordinated imidazole, as well as eight additional phenanthroline peaks in (B), indicates that an imidazole is dissociating to form $Ru(phen)_2(im)(H_2O)^{2+}$. No change was observed in a control NMR tube which was kept in the dark (not shown).

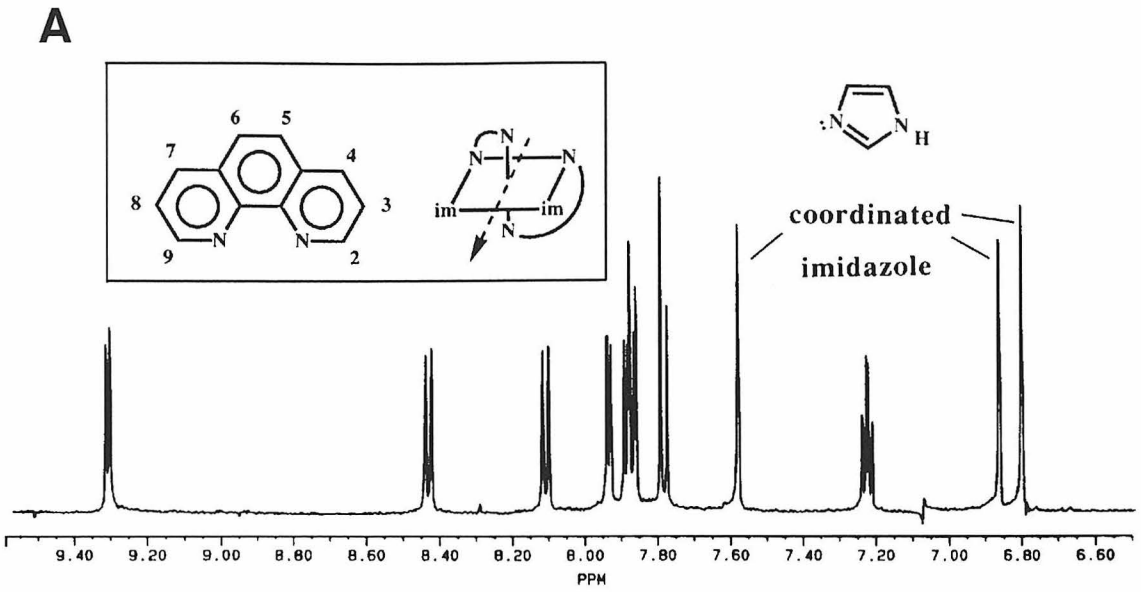
A
6
5
7
4
8
3
9
N
N
2
N
N
N
N
im
im
N
H
coordinated
imidazole
9.40
9.20
9.00
8.80
8.60
8.40
8.20
8.00
7.80
7.60
7.40
7.20
7.00
6.80
6.60
PPM

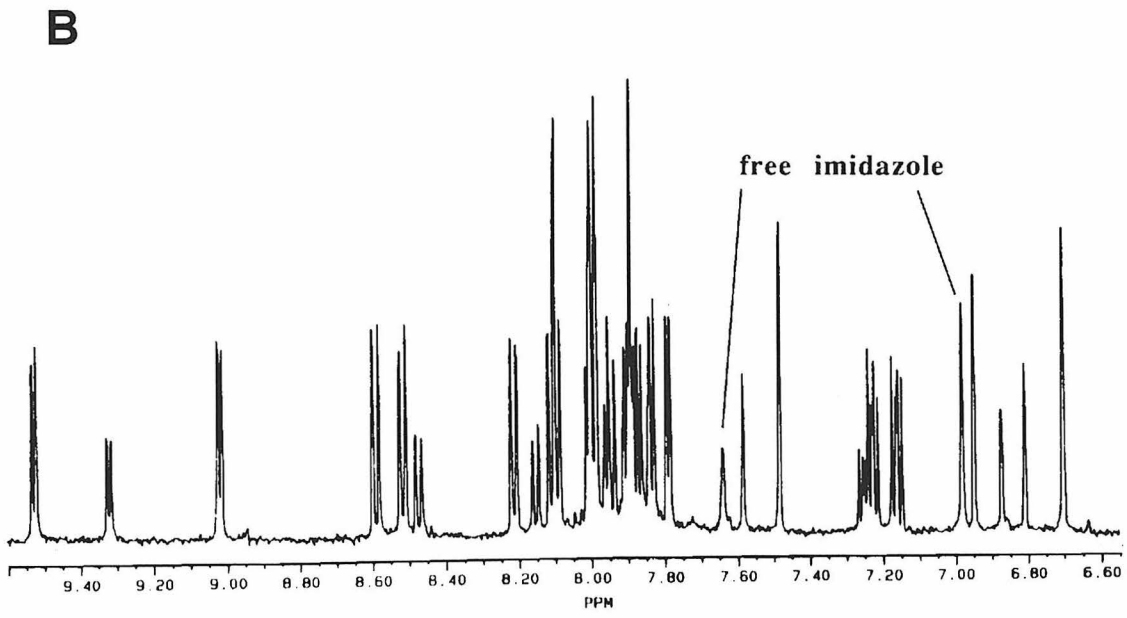
B
free imidazole
9.40
9.20
9.00
8.80
8.60
8.40
8.20
8.00
7.80
7.60
7.40
7.20
7.00
6.80
6.60
PPM

Figure 3.2. Oxidation of Ru(4,4'-$(CH_3)_2$-bpy)$_2$$(im)_2^{2+}$ (A) and Ru(4,4'-$(CONH(C_2H_5))_2$-bpy)$_2$$(im)_2^{2+}$ (B) by cyclic voltammetry. Potentials were measured vs. AgCl/Ag at a platinum working electrode in $\mu = 0.1$ sodium phosphate, pH 7.0.

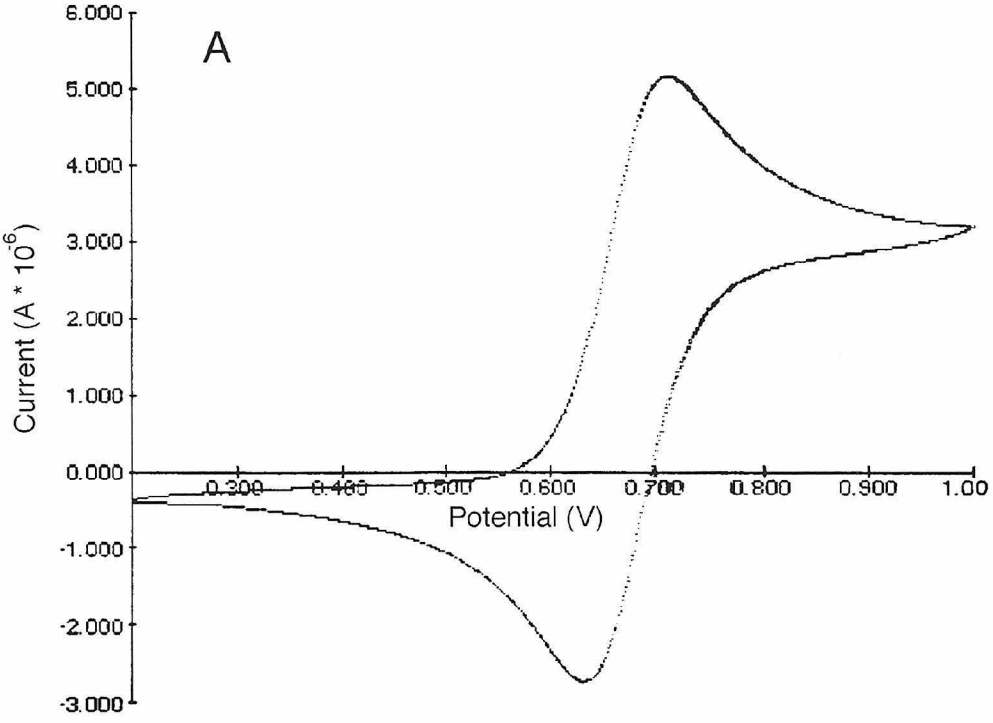
A
6.000
5.000
4.000
3.000
2.000
1.000
0.000
-1.000
-2.000
-3.000
Current (A * 10^-6)
0.300
0.400
0.500
0.600
0.700
0.800
0.900
1.00
Potential (V)

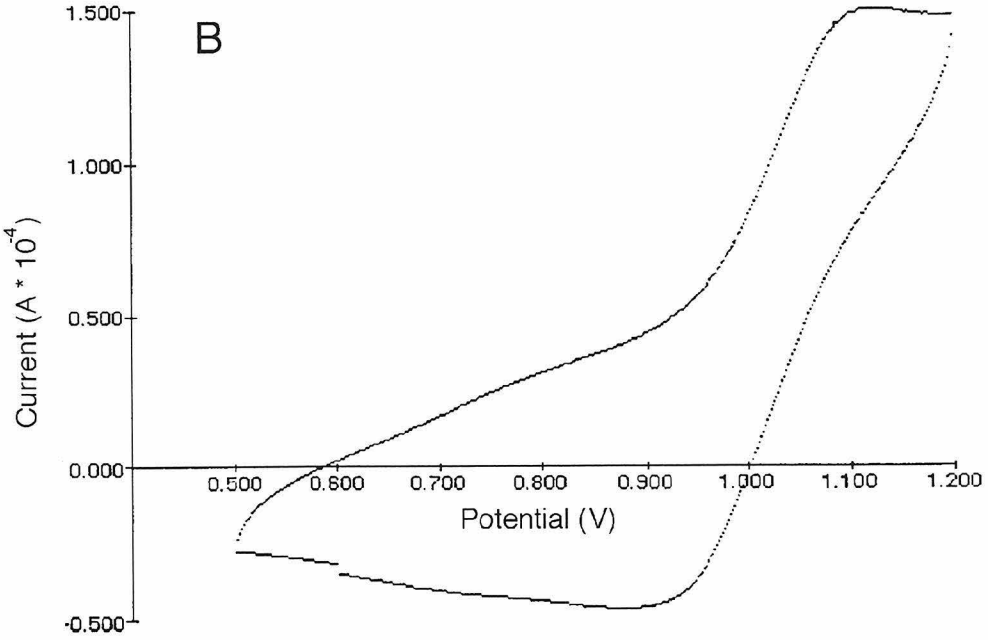
B
1.500
1.000
0.500
0.000
-0.500
Current (A * 10^-4)
0.500
0.600
0.700
0.800
0.900
1.000
1.100
1.200
Potential (V)

Figure 3.3. Reduction of $Ru(phen)_2(CN)(im)^+$ by cyclic voltammetry. The potential was measured vs. AgCl/Ag at an edge-plane graphite electrode in acetonitrile, and was corrected for the junction potential using ferrocenium/ferrocene as an internal standard (see text). 0.1 M tetrabutylammonium hexafluorophosphate was used as the supporting electrolyte.

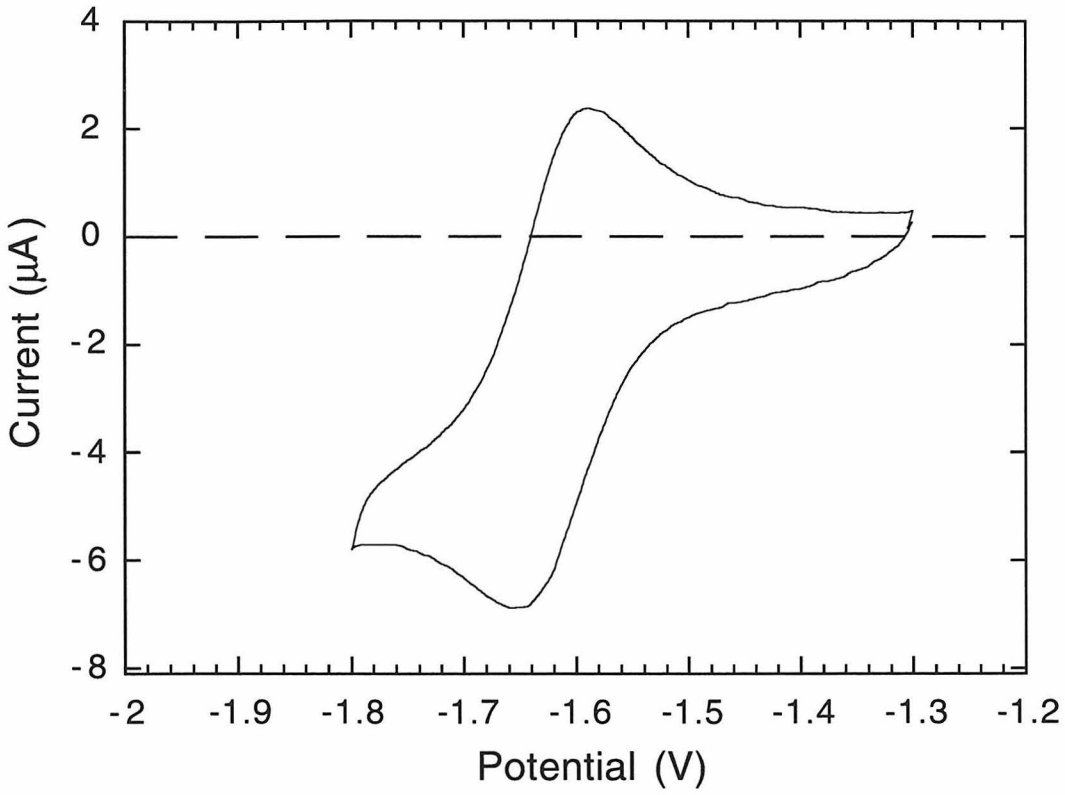
4
2
0
-2
-4
-6
-8
Current (μA)
-2
-1.9
-1.8
-1.7
-1.6
-1.5
-1.4
-1.3
-1.2
Potential (V)

Figure 3.4. Reaction sequences following excitation of Ru^{2+} on oxidized (***1***) or reduced (***6***) cytochrome *c*. Ru represents the various complexes in Table 2, and Fe represents the heme group of cytochrome *c*. Q_1 is $Ru(NH_3)_6^{3+}$; Q_2 is MeODMA.

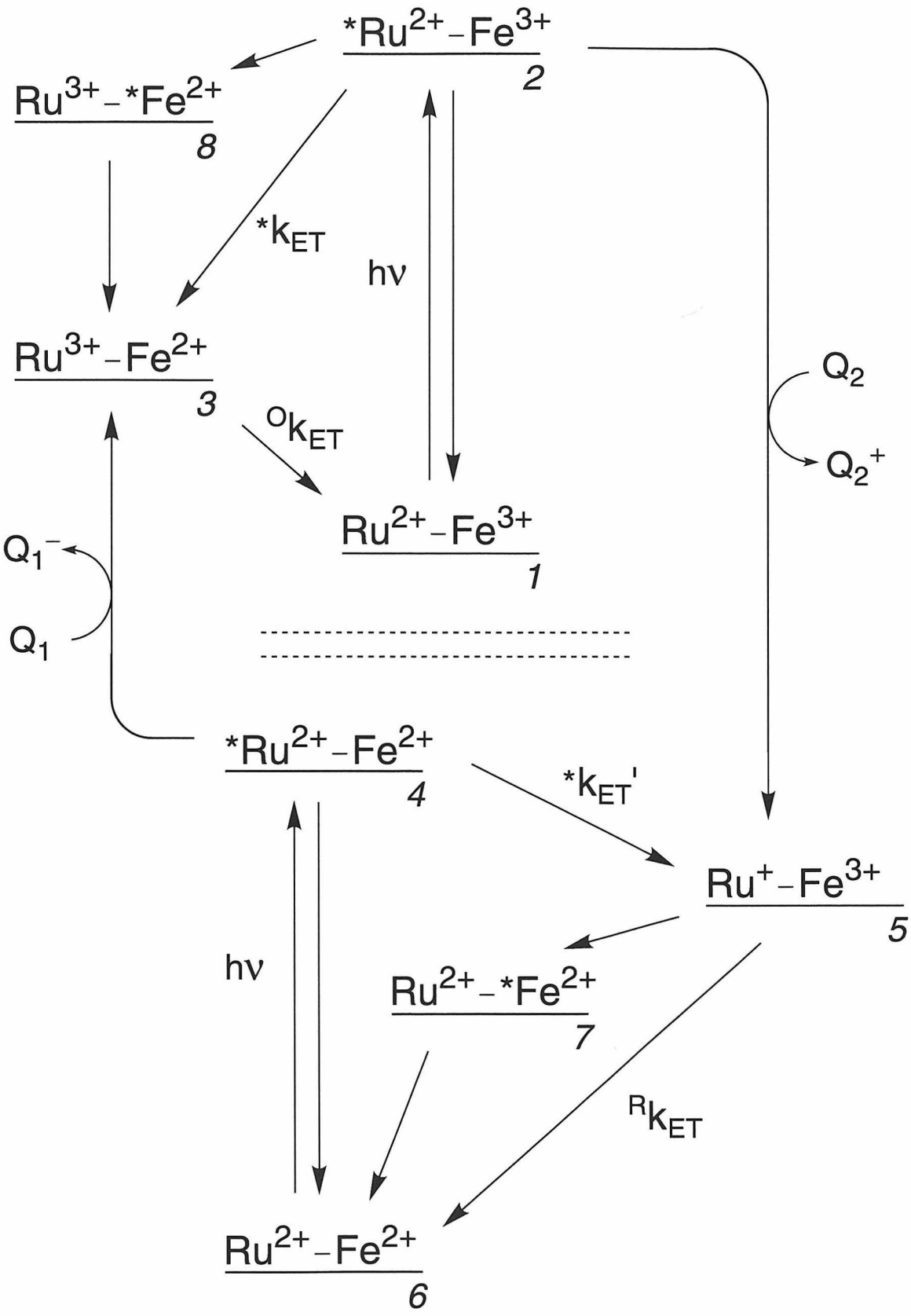
*Ru2+ – Fe3+
2
Ru3+ – *Fe2+
8
*kET
hν
Ru3+ – Fe2+
3
okET
Q2
Q2+
Ru2+ – Fe3+
1
Q1–
Q1
*Ru2+ – Fe2+
4
*kET'
Ru+ – Fe3+
5
hν
Ru2+ – *Fe2+
7
RkET
Ru2+ – Fe2+
6

Figure 3.5. Transient absorption kinetics following excitation of solutions of reduced Ru(4,4',5,5'-$(CH_3)_4$-bpy)$_2$(im)(His33)cyt *c* (A) and Ru(4,4'-$(CONH(C_2H_5))_2$-bpy)$_2$(im)(His33)cyt *c* (B) in the presence of $Ru(NH_3)_6^{3+}$ (Q_1). In (A), [Ru-cyt *c*] = 10 μM, [Q_1] = 6 mM, λ_{ex} = 480 nm, and λ_{obs} = 550 nm. In (B), [Ru-cyt *c*] = 20 μM, [Q_1] = 20 mM, λ_{ex} = 532 nm, and λ_{obs} = 420 nm. Smooth lines are best fits to a single exponential function (the excited state decay/quenching phase was not fit). Parameters and residuals are shown above each trace.

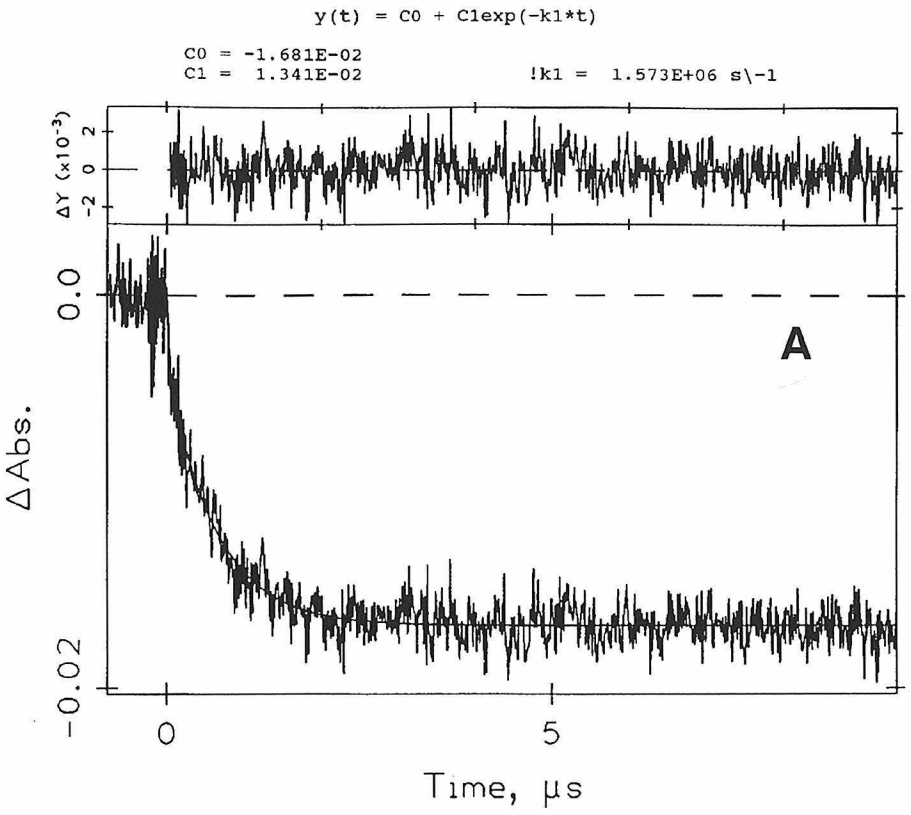
y(t) = C0 + C1exp(-k1*t)
C0 = -1.681E-02
C1 = 1.341E-02
!k1 = 1.573E+06 s\-1
ΔY (x10⁻³)
2
0
-2
0.0
-0.02
ΔAbs.
A
0
5
Time, μs

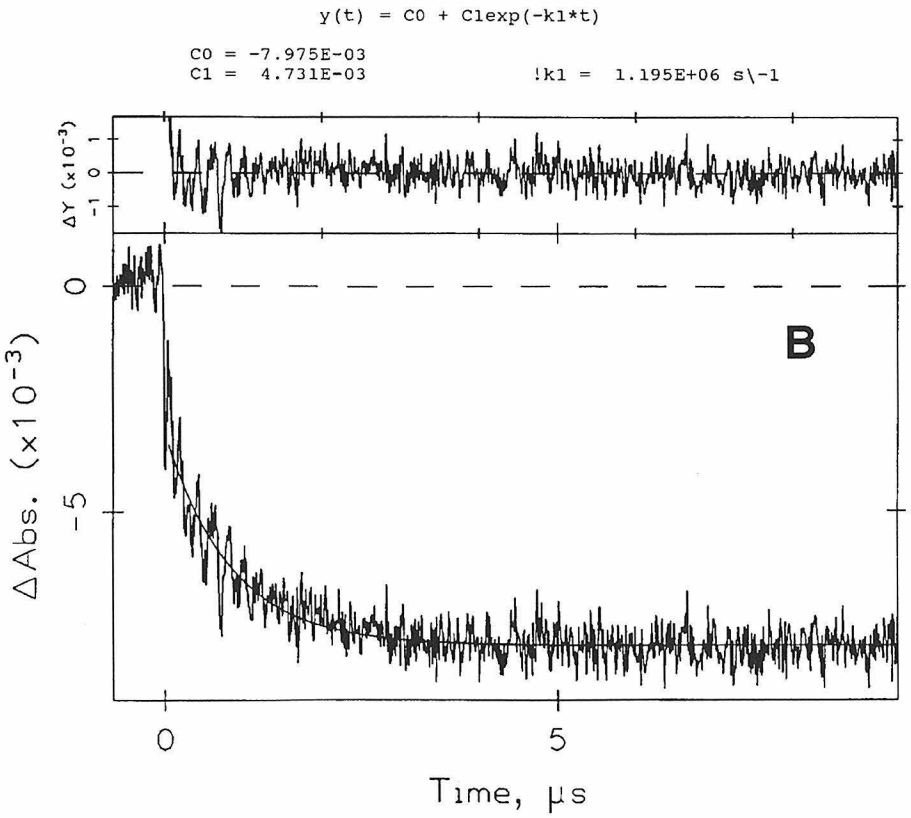
y(t) = C0 + C1exp(-k1*t)
C0 = -7.975E-03
C1 = 4.731E-03
!k1 = 1.195E+06 s\-1
ΔY (x10⁻³)
1
0
-1
0
-5
ΔAbs. (x10⁻³)
B
0
5
Time, μs

Figure 3.6. Transient absorption kinetics of a solution of reduced $Ru(phen)_2(im)(His33)cyt\ c$ (13 μM) and $Ru(NH_3)_6^{3+}$ (4 mM) monitored at 395 nm. The sample had been exposed to ~5000 laser shots before acquisition of this trace. Fits to a biexponential function (the excited state decay/quenching phase was not fit) is designated by the smooth line. The residual and fit parameters are shown above the trace.

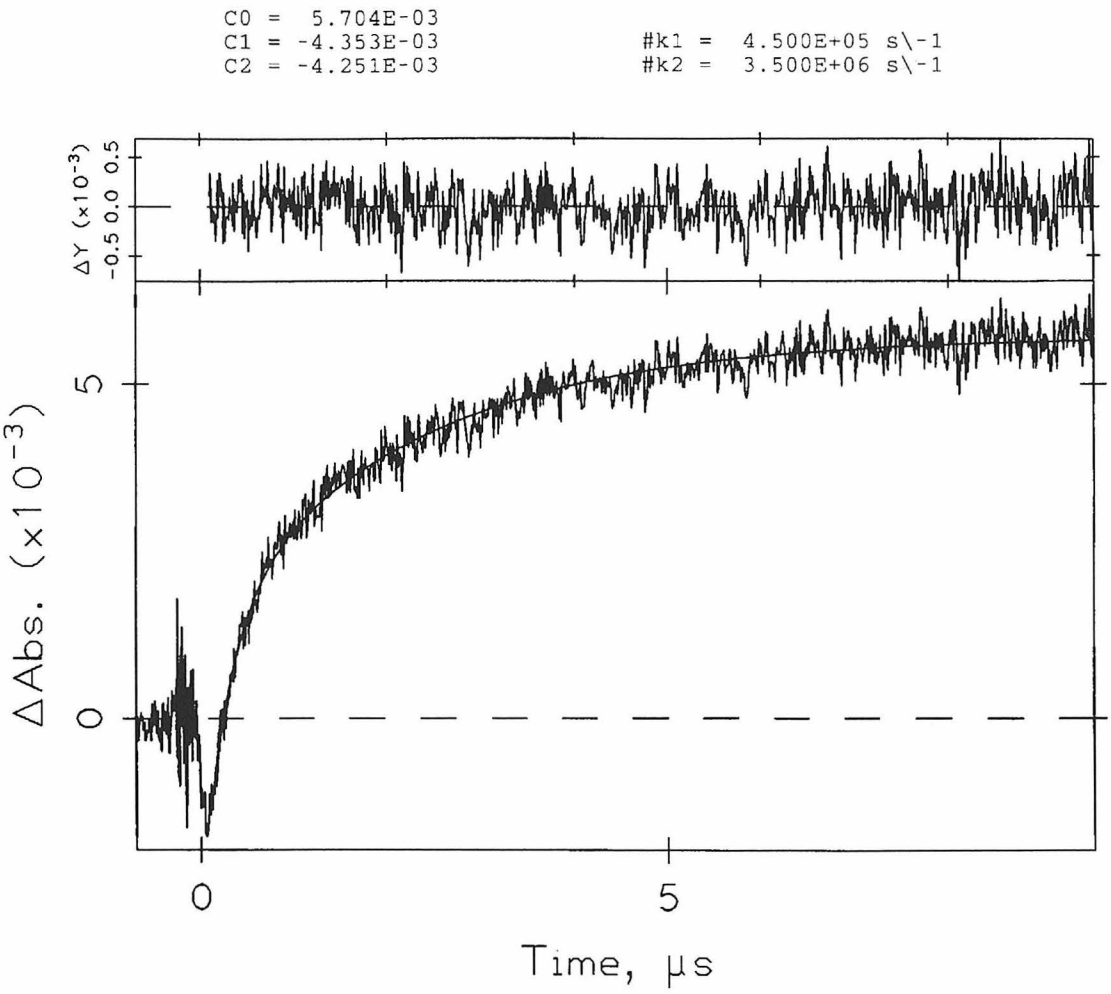
C0 = 5.704E-03
C1 = -4.353E-03
C2 = -4.251E-03
#k1 = 4.500E+05 s\-1
#k2 = 3.500E+06 s\-1
ΔY (x10-3)
-0.5 0.0 0.5
ΔAbs. (x10-3)
5
0
0
5
Time, μs

Figure 3.7. Oxidative flash-quench transient absorption kinetics of photolyzed $Ru(phen)_2(im)(His33)$cyt *c* (A) and pure $Ru(phen)_2(H_2O)(His33)$cyt *c* (B). (A) Kinetics after excitation of a solution of 20 μM reduced $Ru(phen)_2(im)(His33)$cyt *c* and 4 mM $Ru(NH_3)_6^{3+}$ which had been exposed to ~22000 laser shots prior to data acquisition. λ_{obs} = 395 nm. (B) Kinetics following excitation of a solution of reduced $Ru(phen)_2(H_2O)(His33)$cyt *c* (15 μM) and $Ru(NH_3)_6^{3+}$ (4 mM) λ_{obs} = 399 nm. The smooth lines represent best fits to a single exponential function (the excited-state decay/quenching phase was not fit) ($^{O}k_{ET}$ (A) = 4.5 x 10^5 s^{-1}; $^{O}k_{ET}$(B) = 4.3 x 10^5 s^{-1}). Residuals are shown above the trace.

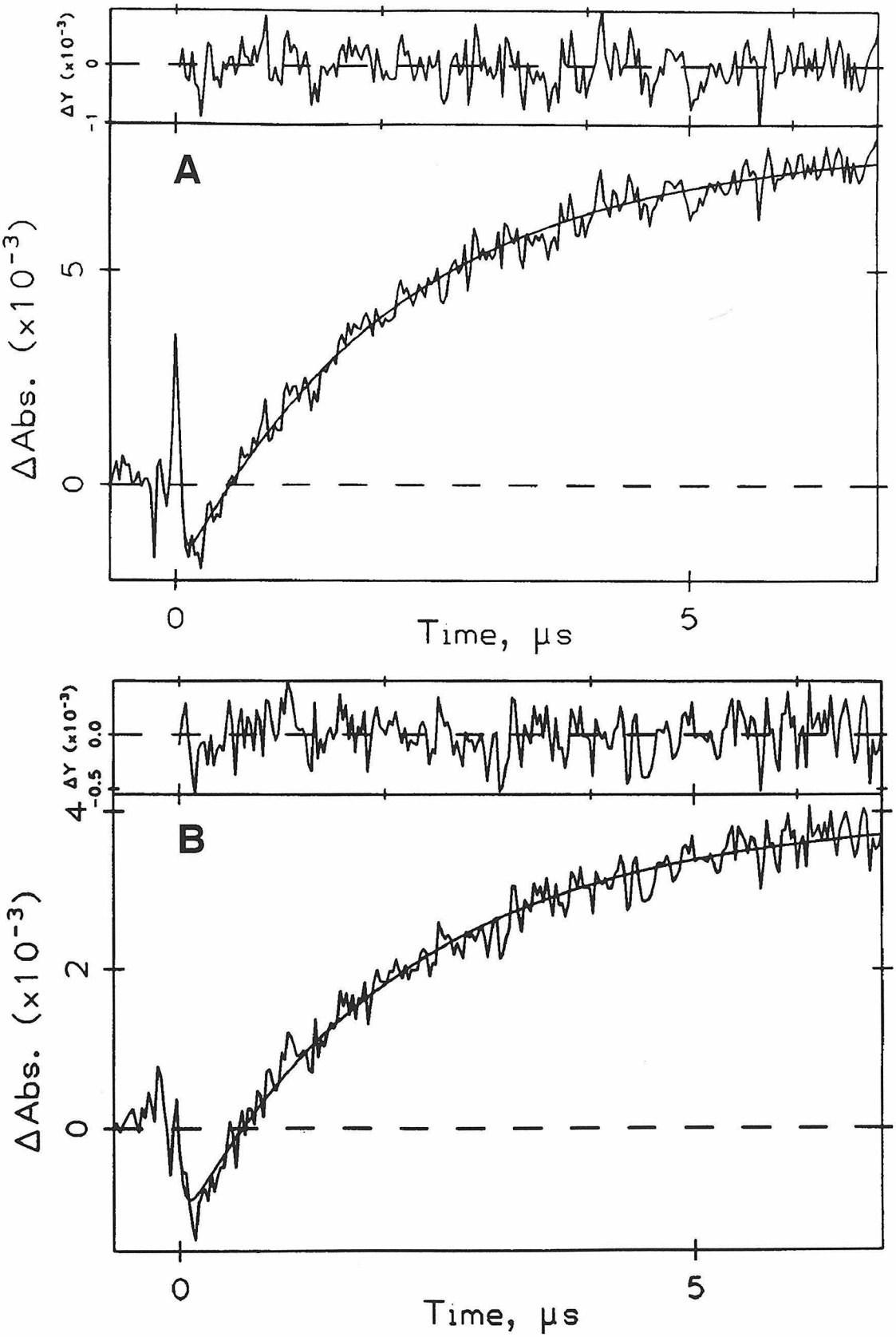
ΔY (x10⁻³)
0
-1
A
ΔAbs. (x10⁻³)
5
0
0
5
Time, μs
ΔY (x10⁻³)
4
0.0
-0.5
B
ΔAbs. (x10⁻³)
2
0
0
5
Time, μs

Figure 3.8. Kinetics following excitation of a solution of oxidized $Ru(bpy)_2(im)(His33)$cyt *c* (20 μM, without quencher, monitored at 420 nm (A) and 370 nm (B). Parameters corresponding to ΔAbs amplitudes were obtained from fits using fixed rate constants determined previously from emission decay profiles and flash-quench kinetics (values above trace marked with "#"). Residuals (above traces) indicate use of these rate constants yield adequate fits to the data. Values of $\Delta\varepsilon_{420}$ ($Fe^{2+} - Fe^{3+}$)cyt *c* = 44300 M^{-1} cm^{-1} (from Margoliash and Frohwirt) and $\Delta\varepsilon_{370}$ ($*Ru^{2+} - Ru^{3+}$) = 8050 M^{-1} cm^{-1} (from a power dependence study performed by Dr. I-Jy Chang) were used to calculate the concentration of Fe^{2+} and $*Ru^{2+}$ produced per laser flash.

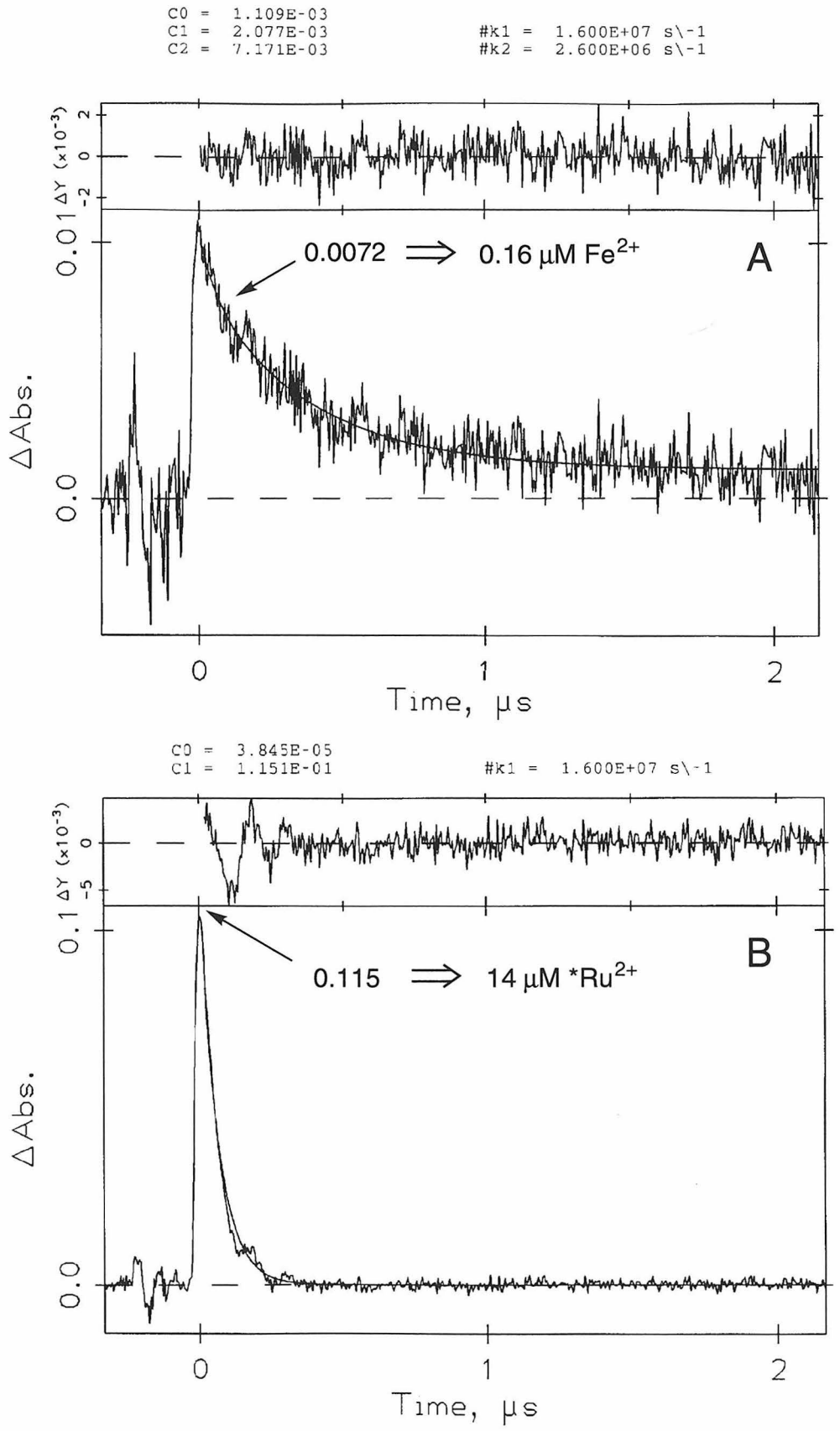
C0 = 1.109E-03
C1 = 2.077E-03
C2 = 7.171E-03
#k1 = 1.600E+07 s\-1
#k2 = 2.600E+06 s\-1
0.01 ΔY (x10⁻³)
2
0
-2
0.0072 ⟹ 0.16 μM Fe2+
A
ΔAbs.
0.0
0
1
2
Time, μs
C0 = 3.845E-05
C1 = 1.151E-01
#k1 = 1.600E+07 s\-1
0.1 ΔY (x10⁻³)
0
-5
0.115 ⟹ 14 μM *Ru2+
B
ΔAbs.
0.0
0
1
2
Time, μs

Figure 3.9. Reductive flash-quench traces produced after excitation of a solution of oxidized Ru(4,4'-(CONH(C_2H_5))$_2$-bpy)$_2$(im)(His33)cyt *c* (10 μM) and MeODMA (4 mM) monitored at 395 nm (A) and 550 nm (B). Single exponential fits to the second kinetic phase are shown by the smooth lines. The rate constants are identical at both wavelengths (see parameters for the fits above each plot). Residuals are shown above each trace.

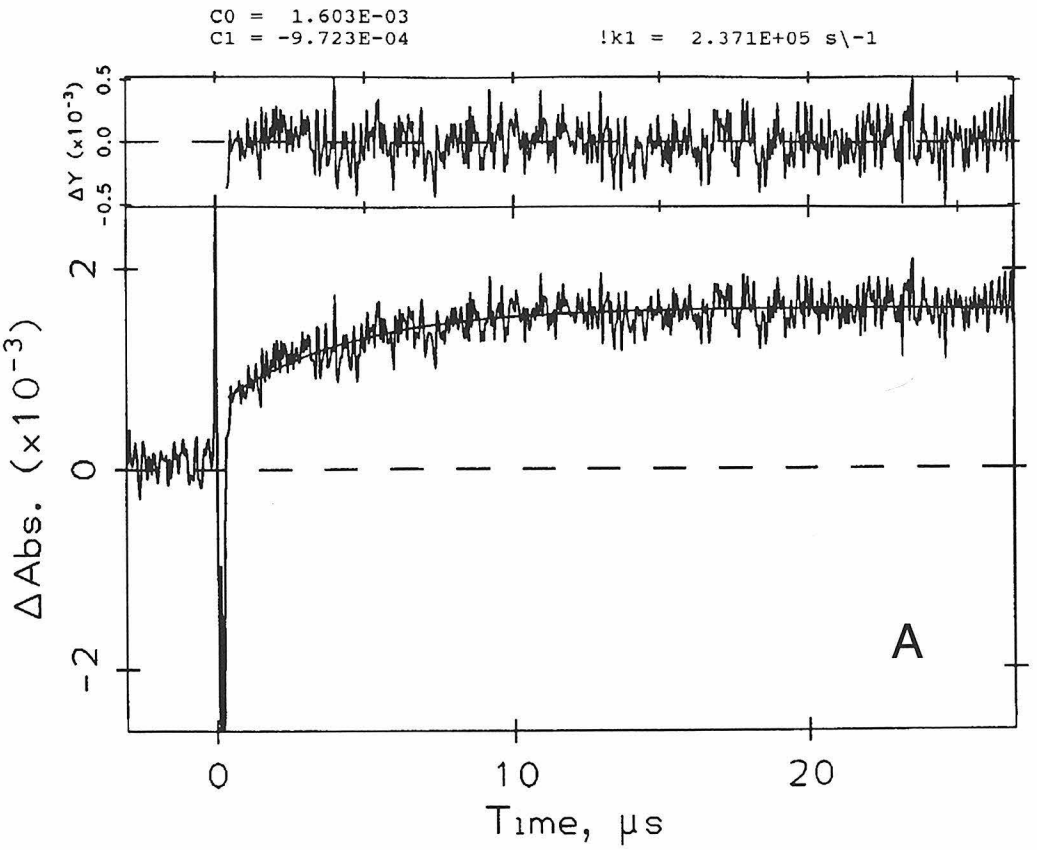
C0 = 1.603E-03
C1 = -9.723E-04
!k1 = 2.371E+05 s\-1
ΔY (x10⁻³)
0.5
0.0
-0.5
2
0
-2
ΔAbs. (x10⁻³)
A
0
10
20
Time, μs

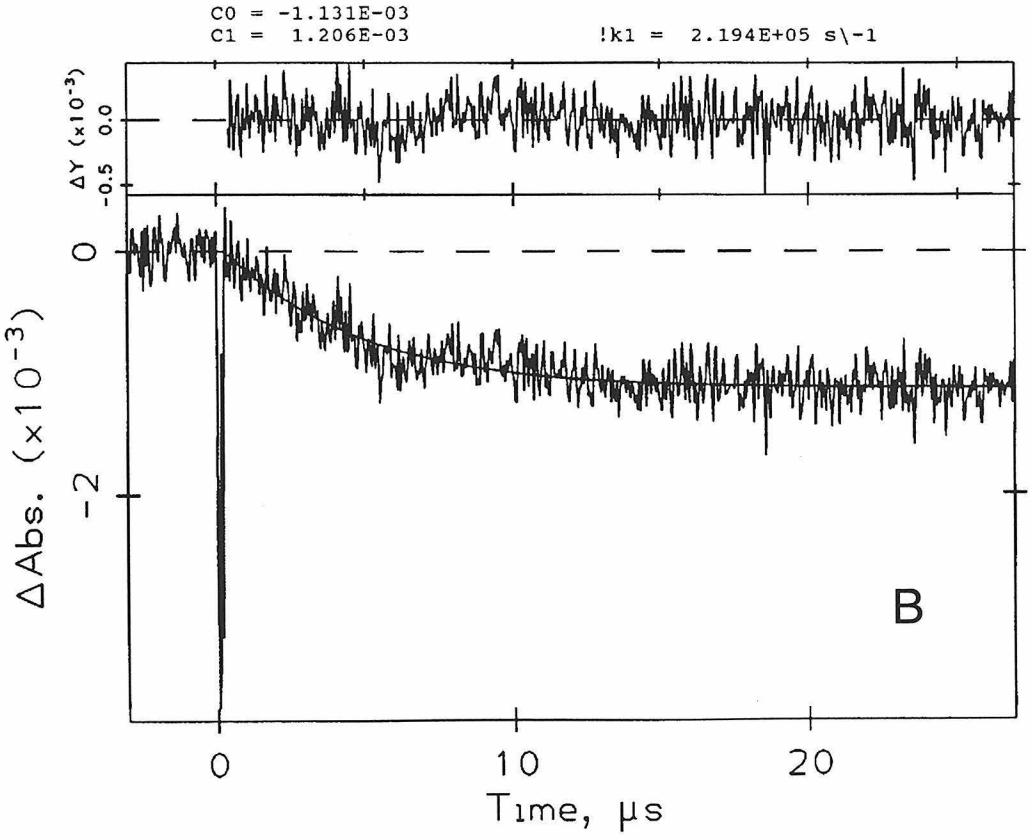
C0 = -1.131E-03
C1 = 1.206E-03
!k1 = 2.194E+05 s\-1
ΔY (x10⁻³)
0.0
-0.5
0
-2
ΔAbs. (x10⁻³)
B
0
10
20
Time, μs

Figure 3.10. Kinetics following excitation of reduced Ru(4,4'-(CONH(C_2H_5))$_2$-bpy)$_2$(im)(His33)cyt *c* (10 μM), with no quencher present, monitored at 550 nm (A) and 395 nm (B). Single exponential fits (smooth lines) yield rate constants identical to one another, and to those seen in Figure 3.9 (see parameters above plots). Residuals are shown above each trace.

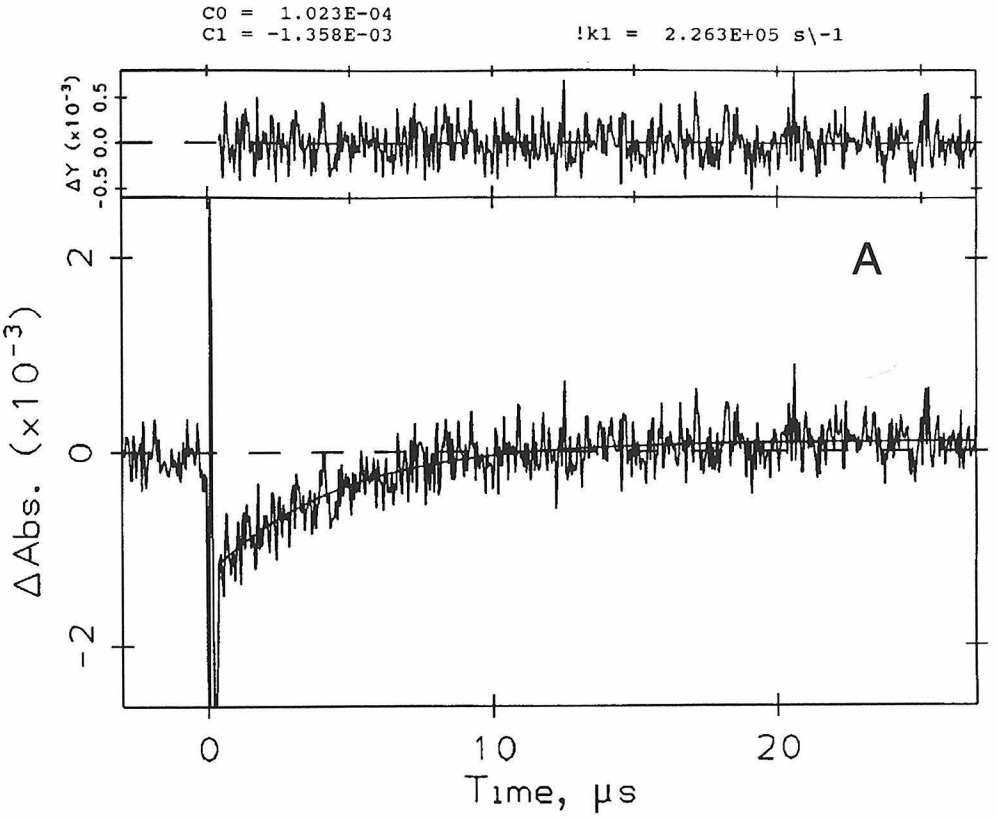
C0 = 1.023E-04
C1 = -1.358E-03
!k1 = 2.263E+05 s\-1
ΔY (x10⁻³)
-0.5 0.0 0.5
A
ΔAbs. (x10⁻³)
2
0
-2
0
10
20
Time, μs

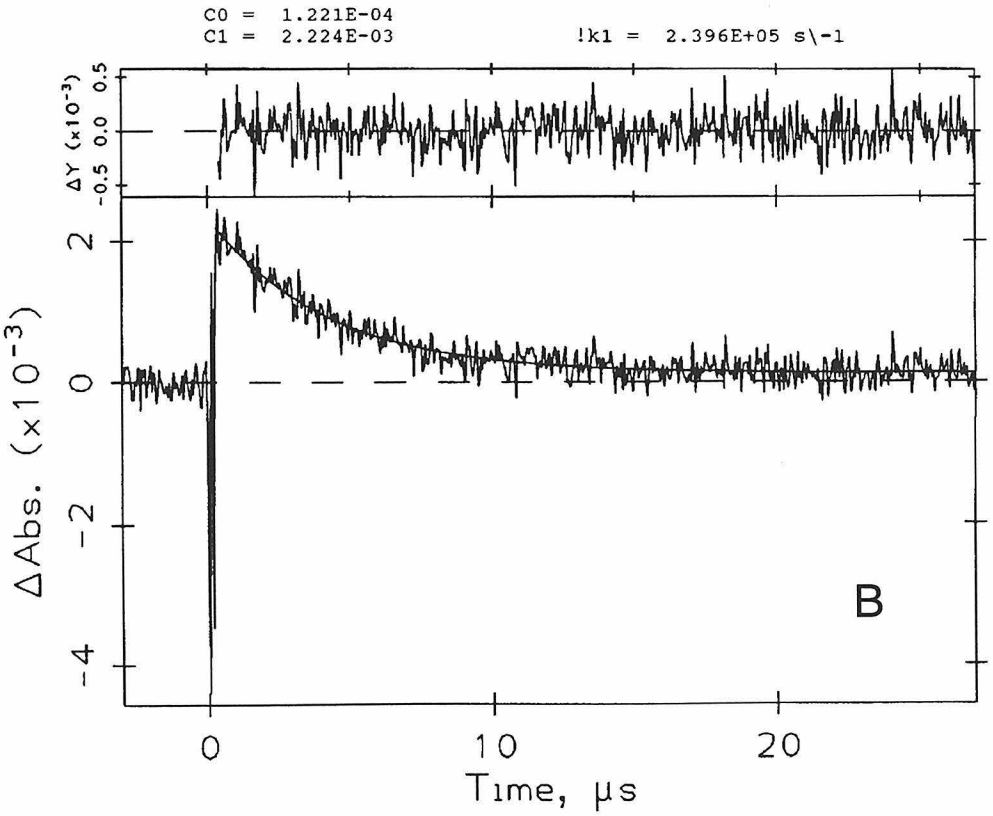
C0 = 1.221E-04
C1 = 2.224E-03
!k1 = 2.396E+05 s\-1
ΔY (x10⁻³)
-0.5 0.0 0.5
B
ΔAbs. (x10⁻³)
2
0
-2
-4
0
10
20
Time, μs

Figure 3.11. Driving-force ($-\Delta G°$) dependence of $Fe^{2+} \rightarrow Ru^{3+}$ rate constants in $RuL_2(im)$(His33)cyt *c*. The lines represent best fits to Equation 3.1. (A) Driving forces determined from the measured $Ru^{3+/2+}$ redox potentials for the model compounds $[RuL_2(im)_2^{2+}]$ corresponding to **I**, **III**, and **VI**. H_{AB} = 0.096(5) cm^{-1}; λ = 0.74(4) eV. (B) Driving forces determined using $Ru^{3+/2+}$ redox potentials for the three model compounds which are adjusted by assuming the values are 85 mV higher when the moieties are bound to His33 in cyt *c* (see text). H_{AB} = 0.100(5) cm^{-1}, λ = 0.83(4) eV.

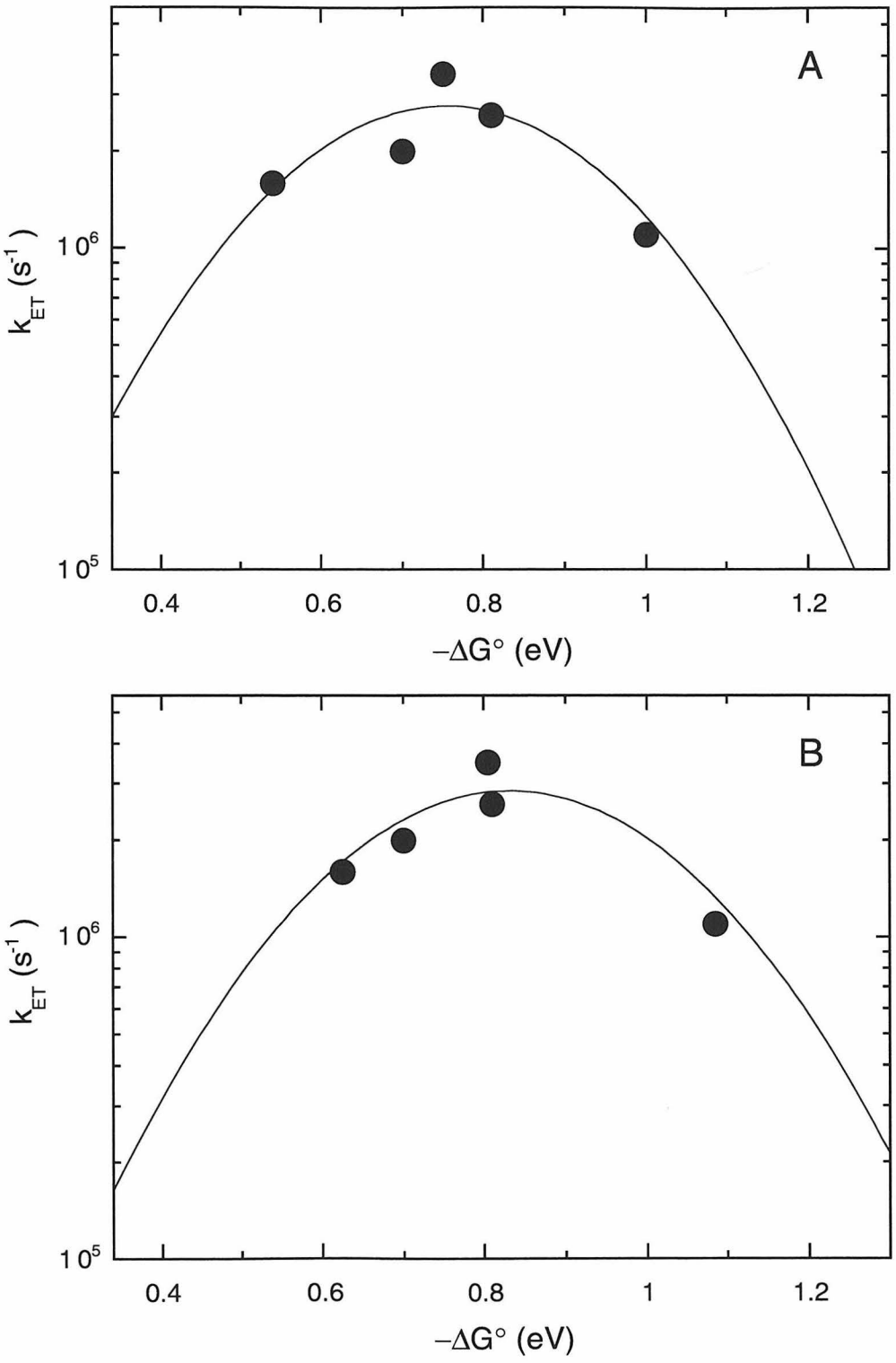
A
B
k_{ET} (s^{-1})
10^6
10^5
0.4
0.6
0.8
1
1.2
$-\Delta G°$ (eV)

Figure 3.12. Replot of the $k_{ET}/-\Delta G^{\circ}$ curves in Figure 3.11 with the addition of $Ru^{+}\rightarrow Fe^{3+}$ (rectangles) and $*Ru^{2+}\rightarrow Fe^{3+}$ (triangles) data. The open symbols represent reactions having rate constants significantly higher than predicted by the theoretical curve describing the $Fe^{2+}\rightarrow Ru^{3+}$ data. (A) and (B) are as described in Figure 3.11.

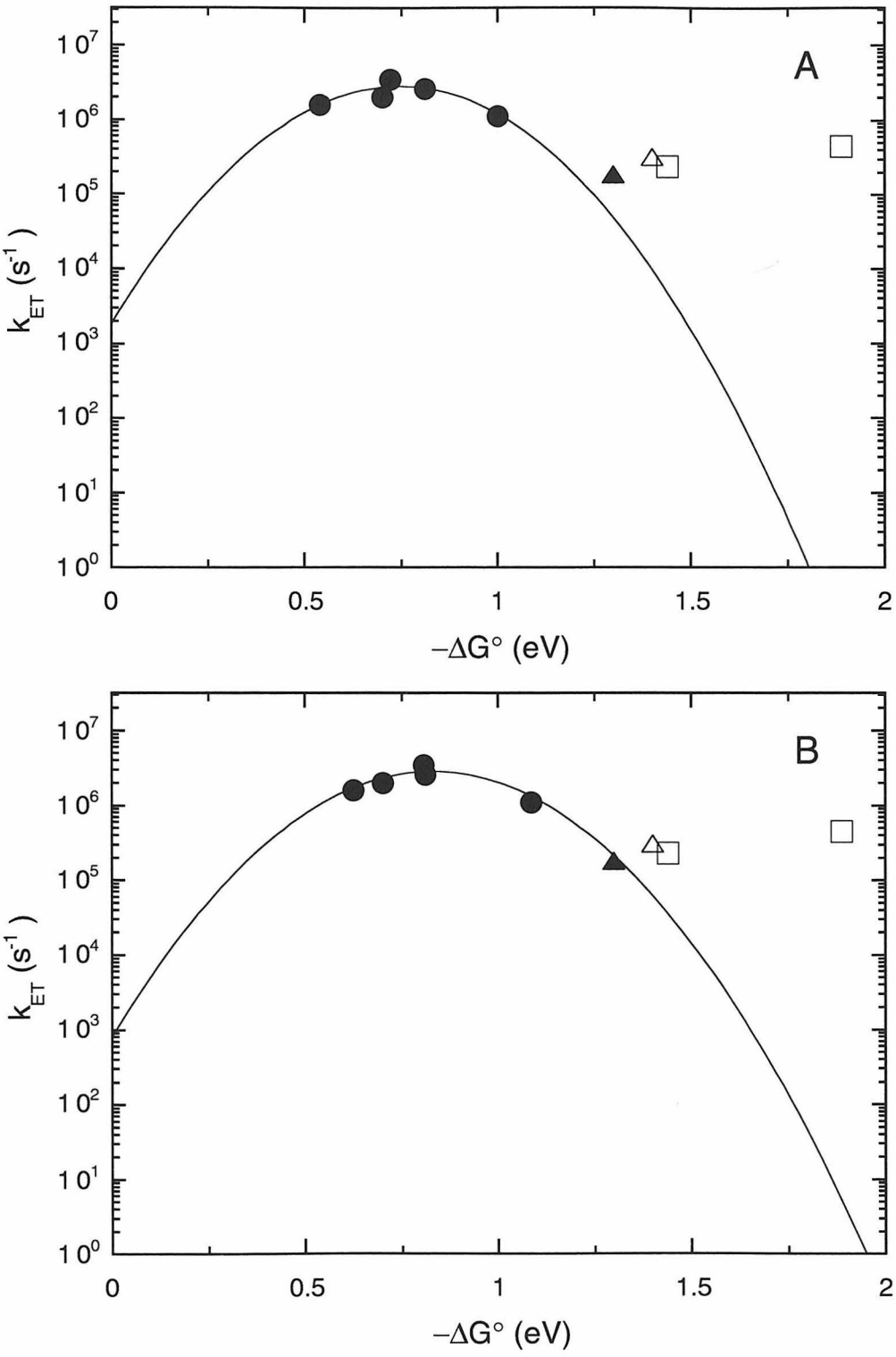
A
B
k_{ET} (s^{-1})
10^0
10^1
10^2
10^3
10^4
10^5
10^6
10^7
0
0.5
1
1.5
2
$-\Delta G°$ (eV)

Figure 3.13. vis/NIR spectrum of ferrocytochrome *c* in deuterated sodium phosphate buffer (μ = 0.1, pD = 7.0 [observed pH = 6.56]). The E^{00} of the lowest energy ^{1}MLCT state is estimated to lie at 1.3 eV. The ^{3}MLCT is too weak to be observed, but is estimated at 1.05 eV (the singlet-triplet energy gap is ~0.25 eV in $Fe(bpy)_3^{2+}$; Kober, E. M.; Meyer, T. J. *Inorg. Chem.* **1982**, *21*, 3967-3977).

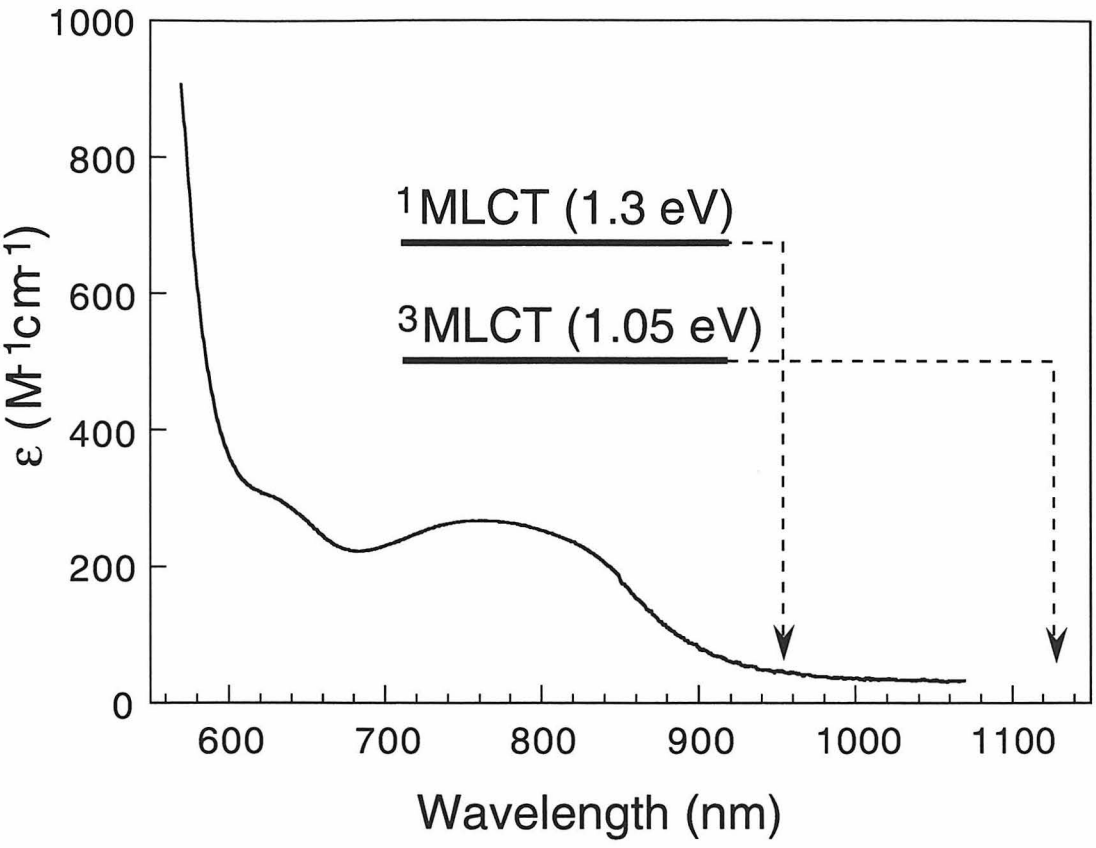
1000
800
600
400
200
0
ε (M⁻¹cm⁻¹)
¹MLCT (1.3 eV)
³MLCT (1.05 eV)
600
700
800
900
1000
1100
Wavelength (nm)

Figure 3.14. Replot of the $k_{ET}/-\Delta G^{\circ}$ curves and rate data in Figure 3.12 assuming that the highly exergonic reactions (gray symbols) involve formation of the ferroheme ^{3}MLCT excited state (~1.05 eV).

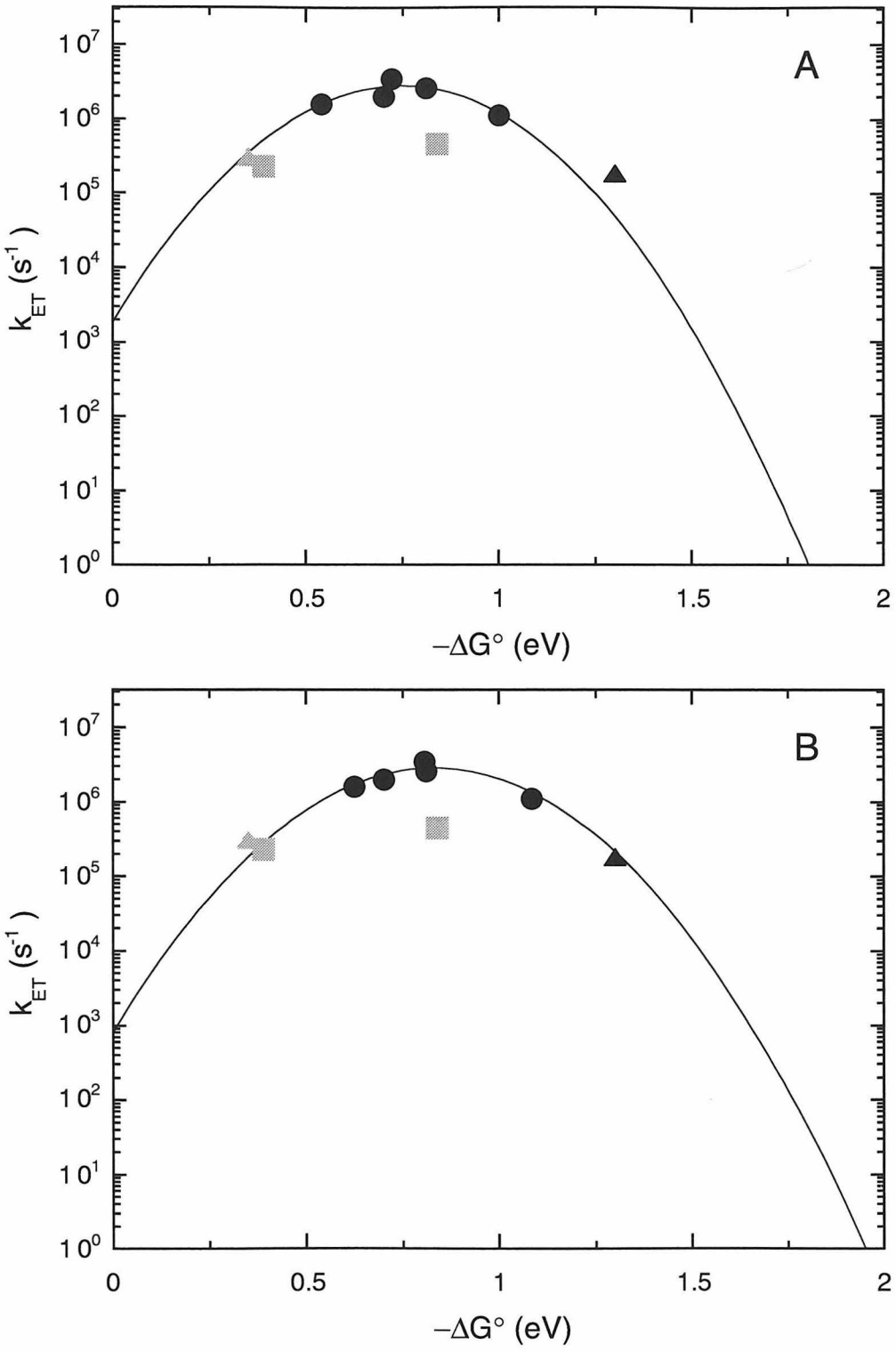
A
B
k_{ET} (s^{-1})
10^0
10^1
10^2
10^3
10^4
10^5
10^6
10^7
0
0.5
1
1.5
2
$-\Delta G°$ (eV)

Chapter 4

Cytochrome *c* Folding Triggered by Electron Transfer

Acknowledgment. The work involving horse cytochrome *c* at 40 °C presented in this chapter was performed by Torbjörn Pascher and John Chesick; they developed the reduction scheme based on $Co(C_2O_4)_3^{3-}$ photolysis which is described.[1]

In the previous chapters photophysical techniques were used to study the nature of intramolecular ET in cytochrome *c*. We now demonstrate an application of photoinduced electron transfer to a fundamental problem in biochemistry: protein folding.

INTRODUCTION

Determining the process by which a polypeptide attains its physiologically relevant conformation is an intriguing problem in biophysical and biochemical research. An experimental approach to solving this problem involves measuring the folding kinetics of proteins in order to elucidate the detailed mechanisms or pathways that are employed and to characterize the interactions which cause these pathways to prevail. A basic requirement for performing kinetic experiments is a means of triggering the event to be studied. The most common means of triggering protein folding involves stopped-flow mixing: solutions of unfolded protein in high concentrations of a chemical denaturant (typically guanidine hydrochloride (GuHCl) or urea) are rapidly mixed with buffer solutions in order to dilute the denaturant concentration to a level at which the folded form is favored. Although this methodology is very useful, it can only be used to observe folding processes which occur on timescales greater than ~1 ms, the minimum time required for solutions to physically mix. Secondary structure fluctuations in short polypeptides can occur on timescales as fast as nanoseconds;[2,3] these motions may play a role in dictating the early events in protein folding reactions.[4] It has also been suggested that the so-called "burst phase" in protein folding, referring to the formation of secondary structure and/or a hydrophobic core, occurs on a submillisecond timescale in many proteins.[5] Indeed, experimental evidence for a burst phase (≤ 5ms) has been reported in at least seven proteins or protein fragments: ubiquitin,[6] hen lysozyme,[7] ferricytochrome *c*,[8,9] ribonuclease A,[10] *trp* aporepressor,[11] barstar,[12,13] and the IgG binding domain of protein G.[14] If one includes measurements made by time-resolved circular dichroism,

which has a dead time of about 10-20 ms, about nine others can be added to the list.[15] Clearly, new techniques must be developed in order to probe these submillisecond events that occur in protein folding.

Several methods have recently been reported which break into this "ms" barrier.[16] Photodissociation of CO from reduced cytochrome *c* has been used to study folding processes occurring in the 10 ns to 1 ms time range.[17] Conventional temperature-jump methodology has been used to study a 300 μs folding event in barstar.[13] Laser-initiated temperature jump experiments were used to measure 250 ns and 3.5 μs kinetic phases in apomyoglobin.[18] Lastly, a continuous-flow mixing apparatus which can achieve time resolution down to 100 μs was used to study fast folding events in ferricytochrome *c*.[9] These methods are promising, but more techniques are needed to fully characterize the submillisecond kinetics of protein folding.

In this chapter, a new method of triggering protein folding using electron transfer is described which has the potential for initiating folding in nanoseconds or faster. This technique is used to investigate the relationship between folding rate and the free-energy of folding in ferrocytochromes *c* from horse (h-cyt *c*) and yeast (y-cyt *c*). These proteins have similar folds, but distinct stabilities due to differences in amino-acid sequence. We find that the rates of the major folding phase in the two proteins differ significantly at a given denaturant concentration, but are comparable when the free energies of folding are matched. This observation provides experimental support for theories suggesting folding free energy is a critical determinant of protein folding rates.

MATERIALS AND METHODS

Some materials and methods pertinent to this chapter are presented in the corresponding section of Chapter 2. Those introduced in this chapter are described below. Note: in this chapter, horse cytochrome *c* (h-cyt *c*) refers to type VI horse heart

cytochrome *c* purchased from Sigma. In addition, the oxidation and conformational states of cyt *c* in this chapter are specified by characters placed directly after the "*c*" in cyt *c*: superscripted Roman numerals (II or III) indicate the oxidation state of the iron, and subscripted capital letters (U or F, corresponding to "unfolded" or "folded") denote the conformational state (e.g., cyt c^{II}_F denotes reduced folded cytochrome *c*).

General

Guanidine hydrochloride (GuHCl), ultrapure grade, was used as received from United States Biochemical. $K_3[Co(C_2O_4)_3]$ was synthesized by Torbjörn Pascher using a published procedure.[19]

Yeast iso-1-cytochrome *c* (Cys102Ser)

The yeast cytochrome *c* protein used in this study (y-cyt *c*) was a mutant of *Saccharomyces cerevisiae* iso-1-cytochrome *c* containing serine at position 102 (h-cyt *c* numbering system) in place of cysteine in order to prevent interprotein disulfide formation.[20] Protein was isolated from 10 L cultures of a previously prepared GM-3C-2 cell line containing a plasmid with the mutant cyt *c* sequence;[21,22] the purification followed the procedure of Smith and coworkers,[23] with the following exception: after dialysis, the protein was loaded onto a cation exchange column (SP Sepharose, 4 cm x 2.5 cm i.d.), and eluted with a linear salt gradient (0 to 1 M NaCl, pH 7.0), rather than subjected to a batch adsorption procedure. Final purification was achieved using cation-exchange FPLC chromatography (Mono S; salt gradient, 0 to 1 M NaCl, pH 7.0); y-cyt *c* eluted at ~0.3-0.33 M NaCl.

Preparation of GuHCl Solutions

Stock solutions (10 or 25 mL) of GuHCl in 50 mM sodium phosphate buffer were prepared by mixing solid GuHCl with an appropriately scaled volume of concentrated (>100 mM) phosphate buffer in a disposable 30 mL graduated cup, dissolving all the

solid (adding nanopure water as necessary), transferring to a volumetric flask, and then diluting with nanopure water to the mark. The pH was adjusted to 7.0-7.3 using a concentrated (6-8 M) aqueous NaOH solution. Addition of phosphate before dilution was performed in order to ensure that the final phosphate concentration was identical in all GuHCl solutions, which was essential for accurately determining the concentration of GuHCl using refractive index measurements (see below). Note: when preparing solutions of >6 M GuHCl, care must be taken not to add too much water in the dissolution step; at these high concentrations, the volume of the solution increases as the solid dissolves, and dissolution occurs slowly (the reaction is endothermic, so warming the solution helps speed things up).

The pK_a of phosphate buffer is strongly dependent on ionic strength, and thus mixing of solutions of phosphate buffer at pH 7.0 with solutions of GuHCl at pH 7.0 can lead to significant lowering of the pH. A large pH shift occurs when a small volume of GuHCl is added to a large volume of phosphate buffer, but the change is fairly minor when a small volume of pH 7.0 phosphate is added to a large volume of pH-adjusted GuHCl/phosphate. Thus, distinct, pH-adjusted solutions of each desired GuHCl concentration were prepared rather than one "stock" solution of concentrated GuHCl. Protein solutions in GuHCl were made by adding a small amount of concentrated protein "stock" solution to 1-2 mL aliquots of the pre-prepared GuHCl solutions. This obviated the need to adjust the pH of every protein solution prepared for equilibrium or kinetic measurements. The pH of samples prepared in this fashion typically decreased by no more than 0.3-0.4 units from the initial (unmixed) value.

Refractive Index Measurements

The concentration of GuHCl in all solutions used in equilibrium or kinetic experiments was determined using the empirical relationship between the concentration

of GuHCl and the refractive index of GuHCl solutions measured by Nozaki and coworkers:[24]

$$[\text{GuHCl}] = 57.147(\Delta N) + 38.68(\Delta N)^2 - 91.60(\Delta N)^3 \quad (4.1)$$

where ΔN is the difference between the refractive index of each solution (N_D) and the refractive index of water (or buffer) ($N_D°$) (the subscript D denotes the light source: D line radiation from sodium). $N_D°$ of 50 mM sodium phosphate buffer was found to be 1.3342(5) (pure water is 1.3330). Refractive index measurements were made using a Milton Roy Abbe-3L Refractometer.

Preparation of Solutions for Equilibrium Unfolding Curves

Oxidized Cytochrome c

25 μL aliquots of a stock solution of ~350 μM ferricytochrome *c* and 0.800 mL aliquots of GuHCl solutions were delivered to 1.5 mL vials using appropriately sized gastight Hamilton syringes to create a series of solutions containing the same concentration of cyt *c* (~10 μM) and a varying concentration of GuHCl (0 M to ~6 or ~8 M). After a minimum of 10 minutes, the 0 M GuHCl solution was placed in a 1.0 x 0.4 cm quartz cuvette having four optically transparent windows, and the absorption and fluorescence spectra were recorded (see below). The 0 M solution was removed from the cuvette, and the next GuHCl solution was transferred to the cuvette for measurement. The cuvette was not rinsed between samples. This procedure was continued until the spectra of all of the samples had been obtained. Refractive index measurements were made on each sample after the experiment to obtain accurate (± 0.02 M) values of the concentration of GuHCl.

Reduced Cytochrome c

A procedure similar to the one outlined above was followed except that excess sodium dithionite ($Na_2S_2O_4$) was present in solution during the measurements, and each sample was prepared under argon just prior to being measured. Specifically, 0.67 g of sodium dithionite was degassed in a Schlenk tube, and 0.5 mL of degassed water was added via cannula under argon ($[S_2O_4^{2-}] = 0.77$ M). ~0.125 mL of ~350 μM ferricytochrome *c* was degassed by repeated pump-fill cycles in a 5 mL conical tube capped with a septum. ~1 μL of the dithionite solution was added to the cyt *c* solution using a gastight syringe (Hamilton). A 1 mL syringe was used to transfer 0.800 mL of the 0 M GuHCl solution to a 1.0 x 0.4 cm quartz cuvette fitted with a 2-3 inch vertical extension of glass tubing (by the manufacturer), and the solution was bubble-degassed with argon for two minutes. 0.5 μL of stock dithionite was added against positive argon pressure, the solution was mixed, and then 25 μL of reduced cyt *c* was added (via syringe) in like fashion (final concentrations: [cyt *c*] ~ 10 μM, $[S_2O_4^{2-}]$ ~500 μM). The tube supplying argon was removed slowly, the cuvette was capped immediately with a septum, and the sample was transferred to the spectrometer for measurement. Samples typically took 5-15 minutes to equilibrate (based on absorption changes); equilibration took longest at the highest GuHCl concentrations. The absorption peak ascribed to dithionite (λ_{max} = 316 nm) typically decreased slowly but steadily during this time, but clearly remained in vast excess throughout the course of both measurements. Although the same amount of stock dithionite solution was added to each sample, the concentration of dithionite, as monitored by the absorption peak at 316 nm, was seen to fluctuate from sample to sample, presumably as a result of the presence of varying amounts of residual oxygen in each sample. This procedure was repeated for all desired GuHCl solutions (working from low to high GuHCl concentration). All spectra in a given set were obtained on the same day, without any rinsing of the cuvette between samples.

Absorption and Fluorescence Measurements

Absorption spectra were measured using a Hewlett-Packard 8452 diode array spectrophotometer. Fluorescence spectra were measured using a Hitachi F-4500 fluorescence spectrophotometer (scan rate 240 nm/min; wavelength range 310-400 nm range; slits 5.0/5.0 nm; PMT 950V; automatic correction set). An excitation wavelength of 292 nm rather than 280 nm was used in order to diminish the relative yield of tyrosine fluorescence. The cuvette was oriented such that the incident beam traveled through the 1.0 cm pathlength in both experiments. The fluorescence was collected at 90° to the sample; thus it traveled through the 0.4 cm pathlength axis of the cuvette en route to the detector. Temperature was maintained using an HP 89090A Peltier Temperature Control Accessory (Hewlett Packard) for absorption measurements and a thermostatted circulating water bath (Lauda/Brinkman) for fluorescence measurements. An external thermocouple was used to determine actual cell temperature. *Note: it is particularly important in the fluorescence experiments to maintain a constant temperature among samples since the fluorescence yield of tryptophan is very sensitive to temperature.*

Corrections to Fluorescence Spectra

The quantum yield for fluorescence of a molecule (Φ_{fl}) equals the fraction of excited molecules which decay by emitting a photon of light:

$$\Phi_{fl} = \left(\frac{\#\ \text{photons emitted}}{\#\ \text{photons absorbed}} \right) \tag{4.2}$$

Φ_{fl} for Trp59 in cyt *c* is sensitive to the conformational state of the protein due to distance-dependent energy-transfer quenching by the heme group: when the protein is folded and the tryptophan is close to the heme, Φ_{fl} is near zero, but when the protein is unfolded and the average distance between the two moieties is large, Φ_{fl} increases

significantly.[25,26] This difference can be exploited to determine unfolding curves for cytochrome *c*.[27]

It is much easier to measure fluorescence intensities (F^{obs}) than quantum yields. Since F^{obs} is proportional to the number of photons emitted, it is evident that

$$\Phi_{fl} \propto \left(\frac{F^{obs}}{I_{abs}^{W}} \right) \tag{4.3}$$

where I_{abs}^{W} is the intensity of photons absorbed by the fluorophore tryptophan (W). Thus when I_{abs}^{W} is the same for two solutions, the ratio of the observed fluorescence intensities of the two solutions equals the ratio of the fluorescence quantum yields, and the F^{obs} values can be compared directly. This is the case for the oxidized cyt *c* unfolding determinations since solutions with equimolar concentration of protein are prepared and no other absorbers are present in solution. However, this is *not* the case for the reduced cyt *c* experiments due to the presence of variable amounts of another absorber, dithionite, in solution. In this case, some of the incident light gets absorbed by dithionite, thereby lowering the number of photons absorbed by tryptophan (I_{abs}^{W}). Note that the need for a correction arises *not* from the presence of another absorber in solution *per se*, but because *different amounts* of it are present in each sample. In this case only F^{obs}/I_{abs}^{W} values can meaningfully be compared; i.e., values of F^{obs} can be compared only if they are corrected for the difference in I_{abs}^{W}. The term $(I_{abs}^{W})^{-1}$ is thus considered a correction factor, and an expression for it in terms of experimental observables is derived below.

Let:

I_o = the intensity of light incident on the sample at the excitation wavelength

I = the intensity of light leaving the sample at the excitation wavelength

A^W = the absorbance due to tryptophan at the excitation wavelength

A^T = the total absorbance of the solution at the excitation wavelength

I_{abs}^W = the intensity of light absorbed by tryptophan at the excitation wavelength

I_{abs}^T = total intensity of light absorbed by the sample at the excitation wavelength

From these definitions it is evident that

$$I_{abs}^T = I_o - I \tag{4.4}$$

and from the definition of absorption:

$$A^T = \log\left(\frac{I_o}{I}\right) \Rightarrow I = I_o(10^{-A^T}) \tag{4.5}$$

Substituting Equation 4.5 into Equation 4.4 yields:

$$I_{abs}^T = I_o(1-10^{-A^T}) \tag{4.6}$$

It is asserted that the *fraction* of I_{abs}^T that is due to absorption by tryptophan is equal to the fractional absorbance of tryptophan in the solution:

$$I_{abs}^W = \frac{A^W}{A^T}(I_{abs}^T) \tag{4.7}$$

Substitution of Equation 4.6 into 4.7 gives:

$$I_{abs}^W = \frac{A^W}{A^T} I_o(1-10^{-A^T}) \tag{4.8}$$

and rearrangement leads to

$$\frac{1}{I_{abs}^W} = \frac{A^T}{(1-10^{-A^T})}\left(\frac{1}{A^W I_o}\right) \tag{4.9}$$

I_o is a constant in the experiments described in this report since the same spectrometer and cuvette are used for each sample. Typically only minor changes in the absorption spectrum of tryptophan are observed upon denaturation of proteins,[28] and for this derivation the assumption is made that the variation is insignificant compared with the differential absorption change caused by the presence of dithionite (i.e., A^W is a constant). Setting these constants arbitrarily to 1 for simplicity, the desired correction factor is obtained:

$$F^{corr} = F^{obs}\left[\frac{A^T}{(1-10^{-A^T})}\right] \tag{4.10}$$

A second correction factor is also necessary in the reduced cyt *c* experiments to correct for the fact that some of the fluorescence intensity is reabsorbed by the sample before emerging from the cuvette to reach the detector. As above, if this reduction were the same in all of the samples no correction would be required, but dithionite is present in varying amounts in each sample and absorbs at 350 nm, the observational wavelength for Trp fluorescence. To determine this correction, one approximates the actual (or corrected) fluorescence intensity to be an incident "beam" of intensity I_o, and the observed fluorescence intensity to be an emergent "beam" of an intensity I, with the light traveling through 0.2 cm of the 0.4 cm pathlength of the cell (half of the cell, on average) en route to the detector. From Equation 4.5 it follows that

$$I_o = I(10^{(0.2)A^T}) \tag{4.11}$$

where A^T represents the total absorption of the sample at the *observational* wavelength for fluorescence (measured through a 1.0 cm pathlength). Thus the secondary correction equation is

$$F^{corr} = F^{obs}(10^{(0.2)A^T}) \quad (4.12)$$

This correction was found to be minor compared to the excitation correction. Nonetheless, the product of both correction factors was used to calculate corrected relative fluorescence intensities.

Thermal Unfolding

The temperature dependence of the absorption spectrum of a solution of 10.6 μM oxidized y-cyt *c* in 0.18 M GuHCl was determined using an HP8452A UV/vis spectrometer fitted with an HP 89090A Peltier Temperature Control Accessory. The temperature was increased from 20 to 82 °C in increments of ≤ 5 °C. Solutions were equilibrated for ~7 minutes at each new temperature. The cuvette was capped with a septum throughout the experiment. After the spectrum at the highest temperature was recorded, the solution was reequilibrated at 25 °C for 25 minutes. Approximately 80% of the original signal was recovered.

Fitting the Equilibrium Unfolding Data

An unfolding equilibrium isotherm (also called an "unfolding curve" or "denaturation curve") describes how the fraction of unfolded protein in a sample (χ_u) varies with the concentration of a chemical denaturant. Unfolding curves for cytochromes *c* were generated from raw absorption or fluorescence data using a standard procedure.[29] Briefly, an assumption was made that only two states of the protein, the folded and unfolded forms, were present at equilibrium at any denaturant concentration:

$$\chi_u + \chi_f = 1 \quad (4.13)$$

where χ_f represents the fraction of folded protein. The y value (absorption or fluorescence value) at any denaturant concentration is thus equal to the sum of the individual contributions of the folded and unfolded states:

$$y = \chi_f y_f + \chi_u y_u \tag{4.14}$$

Substituting Equation 4.13 into 4.14 yields (after rearrangement):

$$\chi_u = \frac{y - y_f}{y_u - y_f} \tag{4.15}$$

The pre- and post-transition data were used to determine the (assumed) linear dependence of y_f and y_u on denaturant concentration:

$$y_f = m_f[\text{GuHCl}] + b_f \tag{4.16}$$

$$y_u = m_u[\text{GuHCl}] + b_u \tag{4.17}$$

Unfolding curves were fit to the following function using the program Kaleidagraph (Abelbeck/Synergy Software):

$$\chi_u = \frac{1}{1 - \exp\left(\frac{m_D([GuHCl]_{1/2} - [\text{GuHCl}])}{RT}\right)} \tag{4.18}$$

in which $[GuHCl]_{1/2}$ is the concentration of GuHCl at which half the protein is unfolded, and m_D is the slope relating the free energy of folding and [GuHCl]:[29,30]

$$\Delta G_f = \Delta G_f^\circ + m_D[\text{GuHCl}] \tag{4.19}$$

ΔG_f° is the free energy of folding with no GuHCl present. Equation 4.18 derives from the fact that in a two-state approximation, χ_u is related to the equilibrium constant for folding [$\chi_u = 1/(1 + K_f)$] which in turn is related to the free energy of folding ($\Delta G_f = -RT\ln K_f$) Note also that in this approximation $\Delta G_f^\circ = -m_D[GuHCl]_{1/2}$. Fitting with Equation 4.18 implicitly assumes that the linear relationship between ΔG and [GuHCl] holds over all denaturant concentrations.

Kinetics Experiments

Solutions containing 15 μM cyt *c* and 2-64 μM (typically 32 μM) $Co(C_2O_4)_3^{3-}$ (1.5 mL, μ = 0.1 sodium phosphate buffer, pH 7.0 ± 0.3) were Ar-degassed via repetitive (5 x 10 cycles each) pump/fill cycles on a Schlenk line in vacuum cells fitted with 1 cm quartz cuvette sidearms. Stock solutions of $Co(C_2O_4)_3^{3-}$ (~5 mM) were used within one day of preparation; light exposure was kept to a minimum. Kinetics were measured by laser-flash photolysis/transient absorption spectroscopy in the Beckman Institute Laser Resource Center. Samples were excited by 25 ns pulses (308 nm, 2-5 mJ/pulse) from a XeCl excimer laser (Lambda Physik LPX201i). Other instrumentation was as described in Chapter 2. Kinetic traces are averages of four laser shots collected at one shot per cycle with the sample stirred between each shot; each sample was subjected to no more than 20 shots in total.

Analysis of Kinetic Data

Kinetic traces were fit using the KINFIT program, which was written by Jay Winkler for the IBM-PC and adapted for use on a Macintosh computer by Torbjörn Pascher. Three different functions were used for fitting the kinetics occurring after the reduction phase (ΔA refers the transient absorption signal which is collected as a difference absorbance): a single exponential function,

$$\Delta A(t) = c_0 + c_1 e^{-k_1 t} \tag{4.20}$$

a biexponential function,

$$\Delta A(t) = c_0 + c_1 e^{-k_1 t} + c_2 e^{-k_2 t} \tag{4.21}$$

and a function which assumes a Gaussian distribution of activation free energies ($\leftrightarrow \ln k$):

$$\Delta A(t) = c_0 + c_1 \int_{-\infty}^{+\infty} G_{\ln \bar{k},\, \sigma}(\ln k) e^{-kt} d(ln\, k) \tag{4.22a}$$

where

$$G_{\ln \bar{k},\, \sigma}(\ln k) = \frac{1}{\sigma\sqrt{2\pi}} e^{-(\ln k - \ln \bar{k})/2\sigma^2} \tag{4.22b}$$

In the first two fitting functions, c_0 is the transient absorption signal at infinite time, c_n is the transient absorption amplitude of the nth kinetic phase, and k_n is the rate constant of the nth kinetic phase. In the third fitting function (referred to hereafter as the "distributed fit"), c_0 is the transient absorption signal at infinite time, and c_1 can be thought of as the amplitude of a kinetic "phase" associated with a distribution of first order rate constants characterized by $\bar{k}$, the rate at the mean activation free energy. σ is the width of the Gaussian distribution (of the activation free energy) and reflects the degree of heterogeneity of the sample; as σ goes to zero, the distribution approximates a delta function, and the fit becomes that of a single exponential function (Equation 4.20).

Single exponential fits were satisfactory for some but not all of the traces; biexponential fits and distributed fits were adequate for all data. Further discussion on this point is deferred until the Results and Discussion section. It should be noted that the

distributed fit algorithm in the current version of KINFIT (β0.3.0, Macintosh) does not converge well; it is often necessary to manually adjust both parameters during the fit to determine if a global minimum has actually been reached. One should use this algorithm very carefully.

Calculation of Folding Rate Constants

Kinetics data presented in this chapter are generally consistent with a model in which the observed kinetic phase after reduction of cyt c^{III}_U under folding conditions corresponds to the sum of two processes: folding and reoxidation (Figure 4.13). In this model, rate constants for folding are extracted from the observed rate constants by multiplying k_{obs} (or $\bar{k}_{obs}$) by the fractional yield of protein folded (Φ_f) (Note the similarity to Equations 2.4 and 2.6):

$$k_{obs} = k_{ox} + k_f \tag{4.23}$$

$$\Phi_f = \frac{k_f}{k_{ox} + k_f} = \frac{k_f}{k_{obs}} \quad \Rightarrow \quad k_f = \Phi_f k_{obs} \tag{4.24}$$

When calculating k_f values from data fitted with a biexponential function, only the fast kinetic phase, which was predominant in all cases, was considered. In the case of the distributed fit model the assumption is implicitly made that the distribution of activation free energies is the same in the folding and oxidation reactions, which need not be the case. The yield of folding was determined by converting the appropriate transient absorption amplitudes (fit parameters) to absolute concentrations using Δε values (at the appropriate wavelengths) for reduced unfolded and reduced folded cyt *c* obtained from optical unfolding equilibrium data:

$$\Phi_f = \frac{\text{cyt } c^{II}{}_F}{\text{cyt } c^{II}{}_U} = \frac{\Delta A_F / \Delta \varepsilon_F}{\Delta A_U / \Delta \varepsilon_U} \tag{4.25}$$

In principle, $\Delta\varepsilon$ values are a function of [GuHCl] and temperature, and need not be identical for yeast and horse cyt *c* proteins. In many cases, however, absorption unfolding data were quite noisy, masking potential differences between proteins, and making extrapolation to different values of [GuHCl] unjustified. For the wavelengths used in our experiments (400, 420, and 550 nm), the pre- and post- transition slopes in the best (least noisy) sets of absorption data (h-cyt *c* at 22.5 °C; Figures 4.10, 4.11) are relatively small, leading to maximal differences between extrapolated and non-extrapolated $\Delta\varepsilon$ values of ~5-10%. These uncertainties are dwarfed by the errors associated with the observed rate constants (see below), and calculation of rate constants in the h-cyt *c* kinetics data set (at 22.5 °C) using constant, unextrapolated values for $\Delta\varepsilon$ yielded rate constants very similar to those obtained using extrapolated values. Furthermore, a temperature unfolding experiment revealed only small spectral changes (~2%) at 400, 420, and 550 nm in cyt c^{III} between 22.5 and 40.0 °C. Given these observations, we elected to use constant values determined from the h-cyt *c* unfolding curves at 22.5 °C to calculate Φ_f in yeast and horse experiments at both temperatures [$\Delta\varepsilon_F$: –46500, 66800, and 21800 M^{-1} cm^{-1} (400, 420, and 550 nm respectively); $\Delta\varepsilon_U$, –53200, 84500, and 13600 M^{-1} cm^{-1} (see Figure 4.9)].

RESULTS AND DISCUSSION

Description of Technique

This study describes a new method for initiating protein folding using electron-transfer (ET) chemistry. Our approach is based on the observation that the formal potentials for metals in redox proteins are often "tuned" by the folding of the polypeptide

chain around them; that is, metals in the hydrophobic interior of a folded protein often exhibit redox potentials which are significantly different from those they would possess in an aqueous environment.[31] A simple thermodynamic cycle (Figure 4.1; P represents a redox protein)[32] indicates that such a shift in redox potential ($\Delta E_{F-U} = E_F - E_U$) reflects a difference in conformational stability between the two redox forms of the protein ($-nF\Delta E_{F-U} = \Delta\Delta G_{f,\,red-ox} = \Delta G_{f,\,red} - \Delta G_{f,\,ox}$). If this stability difference is sufficiently large, it should be possible to find conditions at which one redox form of the protein is unfolded and the other form is folded. For example, if the reduced form of the protein (P_{red}) is more stable than the oxidized protein (P_{ox}), it is expected that a higher concentration of a chemical denaturant will be required to unfold the reduced protein compared to the oxidized protein (Figure 4.2A). In solutions for which the denaturant concentration value lies between the two unfolding curves, reduction of the oxidized protein (unfolded) will lead to the formation of folded reduced protein (Figure 4.2A, arrow). If the reduction is rapid enough, the folding of the reduced protein can be observed (Figure 4.2B). In this scenario, the initiation is limited only by the rate of the electron transfer since no mixing is involved. Owing to the many well established techniques for reducing or oxidizing proteins on time scales on the microsecond timescale or shorter,[33,34] this technique offers promise for studying very early events in protein folding.

The utility of this technique is demonstrated by studying folding in the electron-transfer protein cytochrome *c*. Two features in particular make this protein a good candidate for ET-triggered folding studies. First of all, the heme group is linked to the polypeptide through covalent (thioether) bonds to Cys14 and Cys17. This prevents the heme from diffusing away upon unfolding, thus ensuring that upon reduction, the rate-limiting step is folding instead of bimolecular heme rebinding. Secondly, it is known that the redox potential of folded cyt *c* (260 mV vs. NHE)[35] is ~400 mV higher than the

potential for an exposed heme in aqueous solution (~−150 mV),[36] indicating that the reduced form of the protein is substantially more stable than the oxidized form.[32,37] Thus a wide "window" of denaturant concentrations is predicted for which folding can be triggered by a rapid reduction of the heme. In fact, reduction of GuHCl-unfolded h-cyt c^{III} using electrochemical methods has been shown to yield recovery of a native redox potential, indicating folding.[32] This methodology, however, could not yield kinetic information beyond an upper limit of ~100 ms. Our approach utilizes photoinduced electron transfer, and is therefore capable of accessing kinetic data down to microseconds or faster in principle.

Equilibrium Unfolding Curves

Fluorescence Data

The degree of folding of cyt *c* has been determined by monitoring the intensity of fluorescence from tryptophan 59.[27] The fluorescence is nearly completely quenched in the folded state, presumably via energy transfer to the heme group, due to the proximity of the two chromophores.[25] As the protein is unfolded by denaturant, the distance between the two moieties increases, and the fluorescence signal intensifies dramatically[26] (Figure 4.3).

Unfolding curves generated from fluorescence data for h-cyt *c* and y-cyt *c* in both oxidation states at 22.5 °C and 40.0 °C are well described as two-state transitions in which the free energy of folding is a linear function of denaturant concentration (Figures 4.4, 4.5; Equation 4.19). It is evident from the unfolding curves that at both temperatures in both species of cyt *c*, the reduced form is considerably more stable than the oxidized form, as predicted from electrochemical data. Indeed, the extrapolated values of $\Delta\Delta G_{f,\,red-ox}$ to zero denaturant concentration ($\Delta\Delta G°_{f,\,red-ox}$ = −30 to −35 kJ mol^{-1}; Table 4.1) are close to those estimated from the difference in redox potentials ($\Delta E_f°$ ~ −400 mV = −39 kJ mol^{-1}). It is also seen that in both oxidation states at both

temperatures, y-cyt *c* is considerably less stable than the corresponding h-cyt *c* protein: the ΔG_f values extrapolated to zero GuHCl concentration (ΔG_f°) are ~15 kJ mol^{-1} more positive for y-cyt *c* than for h-cyt *c*, and the unfolding midpoints occur at GuHCl concentrations ~1.5 M lower for y-cyt *c* than for h-cyt *c* (Table 4.1). The observed $[GuHCl]_{1/2}$ and m_D values for h-cyt c^{III} and y-cyt c^{III} at 22.5 °C are consistent with values reported in prior determinations at similar conditions using identical (or nearly identical) proteins.[38-40] The same is true for the values found for y-cyt c^{II} at 22.5 °C.[40]

The stability differences between y-cyt *c* and h-cyt *c* must arise from the side chain variability between the two proteins. Despite the nearly identical backbone folds of h-cyt *c* and y-cyt *c* (about 80% of the main chain to main chain hydrogen bonds are conserved between h-cyt *c* and y-cyt *c*, and the average deviation between main chain atoms is just 0.45 Å),[41] the two sequences are just 60% identical (Figure 4.6).[42] Examination of the X-ray crystal structures of the two proteins reveals that the majority of the changes occur at surface residues, whereas the most highly conserved side chains are those which form the heme environment or are near the exposed heme edge.[41,43,44] This is likely due to the fact that the latter residues play a key role in determining the redox potential of the heme, which allows the protein to carry out its physiological ET function. Six distinct domains can be identified in cytochrome *c*: three α-helical regions (amino terminus, residues 1-13; carboxy terminus, 86-104; 60's helix, 61-69), and three omega loops (residues 20-35, 36-60, and 70-85).[45] Only two of these regions, the 20-35 and 70-85 loops, display a high degree of sequence conservation (> 80% identical) between y-cyt *c* and h-cyt *c*.[42] The amino- and carboxy-terminal helices display the lowest degree of similarity (58% and 37% respectively).

Absorption Data

We have also measured the absorption spectral changes that accompany unfolding of cyt *c* by GuHCl. The primary change observed for oxidized h-cyt *c* at 22.5 °C and pH

7 is a slight shift of the Soret band to higher energy with an accompanying increase in extinction coefficient (Figure 4.7). Changes for the reduced protein (22.5 °C, pH 7) include a small shift to lower energy with an increase in extinction coefficient for the Soret band, and a very slight shift to lower energy with a decrease in extinction coefficient for the peaks at 520 and 550 nm (Figure 4.8).

The spectrum of cyt *c* is dominated by the heme group, and thus the observed absorption changes reflect either differences in axial ligation or heme environment that occur upon unfolding.[46] The axial histidine remains bound to the heme upon unfolding of the oxidized protein at pH values above ~2.5;[47] the axial methionine, however, is thought to be displaced by non-native histidine residues upon denaturation by GuHCl at pH 7.[9,48] Reduced unfolded cyt *c* is less well characterized, but presumably the axial histidine remains bound and the methionine is replaced by another ligand at pH 7.

Difference spectra corresponding to the species expected in the kinetic experiments, the unfolded reduced (cyt c^{II}_U – cyt c^{III}_U) and folded reduced (cyt c^{II}_F – cyt c^{III}_U) proteins, exhibit similar overall shapes, but differing extinction coefficients near 400, 420, and 550 nm, the wavelengths used for most kinetic measurements (Figure 4.9). This difference is more clearly illustrated by plotting the $\Delta\varepsilon$ values at these wavelengths as a function of GuHCl (Figures 4.10, 4.11). Although the pre- and post-transition slopes are nonzero, they are sufficiently small that constant $\Delta\varepsilon$ values have been used determinations of Φ_f (see Materials and Methods). Absorption spectral profiles of oxidized y-cyt *c* (in 0.18 M GuHCl) obtained upon thermal unfolding closely resemble those determined by denaturation with GuHCl (Figure 4.12). The transition is sufficiently steep and occurs at a high enough temperature (T_m ~ 51 °C) that the extinction coefficients at 22.5 and 40.0 °C are nearly identical (≤ 2% different). These results are consistent with our observation that the shapes of GuHCl-induced unfolding curves at both temperatures were similar; differences were not significant compared to

the (relatively large degree of) noise observed in optical titrations carried out at 40.0 °C. Thus the same $\Delta\varepsilon$ values were used for the two temperatures.

Kinetics

Photoreduction Schemes

As discussed above, the ET-triggering method requires rapid reduction of unfolded cyt *c* to initiate folding. The low redox potential and kinetic accessibility of the heme group in unfolded cyt *c* make it a very efficient reductant. This places fairly stringent demands on any potential photochemical reduction scheme: one must not only rapidly generate a potent reductant, but also do so without concomitant generation of oxidants, since reoxidation of the heme removes the driving force for folding. In practice, oxidants can be tolerated as long as the rate of the folding process being observed is competitive with the rate of reoxidation. Microsecond reduction of unfolded cyt *c* by the excited-state of ruthenium-polypyridyl compounds has been achieved in both intramolecular[49] and bimolecular systems,[1] but in both cases, reoxidation is observed by photoproducts on a timescale of about 1 ms. Investigations using the bimolecular approach have indicated that a kinetic phase exhibiting a small relative heme absorption change may occur early in the folding of reduced cyt *c* at pH 7.[1,50] This chapter, however, describes the kinetic events associated with large heme absorption changes which occur on a >1 ms timescale. For these experiments a reduction scheme based on the photochemistry of $Co^{III}(C_2O_4)_3^{3-}$ ($C_2O_4^{2-}$ is oxalate) is used (Figure 4.13). UV-laser excitation of solutions of $Co^{III}(C_2O_4)_3^{3-}$ yields rapid generation of Co^{II}_{aq} and a strong reductant, probably $CO_2^{\bullet-}$ ($E°(CO_2/CO_2^{\bullet-}) = -2.0$ V).[51-53] This chemistry is thought to arise from the distinctive properties of the ligand-to-metal charge-transfer state which is formed upon excitation, $*[(C_2O_4)_2Co^{II}(C_2O_4^{\bullet-})]$: Co^{II} is known to be quite labile,[54] and the oxalate radical anion is known to be unstable with respect to homolytic

carbon-carbon bond cleavage.[55] Importantly, all of the presumed photoproducts in this reaction are either reductants ($CO_2^{\bullet-}$) or are effectively non-redox active (Co^{II}_{aq}, CO_2).

Non-folding Conditions

At very low and very high concentrations of denaturant, reduction of oxidized cyt *c* is not expected to yield folding behavior: at sufficiently low denaturant concentration, oxidized cyt *c* is already folded before the reduction, and at very high GuHCl concentrations, the unfolded reduced cyt *c* that is produced has no thermodynamic driving force to fold (Figures 4.4, 4.5). These conditions have been used to characterize the $Co(C_2O_4)_3^{3-}$/cyt *c* photoreduction system. Kinetics following laser flash photolysis of $Co(C_2O_4)_3^{3-}$ in the presence of oxidized *folded* y-cyt *c* at pH 7 and 40.0 °C (no GuHCl) are monophasic (Figure 4.14A). This phase corresponds to the reduction of y-cyt *c* with a pseudo first order rate constant of ~300 s^{-1}. Notably, no further changes in absorption are observed out to ~1.0 s (Figure 4.14B), indicating that the final product of reduction, y-cyt c^{II}_F, undergoes no observable conformational changes or reoxidation under these conditions. When the same experiment is conducted in the presence of 7.6 M GuHCl, significantly different results are obtained: kinetics are biphasic, with the first phase corresponding to an accelerated reduction of the heme (k_{obs} ~ 10^4 s^{-1}), and the second corresponding to reoxidation of the heme on a ~100 ms timescale (Figure 4.15).

Data gathered at a variety of GuHCl concentrations suggest that the accelerated reduction and oxidation seen at high concentrations of GuHCl do not represent an intrinsic dependence of these rates on the concentration of denaturant, but rather reflect differing properties of the folded and unfolded forms. The faster rate of reduction for the unfolded state is somewhat surprising given that its redox potential is ~0.40 V *lower* than the folded conformation. However, analogous behavior has been observed in microperoxidase 8, and has been attributed to increased accessibility of the heme to

solvent.[56] Accelerated reoxidation of unfolded cyt c^{II} is to be expected if oxidants are present, but it was hoped that the lack of oxidative photoproducts would lead to greater longevity of cyt c^{II}_U than is observed. Unphotolyzed $Co^{III}(C_2O_4)_3^{3-}$ may be acting as the oxidant, although residual traces of oxygen cannot be ruled out as the source of reoxidation. The fact that folded cyt *c* does not reoxidize to any appreciable extent on the timescale of our measurements is a critical observation. Under conditions in which folding experiments are performed, the presence of a signal remaining (a plateau) after ~100 to 500 ms is clear indication that at least some of the protein has folded to a form which has a near-physiological heme environment (redox potential and degree of solvent accessibility). A rate constant for folding can thus be determined even under conditions in which reoxidation competes with the folding reaction.

Folding Experiments

We expect to see protein folding by rapid reduction of ferricytochrome *c* under conditions in which at least 50% of oxidized cyt *c* is unfolded and 90% of reduced cyt *c* is folded. Inspection of the equilibrium folding data (Figures 4.4, 4.5; Table 4.1) yields the following ranges of GuHCl concentration for the designated species and temperature: h-cyt *c*(22.5 °C), 2.8 - 5.0 M; h-cyt *c*(40.0 °C), 2.4 - 4.3 M; y-cyt *c*(22.5 °C), 1.3 - 3.5 M; y-cyt *c*(40.0 °C), 0.8 - 2.9 M). Excitation of $Co(C_2O_4)_3^{3-}$ in the presence of y-cyt *c* at 40.0 °C in 1.0 M GuHCl yields biphasic kinetics (Figure 4.16). The first phase corresponds to rapid reduction of the heme, as seen above: the traces at 420 and 400 nm exhibit a large rise and bleach respectively, and the trace at 550 nm shows a more modest signal increase. The second phase corresponds primarily to folding: the traces at 400 and 420 nm tend toward zero, but plateau after about 100 ms. The 550 nm trace does not exhibit a second phase, but simply plateaus immediately after the reduction phase. This behavior suggests that a fraction of the protein has undergone reoxidation rather than folding since a slight increase is expected at 550 nm for 100% folding, but (partial)

reoxidation would contribute a (small) decrease to the signal. These profiles are nearly identical to those observed with h-cyt *c* in 2.7 M GuHCl at 40 °C, conditions at which essentially 100% of the sample folds. In the latter experiment, a full range of wavelengths was monitored, and the full transient spectra, just after reduction (at ~1 ms) and after completion of the folding phase (at ~50 ms), accord closely with the difference spectra of unfolded and folded reduced cyt *c* respectively (Figure 4.17).[1]

Kinetics of folding of both h-cyt *c* and y-cyt *c* have been measured over a wide range of GuHCl concentrations at both 22.5 °C and 40.0 °C (pH 7). Kinetic traces cannot always be fit adequately by single-exponential functions, but are well described by biexponential decays or functions describing a distribution of first order rate constants (see Materials and Methods) (Figure 4.18). Many kinetic models can lead to the observation of biexponential behavior; in the case of folding, the most common involves the assumption that the reaction goes through a distinct kinetic intermediate, either "on-pathway" or "off-pathway."[57] This could be the case in our system; however, we have no *a priori* reason to suspect that this should be so. The distributed model, on the other hand, is intuitively more attractive in that the source of the nonexponential behavior is attributed to heterogeneity in the sample, which is likely to be the case in reactions such as protein folding. As a test of this model, the reoxidation kinetics at very high concentrations of GuHCl were examined. As in the folding reaction, this process involves the unfolded "state" as a reactant, and is therefore expected to exhibit heterogeneous kinetics. Indeed, reoxidation traces cannot be fit adequately using a monoexponential decay function (Figure 4.19A), but are described well by the distributed function (Figure 4.19B). The kinetics can also be fit to a biexponential function, but a model assuming two kinetic phases seems somewhat arbitrary and chemically unreasonable (one must assume two distinct subpopulations of unfolded molecules with different tendencies for reoxidation). We report and discuss primarily values of $\bar{k}_f$ in this

thesis. It is noted, however, that our spectral kinetics data alone provide insufficient evidence to conclusively distinguish the two models.

For a given protein at 22.5 or 40.0 °C, slower observed rates and smaller final absorption signals are evident as the concentration of GuHCl is increased (Figure 4.20). Analysis using the distributed fit model assuming a competition between folding and reoxidation yields $\bar{k}_f$ values which decrease as the concentration of GuHCl increases, whereas the reoxidation rate is roughly constant as a function of GuHCl and (within error) independent of protein and temperature [($\bar{k}_{ox}$ = 11 ± 5 (h-cyt *c*, 40.0 °C); 14 ± 6 (y-cyt *c*, 40.0 °C); 13 ± 6 (h-cyt *c*, 22.5 °C); 7 ± 3 (y-cyt *c*, 22.5 °C)]. These values for $\bar{k}_{ox}$ are consistent with the observed $\bar{k}_{ox}$ for "pure" reoxidation kinetics of y-cyt $c^{II}{}_U$ at very high concentrations of GuHCl (Figure 4.19B). Values of σ are similar at all concentrations of GuHCl at a given temperature, but are larger at 40.0 °C than at 22.5 °C. Plots of log $\bar{k}_f$ (and thus ln $\bar{k}_f$) vs. [GuHCl] are linear for y-cyt *c* and h-cyt *c* at both temperatures studied (Figure 4.21). Analysis of the data at 22.5 °C using biexponential fits gives very similar results to those found using distributed fits (Figure 4.22); values for k_f are typically within 50% of the corresponding $\bar{k}_f$ values.

The $\bar{k}_f$ values appearing in Figure 4.21 are averages of rates derived from kinetics data at 400, 420, and 550 nm (in cases where 550 nm data are relatively flat as in Figure 4.16, the mean of the 400 and 420 nm values is tabulated). Close inspection of the data before averaging reveals that although the linear behavior is evident, the values extracted from data acquired at different wavelengths often vary substantially. In particular, the values derived from 550 nm data are consistently smaller, often by as much as a factor of 2, than rates derived from 400 and 420 nm data (Figure 4.23; 22.5 °C data shown). While this might simply reflect a large intrinsic uncertainty associated with the complexity of the system and the fact that $\bar{k}_f$ is extracted from the observed rate by calculating Φ_f, it may also be indicative of a systematic error in our analysis. One

possible explanation is that the protein does not achieve the "final" folded form in the kinetic phase that we observe, but rather a *nearly* native state (in which the polypeptide has collapsed around the heme to afford a near-physiological redox potential) which exhibits a decreased intensity at 550 nm in the absorption spectrum relative to the fully folded form (possibly due to the lack of proper Met80 ligation?). This would result in a decreased calculated yield of folding in our analysis of the 550 nm data and could account for the lower $\bar{k}_f$ values that are observed relative to values obtained from 400 and 420 nm traces.

Assuming transition state theory with a constant pre-exponential factor, a linear relationship between ln $\bar{k}_f$ and [GuHCl] corresponds to a linear relationship between the activation free energy of folding ($\Delta G_f^{\ddagger}$) and [GuHCl]:[58,59]

$$\Delta G_f^{\ddagger} = \Delta G_f^{\ddagger\circ} + m_D^{\ddagger}[\text{GuHCl}] \qquad (4.26)$$

where $m_D^{\ddagger}$ equals the slope of a plot of $RT\ln \bar{k}_f$ vs. [GuHCl]. Recalling that ΔG_f is also linearly related to [GuHCl] (Equation 4.19), $\Delta G_f^{\ddagger}$ (and thus ln $\bar{k}_f$) must also be a linear function of ΔG_f with a slope equal to $m_D^{\ddagger} / m_D$. Plots of log $\bar{k}_f$ vs. ΔG_f are shown in Figure 4.24; values of $m_D^{\ddagger}$ and $m_D^{\ddagger} / m_D$ obtained from the plots in Figures 4.21 and 4.24 are tabulated in Table 4.1.

Examination of the rate behavior exhibited by y-cyt *c* and h-cyt *c* yields a remarkable observation: at a given concentration of [GuHCl] at either 22.5 or 40.0 °C, the observed or extrapolated mean folding rate constant for h-cyt *c* is over an order of magnitude larger than that for y-cyt *c*; however, at a given folding free energy at either temperature, the rates of folding in the two proteins are comparable (Figures 4.21, 4.24). This result strongly suggests that the height of the barrier for this step in cyt c^{II} folding depends only on the relative energies of the initial and final states. This finding also

provides compelling experimental support for the theoretical notion that the folding free energy is a key factor in determining the rates of protein folding.[60,61] Furthermore, the fact that the h-cyt *c* and y-cyt *c* values of $\bar{k}_f$ have distinct dependencies on the concentration of GuHCl indicates that this denaturant serves to shift the folding/unfolding equilibrium, but does not have a specific effect in determining the folding rate.

Interpretations and Implications

The Hammond postulate states that for a chemical reaction with a single transition state, $\partial \log k / \partial \log K = \beta$, where β represents the position of the transition state along the reaction coordinate.[62] Fersht and coworkers have applied this principle to the study of protein folding, noting that when Equations 4.19 and 4.26 hold, $\partial \log k / \partial \log K = \partial \Delta G_f^{\ddagger} / \partial \Delta G_f = m_D^{\ddagger} / m_D$ (see also above analysis).[59] Although we have not conclusively observed evidence that cyt c^{II} folding involves an intermediate, neither have we clearly demonstrated that the process is two-state. Nonetheless, recent studies have suggested that cyt c^{III} folding can be a two-state process under certain conditions,[63] and we will proceed with the analysis noting the assumption made. Values of $m_D^{\ddagger} / m_D$ for y-cyt *c* and h-cyt *c* at both temperatures studied are all near 0.4 (Table 4.1), suggesting a relatively early transition state along the folding reaction coordinate. The similarity in these values, a reflection of the striking agreement in rate/free energy behavior noted above, suggests that the residues that are not conserved between the two sequences do not significantly affect the location of the transition state, and the two proteins follow similar folding pathways. Interestingly, the $m_D^{\ddagger} / m_D$ value reported for cyt c^{III} is also near 0.4 (0.46)[63] suggesting that the location of the transition state is also fairly insensitive to the oxidation state of the iron atom.

Another parameter, Φ_F (not to be confused with Φ_f), has been used to assess the degree of foldedness of particular residues (mutations) in the transition state of folding.[64]

Φ_F is defined as $\Delta\Delta G_f^{\ddagger} / \Delta\Delta G_f$, where $\Delta\Delta G^{\ddagger}$ is the difference in the activation free energy of folding between the mutant and the wild-type, and $\Delta\Delta G_f$ is the difference in folding free energy between the two. Its value represents the extent to which the residue(s) involved in the mutation(s) experience(s) a native-like environment (often interpreted as "*structure*") in the transition state; a value of 0 corresponds to an unfolded environment for the residue, whereas a value of 1 implies a completely native-like environment.[65] As in the preceding paragraph, this analysis is only meaningful when applied to a system in which there is only one transition state. Again making this assumption for cyt c^{II}, and viewing y-cyt *c* as a "mutant" of h-cyt *c*, we calculate a Φ_F value of ~0.5 over the concentration range of 1-3 M GuHCl (at 22.5 and 40.0 °C). This value suggests that on average, the ~40 residues which differ between h-cyt *c* and y-cyt *c* find themselves in a partially folded environment in the transition state of folding. With so many mutations between the two proteins, it is difficult to make a specific interpretation of this result. However, the value of ~0.5 is consistent with results of kinetic studies of h-cyt c^{III} which suggest early formation of structure in the N- and C-terminal helices, the two regions with the lowest homology between y-cyt *c* and h-cyt *c*.

CONCLUSION

It has been demonstrated that electron transfer can trigger protein folding. This initiation technique allows direct observation of folding kinetics over a wide range of timescales, including those in the submillisecond regime. This method has been used to compare the folding energetics and kinetics of h-cyt *c* and y-cyt *c*. The results strongly suggest that the folding free energy is a primary factor in determining folding rates. These two proteins, with just 60% sequence identity but very similar backbone structures, fold at very different rates at a given denaturant concentration, but at nearly the same rate when their folding free energies are equal. The differences in the amino-acid sequences

shift the position of the folding/unfolding equilibrium, but do not appear to alter the location of the transition state along the folding reaction coordinate.

REFERENCES AND NOTES

(1) Pascher, T.; Chesick, J. P.; Winkler, J. R.; Gray, H. B. *Science* **1996**, *271*, 1558-1560.

(2) Beals, J. M.; Haas, E.; Krausz, S.; Scheraga, H. A. *Biochemistry* **1991**, *30*, 7680-7692.

(3) Williams, S.; Causgrove, T. P.; Gilmanshin, R.; Fang, K. S.; Callender, R. H.; Woodruff, W. H.; Dyer, R. B. *Biochemistry* **1996**, *35*, 691-697.

(4) Wright, P. E.; Dyson, H. J.; Lerner, R. A. *Biochemistry* **1988**, *27*, 7167-7175.

(5) Ptitsyn, O. B. *Prot. Eng.* **1994**, *7*, 593-596.

(6) Khorasanizadeh, S.; Peters, I. D.; Butt, T. R.; Roder, H. *Biochemistry* **1993**, *32*, 7054-7063.

(7) Itzhaki, L. S.; Evans, P. A.; Dobson, C. M.; Radford, S. E. *Biochemistry* **1994**, *33*, 5212-5220.

(8) Elöve, G. A.; Bhuyan, A. K.; Roder, H. *Biochemistry* **1992**, *33*, 6925-6935.

(9) Takahashi, S.; Yeh, S.-R.; Das, T. K.; Chan, C.-K.; Gottfried, D. S.; Rousseau, D. L. *Nat. Struct. Biol.* **1997**, *4*, 44-50.

(10) Houry, W. A.; Rothwarf, D. M.; Scheraga, H. A. *Biochemistry* **1996**, *35*, 10125-10133.

(11) Mann, C. J.; Matthews, C. R. *Biochemistry* **1993**, *32*, 5282-5290.

(12) Agashe, V. R.; Shastry, M. C. R.; Udgaonkar, J. B. *Nature* **1995**, *377*, 754-757.

(13) Nölting, B.; Golbik, R.; Fersht, A. R. *Proc. Natl. Acad. Sci. U.S.A.* **1995**, *92*, 10668-10672.

(14) Kuszewski, J.; Clore, G. M.; Gronenborn, A. M. *Prot. Sci.* **1994**, *3*, 1945-1952.

(15) Kuwajima, K.; Semisotnov, G. V.; Finkelstein, A. V.; Sugai, S.; Ptitsyn, O. B. *FEBS Lett.* **1993**, *334*, 265-268.

(16) Eaton, W. A.; Muñoz, V.; Thompson, P. A.; Chan, C.-K.; Hofrichter, J. *Curr. Op. Struct. Biol.* **1997**, *7*, 10-14.

(17) Jones, C. M.; Henry, E. R.; Hu, Y.; Chan, C.-K.; Luck, S. D.; Bhuyan, A.; Roder, H.; Hofrichter, J.; Eaton, W. A. *Proc. Natl. Acad. Sci. U.S.A.* **1993**, *90*, 11860-11864.

(18) Ballew, R. M.; Sabelko, J.; Gruebele, M. *Nat. Struct. Biol.* **1996**, *3*, 923-926.

(19) Booth, H. S. *Inorganic Syntheses*; McGraw-Hill Book Company, Inc.: New York, 1939; Vol. 1.

(20) Narita, K.; Titani, K. *J. Biochem (Tokyo)* **1969**, *65*, 259-267.

(21) Bowler, B. E.; Meade, T. J.; Mayo, S. L.; Richards, J. H.; Gray, H. B. *J. Am. Chem. Soc.* **1989**, *111*, 8757-8759.

(22) Mayo, S. L. Ph.D. Thesis, California Institute of Technology, 1988.

(23) Cutler, R. L.; Pielak, G. J.; Mauk, A. G.; Smith, M. *Prot. Eng.* **1987**, *1*, 95-99.

(24) Nozaki, Y. In *Methods in Enzymology*; C. H. W. Hirs and S. N. Timasheff, Eds.; Academic Press: New York, 1972; Vol. 26; pp 43-50.

(25) Fisher, W.; Taniuchi, H.; Anfinsen, C. B. *J. Biol. Chem.* **1973**, *248*, 3188-3195.

(26) Tsong, T. Y. *J. Biol. Chem.* **1974**, *249*, 1988-1990.

(27) Tsong, T. Y. *Biochemistry* **1976**, *15*, 5467-5473.

(28) Tinoco, I., Jr.; Sauer, K.; Wang, J. *Physical Chemistry: Principles and Applications in Biological Sciences;* 2nd ed.; Prentice Hall, Inc.: Englewood Cliffs, 1985, pp 706.

(29) Pace, N. C.; Shirley, B. A.; Thomson, J. A. In *Protein Structure: A Practical Approach*; T. F. Creighton, Ed.; IRL Press: Oxford, 1990; pp 311-330.

(30) Pace, C. N. *CRC Crit. Rev. Biochem.* **1975**, *3*, 1-43.

(31) Churg, A. K.; Warshel, A. *Biochemistry* **1986**, *25*, 1675-1681.

(32) Bixler, J.; Bakker, G.; McLendon, G. *J. Am. Chem. Soc.* **1992**, *114*, 6938-6939.

(33) Wuttke, D. S.; Bjerrum, M. J.; Chang, I.-J.; Winkler, J. R.; Gray, H. B. *Biochim. Biophys. Acta* **1992**, *1101*, 168-170.

(34) Winkler, J. R.; Malmström, B. G.; Gray, H. B. *Biophys. Chem.* **1995**, *54*, 199-209.

(35) Taniguchi, V. T.; Sailasuta-Scott, N.; Anson, F. C.; Gray, H. B. *Pure Appl. Chem.* **1980**, *52*, 2275-2281.

(36) Santucci, R.; Reinhard, H.; Brunori, M. *J. Am. Chem. Soc.* **1988**, *110*, 8536-8537.

(37) Hilgen-Willis, S.; Bowden, E. F.; Pielak, G. J. *J. Inorg. Biochem.* **1993**, *51*, 649-653.

(38) Hickey, D. R.; Berghuis, A. M.; Lafond, G.; Jaeger, J. A.; Cardillo, T. S.; McLendon, D.; Das, G.; Sherman, F.; Brayer, G. D.; McLendon, G. *J. Biol. Chem.* **1991**, *266*, 11686-11694.

(39) McLendon, G.; Smith, M. *J. Biol. Chem.* **1978**, *253*, 4004-4008.

(40) Doyle, D. F.; Waldner, J. C.; Parikh, S.; Alcazar-Roman, L.; Pielak, G. J. *Biochemistry* **1996**, *35*, 7403-7411.

(41) Brayer, G. D.; Murphy, M. E. P. In *Cytochrome c: a multidisciplinary approach*; R. A. Scott and A. G. Mauk, Eds.; University Science Books: Sausalito, 1996; pp 738.

(42) Moore, G. R.; Pettigrew, G. W. *Cytochromes c: Evolutionary, Structural, and Physicochemical Aspects*; Springer-Verlag: New York, 1990, pp 478.

(43) Bushnell, G. W.; Louie, G. V.; Brayer, G. D. *J. Mol. Biol.* **1990**, *213*, 585-595.

(44) Berghuis, A. M.; Brayer, G. D. *J. Mol. Biol.* **1992**, *223*, 959-976.

(45) Bai, Y.; Sosnick, T. R.; Mayne, L.; Englander, S. W. *Science* **1995**, *269*, 192-197.

(46) Margoliash, E.; Schejter, A. *Adv. Protein Chem.* **1966**, *21*, 113-286.

(47) Babul, J.; Stellwagen, E. *Biochemistry* **1972**, *11*, 1195-1200.

(48) Muthukrishanan, K.; Nall, B. T. *Biochemistry* **1991**, *30*, 4706-4710.

(49) Mines, G. A., unpublished results.

(50) Tezcan, F. A.; Telford, J. R., unpublished results.

(51) Breitenkamp, M.; Henglein, A.; Lilie, J. *Ber. Bunsenges. Phys. Chem.* **1976**, *80*, 973-979.

(52) Adamson, A. W.; Sporer, A. H. *J. Am. Chem. Soc.* **1958**, *80*, 3865-3870.

(53) Pina, F.; Mulazzani, Q. G.; Venturi, M.; Ciano, M.; Balzani, V. *Inorg. Chem.* **1985**, *24*, 848-851.

(54) Shinohara, N.; Lilie, J.; Simic, M. G. *Inorg. Chem.* **1977**, *16*, 2809-2813.

(55) Chang, M.-M.; Saji, T.; Bard, A. J. *J. Am. Chem. Soc.* **1977**, *99*, 5399-5403.

(56) McLendon, G.; Smith, M. *Inorg. Chem.* **1982**, *21*, 847-850.

(57) Baldwin, R. L. *Fold. Des.* **1996**, *1*, R1-R8.

(58) Chen, B. L.; Baase, W. A.; Nicholson, H.; Schellman, J. A. *Biochemistry* **1992**, *31*, 1464-1476.

(59) Matouschek, A.; Fersht, A. R. *Proc. Natl. Acad. Sci. U.S.A.* **1993**, *90*, 7814-7818.

(60) Bryngelson, J. D.; Onuchic, J. N.; Wolynes, P. G. *Proteins: Struct. Func. Gen.* **1995**, *21*, 167-195.

(61) Onuchic, J. N.; Wolynes, P. G.; Luthey-Schulten, Z.; Socci, N. D. *Proc. Natl. Acad. Sci. U.S.A.* **1995**, *92*, 3626-3630.

(62) Hammond, G. S. *J. Am. Chem. Soc.* **1955**, *77*, 334-338.

(63) Sosnick, T. R.; Mayne, L.; Englander, S. W. *Proteins: Struct. Func. Gen.* **1996**, *24*, 413-426.

(64) Fersht, A. R.; Matouschek, A.; Serrano, L. *J. Mol. Biol.* **1992**, *224*, 771-782.

(65) Otzen, D. E.; Itzhaki, L. S.; El Masry, N. F.; Jackson, S. E.; Fersht, A. R. *Proc. Natl. Acad. Sci. U.S.A.* **1994**, *91*, 10422-10425.

Table 4.1. Thermodynamic and kinetic parameters for h-cyt *c* and y-cyt *c* folding and unfolding.[a]

Protein	T (°C)	$[GuHCl]_{1/2}$ (M)	$-\Delta G_f^\circ$ (kJ mol^{-1})	m_D (kJ mol^{-1} M^{-1})	$m_D^\ddagger$ (kJ mol^{-1} M^{-1})	$m_D^\ddagger/m_D$
h-cyt c^{III}	22.5(5)	2.8 (1)	40 (1)	14.3 (4)		
h-cyt c^{II}	22.5(5)	5.3 (1)	74 (3)	13.8 (4)	5.2 (5)	0.38
h-cyt c^{III}	40.0(5)	2.4 (1)	30 (1)	12.2 (4)		
h-cyt c^{II}	40.0(5)	4.7 (1)	61 (10)	13.1 (20)	5.5 (5)	0.42
y-cyt c^{III}	22.5(5)	1.3 (1)	24 (1)	18.9 (5)		
y-cyt c^{II}	22.5(5)	3.8 (1)	59 (4)	15.7 (10)	5.4 (5)	0.34
y-cyt c^{III}	40.0(5)	0.8 (1)	15 (1)	18.1 (8)		
y-cyt c^{II}	40.0(5)	3.3 (1)	45 (3)	13.7 (8)	5.8 (5)	0.42

[a] Numbers in parentheses are estimated uncertainties.

Figure 4.1. Thermodynamic cycle illustrating the relationship between folding free energies (ΔG_f) and reduction potentials (E) in a redox protein (P). *n* is the number of electrons transferred, and *F* is the Faraday constant. Subscripts represent the states of the protein: U = unfolded, F = folded; ox = oxidized, red = reduced, except in the case of ΔG_f where the lowercase f designates the reaction type (folding).

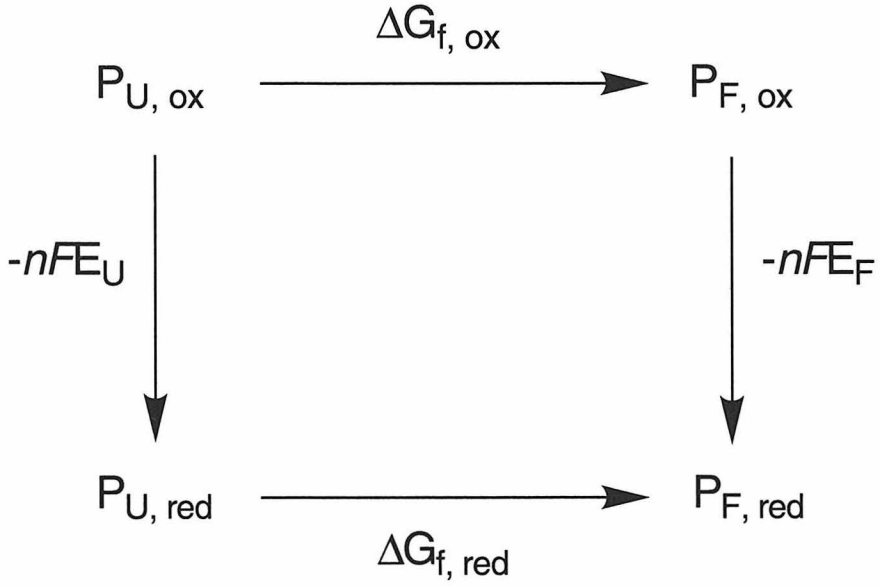

$$\Delta\Delta G_{f,\,red\,-\,ox} = -\,nF(\Delta E_{F\,-\,U})$$

Figure 4.2. Depiction of ET-triggered folding of a hypothetical protein with redox center, P, in which the reduced protein is more stable than the oxidized with respect to unfolding by a chemical denaturant. (A) Unfolding curves. χ_u is the fraction of protein unfolded at equilibrium. Reduction of the oxidized unfolded protein leads to reduced folded protein after equilibrium is reached, when the reduction is carried out at denaturant concentrations that lie between the two curves. (B) Cartoon representation of the triggering. If reduction is fast compared to folding, the latter process can be observed.

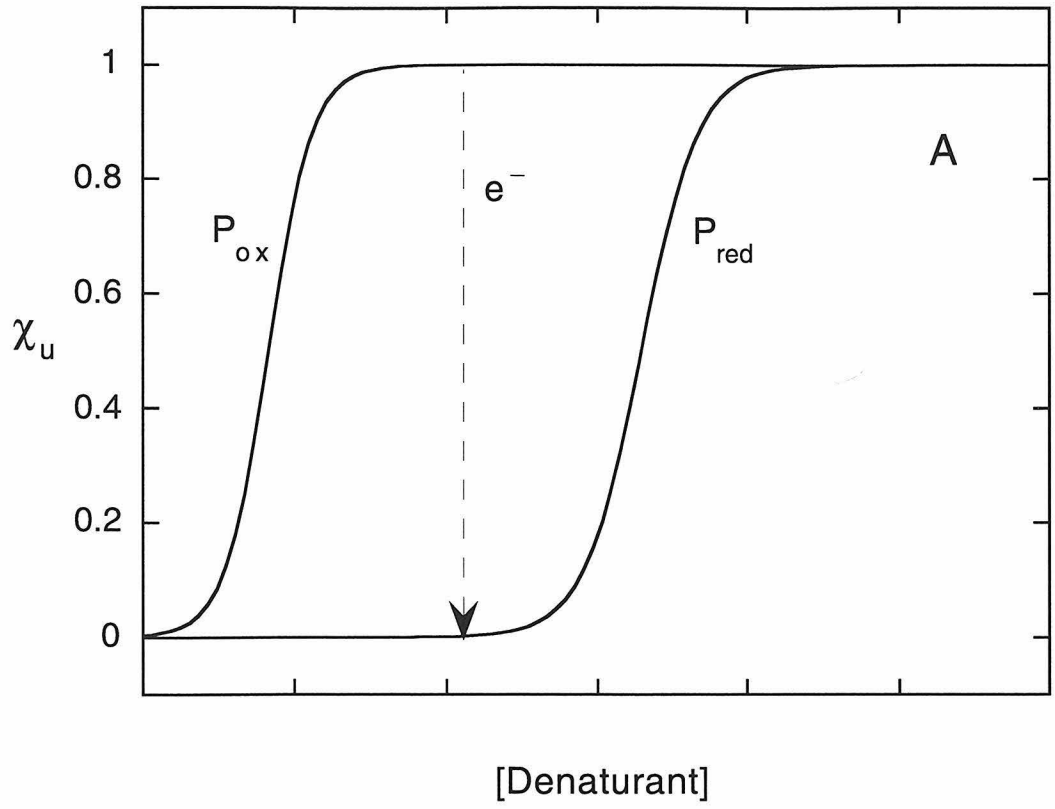
1
0.8
0.6
0.4
0.2
0
χ_u
P_{ox}
e^-
P_{red}
A
[Denaturant]

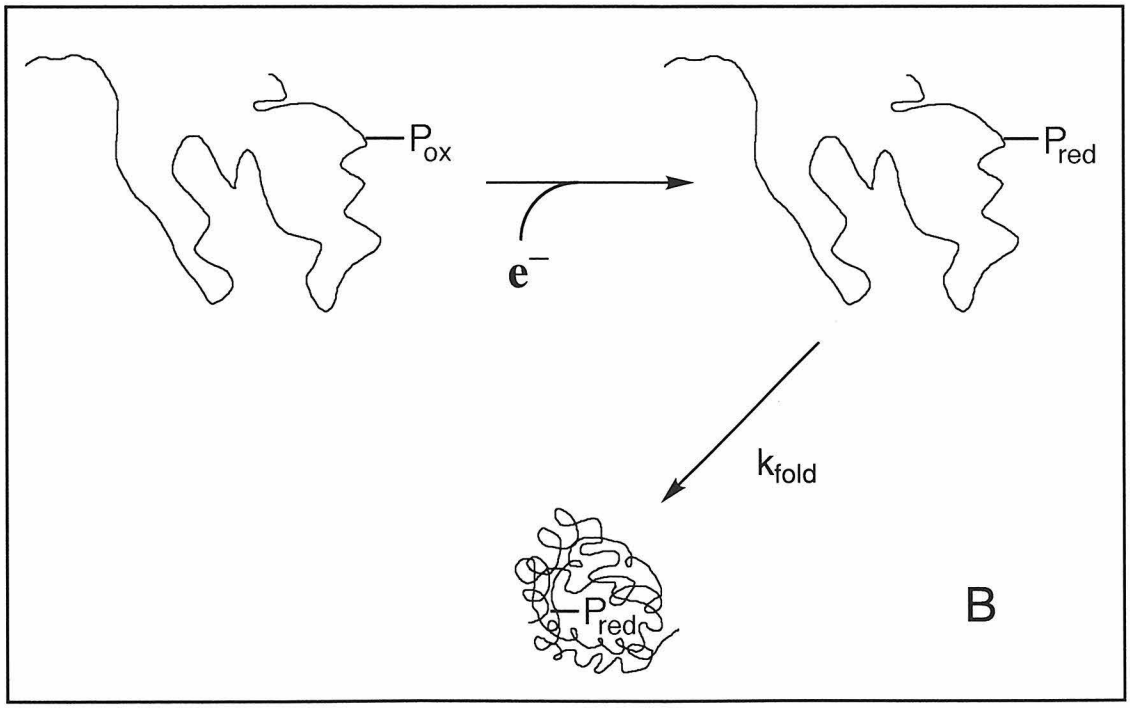
P_{ox}
e^-
P_{red}
k_{fold}
P_{red}
B

Figure 4.3. Unfolding of y-cyt c^{II} by GuHCl at 40.0°C, pH 7, monitored by tryptophan fluorescence. (A) Fluorescence spectra (λ_{ex} = 292 nm) of solutions containing 10.9 μM y-cyt *c*, ~500 μM $S_2O_4^{2-}$ (added), and 0 to ~6 M GuHCl. The intensity units are arbitrary. (B) Corrected fluorescence intensities at 350 nm of the solutions in (A) plotted as a function of [GuHCl]. The correction was carried out using Equations 4.10 and 4.12.

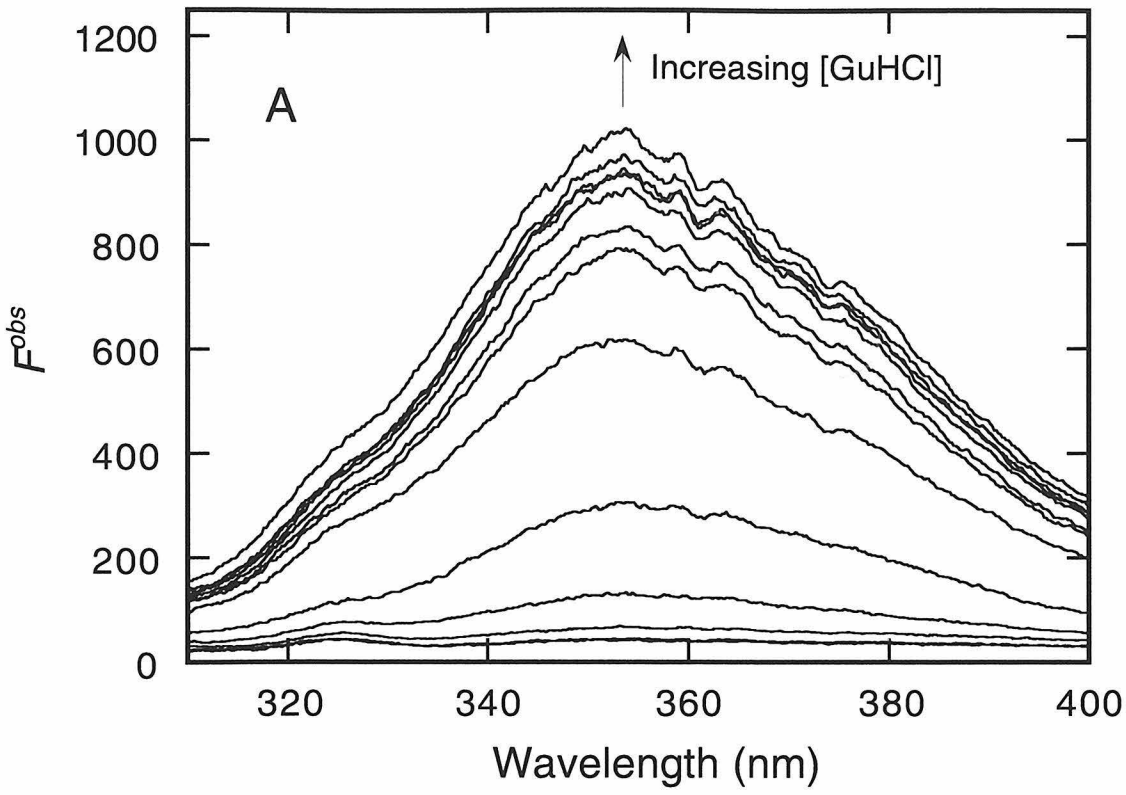
A
Increasing [GuHCl]
1200
1000
800
600
400
200
0
F^{obs}
320
340
360
380
400
Wavelength (nm)

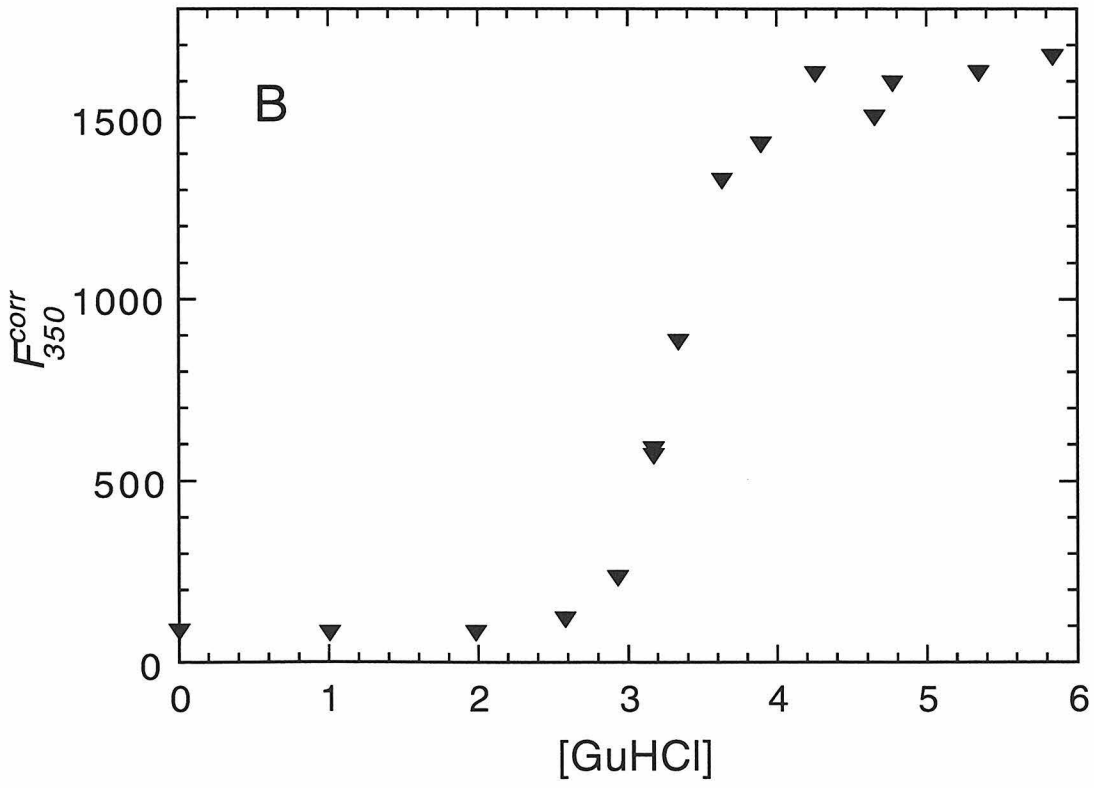
B
1500
1000
500
0
F^{corr}_{350}
0
1
2
3
4
5
6
[GuHCl]

Figure 4.4. Equilibrium unfolding data for h-cyt *c* and y-cyt *c* at 40.0 °C, pH 7. (A) Unfolding curves determined from corrected fluorescence intensity data at 350 nm (y-cyt *c*, inverted triangles; h-cyt *c*, diamonds). Lines are best fits to Equation 4.18: y-cyt c^{III} (long dashes); y-cyt c^{II} (dashes); h-cyt c^{III} (dotted); h-cyt c^{II} (solid). Fit parameters are depicted graphically in (B), which shows plots of ΔG_f vs. [GuHCl] (see Equation 4.19). Fit parameters are also tabulated in Table 4.1.

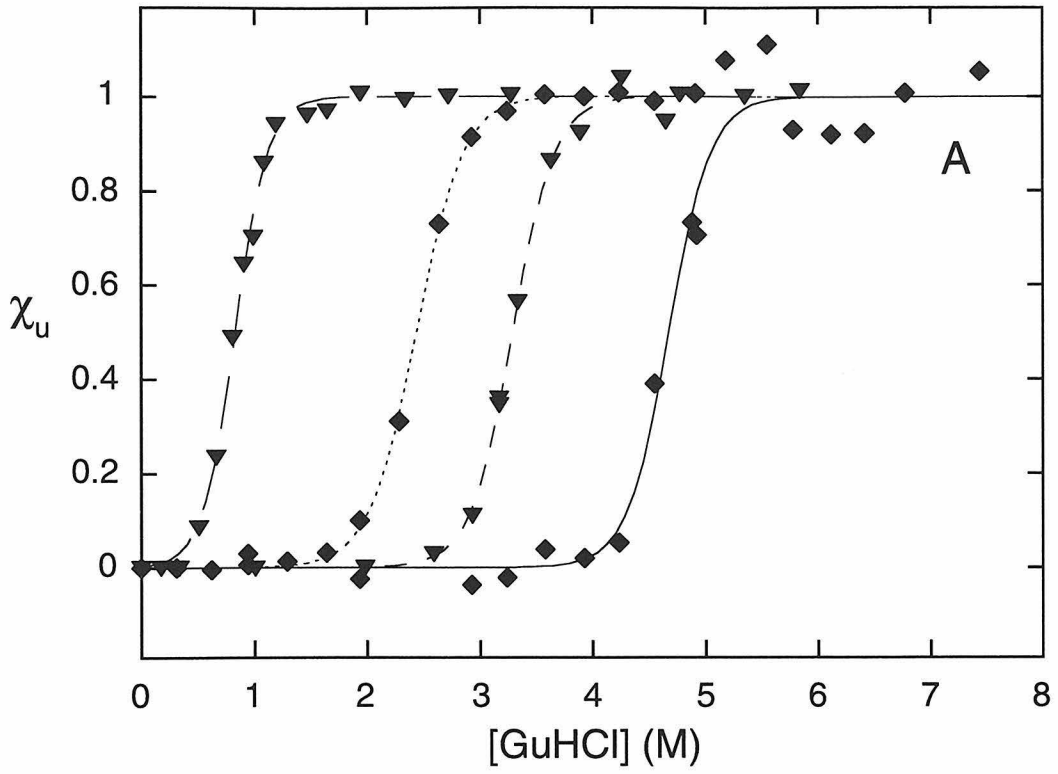
A
χ_u
1
0.8
0.6
0.4
0.2
0
0
1
2
3
4
5
6
7
8
[GuHCl] (M)

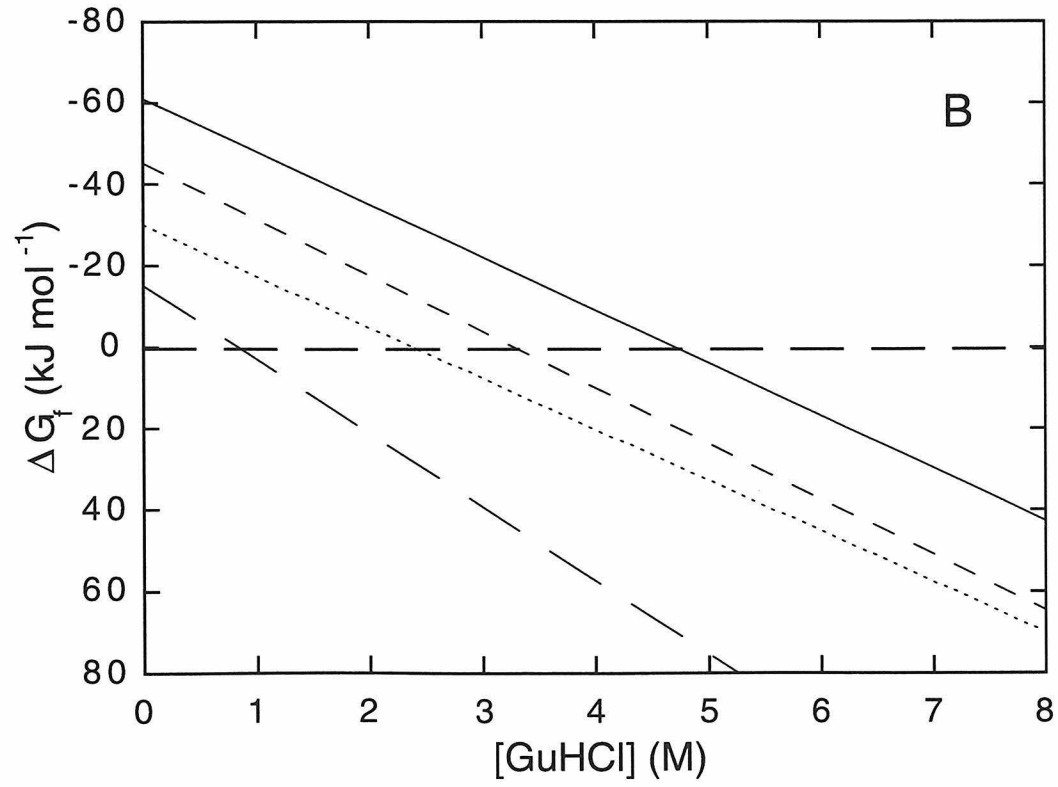
B
ΔG_f (kJ mol^{-1})
-80
-60
-40
-20
0
20
40
60
80
0
1
2
3
4
5
6
7
8
[GuHCl] (M)

Figure 4.5. Equilibrium unfolding data for h-cyt *c* and y-cyt *c* at 22.5 °C, pH 7. (A) Unfolding curves determined from corrected fluorescence intensity data at 350 nm (y-cyt *c*, inverted triangles; h-cyt *c*, diamonds). Lines are best fits to Equation 4.18: y-cyt c^{III} (long dashes); y-cyt c^{II} (dashes); h-cyt c^{III} (dotted); h-cyt c^{II} (solid). Fit parameters are depicted graphically in (B), which shows plots of ΔG_f vs. [GuHCl] (see Equation 4.19). Fit parameters are also tabulated in Table 4.1.

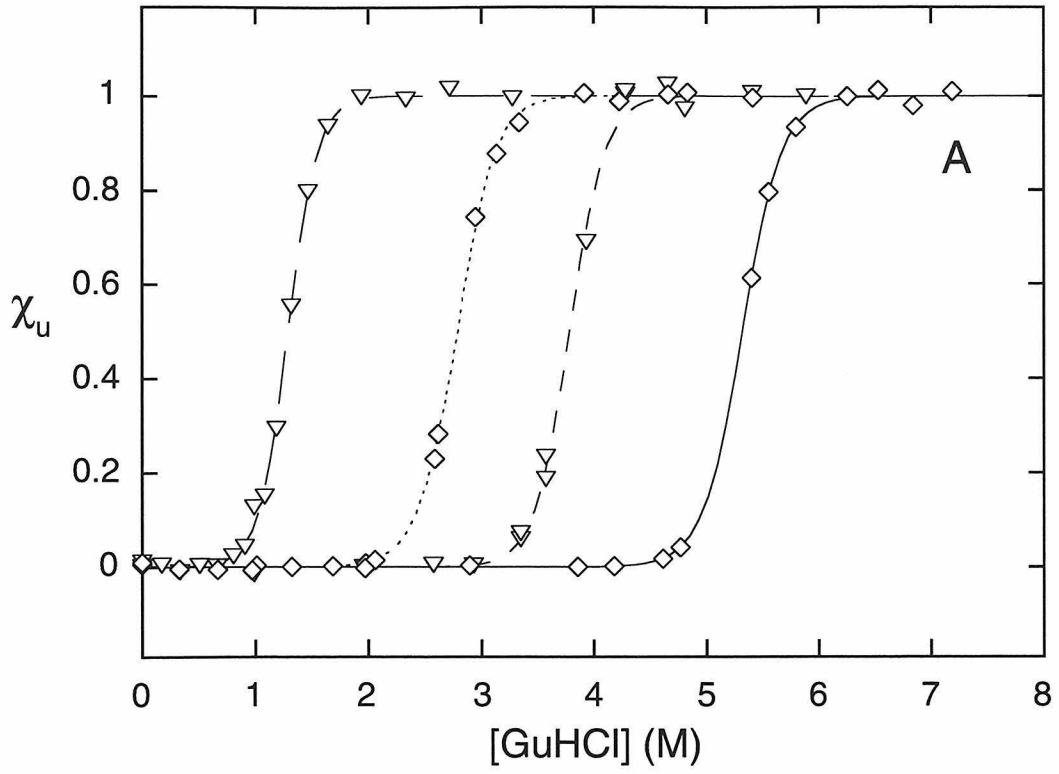
A
χ_u
1
0.8
0.6
0.4
0.2
0
0
1
2
3
4
5
6
7
8
[GuHCl] (M)

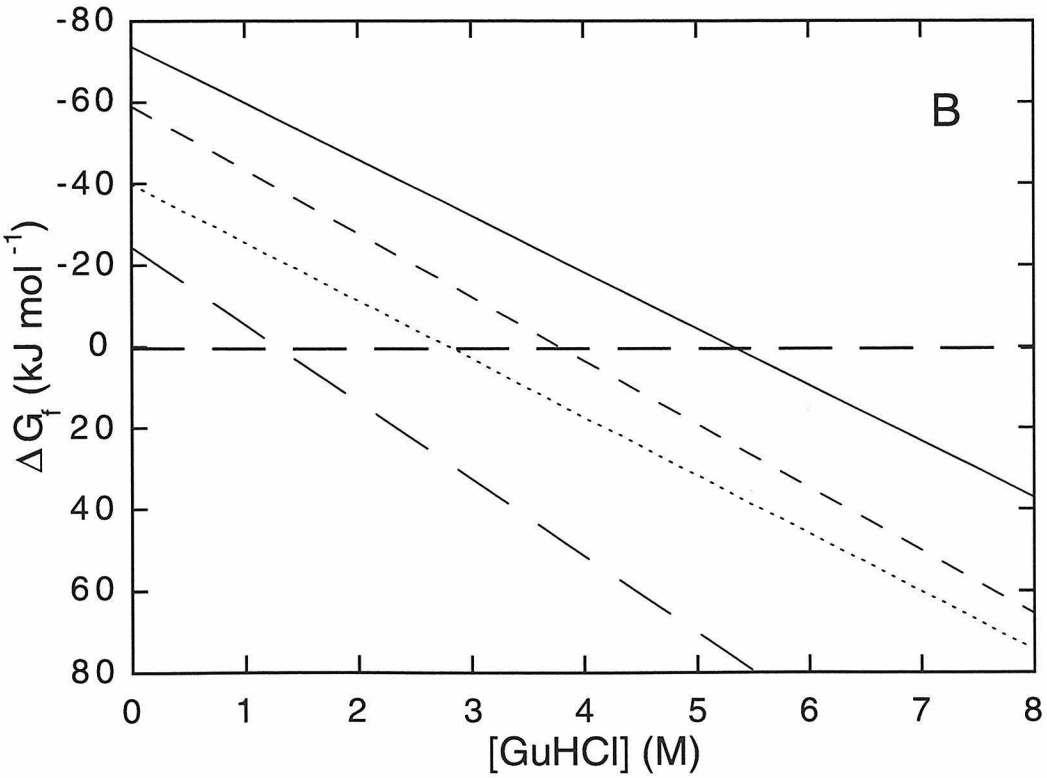
B
ΔG_f (kJ mol^{-1})
-80
-60
-40
-20
0
20
40
60
80
0
1
2
3
4
5
6
7
8
[GuHCl] (M)

Figure 4.6. Structure and sequence comparison of y-cyt *c* and h-cyt *c*. (A) Overlay of the backbone traces of y-cyt *c* (gray) and h-cyt *c* (black) in the standard view. The heme and axial ligands are displayed as well. (B) Sequence comparison of y-cyt *c* and h-cyt *c*. Differences are bolded and underlined for emphasis.

```
          -5          1                   10                  20
horse:                G  D V E  K G  K K I  F  V Q K  C  A  Q C H T V
yeast:     T E F K A  G  S A K  K G  A T L  F  K T R  C  L  Q C H T V

21                  30                  40                  50
 E K G G  K  H K  T  G P N L H G  L  F G R  K T  G Q A  P  G  F T  Y T D
 E K G G  P  H K  V  G P N L H G  I  F G R  H S  G Q A  E  G  Y S  Y T D

51                  60                  70                  80
 A N K N  K  G I T  W  K  E  E T L M  E Y L  E  N P K K Y I P G T K M
 A N I K  K  N V L  W  D  E  N N M S  E Y L  T  N P X K Y I P G T K M

81                  90                  100
 I  F A G  I  K K  K T E  R  E  D L I  A  Y L K K A  T N E
 A  F A G  L  K K  E K D  R  N  D L I  T  Y L K K A  S E
```

Figure 4.7. Absorption spectral changes accompanying unfolding of h-cyt c^{III} by GuHCl at 22.5 °C, pH 7 ([cyt *c*] = 7.3 μM; range of [GuHCl], 0 to 7.3 M). (A) Full spectrum. (B) Close-up of the Soret band region. (C) Close-up of the Q-band region. Arrows indicate increasing concentration of GuHCl.

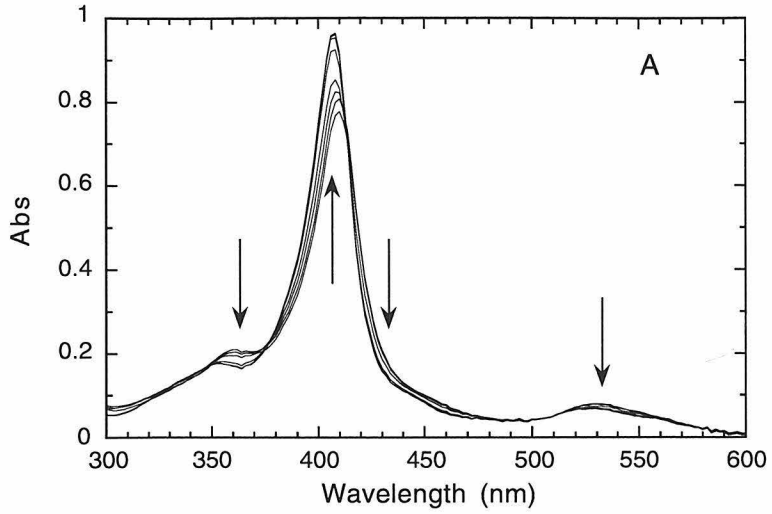
A
Abs
Wavelength (nm)
1
0.8
0.6
0.4
0.2
0
300
350
400
450
500
550
600

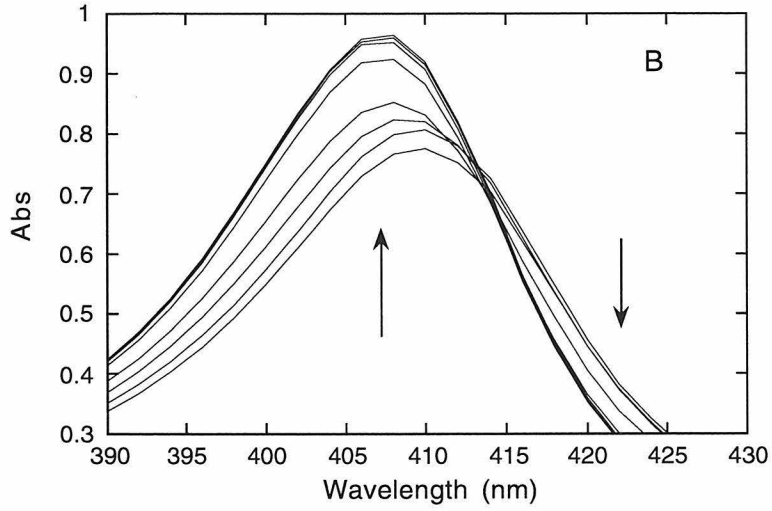
B
Abs
Wavelength (nm)
1
0.9
0.8
0.7
0.6
0.5
0.4
0.3
390
395
400
405
410
415
420
425
430

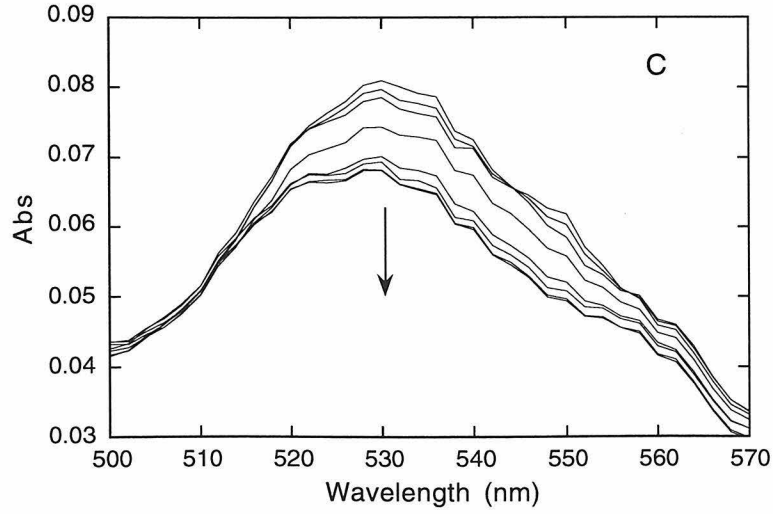
C
Abs
Wavelength (nm)
0.09
0.08
0.07
0.06
0.05
0.04
0.03
500
510
520
530
540
550
560
570

Figure 4.8. Absorption spectral changes accompanying unfolding of h-cyt c^{II} by GuHCl at 22.5 °C, pH 7 ([cyt *c*] = 11.8 μM; $[S_2O_4^{2-}]$ ~ 500 μM (added); range of [GuHCl], 0 to 7.6 M). (A) Full spectrum. The large absorbance near 316 nm is due primarily to $S_2O_4^{2-}$. (B) Close-up of the Soret band region. (C) Close-up of the Q-band region. Arrows indicate increasing concentration of GuHCl.

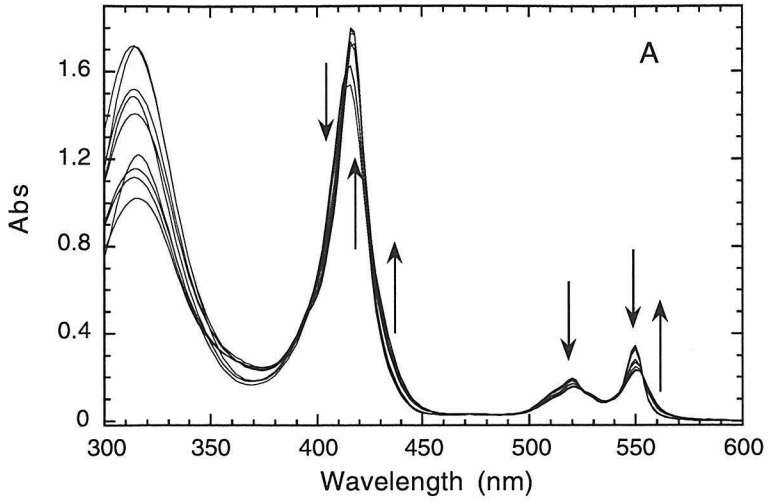
A
Abs
1.6
1.2
0.8
0.4
0
300
350
400
450
500
550
600
Wavelength (nm)

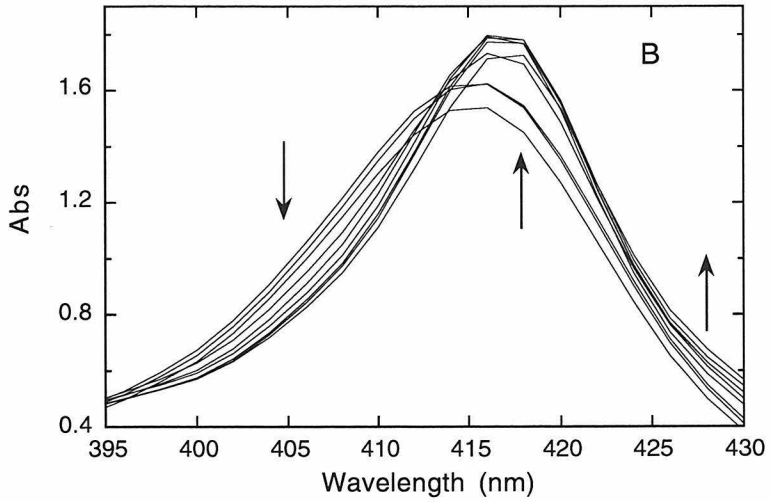
B
Abs
1.6
1.2
0.8
0.4
395
400
405
410
415
420
425
430
Wavelength (nm)

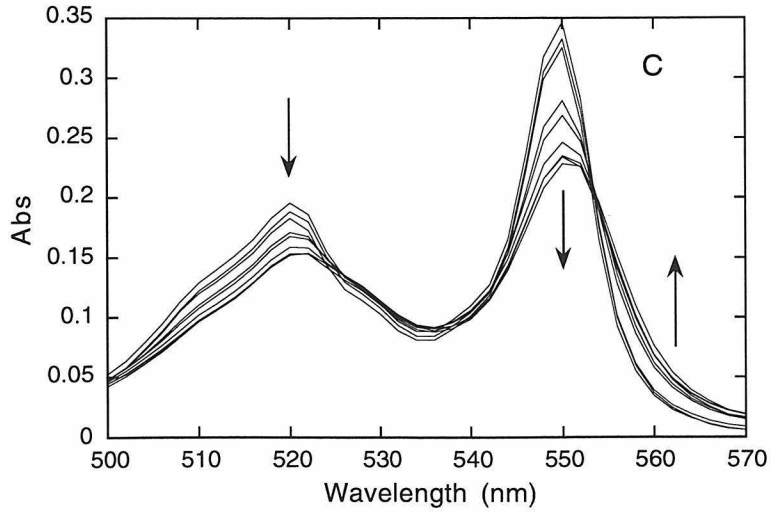
C
Abs
0.35
0.3
0.25
0.2
0.15
0.1
0.05
0
500
510
520
530
540
550
560
570
Wavelength (nm)

Figure 4.9. Estimated difference spectra of folded and unfolded reduced cyt *c* at pH 7. (A) Spectra representing cyt $c^{II}{}_U$ (solid line; h-cyt c^{II} acquired at 22.5 °C in 6.3 M GuHCl), cyt $c^{II}{}_F$ (dashed line; h-cyt c^{II} acquired at 22.5 °C in 4.6 M GuHCl), and cyt $c^{III}{}_U$ (dotted line; h-cyt c^{III} measured at 22.5 °C in 3.9 M GuHCl). (B) Difference spectra determined from the spectra in (A). Reduced unfolded (solid line; cyt $c^{II}{}_U$ – cyt $c^{III}{}_U$), reduced folded (dashed line; cyt $c^{II}{}_F$ – cyt $c^{III}{}_U$).

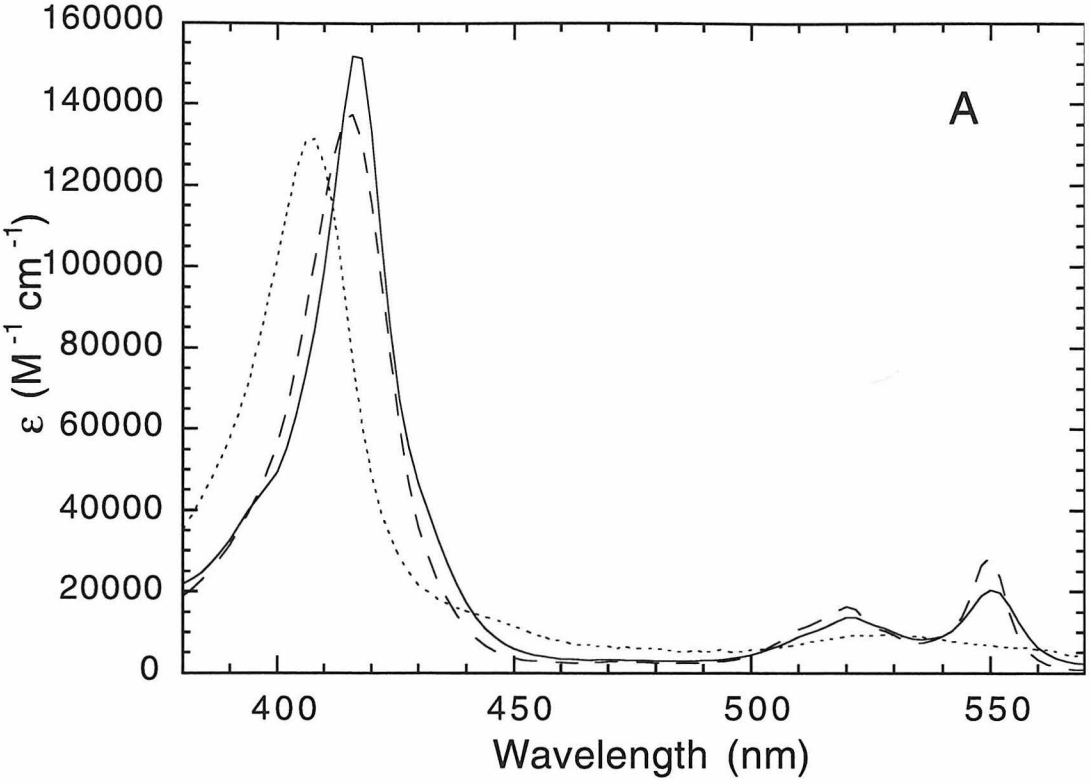
160000
140000
120000
100000
80000
60000
40000
20000
0
ε (M-1 cm-1)
A
400
450
500
550
Wavelength (nm)

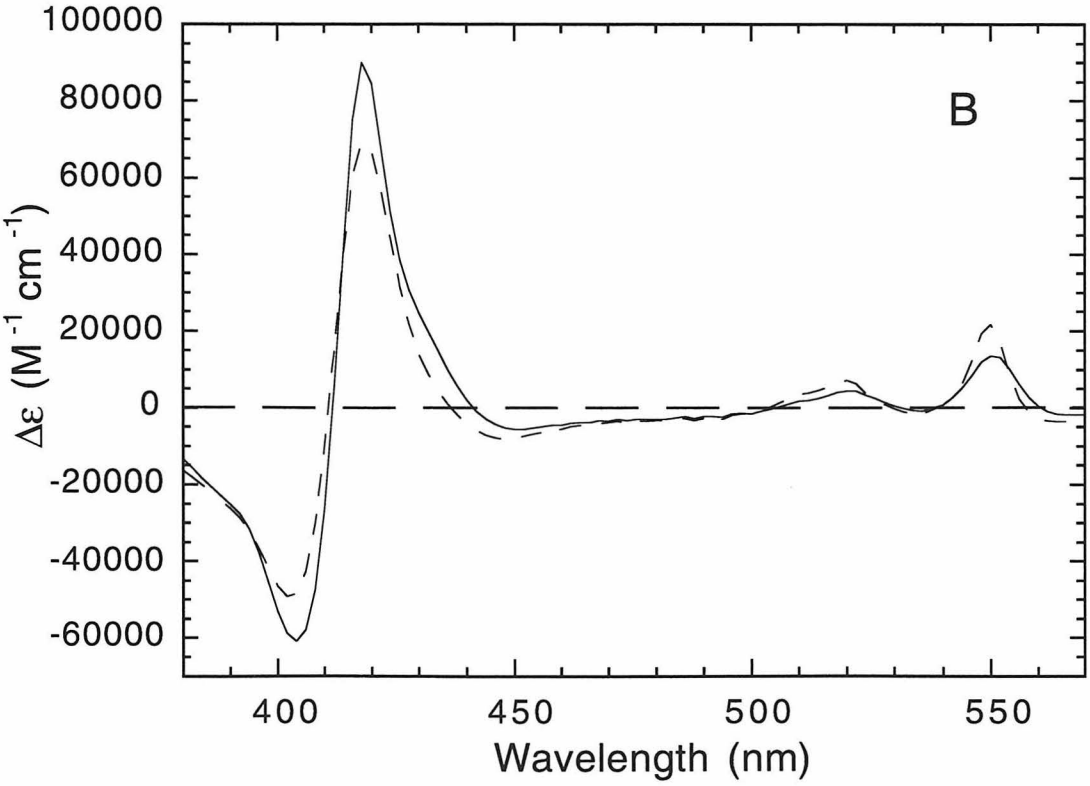
100000
80000
60000
40000
20000
0
-20000
-40000
-60000
Δε (M-1 cm-1)
B
400
450
500
550
Wavelength (nm)

Figure 4.10. Absorption spectral changes at 400 nm (A), 420 nm (B), and 550 nm (C) accompanying unfolding of h-cyt c^{III} by GuHCl at 22.5 °C, pH 7. Data are from Figure 4.7, plotted as ε values (using [h-cyt *c*] = 7.3 μM). Linear fits to the filled symbols represent the dependence of the spectrum of h-cyt c^{III}_U on the concentration of GuHCl.

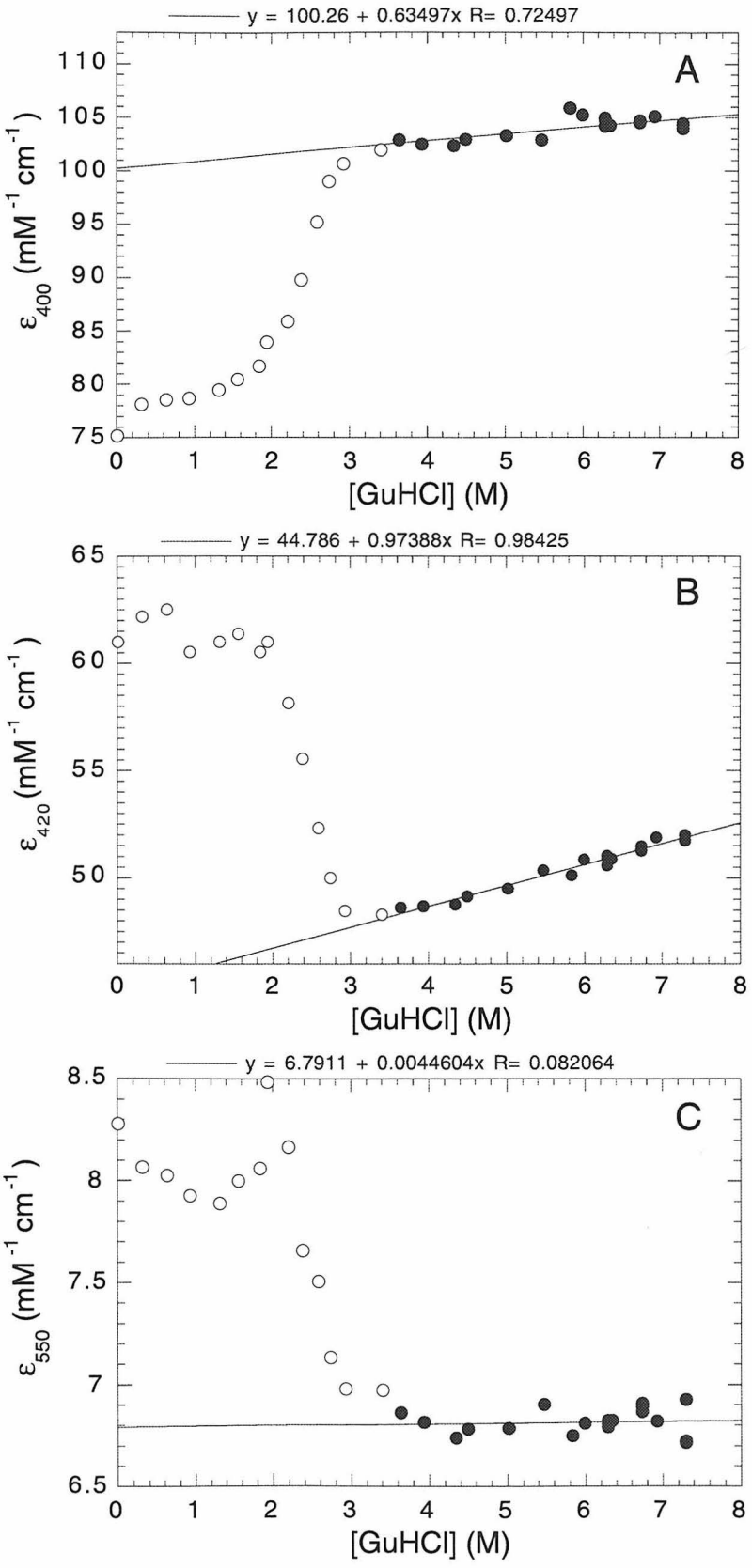
y = 100.26 + 0.63497x R= 0.72497
A
ε_{400} (mM^{-1} cm^{-1})
[GuHCl] (M)
y = 44.786 + 0.97388x R= 0.98425
B
ε_{420} (mM^{-1} cm^{-1})
[GuHCl] (M)
y = 6.7911 + 0.0044604x R= 0.082064
C
ε_{550} (mM^{-1} cm^{-1})
[GuHCl] (M)

Figure 4.11. Absorption spectral changes at 400 nm (A), 420 nm (B), and 550 nm (C) accompanying unfolding of h-cyt c^{II} by GuHCl at 22.5 °C, pH 7. Data are from Figure 4.8, plotted as ε values (using [h-cyt *c*] = 11.8 μM). Linear fits to the filled rectangles represent the dependence of the spectrum of h-cyt c^{II}_U on the concentration of GuHCl; fits to the filled circles define the GuHCl dependence of the spectrum of h-cyt c^{II}_F.

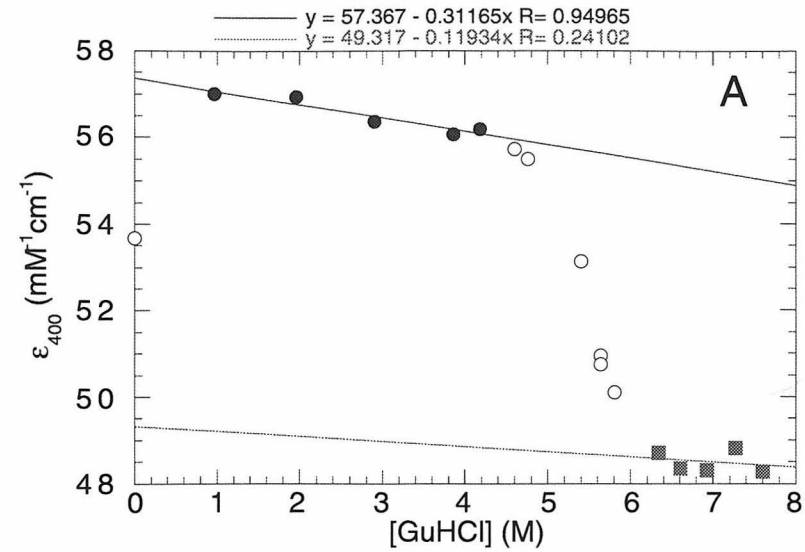
y = 57.367 - 0.31165x R= 0.94965
y = 49.317 - 0.11934x R= 0.24102
A
ε_{400} (mM^{-1}cm^{-1})
[GuHCl] (M)

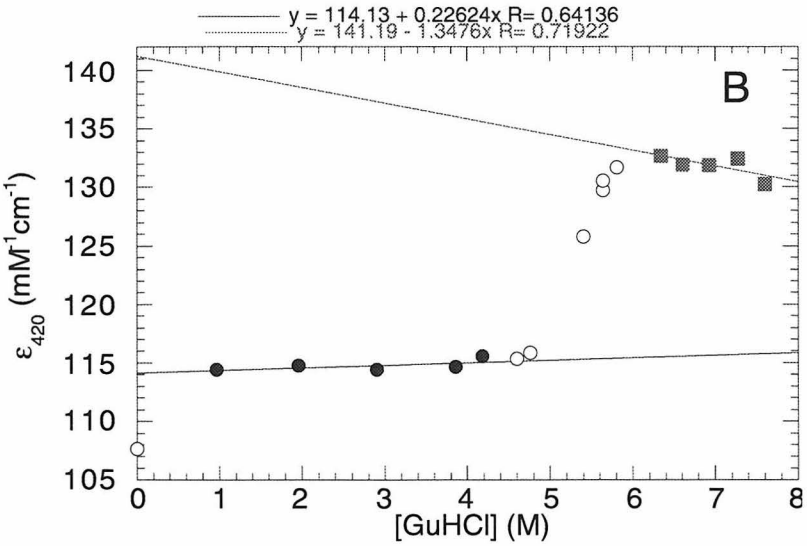
y = 114.13 + 0.22624x R= 0.64136
y = 141.19 - 1.3476x R= 0.71922
B
ε_{420} (mM^{-1}cm^{-1})
[GuHCl] (M)

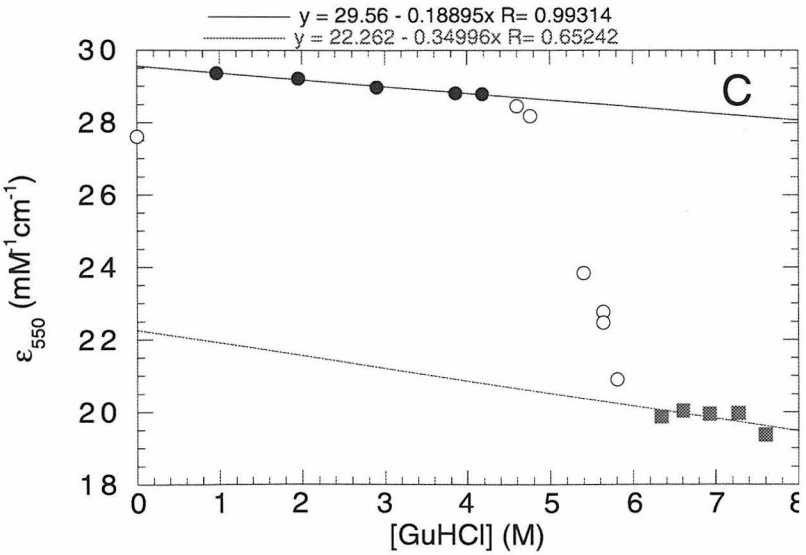
y = 29.56 - 0.18895x R= 0.99314
y = 22.262 - 0.34996x R= 0.65242
C
ε_{550} (mM^{-1}cm^{-1})
[GuHCl] (M)

Figure 4.12. Absorption changes at 400 nm (A), 420 nm (B), and 550 nm (C) accompanying thermal unfolding of y-cyt c^{III} (10.6 μM) at pH 7 in 0.18 M GuHCl.

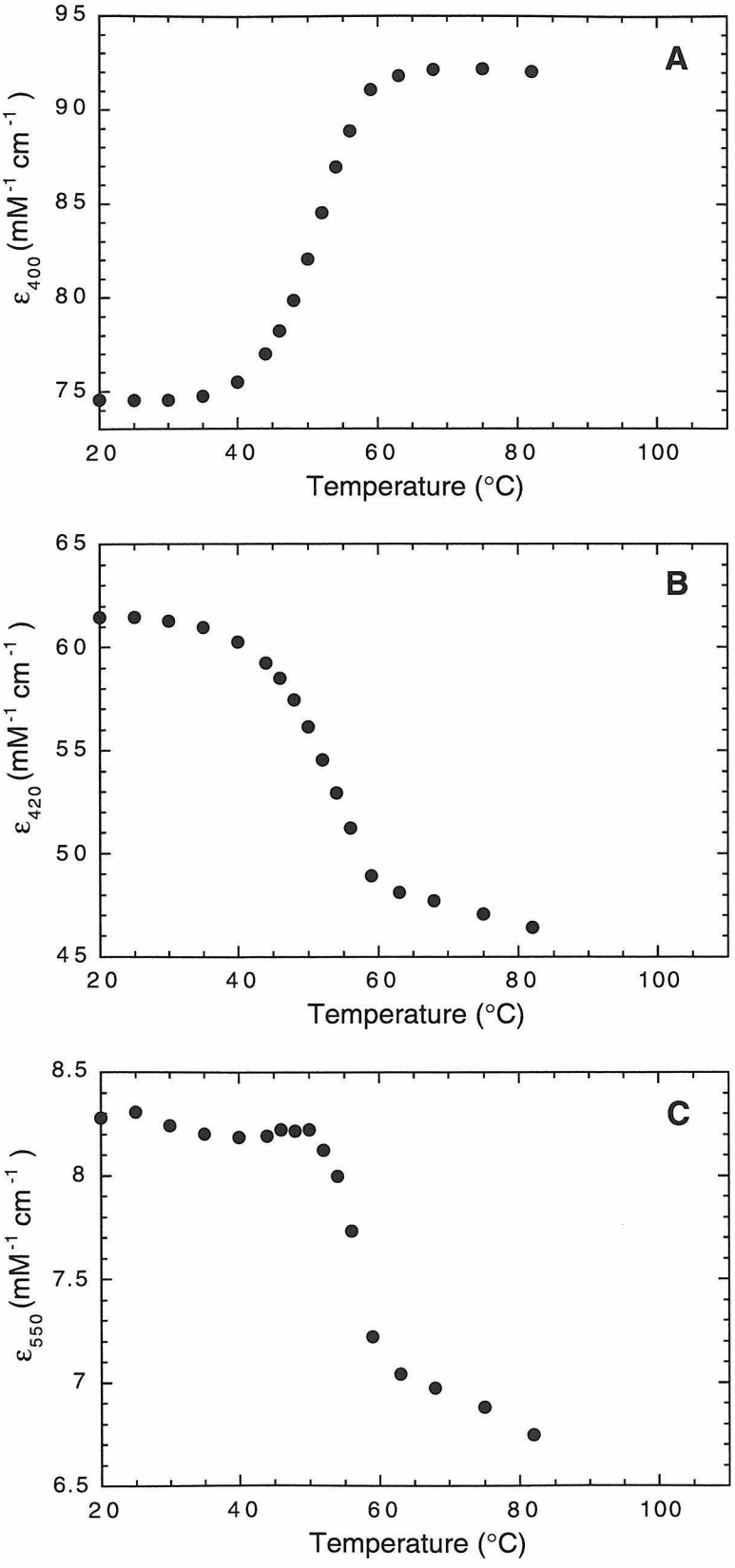
A
ε_{400} (mM^{-1} cm^{-1})
95
90
85
80
75
20
40
60
80
100
Temperature (°C)
B
ε_{420} (mM^{-1} cm^{-1})
65
60
55
50
45
20
40
60
80
100
Temperature (°C)
C
ε_{550} (mM^{-1} cm^{-1})
8.5
8
7.5
7
6.5
20
40
60
80
100
Temperature (°C)

Figure 4.13. Reaction scheme for photoinduced ET-triggered folding of cytochrome *c*.

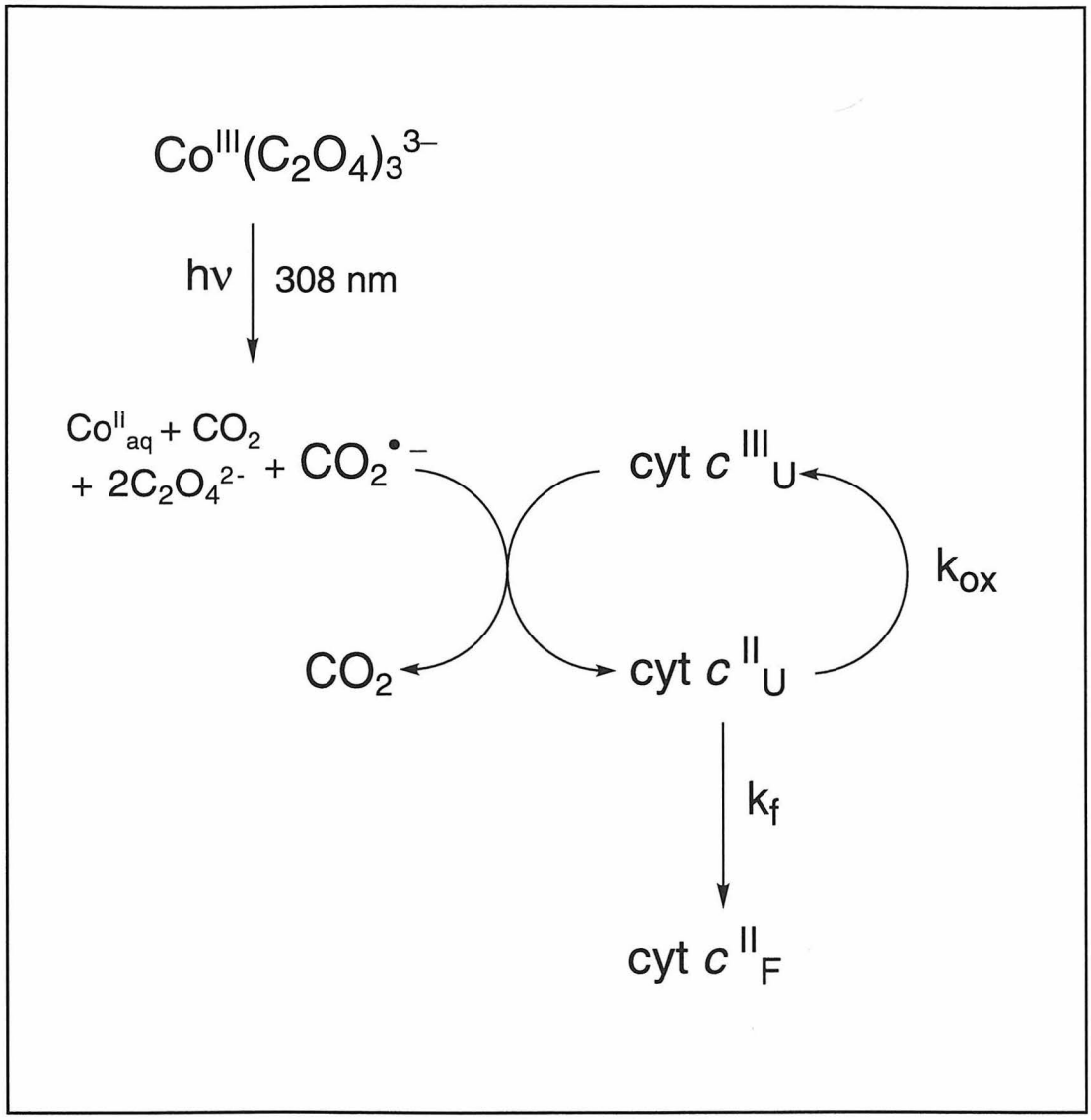
Co^III(C2O4)3^3–
hν
308 nm
Co^II_aq + CO2
+ 2C2O4^2- + CO2•–
cyt c^III_U
kox
CO2
cyt c^II_U
kf
cyt c^II_F

Figure 4.14. Transient absorption kinetics monitored at 420 nm following excitation (λ_{ex} = 308 nm) of a solution of y-cyt c^{III}_F (~15 μM) and $Co(C_2O_4)_3^{3-}$ (32 μM) in 0 M GuHCl (pH 7, 40 °C). (A) 20 ms timescale. (B) 800 ms timescale.

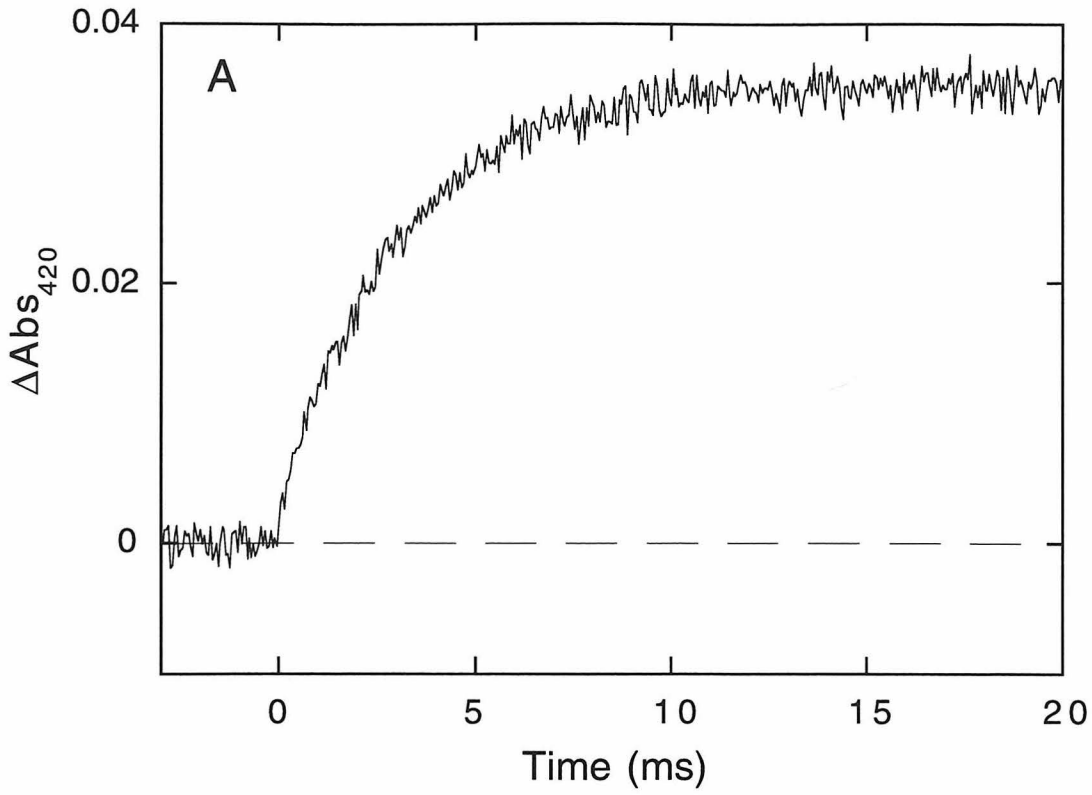
A
0.04
0.02
0
ΔAbs420
0
5
10
15
20
Time (ms)

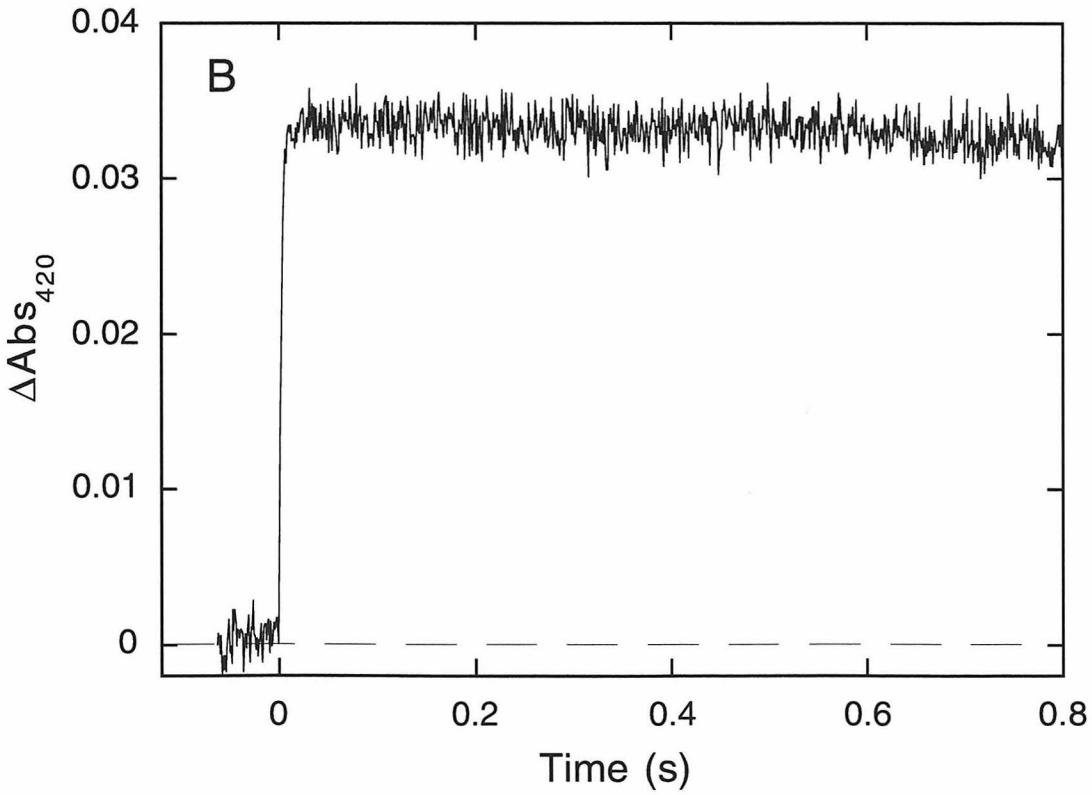
B
0.04
0.03
0.02
0.01
0
ΔAbs420
0
0.2
0.4
0.6
0.8
Time (s)

Figure 4.15. Transient absorption kinetics monitored at 420 nm following excitation of a solution of y-cyt c^{III}_{U} (~15 μM) and $Co(C_2O_4)_3^{3-}$ (32 μM) in 7.6 M GuHCl (pH 7, 40 °C). (A) 0.6 ms timescale. (B) 800 ms timescale.

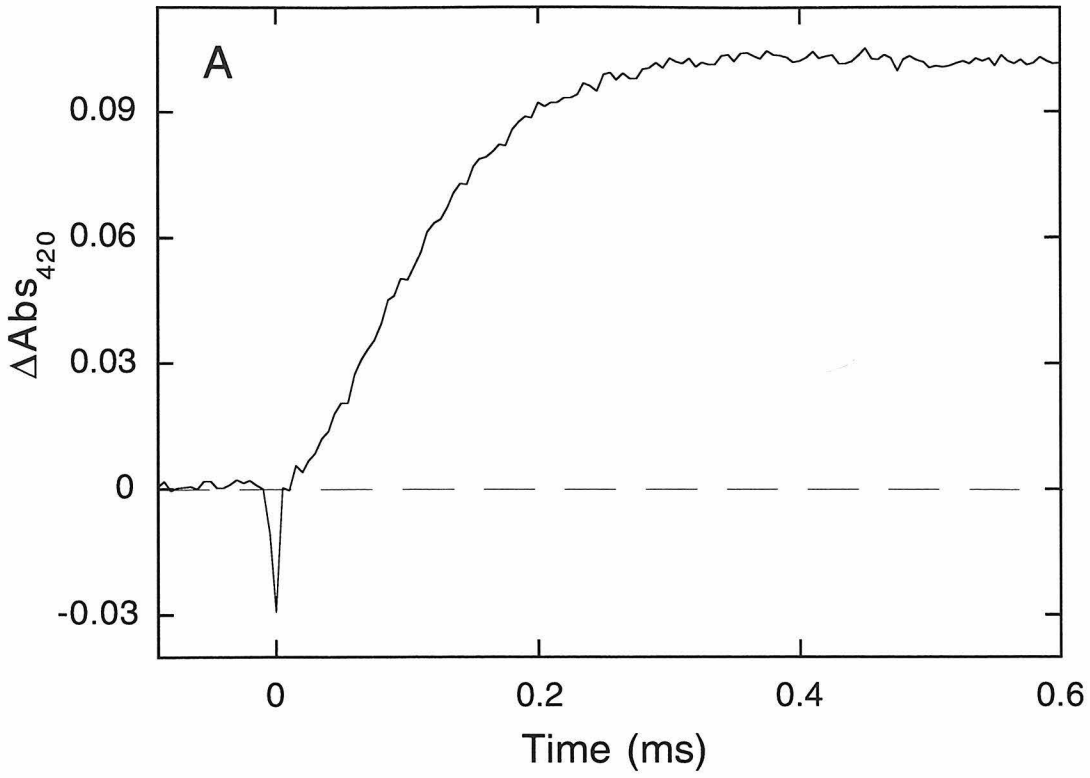
A
0.09
0.06
0.03
0
-0.03
ΔAbs420
0
0.2
0.4
0.6
Time (ms)

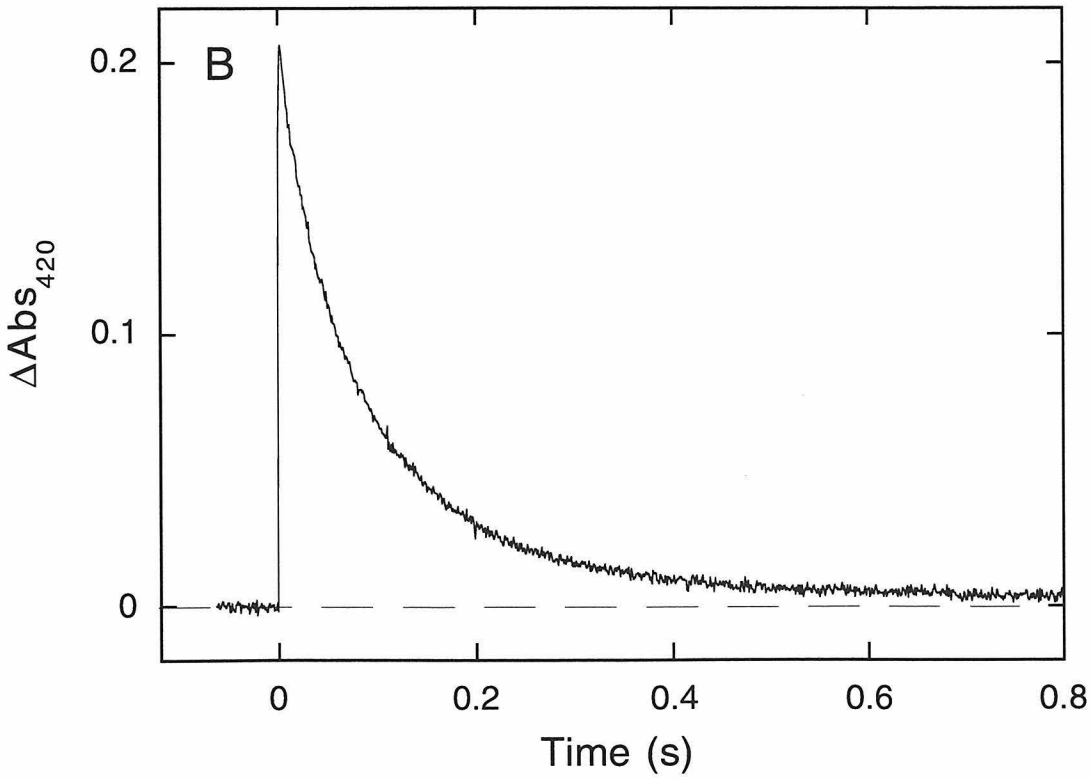
B
0.2
0.1
0
ΔAbs420
0
0.2
0.4
0.6
0.8
Time (s)

Figure 4.16. Transient absorption kinetics following excitation of a solution of y-cyt c^{III} (~15 μM) and $Co(C_2O_4)_3^{3-}$ (32 μM) in 1.0 M GuHCl (pH 7, 40 °C) monitored at 420, 550, and 400 nm. Compare with Figures 4.14, 4.15.

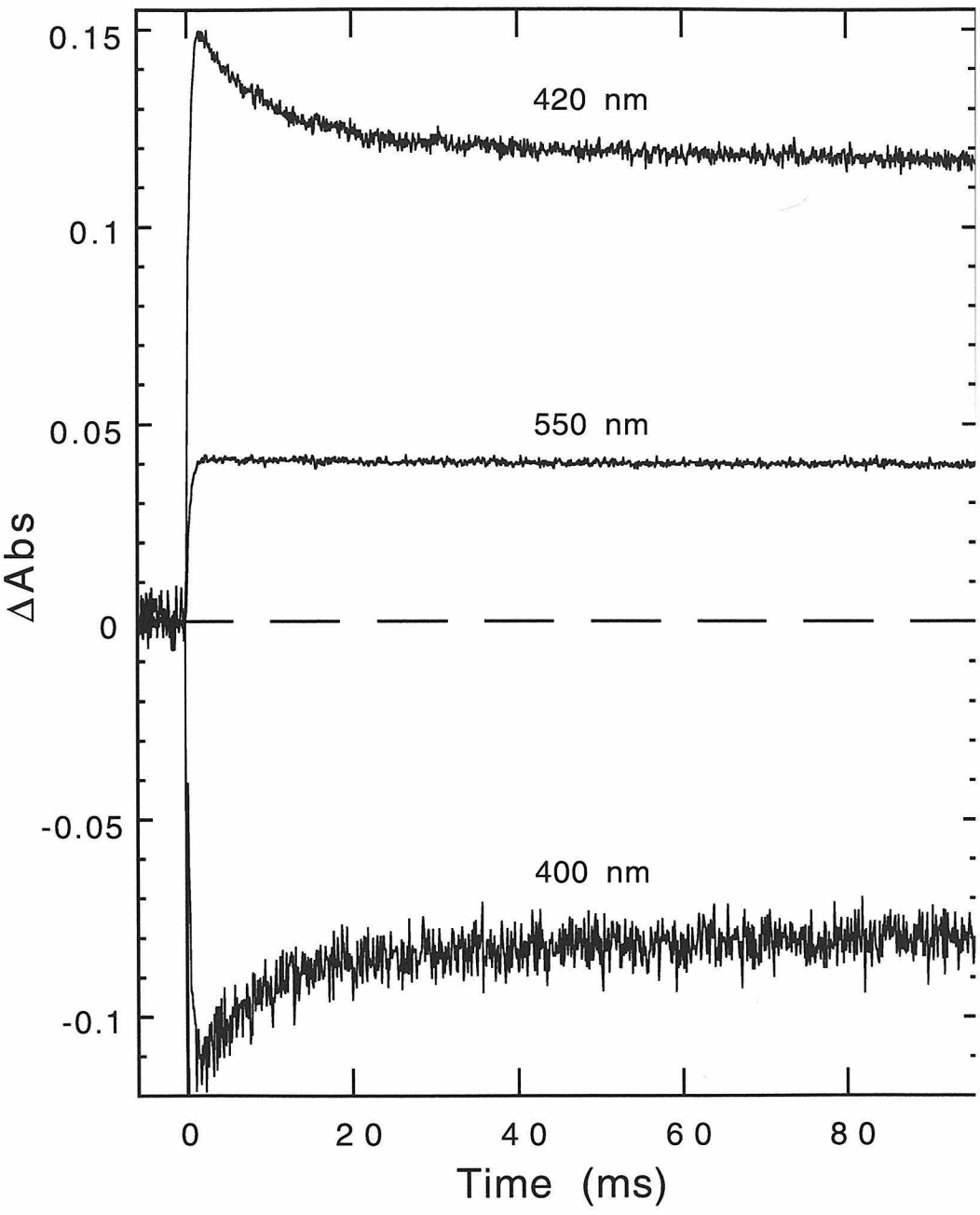
0.15
0.1
0.05
0
-0.05
-0.1
ΔAbs
420 nm
550 nm
400 nm
0
20
40
60
80
Time (ms)

Figure 4.17. Transient absorption spectra recorded at ~1 ms (solid line) and 50 ms (dashed line) after photolysis of $Co(C_2O_4)_3^{3-}$ in the presence of h-cyt c^{III}_U in 2.7 M GuHCl (40.0 °C, pH 7). 1 ms corresponds to immediately after the reduction phase, and 50 ms is near completion of the folding phase.

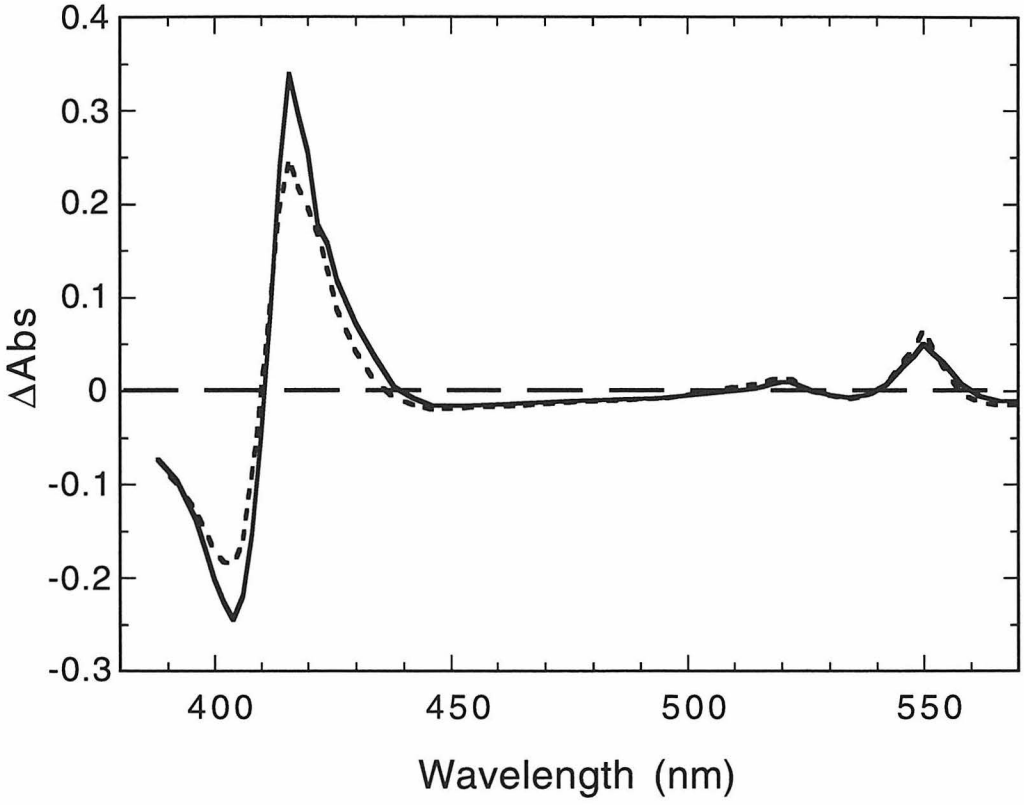
0.4
0.3
0.2
0.1
0
-0.1
-0.2
-0.3
ΔAbs
400
450
500
550
Wavelength (nm)

Figure 4.18. Folding (+ reoxidation) kinetics of y-cyt c^{II} in 1.6 M GuHCl (pH 7, 40 °C; λ_{obs} = 420 nm). The smooth lines are best fits to a distribution function (Equation 4.22) (A) and a biexponential function (Equation 4.21) (B). Residuals (the difference between the data and the fit values at each time point) are shown above each trace. The observed rate at the mean activation free energy obtained from the distributed fit ($\bar{k}_{obs}$ = 31 s^{-1}) is similar to the observed rate constant of the fast phase returned by the biexponential fit (k_{obs} = 37 s^{-1}).

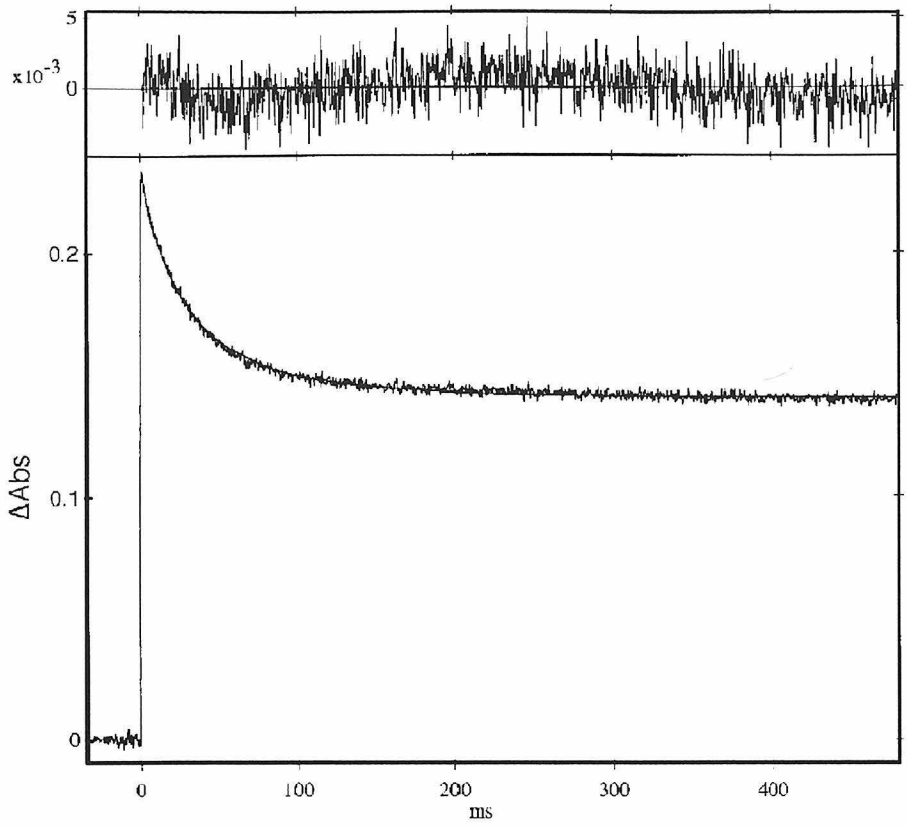
5
x10-3
0
0.2
0.1
0
ΔAbs
0
100
200
300
400
ms

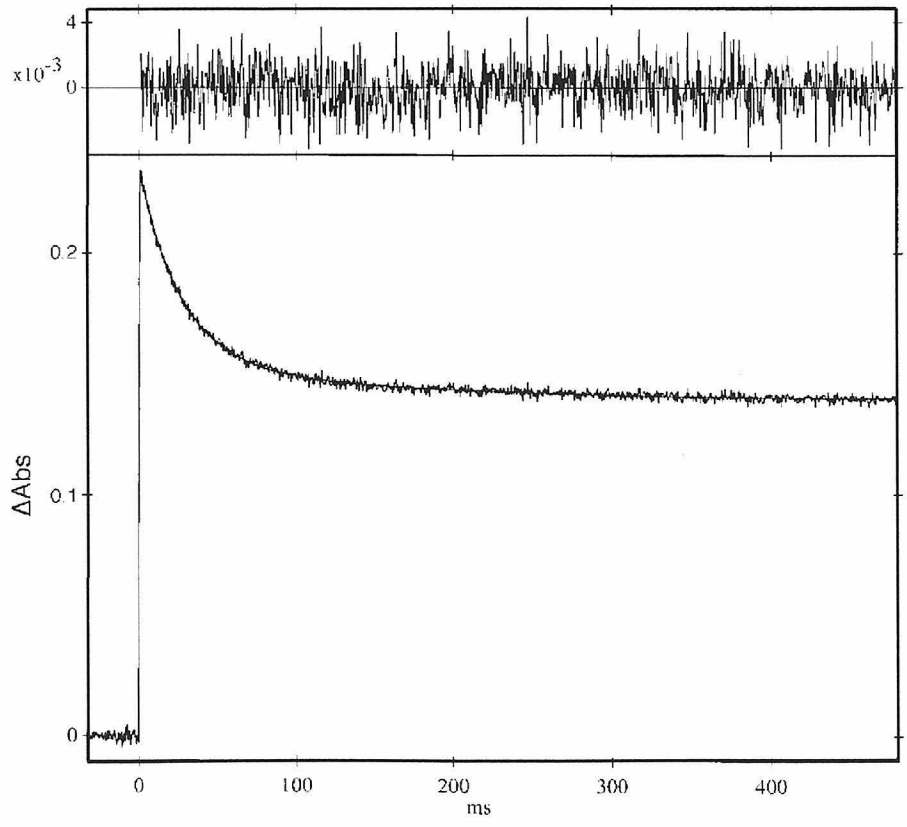
4
x10-3
0
0.2
0.1
0
ΔAbs
0
100
200
300
400
ms

Figure 4.19. Fits of reoxidation kinetics of unfolded y-cyt c^{II} (Figure 4.15B) using a single exponential decay (Equation 4.20) (A) or a distributed fit function (Equation 4.22) (B). Residuals are shown above each trace. The single exponential function clearly does not adequately represent the kinetics. The value of $\bar{k}_{ox}$ = 11 s^{-1} obtained from the distributed fit is identical, within error, to values extracted from raw data at lower concentrations where folding occurs (see text).

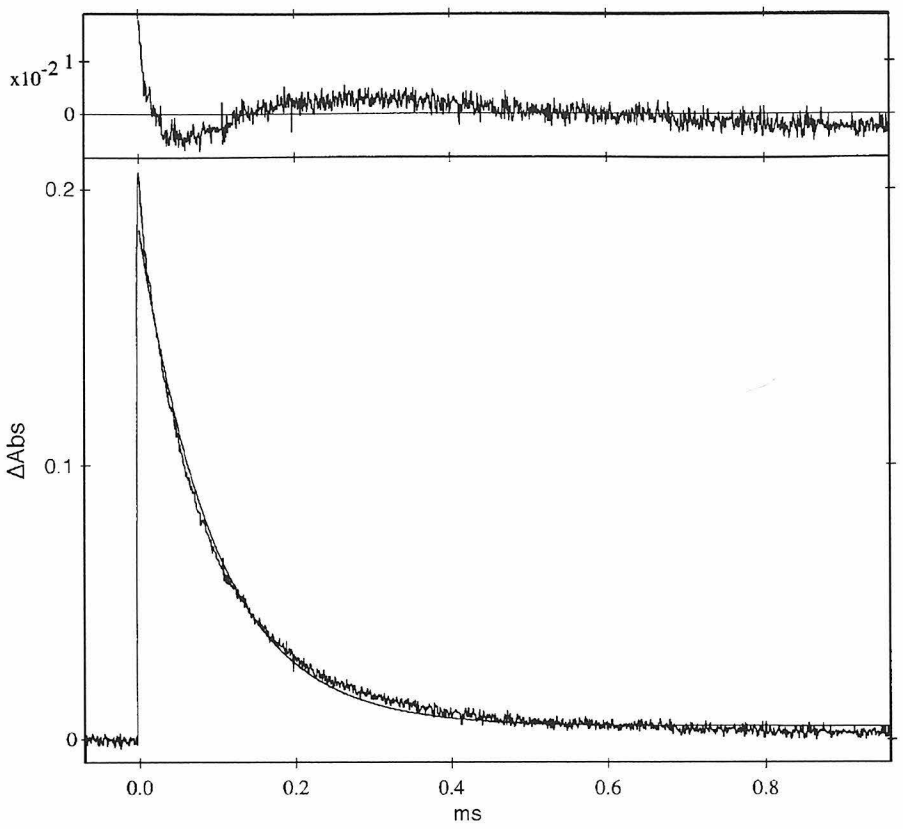
x10-2
1
0
0.2
0.1
0
ΔAbs
0.0
0.2
0.4
0.6
0.8
ms

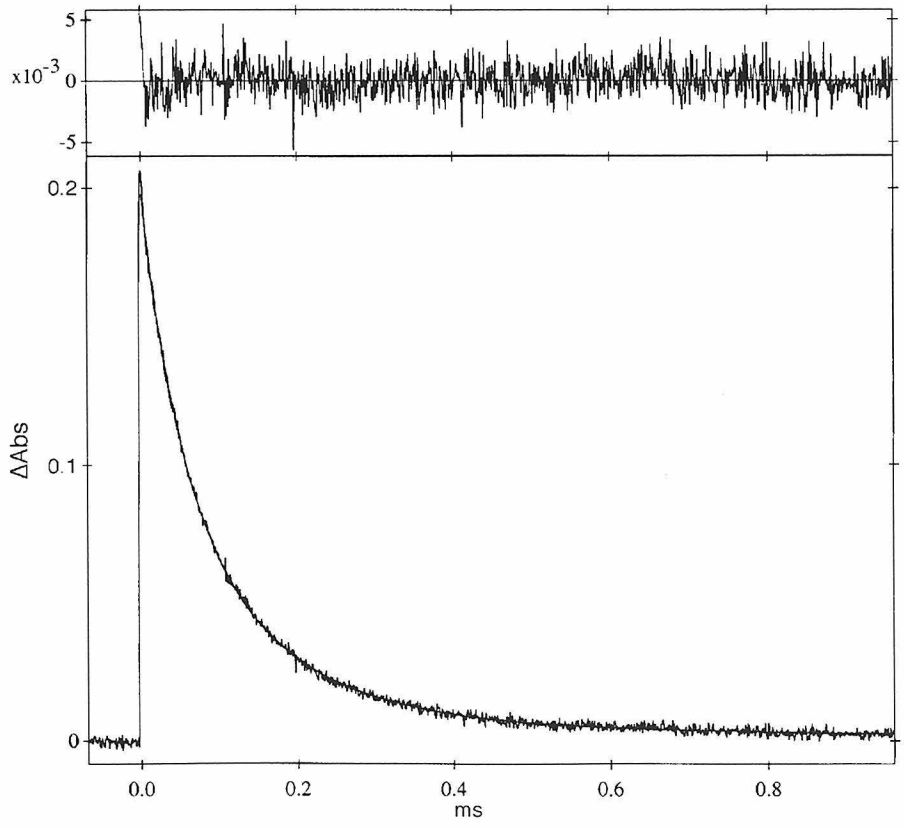
5
x10-3
0
-5
0.2
0.1
0
ΔAbs
0.0
0.2
0.4
0.6
0.8
ms

Figure 4.20. Kinetic profiles of folding/reoxidation of y-cyt c^{II} in solutions of varying concentrations of GuHCl (λ_{obs} = 420 nm; [GuHCl] = 1.3 to 2.6 M). Traces are scaled to 1 at t = 0 for ease of comparison.

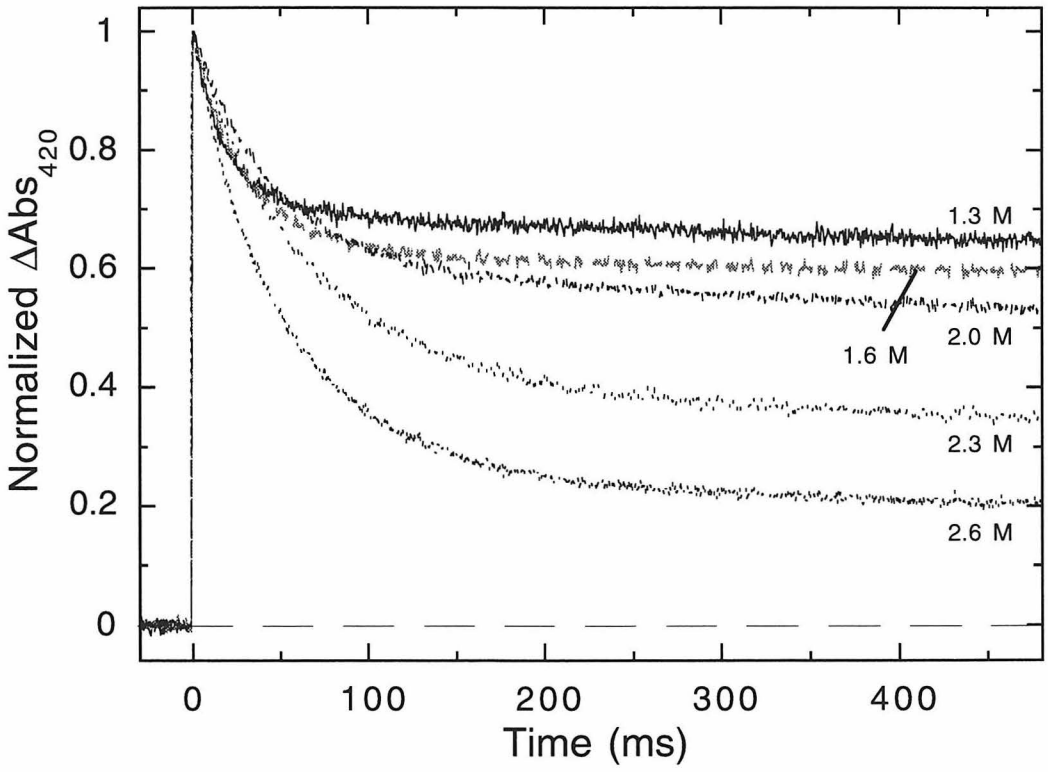
Normalized ΔAbs420
1
0.8
0.6
0.4
0.2
0
0
100
200
300
400
Time (ms)
1.3 M
2.0 M
1.6 M
2.3 M
2.6 M

Figure 4.21. Plot of the folding rates extracted using distributed fits ($\bar{k}_f$) as a function of GuHCl concentration for y-cyt *c* (inverted triangles) and h-cyt *c* (diamonds) at 22.5 °C (open symbols) and 40.0 °C (filled symbols). Note that the y-axis is a log scale; thus linear fits to the data (solid lines, h-cyt *c*; dashed, y-cyt *c*) indicate a linear relationship between $\Delta G_f^{\ddagger}$ and the concentration of GuHCl.

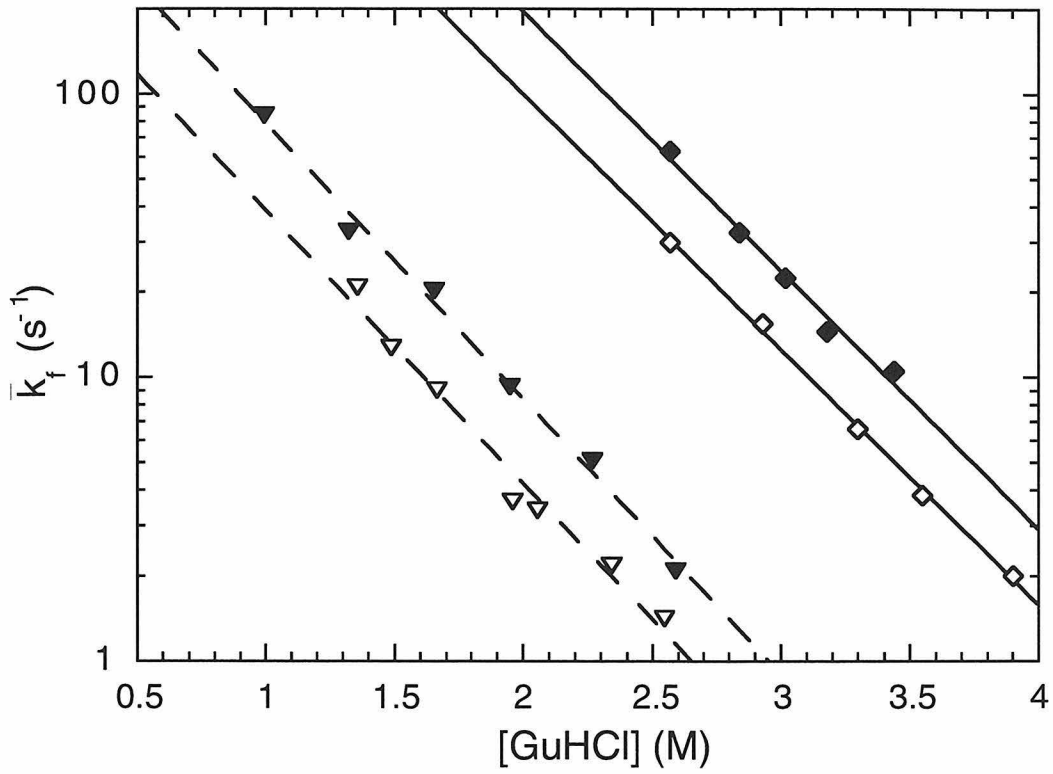
100
10
1
$\bar{k}_f$ (s^{-1})
0.5
1
1.5
2
2.5
3
3.5
4
[GuHCl] (M)

Figure 4.22. Plot of the folding rates extracted using biexponential fits (k_f) as a function of GuHCl concentration for y-cyt *c* (inverted triangles) and h-cyt *c* (diamonds) at 22.5 °C.

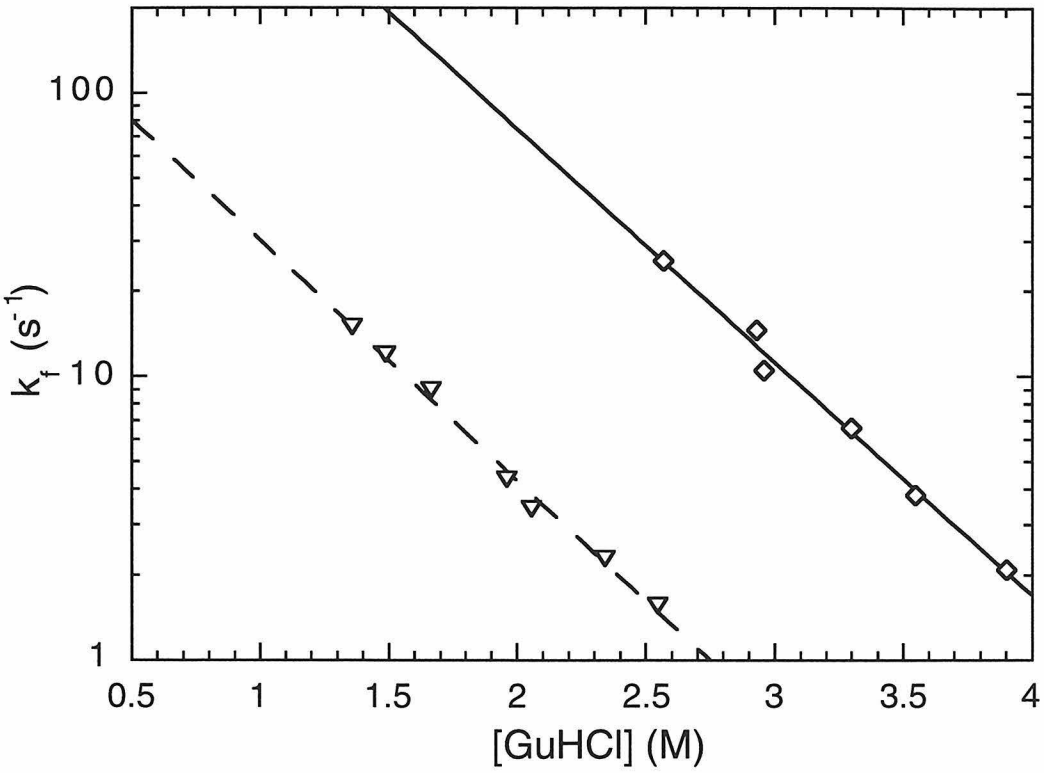
100
10
1
k_f (s^{-1})
0.5
1
1.5
2
2.5
3
3.5
4
[GuHCl] (M)

Figure 4.23. Replot of the 22.5 °C data in Figure 4.21 showing the values of $\bar{k}_f$ extracted from kinetics at each of the three wavelengths monitored: 420 nm (triangles), 400 nm (squares), and 550 nm (diamonds). y-cyt *c* is designated by open symbols; h-cyt *c* by filled (gray) symbols.

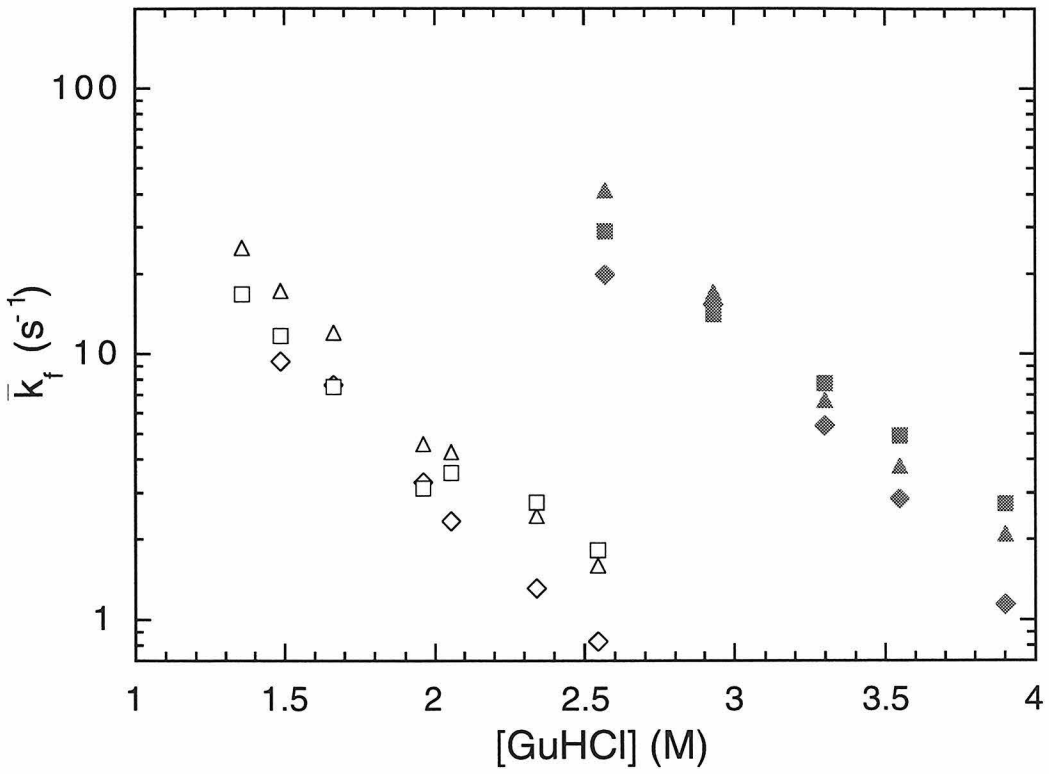
100
10
1
$\bar{k}_f$ (s^{-1})
1
1.5
2
2.5
3
3.5
4
[GuHCl] (M)

Figure 4.24. Plot of $\bar{k}_f$ vs. ΔG_f for y-cyt *c* (inverted triangles) and h-cyt *c* (diamonds) at 22.5 °C (open symbols) and 40.0 °C (filled symbols). Note that the y-axis is a log scale; thus linear fits to the data (solid lines, y-cyt *c*; dashed, h-cyt *c*) indicate a linear relationship between $\Delta G_f^{\ddagger}$ and ΔG_f.

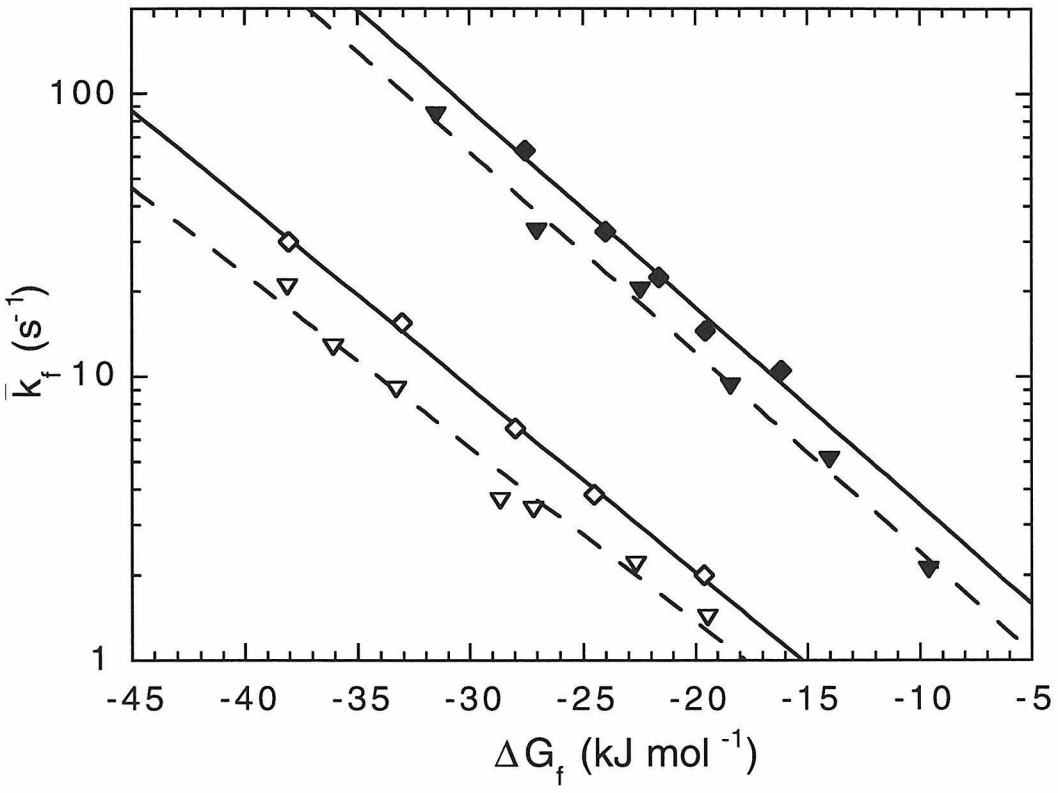
100
10
1
$\bar{k}_f$ (s^{-1})
-45
-40
-35
-30
-25
-20
-15
-10
-5
ΔG_f (kJ mol^{-1})

Appendix A

Characterization Data for Some $RuL_2(X)(im)$ Complexes

Figure A.1. Absorption spectra of $Ru(phen)_2(im)_2^{2+}$ (dotted), $Ru(4,4'\text{-}(CH_3)_2\text{-}bpy)_2(im)_2^{2+}$ (solid), $Ru(bpy)_2(im)_2^{2+}$ (dashed), $Ru(4,4'\text{-}(CONH(C_2H_5))_2\text{-}bpy)_2(im)_2^{2+}$ (long dash-short dash-long dash), and $Ru(phen)_2(CN)(im)^{+}$ (solid-dotted) in $\mu = 0.1$ sodium phosphate, pH 7.0.

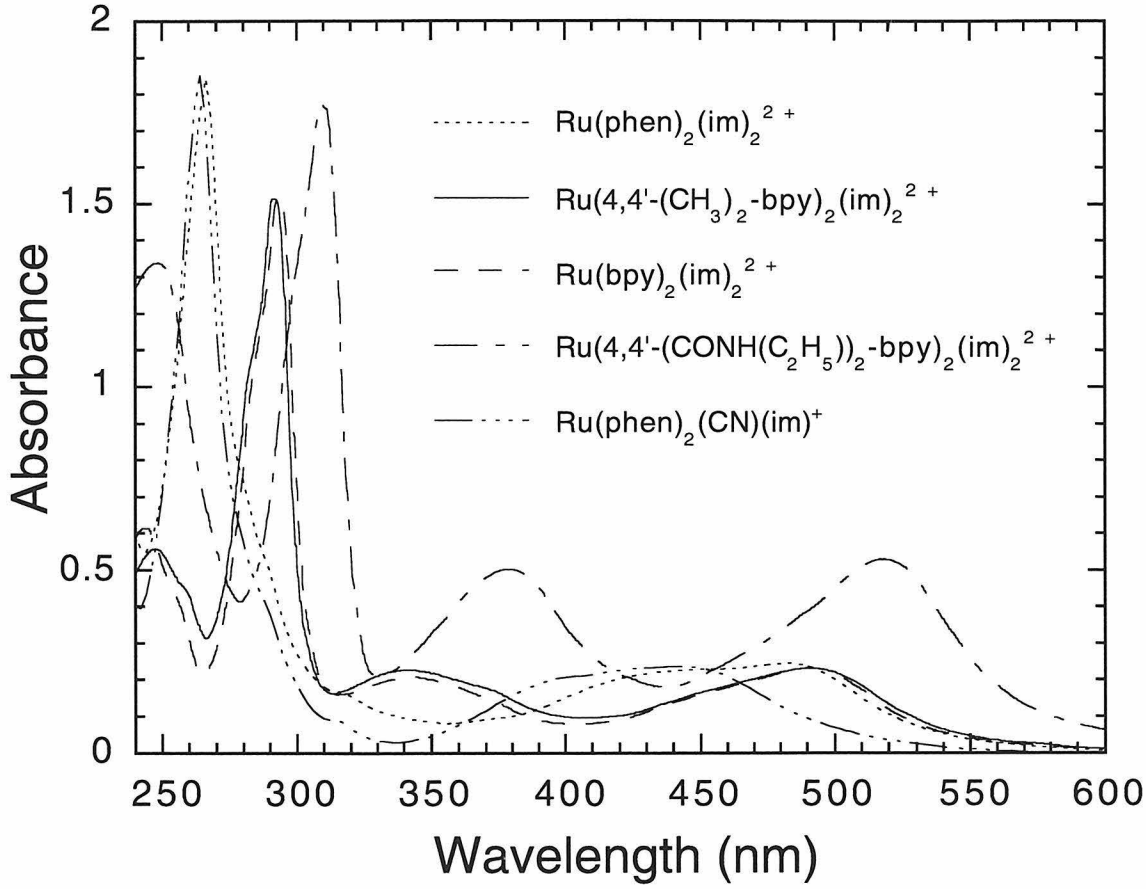
Absorbance
Wavelength (nm)
0
0.5
1
1.5
2
250
300
350
400
450
500
550
600
Ru(phen)2(im)2 2 +
Ru(4,4'-(CH3)2-bpy)2(im)2 2 +
Ru(bpy)2(im)2 2 +
Ru(4,4'-(CONH(C2H5))2-bpy)2(im)2 2 +
Ru(phen)2(CN)(im)+

Figure A.2. Uncorrected emission spectra of $Ru(phen)_2(im)_2^{2+}$ (dotted), $Ru(bpy)_2(im)_2^{2+}$ (dashed), $Ru(4,4'\text{-}(CONH(C_2H_5))_2\text{-}bpy)_2(im)_2^{2+}$ (long dash-short dash-long dash), and $Ru(phen)_2(CN)(im)^+$ (solid-dotted) in $\mu = 0.1$ sodium phosphate, pH 7.0. $\lambda_{ex} = 436$ or 490 nm. The abrupt change in the spectrum of $Ru(phen)_2(CN)(im)^+$ at ~710 nm is presumably due to a lamp fluctuation.

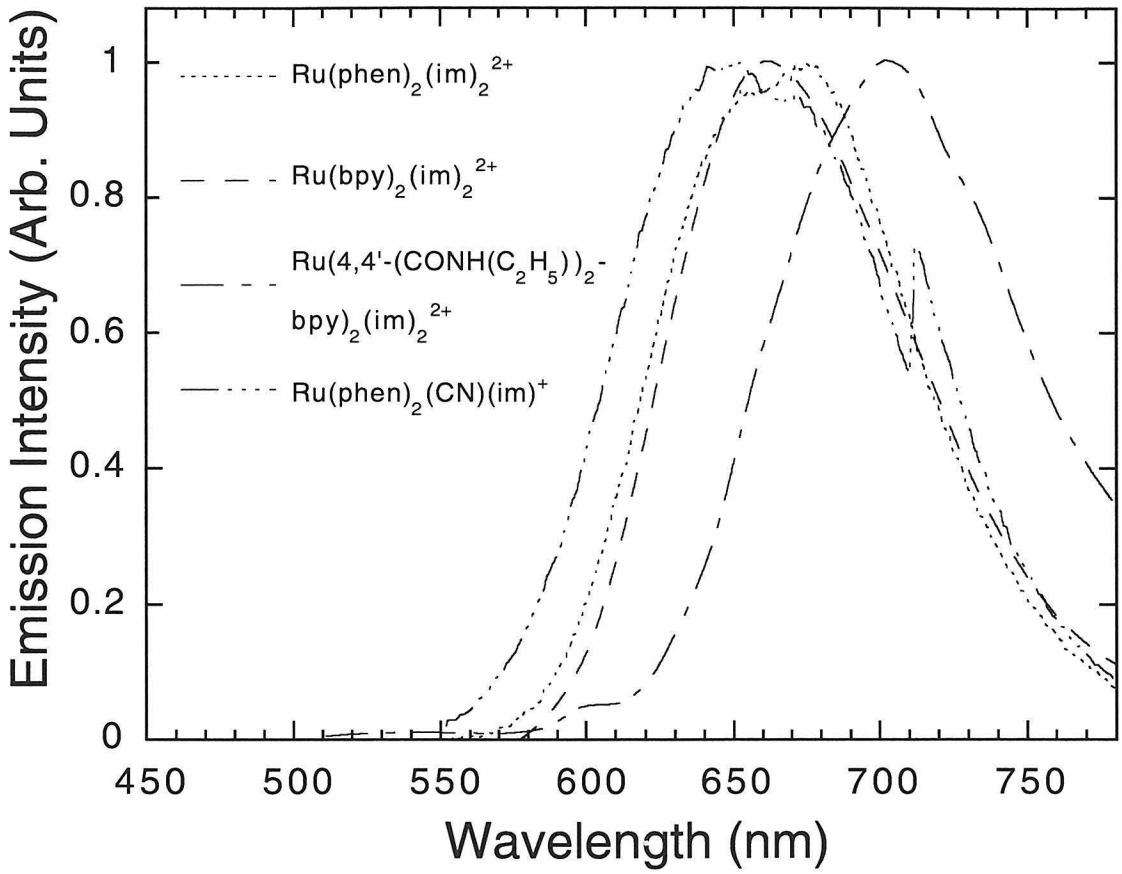
Emission Intensity (Arb. Units)
Wavelength (nm)
0
0.2
0.4
0.6
0.8
1
450
500
550
600
650
700
750
Ru(phen)2(im)2 2+
Ru(bpy)2(im)2 2+
Ru(4,4'-(CONH(C2H5))2-bpy)2(im)2 2+
Ru(phen)2(CN)(im)+

Figure A.3. ^{1}H NMR spectrum of $Ru(4,4'\text{-}(CONH(C_2H_5))_2\text{-}bpy)_2(im)_2^{2+}$ in D_2O.

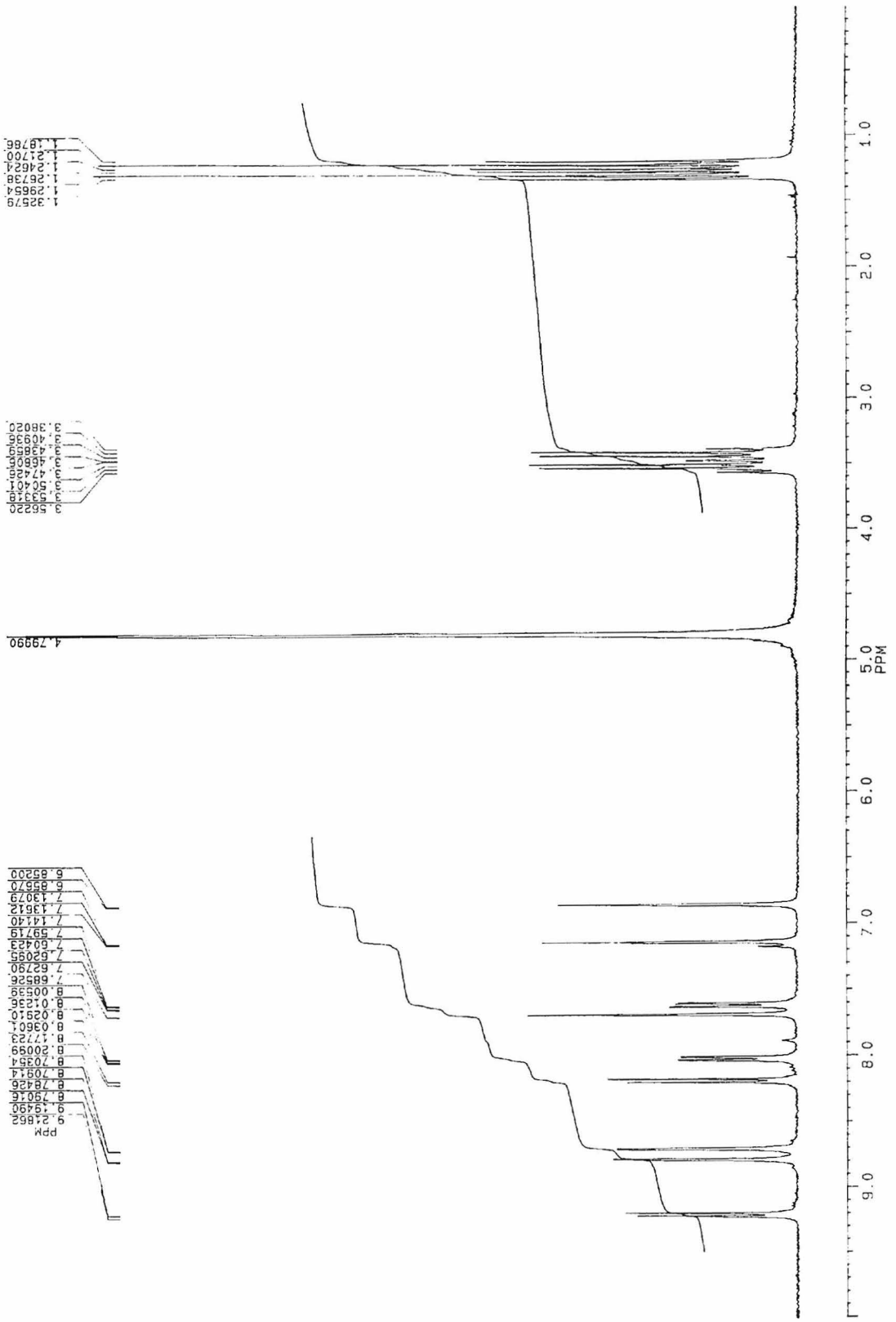
PPM
1.0
2.0
3.0
4.0
5.0
6.0
7.0
8.0
9.0

Figure A.4. ^{1}H NMR spectrum of $Ru(bpy)_2(im)_2^{2+}$ in D_2O.

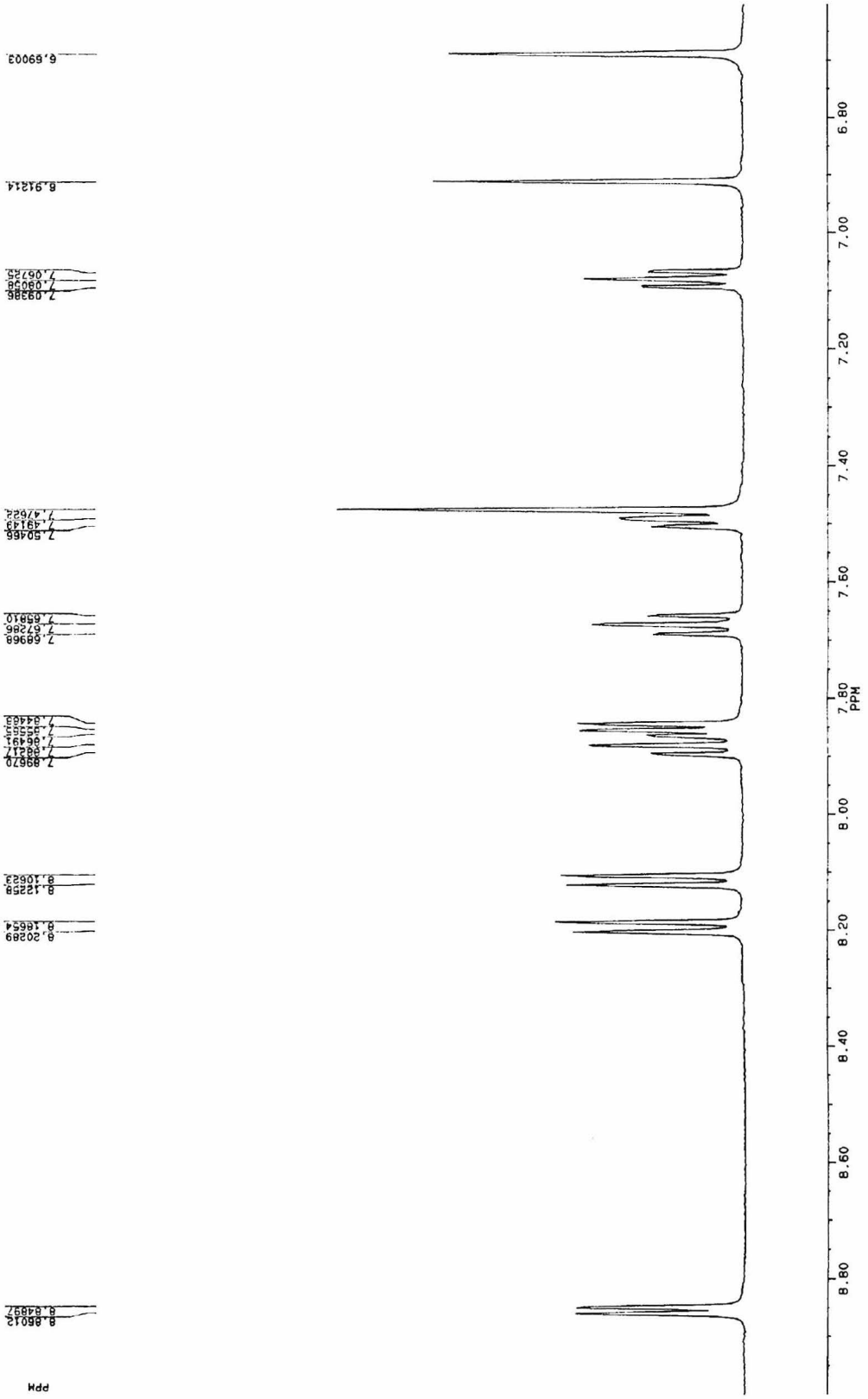
6.89003
8.92214
7.06725
7.05386
7.47622
7.49149
7.50466
7.65810
7.67286
7.68968
8.84463
7.95545
7.96492
7.98217
7.99570
8.12589
8.18654
8.20289
8.84897
8.86012
PPM
6.80
7.00
7.20
7.40
7.60
7.80
8.00
8.20
8.40
8.60
8.80
PPM